A Thesis Submitted for the Degree of PhD at the University of Warwick

Permanent WRAP URL:

http://wrap.warwick.ac.uk/186324

warwick.ac.uk/lib-publications

Coordination chemistry of rationally designed, multidentate phosphine ligands

Jennifer Emily Smart

A thesis submitted in partial fulfilment of the
requirements for the degree of
Doctor of Philosophy in Chemistry

University of Warwick
Department of Chemistry

May 2023

In loving memory

of

Abigail Rose Craddock

Table of Contents

Acknowledgements

Sébastien, thank you for always being willing to help, I really appreciate it. It's been great working with someone who shares my love of food, even though we may never agree on crispy bacon…

Finally, Tom, welcome back! It's been so much fun having you in the group again. Thanks for getting me hooked on gin and musicals and for your help during the final few weeks. I don't know what I would've done without you there to read my drafts and answer all my thesis-related questions.

I would also like to thank the Pringle group. To Rachel, Dan and Josh, you made me feel so welcome during my brief visit, and thank you Bex for everything you taught me! I really enjoyed my time in Bristol.

Big thanks also go to my Sussex friends. Shane, thank you for always believing in me and for sending me all those dinner photos… I kept breathing – I'm a swan, remember?! Rebecca, thank you for our days out – I really enjoyed our trips to Kenilworth, Blenheim and even the freezing pizza night on Worthing Pier! And to Abie, thank you so much for your friendship – you taught me so much and your bravery and determination have been a real inspiration to me.

This section wouldn't be complete without a massive thank you to Ronnie and Holly – 15 years of friendship and counting! You're support means so much to me. The Dursley weekends, the Bride Tribe fun and all the amazing things we've done together over the last few years have been a welcome distraction. You've helped to remind me that there is a world outside of the lab! See you in Lanzarote, love you both so much!!

I am also grateful for the support of my new CLS friends, in particular Jack, Giulia, Ross and Vincent. Thank you for your support and encouragement, it really helped me get through the final battle!

Finally, this wouldn't have been possible without the support of my amazing family, in particular Mum and Dad. Thank you so much for always believing in me and for all your support. I really appreciate everything you have done to help me - all the lifts to the Midlands and back, the cleaning and the laundry, for being a parcel collection service, for letting me move back in during lockdown and for everything you did for me when I broke my arm. I'm so lucky to have such supportive parents, I love you so much!

Declaration of Collaborative and Published Work

This thesis is submitted to the University of Warwick in support of my application for the degree of Doctor of Philosophy. It has been composed by myself and has not been submitted in any previous application for any degree.

The work presented (including data generated and data analysis) was carried out by the author except in the cases outlined below:

- Crystallographic data for all compounds was collected by Dr Adrian B. Chaplin, Reader, University of Warwick.

- gNMR simulations of the VT NMR spectra of 2,2'-biphenyl complexes **6** and **7** (**Chapter 2**) was performed by Dr Baptiste Leforestier, PhD graduate, Chaplin group, University of Warwick.

- Complexes **A167** (**Chapter 3**) and **A97** (**Chapter 4**) were synthesised by Dr Jack Emerson-King, PhD graduate, Chaplin group, University of Warwick.

- Hydroformylation catalysis (**Chapter 4**) was performed in collaboration with Prof. Paul G. Pringle, Professor of Inorganic Chemistry, University of Bristol. Initial optimisation of conditions, all reactions with complex **43** and some reactions with complex **44** were performed by Dr Rebekah J. Jeans, Postdoctoral Researcher, Pringle group, University of Bristol.

- High pressure NMR investigations into the activation of complex **44** were performed by Dr Alejandro Bara Estaún, PhD graduate, Hintermair group, University of Bath.

- Ambient pressure NMR investigations into the activation of complex **44** were performed by Dr Rebekah J. Jeans.

List of Abbreviations

%V_{bur}	Percent buried volume
β_n	Natural bite angle
δ	NMR shift
η	Hapticity
θ	Cone angle
κ	Denticity
ν	Tolman Electronic Parameter (see TEP)
χ_i	Substituent contributions to ν
Å	Ångström
acac	Acetylacetonate
An	Anthracenyl
app.	Apparent
Ar	Aryl
ATR	Attenuated Total Reflection
ax	Axial
biph	2,2'-Biphenyl
b/l	Branched-to-linear ratio
Bn	Benzyl
br	Broad
calcd	Calculated
CAAC	Cyclicalkyl(amino)carbene
COA	Cyclooctane
COD	1,5-Cyclooctadiene (lower case denotes coordination to metal)
COE	Cyclooctene (lower case denotes coordination to metal)
COSY	Correlated Spectroscopy
Cy	Cyclohexyl
d	Doublet
DFT	Density Functional Theory
dppe	1,2-Bis(diphenylphosphino)ethane
dtbpm	Bis(di-*tert*-butylphosphino)methane
ee	Enantiomeric excess
en	*endo*
eq	Equatorial
er	Enantiomeric ratio
ESI	Electrospray Ionisation

Et	Ethyl
ex	*exo*
fwhm	Full-width, half-maximum
HMBC	Heteronuclear Multiple Bond Correlation
HMDS	Hexamethyldisilazide
HOMO	Highest Occupied Molecular Orbital
HR	High Resolution
HSQC	Heteronuclear Single Quantum Coherence
i-	*ipso*
^{i}Bu	*iso*-Butyl
^{i}Pr	*iso*-Propyl
IR	Infrared
J	Spin-spin coupling constant
k^a	Local force constant
LR	Low Resolution
LUMO	Lowest Unoccupied Molecular Orbital
m	Multiplet
m-	*meta*
Me	Methyl
mer	Meridional
Mes	Mesityl
MLEP	Metal Ligand Electronic Parameter
MS	Mass Spectrometry
m/z	Mass-to-charge ratio
NBA	Norbornane
NBD	Norbornadiene (lower case denotes coordination to metal)
NBO	Natural Bond Orbital
^{n}Bu	*n*-Butyl
NCI	Non-Covalent Interaction
NHC	*N*-Heterocyclic Carbene
^{n}Hept	*n*-Heptyl
NMR	Nuclear Magnetic Resonance
^{n}Oct	*n*-Octyl
Naph	Naphthyl
NOESY	Nuclear Overhauser Effect Spectroscopy
Np	*Neo*pentyl

^{n}Pent	*n*-Pentyl
^{n}Pr	*n*-Propyl
o-	*ortho*
OAc	Acetate
p-	*para*
Ph	Phenyl
ppm	Parts per million
Py	Pyridine
q	Quartet
QTAIM	Quantum Theory of Atoms In Molecules
rac	*Racemic*
R_F	Retention Factor
ROESY	Rotating-frame nuclear Overhauser Effect Spectroscopy
r.t.	Room temperature
s	Singlet
SC-SC	Single-Crystal-to-Single-Crystal
sept	Septet
SMOM	Solid state Molecular Organometallic
t	Triplet
TBAF	Tetrabutyl ammonium Fluoride
^{t}Bu	*tert*-butyl
TEP	Tolman Electronic Parameter (see *v*)
THF	Tetrahydrofuran (lower case denotes coordination to metal)
TMEDA	*N,N,N',N'*-Tetramethylethylenediamine
TMS	Tetramethylsilane
TON	Turnover Number
UV	Ultraviolet
vbr	Very broad
vt	Virtual triplet
VT	Variable Temperature
XRD	X-Ray Diffraction
Xy	Xylyl

Abstract

Rational ligand design is a powerful strategy in organometallic chemistry. By carefully considering what features a ligand will need to possess for certain applications, drawing on information in the literature and, perhaps, computational insight, appropriate systems can be designed, enabling more efficient experiments to be conducted. This could have wide-ranging application in coordination chemistry and catalysis, with the potential to influence metal-based reactivity through modification of the coordination spheres. In this thesis, the application of ligand design strategies to three projects is presented. The roles of the primary and secondary coordination spheres are evaluated and the group 9 coordination chemistry of three multidentate phosphine ligands is investigated. These ligands were designed or chosen to achieve particular goals.

By considering the role of pincer ligands in the primary coordination sphere, [M(PNP-Np)(biph)][BAr$^F_4$] complexes were synthesised (biph = 2,2'-biphenyl, M = Rh/Ir, BAr$^F_4$ = B[3,5-(CF$_3$)$_2$C$_6$H$_3$]$_4$), exploiting the flexibility of the *neo*pentyl chains to investigate agostic interactions in these complexes. The results are in contrast to PNP-^{t}Bu analogues, which do not possess significant agostic interactions.

The versatility of pincers is also utilised, in combination with secondary coordination sphere considerations, for the design and synthesis of a resorcinarene-derived pincer ligand. The overarching aim was to design a system that could stabilise an alkane ligand in the solid and solution states. Whilst not yet achieved, this synthesis is described, and rhodium carbonyl complexes of this ligand are presented.

Finally, the focus was shifted to reaction control in the secondary coordination sphere, and a resorcinarene-derived phosphine-phosphite, previously synthesised in the Chaplin group, was investigated in the rhodium-catalysed hydroformylation of alkyl alkenes. The system showed branched selectivity that increased significantly with increasing alkene chain length, attributed to cavity effects.

Overall, this work highlights how the implementation of rational ligand design approaches can be a useful strategy for chemists.

| Chapter 2 | Chapter 3 | Chapter 4 |
| Agostic interactions | Bespoke pincer design | Branched-selective hydroformylation |
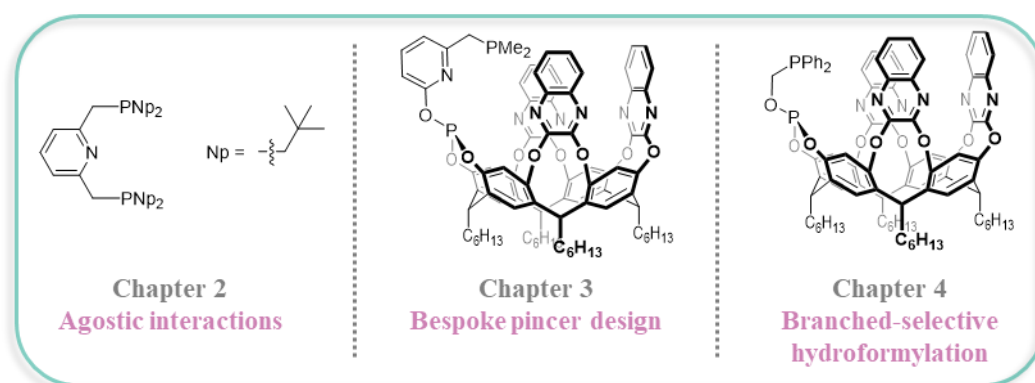
1. <u>Introduction</u>

1.1. <u>Reaction Control in the Primary and Secondary Coordination Spheres</u>

Traditionally, organometallic chemistry has involved the use of ancillary ligands to stabilise a metal ion and allow reactivity of interest to occur at the remaining coordination sites (usually behaving as spectators but in some cases becoming involved themselves). The range of ligands that can perform this role is vast, but common examples include two-electron 'L' donors such as trivalent phosphorus- and nitrogen-containing compounds, and *N*-heterocyclic carbenes (NHCs). Arenes, such as benzene-based compounds and the now-ubiquitous cyclopentadienyl ligand also have many applications, but it is chelating ligands that are now of considerable interest, stabilising complexes through the chelate effect and their increased rigidity and size when compared to non-chelating ligands.

The use of ligands such as those mentioned above allows the chemist to influence reactivity in the primary coordination sphere, by modification of the steric and electronic properties of these systems. Although these properties are often interrelated, there are several parameters which enable them to be quantified (**Figure 1.1**). The steric and electronic properties of phosphorus-containing ligands was extensively investigated by Tolman.[1] Here, the Tolman electronic parameter (TEP/v) was introduced, for quantifying the effect of donor strength of a phosphine when the substituents (contributions χ_i) are varied. It was originally obtained from one of the two carbonyl stretching bands of $[Ni(CO)_3L]$, where L is the phosphine of interest. Since this initial report, the concept of the TEP has been extended to other transition metal complexes, with more synthetically accessible complexes of the formula *cis*-$[M(L)(CO)_2Cl]$ being widely used (M = Rh, Ir; L = phosphine,[2,3] NHC[4-6]). Here, the two carbonyl stretching vibrations are averaged. The π-acidic carbonyl ligand is a good reporter of electron density at the metal centre to which it is bound, and, by extension, of the bonding situation between the metal and L.

This parameter has seen widespread application when describing the properties of ligands. However, Cremer has argued that the strength of a metal-ligand (M-L) bond cannot be quantitatively described by the carbonyl stretching frequency, rendering the TEP an unreliable parameter.[7,8] It is based on an oversimplified electronic bonding model and is not based on mode-decoupled carbonyl stretching frequencies, which introduces error. It has been proposed that by measuring the far infrared M-L stretching frequencies (which is now much simpler to achieve) and converting these normal (coupled) mode frequencies into local (decoupled) mode frequencies, the local force constant (k^a(M-L)) can be extracted.

Alternatively, this can be calculated using quantum chemical methods. With these values in hand, bond strength order values can be derived. These have also been termed metal-ligand electronic parameters (MLEP) and allow different M-L bonds to be compared.

When dealing with phosphorus-based ligands, the σ-donor capabilities of trivalent phosphorus groups can be probed by ^{31}P NMR spectroscopy, following preparation of the phosphorus selenide compound. The [31]P-[77]Se coupling constant is generally smaller for a more basic phosphorus centre: the presence of electron-donating substituents at phosphorus will lead to decreased s character of the phosphorus lone pair and a decrease in $^1J_{SeP}$, whilst electron-withdrawing substituents result in increased s character of the phosphorus lone pair and a larger $^1J_{SeP}$ value. This value can also convey some information about the steric properties of the ligand, as bulky substituents at phosphorus also lead to decreased s character of the lone pair (due to a widening of bond angles) and, subsequently, a smaller coupling constant.[9,10]

In order to consider the steric properties of a ligand, the cone angle (θ) was also introduced by Tolman to quantify the steric effect of the substituents of a phosphorus-containing ligand: this is the apex angle of the cylindrical cone defined by the metal and the phosphine substituents.[1] It can be modified to include examples where the three substituents are inequivalent, and also extended to include bidentate phosphines. However, this has largely been replaced by the percent buried volume (%V_{bur}). This is defined as the percent of the total volume of a sphere occupied by a ligand, where the sphere has a defined radius, with the metal centre at its core.[11,12] The volume of the sphere represents the primary coordination sphere (the space occupied by the ligands directly coordinated to the metal). It can be calculated using crystallographic data and is applicable to a wide range of ligands, rather than just tertiary phosphines.

When dealing with chelating ligands, it is often helpful to refer to the bite angle as an appropriate parameter. This is loosely defined as the angle made by the donor groups at the metal. However, this is complicated by the fact that the ligand-preferred bite angle (or natural bite angle, based on the steric constraints of the system) is not necessarily the same as the metal-preferred bite angle, which is impacted by electronic factors imposed by the metal centre. Both of these situations combine to give the observed bite angle.[13] Van Leeuwen and co-workers have performed detailed investigations into the effect of the natural bite angle (β_n) of chelating phosphorus-based ligands in homogeneous transition metal-catalysed processes.[14-19] This is now the most common parameter referred to when discussing bidentate ligands.

The use of the parameters discussed here enables researchers to consider the effects that the steric and electronic properties of various ligands (and their substituents) may have on the organometallic chemistry of their complexes, providing useful insight which can benefit the

ligand design process. However, in recent years there has been an increasing interest in manipulating interactions in the secondary coordination sphere to exert additional control over reactivity. This can allow new activity and/or selectivity to be introduced to a system where modification of the primary coordination sphere is not sufficient.
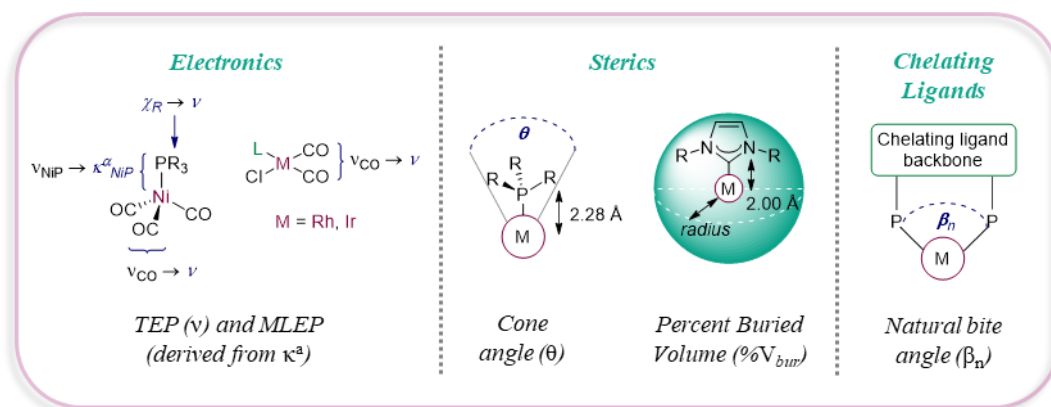
Figure 1.1. Ligand parameters used to quantify electronic and steric effects, where M is any metal (in the case of natural bite angle, M is a dummy metal with no electronic effects).

The use of secondary interactions in order to control organometallic reaction outcomes is inspired by the extremely high reactivity and selectivity displayed by enzymes. These are much greater in size compared to a synthetic organometallic catalyst, with a well-defined, confined space surrounding the active site. The pre-organisation brought about by this confinement, along with the presence of directing groups, can allow these natural catalysts to out-perform synthetic systems. In an attempt to mimic certain features of these enzymatic systems, combining elements of supramolecular chemistry with organometallic synthesis and transition metal catalysis is currently an area of significant interest.[20-22] By introducing potential for the formation of non-covalent interactions (NCIs) (e.g. *via* confinement[23-27,28-34] or other directing effects[22,35]) into the secondary coordination sphere, this could enable catalysts to be designed which display divergent reactivity, when compared with related non-supramolecular analogues. It could also enable the stabilisation of reactive species that would not otherwise be observed.

Ultimately, this thesis will focus on two relevant themes that underpin the work presented: pincer ligand design for controlling organometallic reactivity in the primary coordination sphere and the introduction of confinement *via* supramolecular ligand architectures in the secondary coordination sphere (**Figure 1.2**). In particular, the group 9 coordination chemistry of the ligands discussed will be the main focus, exploring ways in which the design of these ligands has enabled this reactivity.

Primary coordination sphere:
Coordinated ligands (e.g. pincer ligands) where the nature of **X**, **Y** and **Z** can influence sterics and electronics at the metal centre

Secondary coordination sphere:
Extended environment that can impact substrate (**S**) binding through encapsulation, non-covalent interactions or directing effects

Directing groups:
Directing groups can be incorporated to direct substrate binding, or NCIs with the microenvironment can stabilise substrate

Figure 1.2. *Illustrative depiction of the primary and secondary coordination spheres of an organometallic system confined within a supramolecular architecture.*

1.2. <u>Pincer Ligands</u>

1.2.1. <u>Overview</u>

A key requirement of ligand design is choosing a scaffold in which the donor properties can be varied with relative ease. Such a versatile system could have wide-ranging applications. Pincers are a category of ligand that fit this description well. The pincer ligand motif has become incredibly useful in organometallic chemistry over the last few decades, with many applications in areas such as homogenous catalysis and bond activation reactions.[36-43] Pincer ligands are defined as tridentate ligands that coordinate to a metal with a meridional (*mer-*) geometry (thereby distinguishing them from facially coordinating scorpionates), although there are some exceptions to this.[44] As a result of this coordination mode and the fixity of the donor groups, they are very rigid ligands, able to impart thermal stability and robustness at metal centres to which they are coordinated. This property is very useful when it comes to studying systems under catalytic conditions, where high temperatures and pressures may be required. It is also of use when observing coordinatively unsaturated metal centres, as the primary coordination sphere is occupied by the three donor groups and the steric effects of the substituents can prevent coordination at a vacant site.

Figure 1.3A highlights the general structure of a pincer ligand. The nomenclature is derived from the central atom of the three donor groups (**X** and **Z**), along with the linker atoms (**Y**). It is these three components that are typically modified, enabling a plethora of ligands to be synthesised that display rigid, *mer*-coordination, but wide-ranging steric and electronic properties. For example, a simple modification could be adjusting the substituents on the **Z** donors, changing the steric profile of the ligand and, therefore, affecting the environment at a metal centre. Additionally, changing the nature of the **Z** donor can affect both the sterics and electronics of the system. The introduction of phosphine or phosphinite groups also provides a useful NMR spectroscopic handle. Other donor groups are known, including carbenes,[45] amines, imines and phosphaalkenes,[36-38] although these are less common. Changing the nature of the linking **Y** atoms/groups can affect the electronics of the system and, also, the bite angle of the two **Z** donors. The typical pincer ligands are symmetric, such as PCP (X = C$^-$, Y = CH$_2$, Z = P) or PONOP (X = N, Y = O, Z = P) but asymmetric variants are also known.[46] This is a powerful approach as it potentially allows a system with two differing donor groups (different steric profiles, different electronics *etc.*) to be synthesised, which can have a considerable effect on the chemistry of an organometallic system. In **Figure 1.3B**, a small selection of pincer ligands (**A1**-**A15**) is shown which demonstrate how **X**, **Y** and **Z** can be varied to give ligands with diverse structures and properties.[36,38,46,47] A thorough discussion of these different structures is not possible here, and so the focus of the following sections will be on pincer ligands that possess scaffolds resembling those of the ligands described in this thesis.
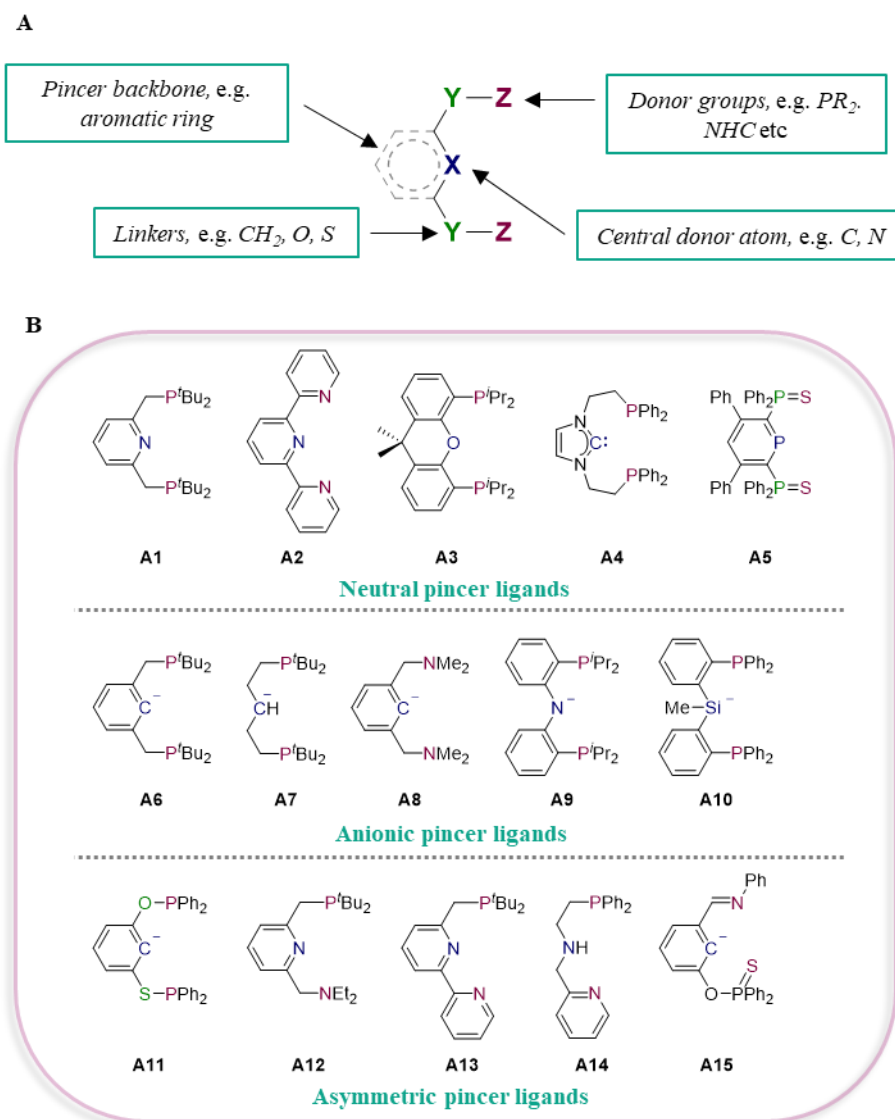
Figure 1.3A) *The generalised structure of a pincer ligand with donor groups **X** and **Z** and linkers **Y**;*
B) *a selection of examples of neutral (**A1-A5**), anionic (**A6-A10**) and asymmetric (**A11-A15**) pincer*
*ligands, highlighting how **X**, **Y** and **Z** can be modified.*

1.2.2. Phosphine-Based Pincer Ligands with an Aromatic Backbone

A large and important class of pincer ligands feature either a benzene or pyridine backbone
($X = C^-$/N), with methylene or oxygen linkers (Y) and phosphine donors (Z). Pincer ligands
based on these scaffolds were the first among this class of ligand to be investigated and they
have become a common feature of modern organometallic chemistry. In the case of
PNP/PONOP (**Scheme 1.1A-B**), the resulting ligand is an L_3 donor, whilst PCP/POCOP
(**Scheme 1.1C-D**) are L_2X donors, requiring an additional step, such as C-H activation of a
proligand (C-C and C-Br activations have also been implemented), before coordination to a
metal can occur.[36-38] Pincer ligands of this type are relatively easy to synthesise, starting from
readily available precursors such as 1,3-bis(halomethyl)benzene, lutidine and resorcinol.

6
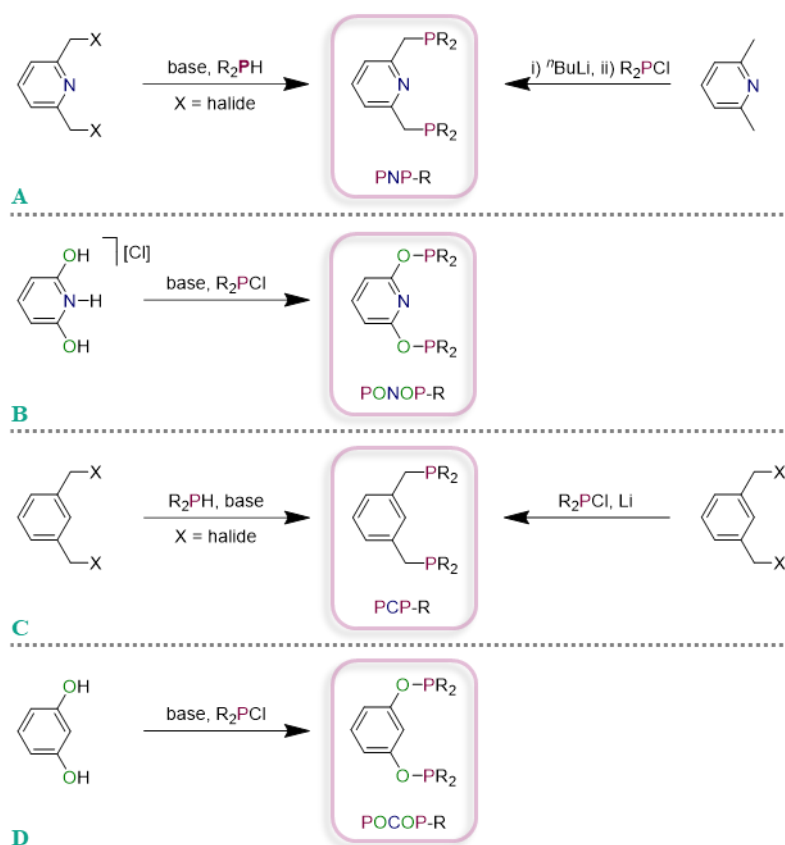
Scheme 1.1. *Synthetic routes to pincer ligands of the form* **PYXYP** *(X = N, C; Y = CH₂, O)*.

The first pincer ligand, PNP-Ph, was reported by Nelson in 1971,[48] along with an investigation of its iron, cobalt and nickel coordination chemistry. Moulton and Shaw reported the synthesis of PCP-*t*Bu soon after,[49] and characterised a range of transition metal complexes, including group 9 hydrides and carbonyl complexes. Since then, these and related pincer complexes have been shown to be effective catalysts in a variety of transformations, including C-C and C-O bond forming reactions, palladium and nickel-catalysed cross-coupling reactions, transfer hydrogenation, alkane dehydrogenation and asymmetric catalysis. They have also found application in small molecule activation, bond activation reactions (including C-H bonds) and in the stabilisation of unusual complexes or metal oxidation states. Their ability to act as non-innocent ligands and participate in metal-ligand cooperativity (often *via* dearomatisation in PNP systems) is also an important mode of reactivity.[36-43]

Milstein was the first to synthesise the now well-known PNP-*t*Bu.[50] It's iridium coordination chemistry was explored, and it was found that reaction with [Ir(coe)₂Cl]₂ (coe = cyclooctene) resulted in the product of C(sp²)-H activation (**A16**, **Scheme 1.2**). Further investigation enabled the synthesis of the cationic iridium(I) coe complex **A17**, which underwent C-H activation in the presence of benzene.[51,52] The product **A18** is a rare example of a thermally stable, square pyramidal, aryl hydride complex, in contrast to the analogous PCP-*t*Bu complex **A19**, which is not thermally stable.[53] Despite the lower electron density in

cationic **A18** (*cf.* neutral **A19**), the carbon donor in **A19** exerts a stronger *trans* influence, resulting in a longer Ir-C bond and a complex unstable to reductive elimination. The propensity of **A17** to undergo aromatic C-H activation was extended to aryl halides, where it was found that C-H activation was preferred to C-X activation (X = F, Cl, Br). In the case of fluorobenzene activation (**A20**), no selectivity was observed and the kinetic products were formed (*i.e.* the products of *ortho-*, *meta-* and *para-*C-H activation). However, reaction with chlorobenzene, bromobenzene and anisole ultimately led to complete conversion to the thermodynamic *ortho-*products **A21**-**A23**, in which coordination of the heteroatom drives the formation of this product.
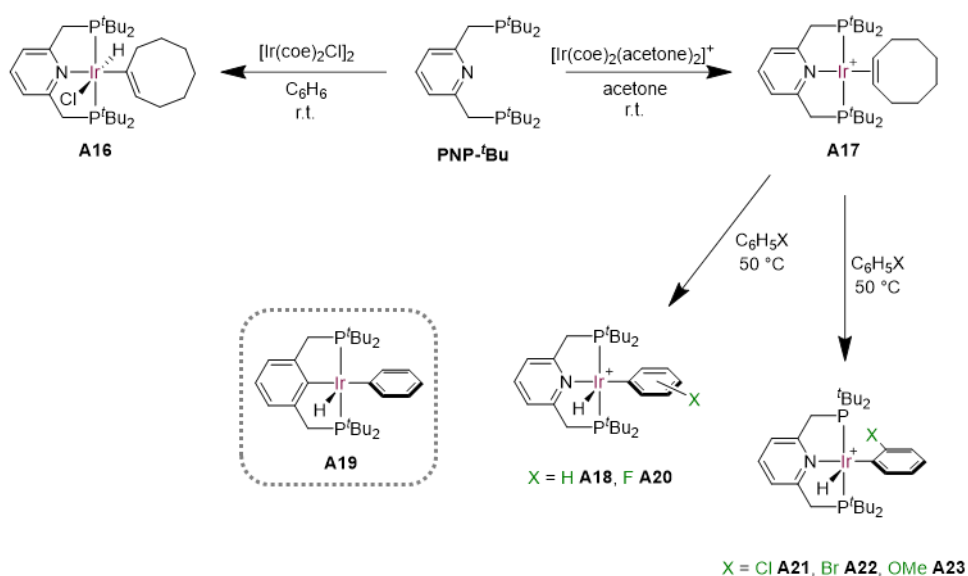
Scheme 1.2. C(sp^2)-H activation in iridium complexes of PNP-^{t}Bu, reported by Milstein,[50-52] with Goldman's PCP-^{t}Bu complex A19 shown alongside for comparison.[53] [PF$_6$]$^-$ counterions are omitted for clarity.

The rhodium chemistry was also explored, but vinylic C-H activation of COE was not observed in this case.[50] Other groups have extended the rhodium coordination chemistry of PNP-^{t}Bu[54-58] to include carbonyl, dihydrogen and dinitrogen adducts.[54,55,57] Goldberg and Heinekey observed C-H activation of benzene by rhodium(I) hydroxide and trifluoroethoxide complexes **A24**-**A25** (**Scheme 1.3**).[59,60] Recently in the Chaplin group, a series of rhodium(I) complexes of PNP-^{t}Bu and PONOP-^{t}Bu were synthesised from the 1,5-cyclooctadiene (COD) complexes **A27**-**A30** (**Scheme 1.4**).[61] The lability of the bound cod provided a simple route to reach the known carbonyl (**A31**-**A32**), dihydrogen (**A33**-**A34**) and dinitrogen (**A35**-**A36**) adducts, along with the novel water (**A37**-**A38**) and nitrous oxide complexes (**A39**-**A40**).[62] The coordination chemistry of nitrous oxide is an area of great current interest, due to it's environmental concerns, but efforts have been hampered by the poor ligating ability of this greenhouse gas. It is both a weak σ-donor and π-acceptor and N-N or N-O bond cleavage are often preferred modes of reactivity following coordination to a metal.[63] The pincer ligands PNP-^{t}Bu and PONOP-^{t}Bu possess rigid, stabilising backbones, which, along with the steric

buttressing provided by the *tert*-butyl groups around the metal centre, stabilises the weakly bound N_2O ligand.
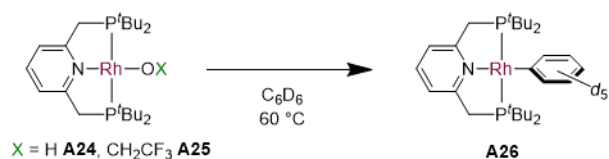
Scheme 1.3. *$C(sp^2)$-H activation of benzene by rhodium(I) phenoxide and trifluoroethoxide complexes **A24** and **A25**.*[59,60]

The activation of terminal alkynes using **A27** and **A28** was then investigated (**Scheme 1.5**). In both cases, this gave rise to the vinylidene complexes **A41**-**A44**, although in the case of PONOP-*t*Bu complex **A44**, this was only obtained as a minor product, alongside the alkyne π-complex. This work serves to highlight the ease with which the rhodium coordination chemistry of these pincers can be accessed.
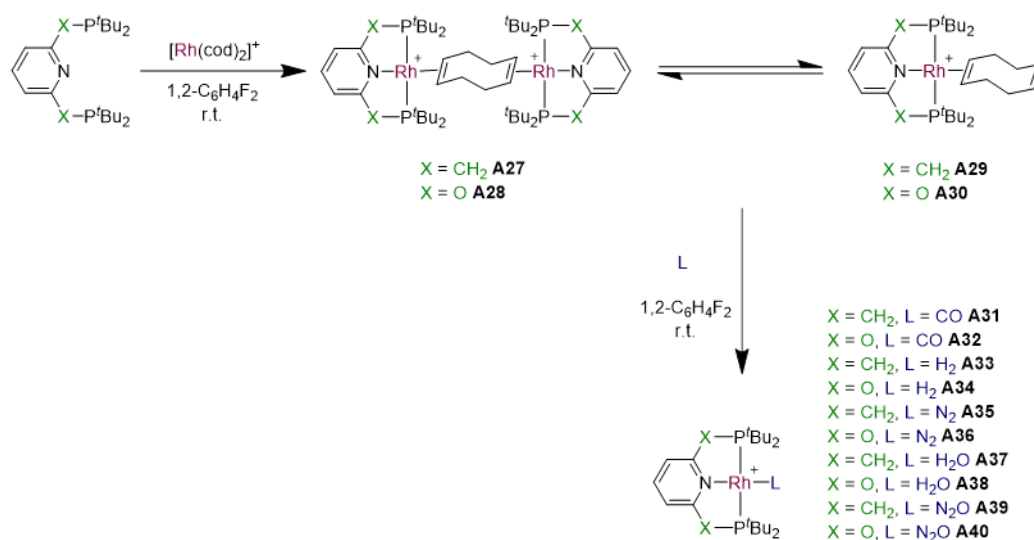
Scheme 1.4. *Synthesis of rhodium(I) cod complexes **A27**-**A30** and the subsequent preparation of adducts **A31**-**A40**.*[61,62] *$[BAr^F_4]^-$ counterions are omitted for clarity ($BAr^F_4 = B[3,5-(CF_3)_2C_6H_3]_4$).*
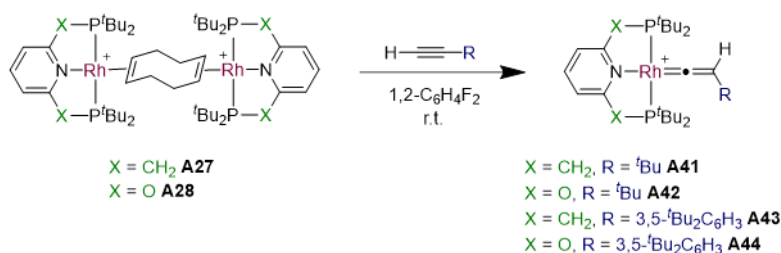
**Scheme 1.5.** *C(sp)-H activation of terminal alkynes by A27 and A28.*[61] *[BAr$^F_4$]$^-$ counterions are omitted for clarity.*

A relatively unexplored ligand in this family is PNP-Np (Np = *neo*pentyl), synthesised by Yamashita and Nozaki.[64] Only its iridium chemistry has been investigated, and there are no reports of PONOP-Np. Although limited in scope, these results are relevant in the context of the work presented here. Reaction of PNP-Np with [Ir(cod)$_2$][BF$_4$] rapidly proceeded to give cationic iridium(III) cyclometallated complex **A45** (**Scheme 1.6**). Subsequent reaction with acetonitrile preserved the metallacycle, giving 18-electron complex **A46**, whilst reductive elimination of the cyclometallated group was found to occur on addition of a series of π-acceptor ligands **A47**-**A49**. The reaction with carbon monoxide was studied by ^{31}P{^{1}H} NMR spectroscopy and an 18-electron iridium(III) reaction intermediate was identified, which then underwent reductive elimination to give 16-electron iridium(I) complex **A47**. Under an atmosphere of dihydrogen, dihydride **A50** was synthesised, displaying an agostic interaction at the vacant coordination site. Complex **A51**, with a dearomatised pyridine backbone, was synthesised *via* reaction of complex **A45** with lithium hexamethyldisilylamide.[65]

Inspired by the work of Milstein on the related PNP-^{t}Bu iridium system **A17** (**Scheme 1.2**),[50-52] the authors wanted to investigate the potential for benzene activation with **A45**. However, the expected product of C-H activation was not observed. In the PNP-^{t}Bu system, iridium(I) complex **A17** and the product of C-H activation, **A18**, are energetically similar, with only a small overall loss of entropy occurring in this transformation. However, PNP-Np complex **A45** is more stabilised due to the cyclometallation of a *neo*pentyl group, with reductive elimination required to form an iridium(I) intermediate that can undergo C-H activation, rather than ligand dissociation. This transformation is, subsequently, entropically unfavourable, and so not observed.
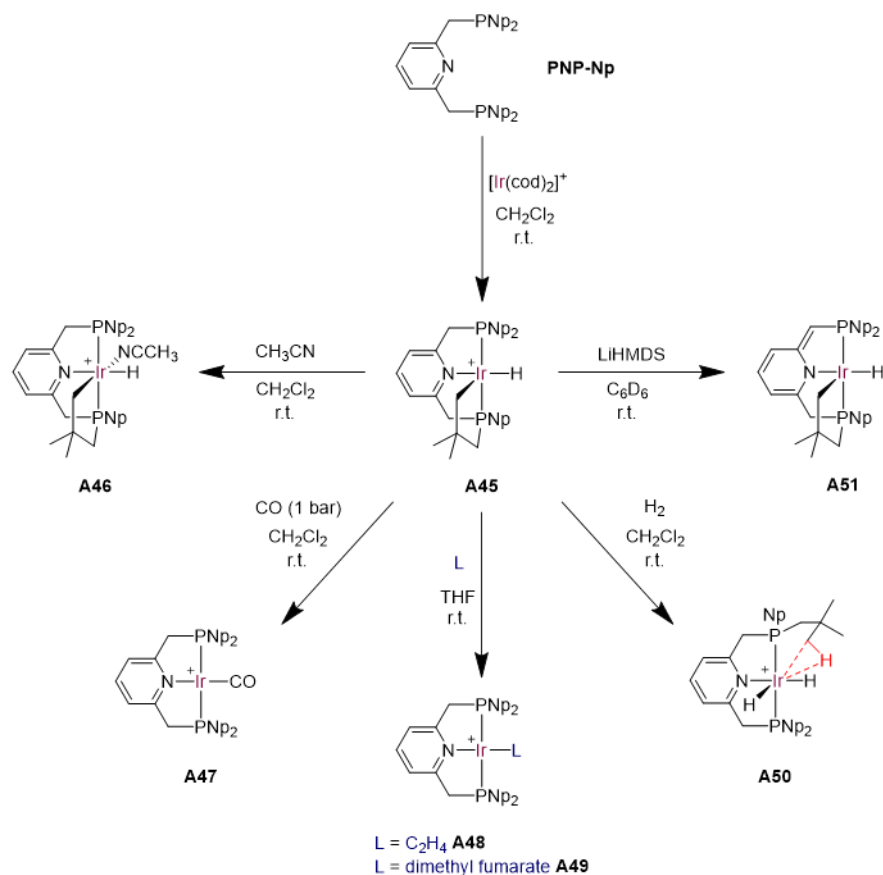
Scheme 1.6. *Iridium coordination chemistry of PNP-Np.*[64,65] *[BF₄]⁻ counterions are omitted for clarity.*

However, when heated with nitrobenzene or acetophenone, complex **A45** did undergo C-H activation, with total selectivity for the *ortho*-position (**Scheme 1.7**). Again, the authors compared this to the C-H activation of chloro-/bromo-benzene and anisole by the PNP-ᵗBu system.[51,52] In the same way, it is proposed that a mixture of products is formed, with the *ortho*-product being the most thermodynamically stable and the only product observed at the high temperatures required to reductively eliminate the cyclometallated *neo*pentyl group. The resulting iridium(III) aryl hydrides feature coordination of the acetyl (**A52**) or nitro (**A53**) groups to the metal. This additional stabilisation explains why these products were formed, but not the C-H activation product of benzene. Finally, a later study investigated the ability of the cyclometallated iridium complex **A45** to catalyse the dimerisation of alkylamines to form dialkylamines, in the presence of sodium hydride.[65]
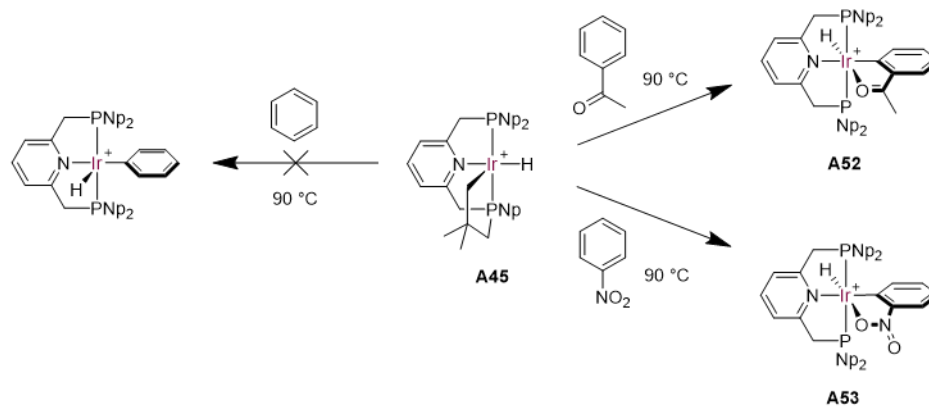
Scheme 1.7. *C(sp^2)-H activation by PNP-Np complex **A45**.[64] [BF$_4$]$^-$ counterions are omitted for clarity.*

These selected examples serve to highlight the breadth of reactivity of group 9 complexes that can be explored with phosphine-based pincers possessing an aromatic backbone. In order to maximise this potential, the choice or design of an appropriate ligand is a very useful strategy.

1.2.3. Rational Design of Pincer-Ligated Systems

To demonstrate the concept and potential of rational design of a pincer ligand to achieve a certain outcome, several recent examples will be discussed. These will cover the broad themes of i) enabling new modes of reactivity (including application in catalysis), ii) stabilising unusual complexes iii) preventing unwanted reactivity in a system and iv) enabling tunable reactivity. They also serve to demonstrate the synthetic versatility of the pincer scaffold.

An example of the design of a bespoke pincer ligand was described by van der Vlugt and de Bruin in 2015.[66] The aim was to design a system containing both nucleophilic and electrophilic sites that could engage in dual-mode ligand-based reactivity. This mode of reactivity is much less explored than metal-ligand cooperation, where the ligand typically possesses a Lewis basic site and the metal centre acts as a Lewis acid. Building on the known dearomatisation chemistry of phosphinomethylpyridine compounds and combining this with the propensity of *sec*-amidopyridine ligands to lose a hydride and form an imine (and, therefore, an electrophilic site), the new pincer ligand PNN^{H3} was synthesised.

The rhodium chemistry of this ligand was then explored, following reaction with [Rh(CO)$_2$Cl]$_2$ (**Scheme 1.8**). The rhodium(I) complex of PNN^{H3}, **A54**, was isolated and characterised. Subsequent treatment with potassium *tert*-butoxide gave the neutral amido (PNN^{H2}) complex **A55**, which was reported to be unstable at room temperature. This was reacted with sodium bicarbonate *in situ* (*i.e.* in the presence of potassium hexafluorophosphate) to give a major compound, assigned as PNN^H complex **A56**, alongside a minor product, assigned as PNN' complex **A57**. Two possible pathways were proposed, involving either hydride transfer from the amido group in **A55** to the proton of sodium bicarbonate, generating the imine functionality in **A56**, along with dihydrogen and potassium sodium carbonate, or spontaneous loss of dihydrogen from **A55** to form dearomatised **A57**, which is protonated by sodium bicarbonate to rearomatise the pyridine backbone. Dihydrogen was detected in the headspace, consistent with both pathways, and no evidence for generation of formate was observed, so carbonate does not act as a hydride acceptor. Whichever pathway is operating, these results demonstrate the ability of this system to undergo ligand-based reactivity at both the nucleophilic and electrophilic sites, as desired. To further investigate this system, imine complex **A56** was found to undergo dearomatisation, forming **A57**, upon treatment with potassium *tert*-butoxide. Furthermore, a benzene solution of **A55** underwent formal loss of hydride from the imine and a proton from the phosphinomethyl group at room temperature to form **A57**, lending support to the second proposed reaction pathway. Finally, overnight reaction of **A54** with sodium hydroxide also generated **A57**.
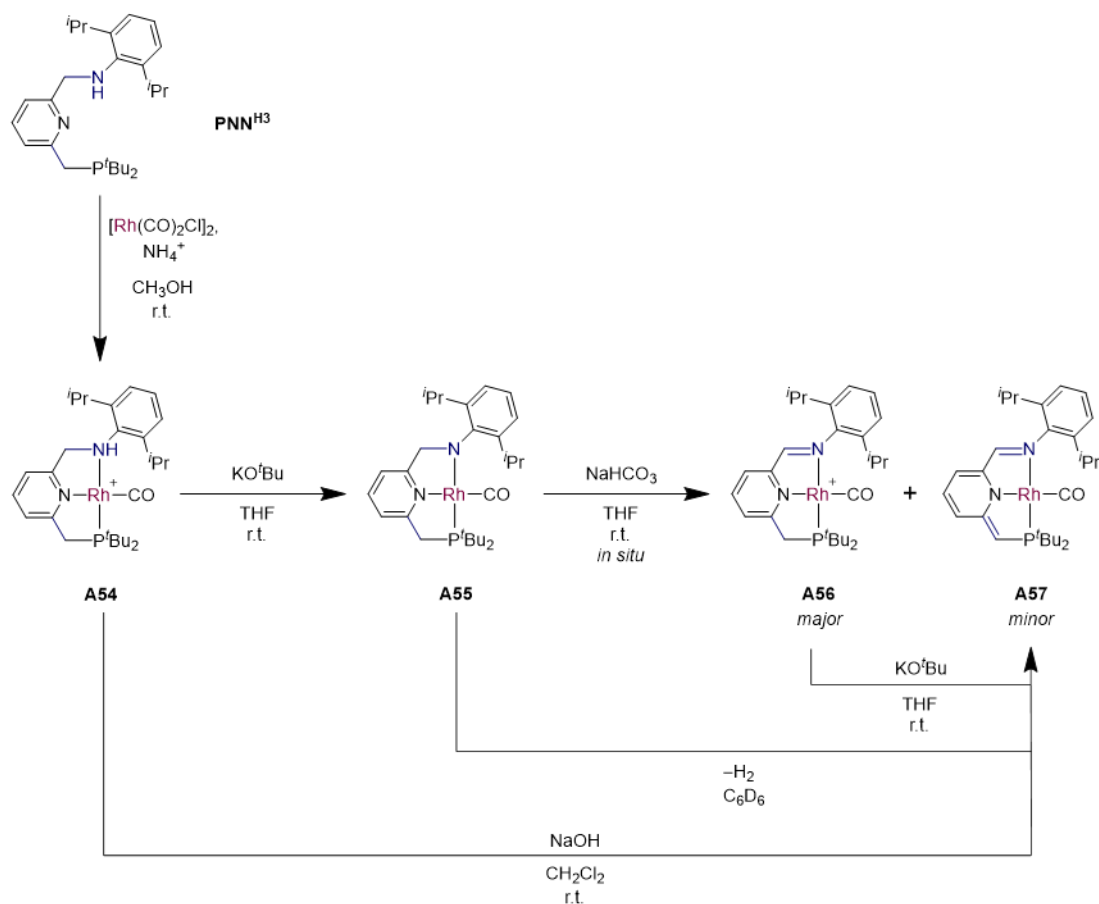
Scheme 1.8. *Formation of PNN^{H3} complex **A54** and subsequent proton/hydride transfer chemistry of this system.[66] [PF_6]^− counterions are omitted for clarity.*

The crystal structures of **A54**, **A56** and **A57** confirm the assignments and highlight that little perturbation from square planar geometry occurs across the transformations described, attributed to the rigidity of the pincer backbone. DFT analysis of **A57** confirms that the HOMO is centred on the phosphinomethyl arm, whilst the LUMO is centred on the imine functionality. This is a rare situation, supporting the observed ligand-based reactivity and lending support to the initial proposal that the pincer ligand should contain both nucleophilic and electrophilic sites. The LUMO of **A56** was found to resemble that of **A57**, suggesting that the electrophilicity of the imine is maintained even after protonation of the phosphinomethine arm.

Upon treatment of **A57** with *o*-toluenesulfonamide, aminal complex **A58** was isolated (**Scheme 1.9**). This is likely to be the first well-characterised example of a rhodium-bound aminal. Protonation of the phosphinomethine group by *o*-toluenesulfonamide has occurred, leading to rearomatisation, either by an outer sphere mechanism, or *via* coordination of *o*-toluenesulfonamide to rhodium. It is proposed that a rhodium sulfonamido intermediate is formed, which undergoes nucleophilic addition to the imine group, followed by a 1,3-proton shift, to form the aminal. In solvents such as tetrahydrofuran-*d_8*, **A58** reverts to **A57**. This

14

ability to form and cleave the C-N bond of the aminal led the authors to assess the ability of this system to catalyse sulfonamide coupling reactions. Reaction of **A58** with methyl iodide gave the coupled *N*-methylsulfonamide product and **A60** (the iodide salt of **A56**). Treatment with base allowed **A57** to be regenerated. A catalytic cycle was proposed (**Scheme 1.10**), although no evidence for the formation of rhodium(III) oxidative addition product **A59** was found. However, these reactions were only carried out stoichiometrically and turnover could not be achieved, attributed to deactivating side reactions. Complexes **A61** and **A62** were observed in the reaction mixture, originating from hydrolysis of the aminal (**Scheme 1.10**). Despite this, this work is useful as a proof of concept: the authors have designed a pincer ligand that is rare in possessing both nucleophilic and electrophilic sites and that can engage in ligand-based reactivity. When this is combined with metal-based reactivity, unusual complexes can be stabilised and C-N coupling could be achieved.
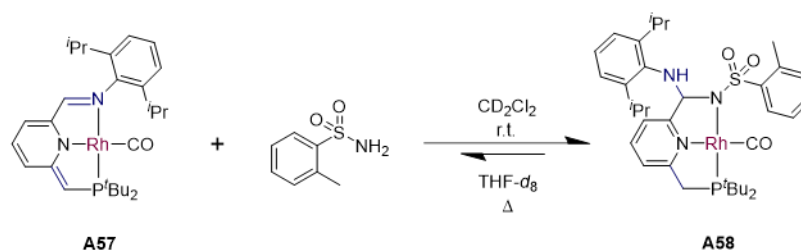

Scheme 1.9. *Reaction of **A57** with* o-*toluenesulfonamide, yielding rhodium aminal **A58**.*[66]
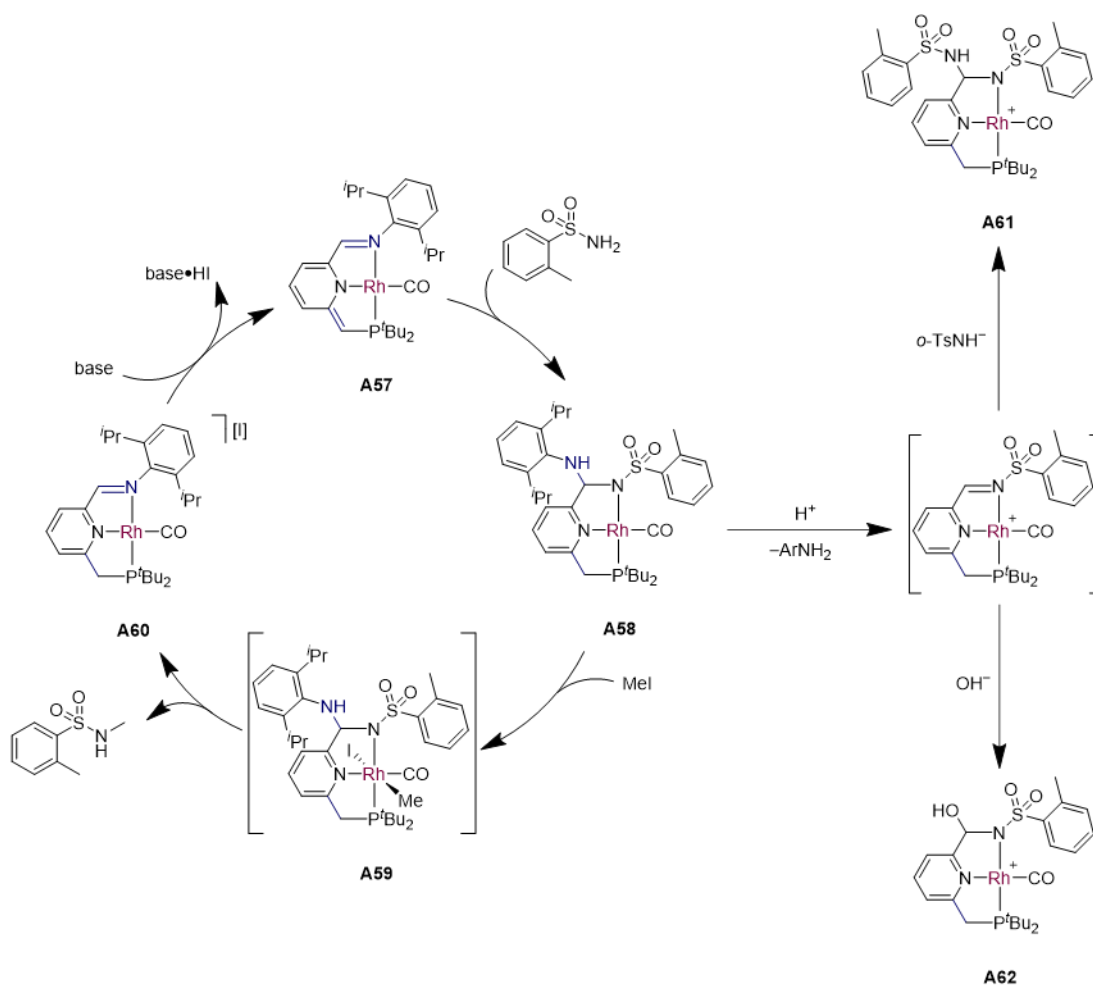
*Scheme 1.10. Proposed cycle for the catalytic coupling of sulfonamides and alkyl halides using **A57** as a catalyst, with aminal hydrolysis leading to the formation of byproducts **A61** and **A62**.[66]*

Rational ligand design is a powerful tool that can enable researchers to carry out more efficient experimental procedures, especially when it is informed by computational insight. This has recently been demonstrated by Nakano and co-workers, who reported the design and synthesis of the first pincer-ligated rhodium(I) catalyst for the synthesis of acrylate from carbon dioxide and ethylene.[67] This process is of considerable interest because of the application it provides for abundant carbon dioxide.[68] The authors proposed that application of a bespoke pincer ligand could increase the thermal stability of the catalyst, whilst also providing the first example of a group 9 catalyst in this transformation. Computational investigations, using DFT, were undertaken to investigate which structural features were important, so that they could be incorporated into design of an optimum pincer ligand. Following ethylene coordination, reaction with carbon dioxide forms a metallalactone (**Scheme 1.11**). The thermodynamics and kinetics of rhodalactone formation were, therefore, studied theoretically, using different electron-rich pincer fragments. σ-Donating ligands are known to be effective in d^{10} systems[68] and so this formed the starting point for the computational investigation, with ligands **A63**-

A65 initially proposed (**Figure 1.4A**). These are based on well-established, synthetically accessible pincer frameworks, with strongly σ-donating dimethylphosphino-based side arms.
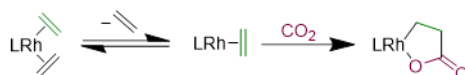
Scheme 1.11. Rhodalactone formation from ethylene and carbon dioxide.

It was found that all three of these standard pincer frameworks resulted in a highly endergonic profile for rhodalactone formation, starting from the bis-ligated ethylene complex. However, the profile of the phenyl-based system **A65** was the most kinetically and thermodynamically favourable, so this was chosen as the ligand backbone on which to base further investigations.

Attention was then turned to modifying the side-arms and donor groups, in order to influence the energetic profile. A series of different side-arms were investigated (**A66**-**A69**, **Figure 1.4B**), based on donors with better σ-donating and weaker π-accepting properties than phosphines. NHC, cyclicalkyl(amino)carbene (CAAC) and guanidine donors were investigated computationally. Ultimately, it was found that weaker π-acceptors were the most beneficial. When the pincer bore guanidine side-arms, rhodalactone formation was almost isothermic. The guanidine system **A69** was found to be the most energetically favourable as a result of hydrogen-bonding between N-H and the oxygen of carbon dioxide, promoting cyclisation, whilst the alkyl substituents in **A68** led to steric repulsion. Furthermore, it was found that repulsion between p_π electrons of the guanidine groups and the occupied d_{yz} at the rhodium centre had the overall effect of increasing electron density at the metal and raising the energy of the frontier orbitals, such that the system more closely resembled a truncated model of a tetraphosphine ruthenium(0) complex, previously used in catalytic acrylate synthesis.[69,70]
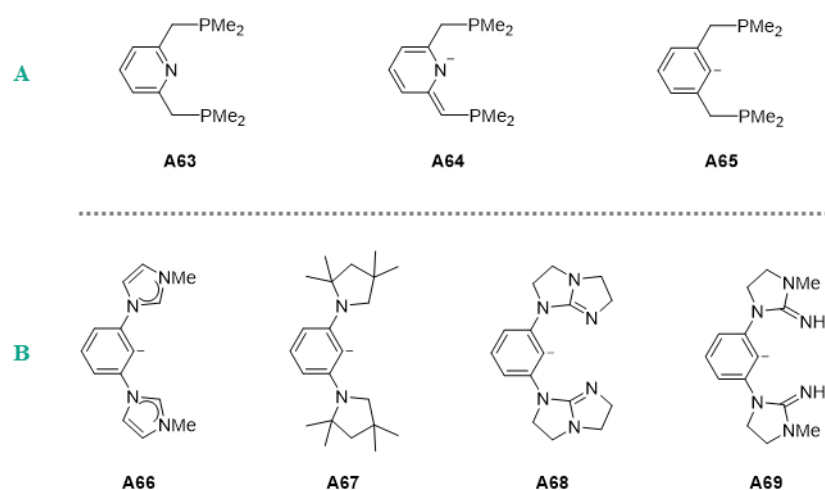
Figure 1.4. A) Pincer scaffolds and B) donor groups investigated using DFT methods.[67]

The information obtained from this theoretical study suggested that a guanidine-based pincer ligand, with a similar structure to **A69**, would allow a rhodium(I) complex to behave in a similar way to the previously reported ruthenium(0) system and catalyse the synthesis of acrylate from ethylene and carbon dioxide. Informed by this, the guanidine-based NCN ligand **A70** was synthesised, along with a series of rhodium complexes, including the chlorohydride **A71**, benzene (**A72**) and *N*-methylmaleimide adducts (**A73**) and the desired rhodalactone **A74** (**Scheme 1.12**). With this result confirming the predictions made by the computational study, catalytic acrylate synthesis was investigated, using **A74** as a pre-catalyst. Under 20 bar of ethylene and carbon dioxide, with sodium *tert*-butoxide in benzene at 160 °C, a turnover number (TON) of 16 was observed. Although this result is not as impressive as those obtained with catalysts based on group 10 metals,[71] it is comparable to the ruthenium(0) system[69,70] and confirms that the strategic design of this pincer-ligated system, based on computational analysis, does, indeed, result in an active catalyst.
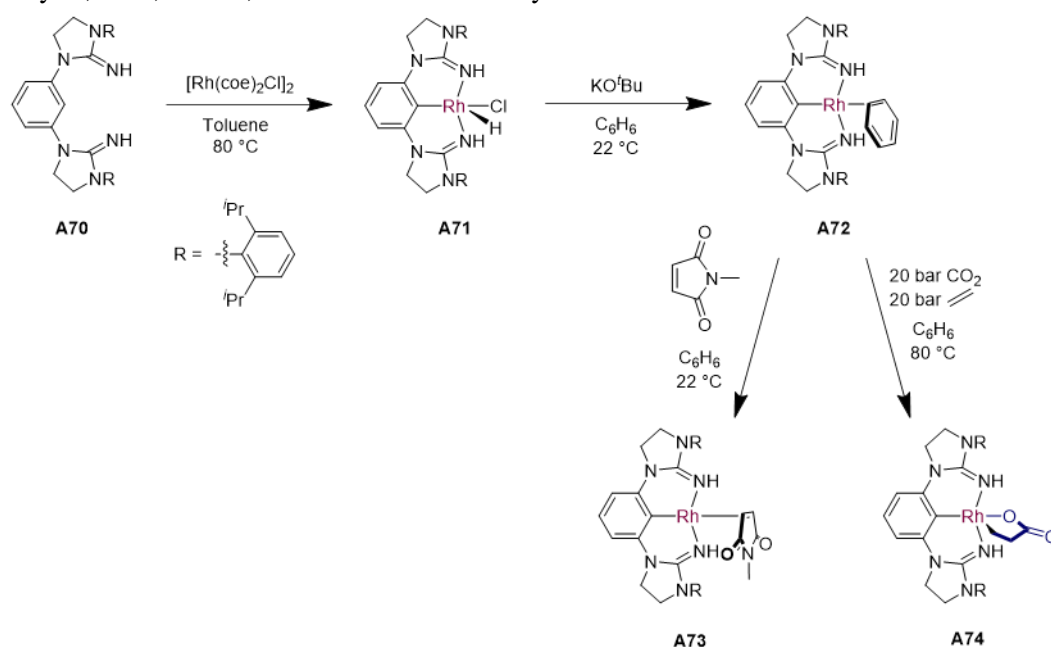

Scheme 1.12. *Rhodium coordination chemistry of a guanidine-based NCN pincer.[67]*

The next example was chosen to illustrate the concept of ligand design in order to alter the reactivity of a system, thereby enabling unusual chemistry to be explored. The pincer ligand termed Me$_4$PNP-^{i}Pr resembles PNP-^{i}Pr but possesses methylated linkers.[72] As well as increasing the steric profile of this pincer, these methyl groups block the deprotonation of this position that often occurs in PNP systems, preventing processes such as dearomatisation, or the abstraction of a hydrogen atom, which results in formation of a ligand-centred radical. This mode of reactivity has been observed in cobalt complexes of PNP ligands,[73] and it is proposed that this can lead to the complexes engaging in radical reaction pathways. It was

hoped that cobalt complexes of Me$_4$PNP-^{i}Pr would instead behave more like their heavier congeners.

The cobalt(I) methyl complex **A75** was found to catalyse the hydrogenation of alkenes and alkynes, and a reaction mechanism was proposed, based on a series of oxidative addition and reductive elimination steps. Some of these putative steps were supported by experimental evidence. The proposed cycle is shown in **Scheme 1.13**. Oxidative addition of dihydrogen to cobalt(I) methyl complex **A75** is proposed to give cobalt(III) methyl dihydride intermediate **A76**, which then reductively eliminates methane to form cobalt(I) monohydride **A77**. Subsequent (reversible) oxidative addition of a second molecule of dihydrogen yields stable cobalt(III) trihydride **A78**, which is the observed product when **A75** is exposed to dihydrogen. The authors propose that the monohydride is the active catalytic species, undergoing 1,2-migratory insertion with an alkene (or alkyne). The resulting alkyl species **A79** is the observed product when trihydride **A78** is treated with ethylene. Exposure of complex **A79** to dihydrogen liberates ethane. This is likely to occur *via* oxidative addition of dihydrogen (**A80**), followed by reductive elimination of the alkane, reforming monohydride species **A77**. Although more detailed investigation is required to confirm the operation of a mechanism based on two-electron reactivity, these results are promising and imply that the proposed strategy was successful. Application of the Me$_4$PNP-^{i}Pr pincer in other reactions would help to confirm that the additional methyl groups in this ligand result in modified reactivity of its cobalt complexes.
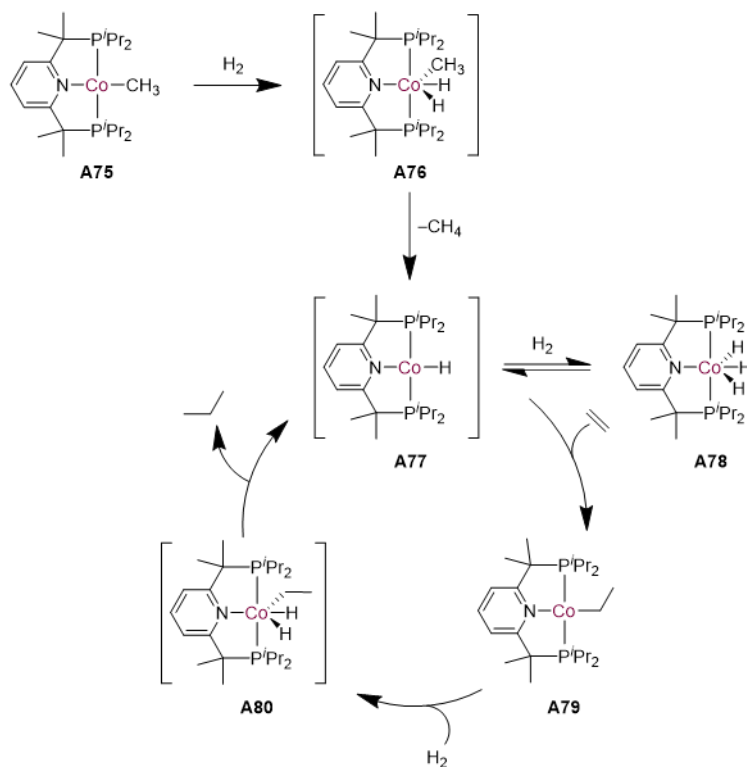

Scheme 1.13. Proposed catalytic cycle for the hydrogenation of alkenes and alkynes using A75 as a pre-catalyst.[72]

The varied examples presented in this section are just some of the many ways in which pincer ligands have been designed and used to bring about desired transformations or stabilise unusual complexes. The ability to modify the backbone and incorporate different donor groups gives these ligands huge potential for influencing reactivity in the primary coordination sphere of a transition metal.

The final example of rational pincer ligand design to be discussed here was provided by the group of Miller, where asymmetric pincer ligands featuring appended aza-crown ethers have been reported.[74] These systems were targeted because of a desire to design a system in which the activity of the catalyst could be controlled by employing ligand hemilability, and, therefore, substrate gating. By combining the rigidity and thermal stability of a pincer ligand with the weakly coordinating ability of a crown ether, it was proposed that such control could be exerted over a catalytic system, relying on NCIs to modulate reactivity. This approach, using a single combination of metal and ligand, alongside external additives, would be simpler to achieve than the synthesis and investigation of a library of related ligands with small structural differences.

To this end, ^{15c5}NCOP was designed and its chemistry investigated.[75] Iridium(III) hydrido chloride complex **A81** was prepared, displaying a κ^4 binding mode of the pincer (with coordination of a crown ether oxygen, **Scheme 1.14**). Abstraction of the chloride led to the formation of iridium(III) hydride **A82**, with a κ^5 pincer coordination mode (an additional ether oxygen occupying the vacant coordination site). The ability of **A82** to activate dihydrogen was then investigated. Under an atmosphere of D_2, little H/D exchange was observed, as D_2 is too weakly coordinating to displace an ether group. However, in the presence of $Na[BAr^F_4]$, a 20-fold rate enhancement was observed. This was increased to 250-fold in the presence of $Li[BAr^F_4]$. The proposed mechanism involved chelation of the cation by the macrocycle and, consequently, dissociation of the iridium-bound ether groups, formation of a D_2 σ-complex, H/D exchange, release of the cation and recoordination of the ether groups. The greater rate enhancement observed in the presence of the lithium salt was attributed to stronger interactions between the aza-crown ether and the lithium cation, resulting in a larger shift in the ligand substitution equilibrium, favouring D_2 displacement of the coordinated ether group.
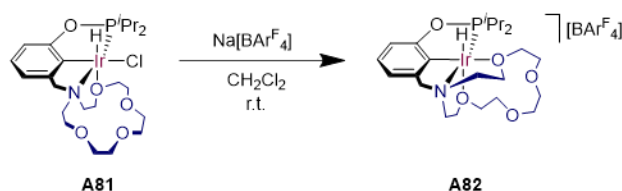
Scheme 1.14. *Chloride abstraction from κ^4 complex **A81** to give κ^5 complex **A82**.*[75]

These initial results suggested that the use of a pincer ligand possessing an appended aza-crown ether, along with cationic additives, could influence catalysis by allowing the primary coordination sphere of iridium to be modified *via* dynamic hemilability of the ether groups. The reactivity of this system was extended to include iridium carbonyl complexes and methanol carbonylation,[76,77] and allylbenzene isomerisation,[78] where similar cation enhancement effects were observed, effectively allowing the rate of catalysis to be modulated *via* cation control (**Scheme 1.15**). The system could also be switched between active and inactive states: whereas hydrido chloride **A81** was inactive, **A82** displayed sluggish activity which was dramatically enhanced in the presence of alkali metal cations, proceeding *via* κ^3 complex **A83**.
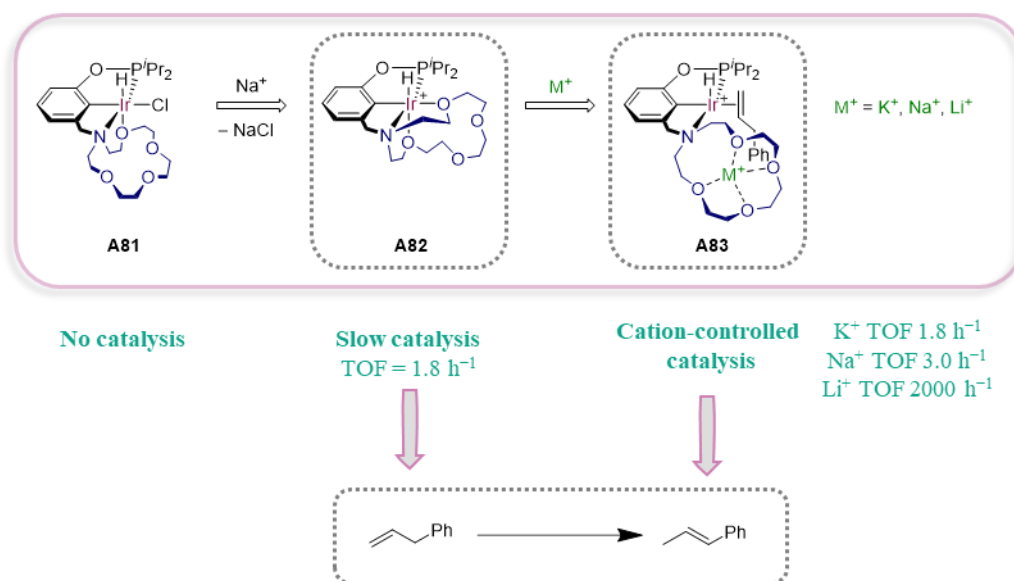
Scheme 1.15. *The three states of ^{15c5}NCOP iridium catalyst: inactive **A81**, slow κ^5 complex **A82** and κ^3 complex **A83**, with encapsulated cation.*[74,78]

More recently, the related ^{18c6}NCOP ligand has been synthesised, featuring a methoxy substituent on the pincer backbone.[79] This was informed by studies on catalyst decomposition,[80] where it was found that pincer demetallation and remetallation at this position on the aromatic ring was occurring. The methoxy group was placed here to block this deactivation pathway. The larger aza-crown ether was chosen as it has a higher affinity for sodium ion binding than the 15-c-5 analogue.[81] This should result in a higher activity in olefin isomerisation, potentially allowing for the double bond chain walking required for multiple isomerisations. Cation responsive olefin isomerisation was pursued, and it was found that complex **A84** was able to catalyse the isomerisation of 4-phenyl-1-butene derivatives to 2-butenes, with high *E* selectivity (**Scheme 1.16**). However, when the reactions were carried out in the presence of Na[BAr$^F_4$], 3-butenes were typically formed with high regioselectivities, again stereoselective for the *E* isomers. This striking change in selectivity upon addition of sodium salt has been attributed to cation-macrocycle interactions. In the absence of cationic

additive, the pincer ligand maintains κ^4 coordination during catalysis (as in complex **A85**), with dissociation of a single ether group allowing for substrate coordination and isomerisation. However, sodium ions are encapsulated by the macrocycle, resulting in dissociation of two ether groups and a κ^3 pincer coordination mode during catalysis (as in complex **A86**). The additional vacant site allows for coordination of internal olefins, and, subsequently, a second isomerisation. DFT calculations demonstrated that the 3-alkene products, formed in the presence of sodium ions, are more thermodynamically stable than their 2-alkene isomers. It was concluded that in the absence of sodium salt, the reaction is under kinetic control, whereas addition of salt results in the thermodynamic product. In the cases where the 2-alkene was calculated to be more thermodynamically stable, this was the product observed in the presence of Na[BAr$^F_4$].
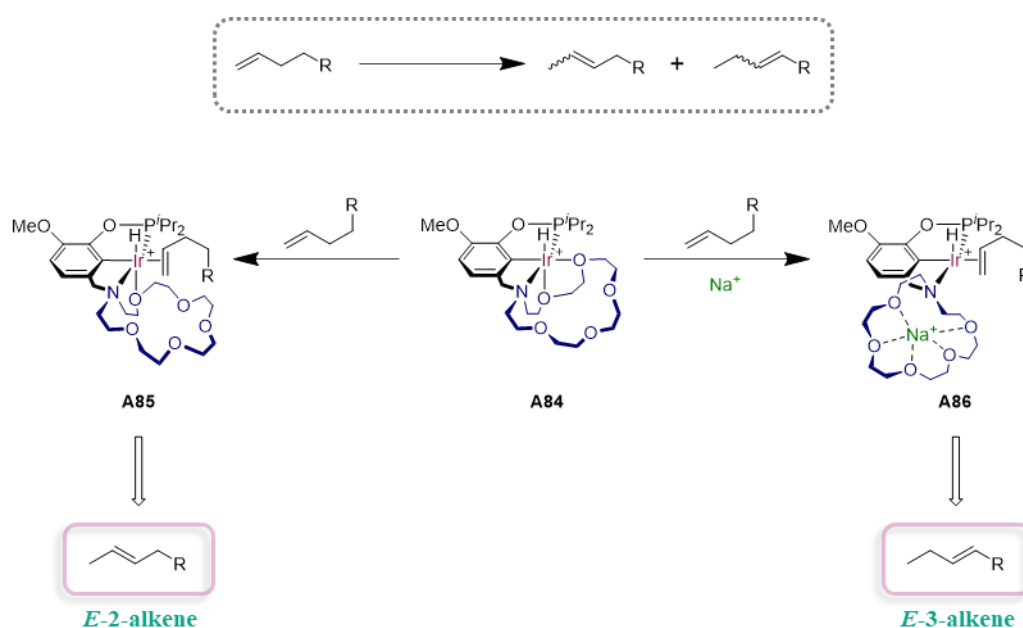
Scheme 1.16. E-*selective, single isomerisation is observed with* **A84** *in the absence of salts, proceeding* via κ^4-**A85**; E-*selective double isomerisation is observed in the presence of salts, proceeding via* κ^3-**A86**. [BAr$^F_4$] *counterions are omitted for clarity.*[79]

This work provides a rare example of a cation-responsive catalyst, in which selectivity can be switched by modification of NCIs. It nicely demonstrates how interactions in the secondary coordination sphere (cation binding at the macrocycle) can influence reactivity at the primary coordination sphere (dissociation of the ether moieties and coordination of substrates). This approach differs from others that employ NCIs in the secondary coordination sphere to control reaction outcomes, as these do not usually involve a change in the coordination number at the metal centre. However, this latter approach is itself becoming an increasingly interesting strategy in ligand design and will form the basis of the following sections.

1.3. Supramolecular Ligands

1.3.1. Organometallic Chemistry in a Confined Space

Introducing confinement into the secondary coordination sphere of a homogeneous catalyst is an intriguing way to harness the principles of supramolecular chemistry to influence reactivity in organometallic systems. This can be achieved in various ways, but there are some key categories, into which the majority of examples fall.[20,21] **Figures 1.5**-**1.8** highlight a select few examples of these strategies.

By employing classic host-guest chemistry, a discrete organometallic catalyst can be encapsulated within a container molecule. This can offer various benefits, such as increasing catalyst stability, introducing size selectivity to the system or modifying reactivity. The anionic cage **A87**,[82,83] depicted in **Figure 1.5**, has seen application as a host for several organometallic complexes. These include iridium(III) complex **A88**,[84] enabling size- and shape-specific stoichiometric C-H activation of aldehydes, and rhodium (I) complex **A89**,[85] a size-selective catalyst for the isomerisation of allylic alcohols and ethers to the corresponding aldehydes and enol ethers. Gold(I) complex **A90** displayed enhanced activity as a catalyst for intramolecular cyclisations when encapsulated, and is stable to aqueous, aerobic conditions due to its encapsulation within **A87**.[86,87] Self-assembled, hexameric resorcin[4]arene capsules have been employed to protect olefin metathesis catalysts, as in **A91** and **A92**, increasing the activity of ruthenium complexes under aqueous conditions,[88] whilst host-guest system **A93** displayed size-selectivity in the catalytic oxidation of alcohols.[89] A host-guest complex of resorcin[4]arene **A94** and rhodium complex **A95** was found to catalyse the hydrogenation of norbornadiene, resulting in reduced dimerisation compared to the unencapsulated **A95**. The transition state for dimerisation is presumably hampered by the confinement of the resorcin[4]arene host.[90]
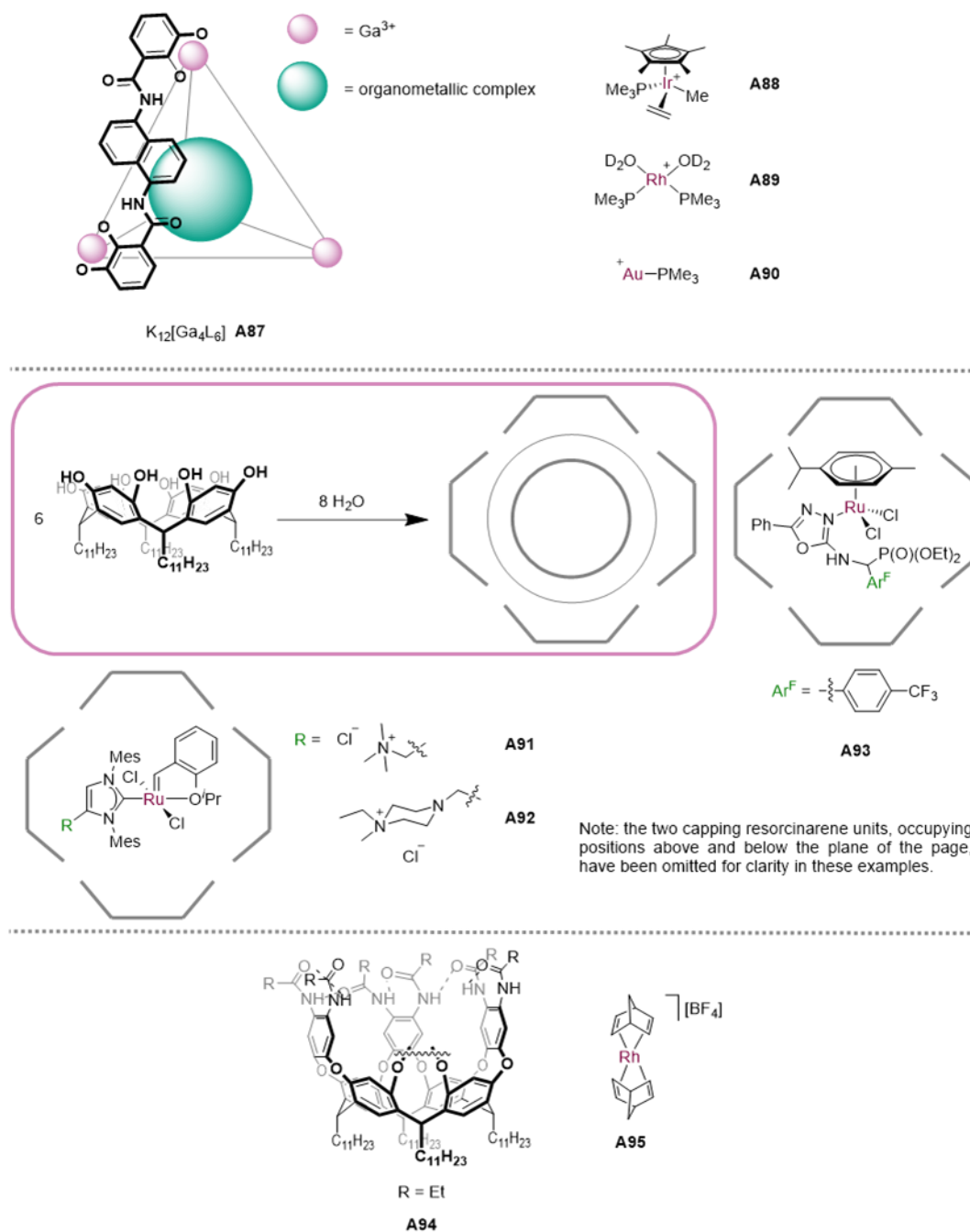
Figure 1.5. Selected examples of organometallic complexes that have been confined within host molecules, in order to influence their reactivity.[82-90]

Another strategy is to use a ligand-templated approach, where ligands in the primary coordination sphere encourage formation of a cage or capsule around the catalyst.[21,25,32] A seminal example of this approach is the hydroformylation catalyst reported by Reek.[91-96] This features a tripyridyl phosphine, in which the nitrogen atoms coordinate to zinc porphyrin units, enabling a capsule to form by ligand-templated self-assembly (**A96, Figure 1.6**). Confinement of the coordinated rhodium(I) centre results in good selectivity for the branched aldehyde products. This methodology has recently been extended to include the chiral capsule **A97**, enabling asymmetric branched-selective hydroformylation.[97] Metalloporphyrins are a

privileged motif in enzymes, and the ability to modify the porphyrin scaffold and introduce various metals into the binding site makes these complexes very versatile and useful for incorporating into supramolecular organometallic systems.[20,21,23,27,98,99]
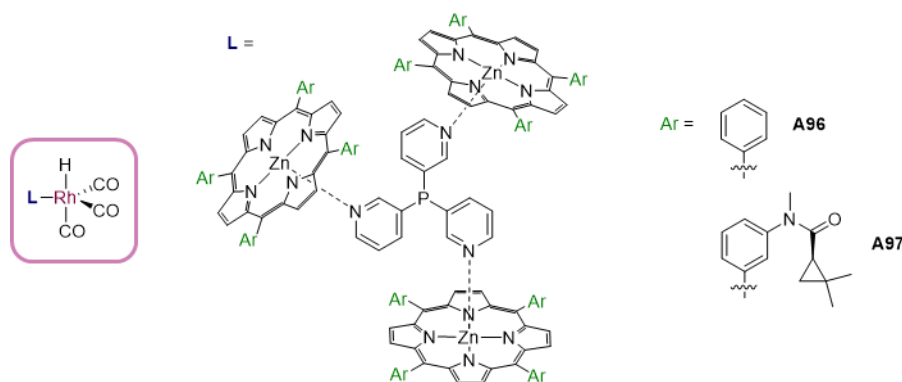
Figure 1.6. Ligand-templated, self-assembled, phosphine-containing capsules as ligands for branched-selective rhodium-catalysed hydroformylation.[91-97]

Lastly, and the approach that will be discussed here, is that of introducing confinement by covalently linking a container molecule, such as a cavitand, to a ligand, which can then coordinate to the metal centre of interest.[20,21,23,24,26-28,30,31,33,34] Cram first coined the term *cavitand* to refer to 'synthetic organic compounds that contain enforced cavities of dimensions at least equal to those of the smaller ions, atoms, or molecules'.[100] The term can now be considered to include classes of compounds such as cyclodextrins, spherands, calixarenes, resorcinarenes and pillarenes (**Figure 1.7**). The strategy of appending these molecules to donor groups, such as phosphines and NHCs, has significant potential, allowing a ligated metal to reside within or in proximity to the cavity.
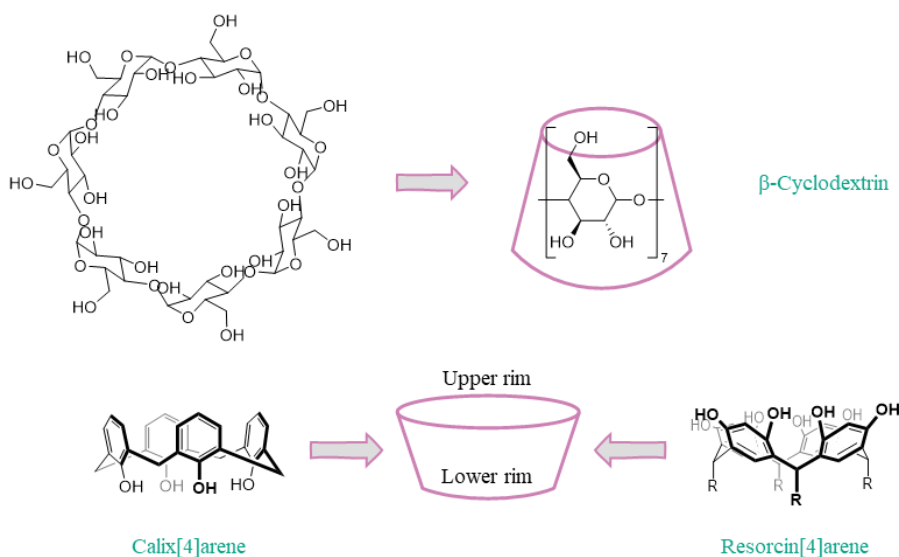

Figure 1.7. Cyclodextrins, calixarenes and resorcinarenes are prominent examples of cavitands, featuring conical structures with upper and lower rims that can be functionalised further.

25

Figure 1.8 shows some of the varied ways in which these ligands can be employed. Palladium(II) complex **A98** possesses a diamine ligand based on a β-cyclodextrin and catalyses Suzuki-Miyaura cross-coupling reactions, encapsulating the substrate within the cavity and enabling the reaction to be carried out under aqueous conditions.[101] Sémeril has reported on the use of NHC-functionalised cavitands as ligands in palladium-[102-104] and nickel-catalysed[105,106] cross-coupling reactions, including calix[4]arene complexes **A99**-**A100** and resorcin[4]arene complex **A101**.[104] These catalysts performed well, attributed to the steric influence of the cavitand, as opposed to confinement effects (as the metal centres do not reside in the cavity). Roland and Sollogoub synthesised a series of NHC-capped cyclodextrins in order to investigate metal confinement effects.[107-110] Pre-catalysts **A102** and **A103** were employed in the hydroboration of alkynes, where they gave opposite regioselectivities. The larger cavity of the β-cyclodextrin in **A103** induced a mechanistic switch, explaining this outcome.[109] As well as their emerging role in catalysis, cavitand-based ligands have been utilised to observe unusual reactivity, as demonstrated by complex **A104**. Using a calix[4]arene in which two phosphine donors have been appended to the upper rim,[111] a rare example of a rhodium(III) molecular dinitrogen complex was observed.[112] Solvent exclusion by the calix[4]arene enables stabilisation of this weakly bound ligand.

Of interest in the context of this project is the less common class of molecules referred to as deep cavitands,[113] based on a resorcin[4]arene structure. Resorcin[4]arene was first systematically investigated and fully characterised by Hörberg[114] and Cram[115] in the early 1980s and is formed from four linked resorcinol units - the name will be simplified to *resorcinarene* from here on. The presence of hydroxyl groups on the upper rim of resorcinarene allows functionalisation to be carried out with relative ease (**Figure 1.7**). As well as introducing donor functionalities directly onto the upper rim, aromatic 'walls', such as quinoxaline groups, can be introduced, which have the overall effect of creating a deeper, less conformationally flexible cavity. Ligands derived from deep cavitands place the organometallic fragment further inside the cavity, rather than above or below it, ensuring that confinement plays a role in substrate binding at the metal.[34]
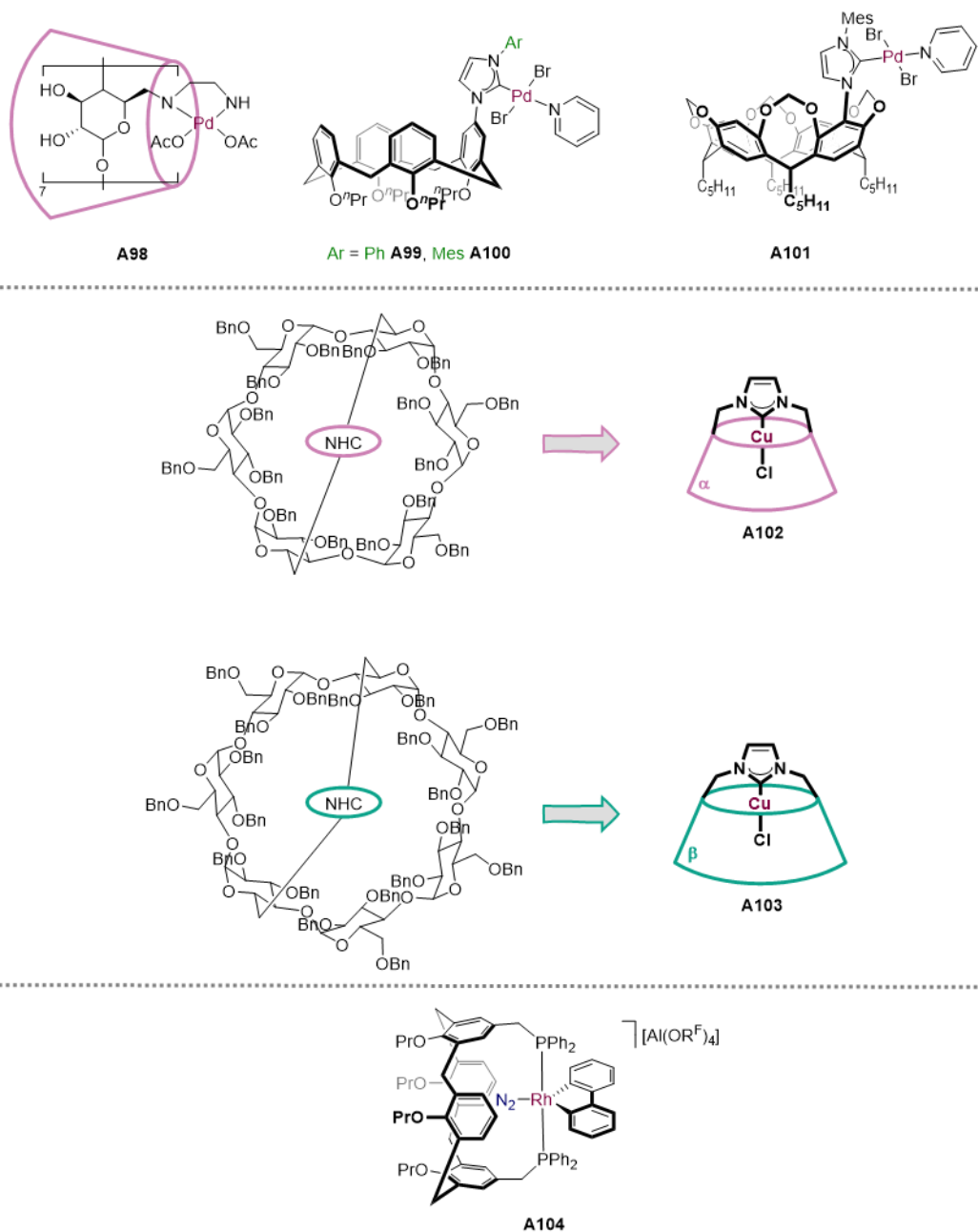
Figure 1.8. *Selected examples of organometallic complexes of cavitands featuring appended donor groups ($OR^F = OC(CF_3)_3$).*[101,104,109,112]

1.3.2. Coordination Chemistry of Resorcinarene-Based Ligands

The first example of a ligand based on a resorcinarene scaffold being used in transition metal catalysis was provided by Rebek in 2002. Ligand **A105** is a deep cavitand with a pendant, chelating phosphite-oxazoline and was employed in palladium-catalysed allylic alkylation (**Scheme 1.17**), displaying a degree of substrate specificity in competition experiments.[116]
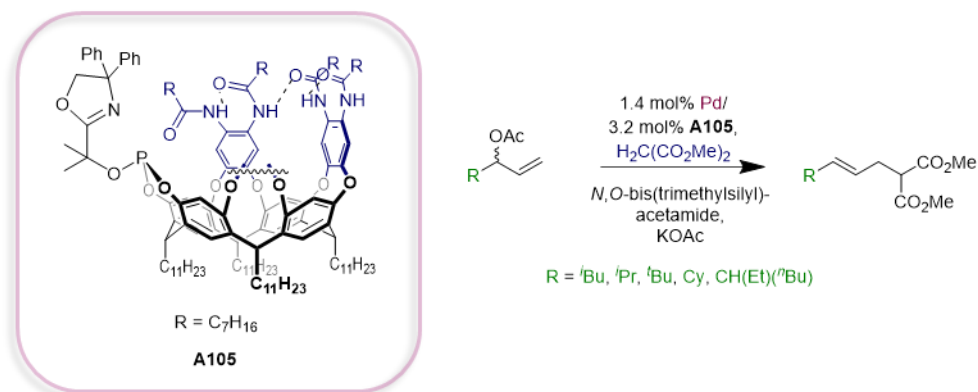

*Scheme 1.17. Pd-catalysed allylic alkylation using deep-cavity resorcinarene ligand **A105**.[116]*

The coordination chemistry of deep cavity resorcinarene ligands has been pursued by the groups of Iwasawa, Schramm and Sémeril.[117-126] Following a report that quinoxaline walls of functionalised resorcinarene can be cleaved with nucleophilic reagents,[127] this opened up the potential for the introduction of donor groups into these systems. The '*tris*-walled' ligand (*i.e.* the resorcinarene bears three quinoxaline groups, with one removed to allow for installation of the donor functionality) **A106** was synthesised and its confining effect on the gold-catalysed cyclisation of γ-alkynoic acids was investigated (**Scheme 1.18A**).[124]

It was proposed that large R/R' groups could prevent substrate encapsulation, allowing easier access of the alkyne to the gold(I) centre and, therefore, a faster rate of reaction. The nature of R' was found to have the greatest effect. When it contained a group that shows affinity for binding in resorcinarene cavities (such as benzyl),[128,129] the rate slowed, whereas bulky substituents containing groups that are known to be excluded from the cavity (such as naphthyl, xylyl and mesityl) displayed faster rates.

Similar cavity effects were observed in the gold(I)-catalysed cycloisomerisation of aryl-alkynes (**Scheme 1.18B**).[126] The results were contrasted with those obtained using an electronically similar, non-supramolecular ligand. Increasing the alkyl chain length at the alkyne functionality had little effect, but when the bis-aryl backbone featured a tolyl or phenyl group (these being better guests for resorcinarenes than *m*-xylyl), very minimal conversion was observed compared to the non-supramolecular catalyst. These results highlight the important effect of the cavity upon the outcomes of catalysis, but as yet, a clear understanding of the role it plays has not been obtained.
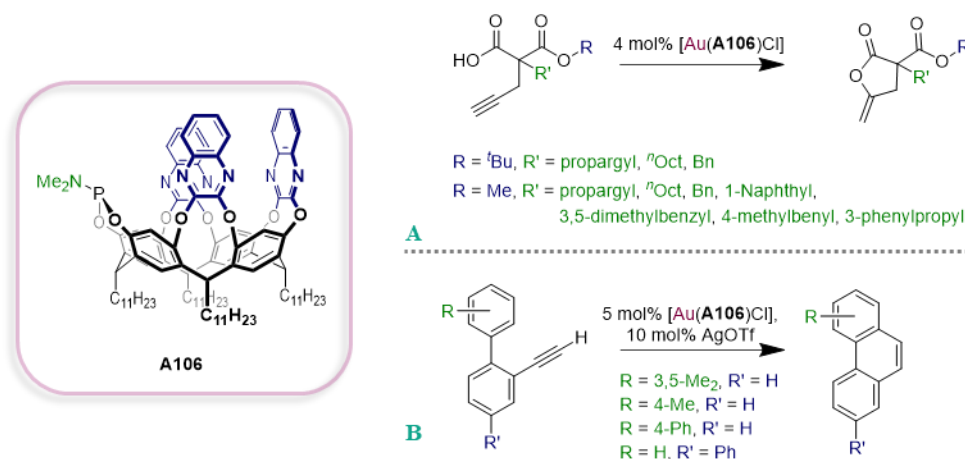
Scheme 1.18. *Gold-catalysed cyclisations using ligand A106.*[124,126]

Related to the *tris*-walled ligand **A106** are the *bis*-walled ligands **A107-A108**. These were investigated in the gold(I)-catalysed hydration of internal alkynes (**Scheme 1.19**) and feature an oxidised phosphorus, to deliver a water molecule to the bound alkyne, with the oxygen acting as a hydrogen-bonding directing group. It was proposed that the presence of the cavity may allow regioselective addition of water to the alkyne.[122,123] Only when the substrate contained a methyl or ethyl group did the catalyst display significant conversion, with almost perfect selectivity for ketone **II** (82-98 %). This was attributed to the high binding affinity of these alkyl chains, making the gold centre more accessible to these substrates, compared to bulkier ones. The catalyst showed almost no selectivity with 2-pentyne as a substrate (59 % **I** : 41 % **II**), due to the affinity of both methyl and ethyl groups for the cavity, such that it is unable to distinguish between them and the regioselectivity is lost. A mechanism was proposed in which the methyl or ethyl chain resides within the cavity, allowing regioselective delivery of water to this end of the triple bond (**Figure 1.9**). In comparison, barely any reaction was observed with *tris*-walled **A106**, highlighting the importance of the directing group.

The effect of the quinoxaline-walled cavity was also investigated: whilst the gold(I) complex of pyrazine-walled **A109** displayed similar activity and selectivity to **A108**, unwalled **A110** resulted in negligible hydration of most substrates and *cis*-disposed **A111** also resulted in low activity and selectivity.[125] This highlights the important role played by the deep cavity – presumably stabilisation of intermediate species occurs as a result of interaction with the π-electron cloud of the quinoxaline (or pyrazine) groups. The *trans* arrangement of quinoxaline groups also appears to be crucial for creating this well-defined cavity, compared with the more open structure created by *cis*-disposed walls.
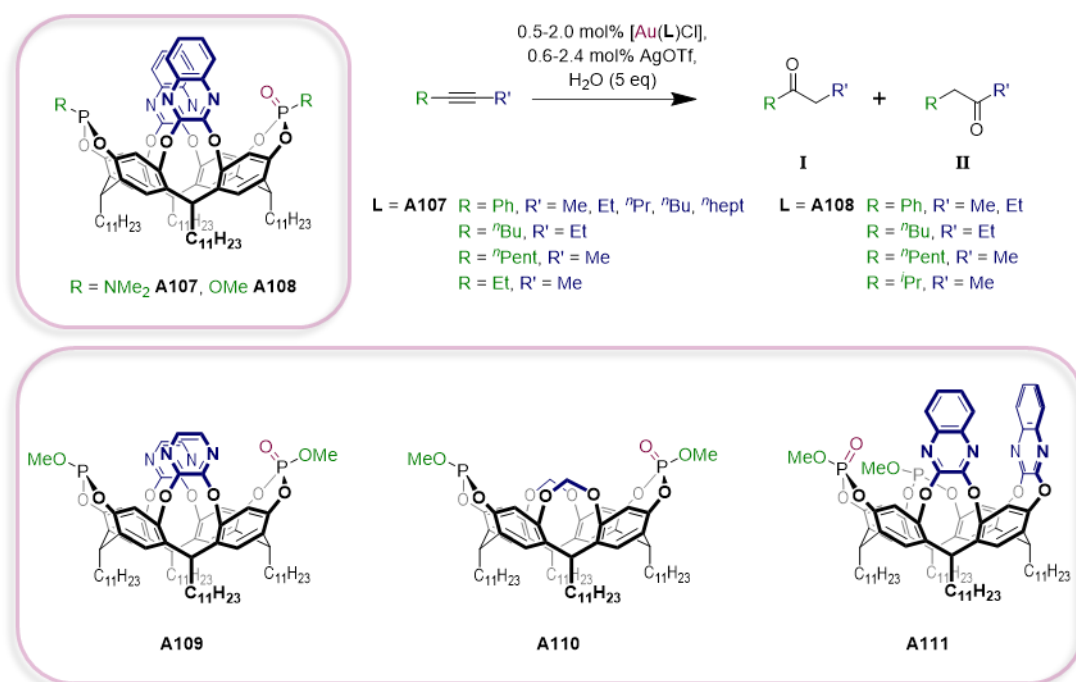
Scheme 1.19. *Gold-catalysed hydration of internal alkynes using ligands* **A107-A111**.[122,123,125]
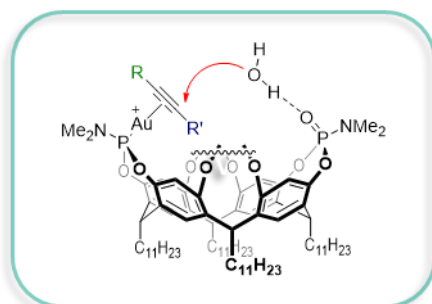
Figure 1.9. *Proposed mechanism for the delivery of water to a bound alkyne in the resorcinarene cavity, where R' = Me or Et.*[122,123]

Echavarren and co-workers have also reported on the gold(I) chemistry of similar cavitands (**A112-A123**). Ligands **A112**, **A113**, **A116-A119** displayed activity in the reaction shown in **Scheme 1.20A**.[130] Interestingly, whilst model ligands such as triphenylphosphine and trimethylphosphine resulted in formation of exocyclic single-cleavage skeletal rearrangement product **I**, use of the cavitand-derived ligand **A112** changed the regioselectivity of this reaction, forming the endocyclic product **II** with 83 % selectivity. The other ligands resulted in lower amounts of **II** (11-67 %). The chiral ligands **A114**, **A115**, **A120-A123** were investigated in the asymmetric alkoxycyclisation of 1,6-enynes (**Scheme 1.20B**). Mononuclear complexes of **A114** and **A115** displayed good activity but poor enantioselectivity (51:49, 59:41 *er*). Dinuclear complexes of **A120**, **A121** and **A123** displayed much higher enantioselectivities (72-78 % *ee*), and there was no significant impact of replacing the quinoxaline walls with naphthoquinone groups, or of modifying the phosphoramidite (although1-naphthyl-containing **A122** did not perform as well). Comparison

with isomers of the ligands where one amide group is directed into the cavity (and, hence, the gold(I) centre directed outward) highlight the importance of placing the gold(I) centres inside the cavity to achieve high enantioselectivities. These experimental observations were probed with DFT calculations, which indicate that NCIs between the aromatic ring of the substrate and the cavity contribute to a lowering of the transition state energy for the observed product.
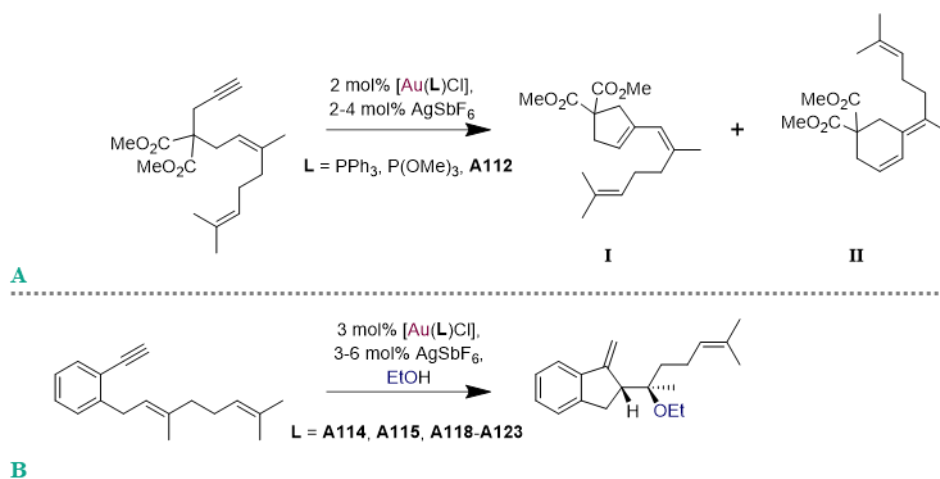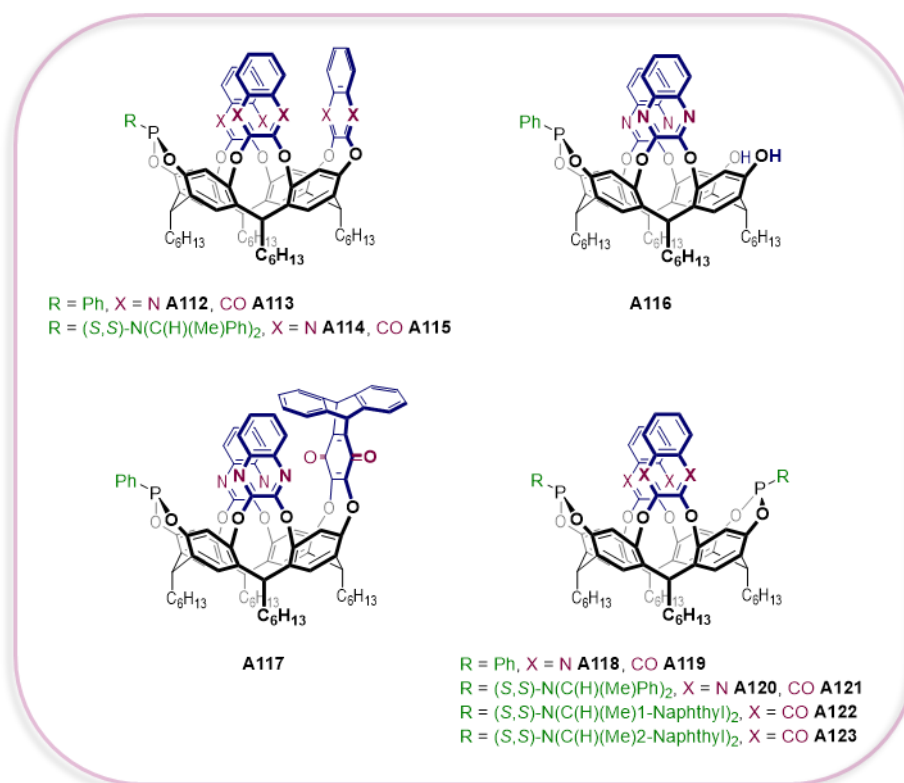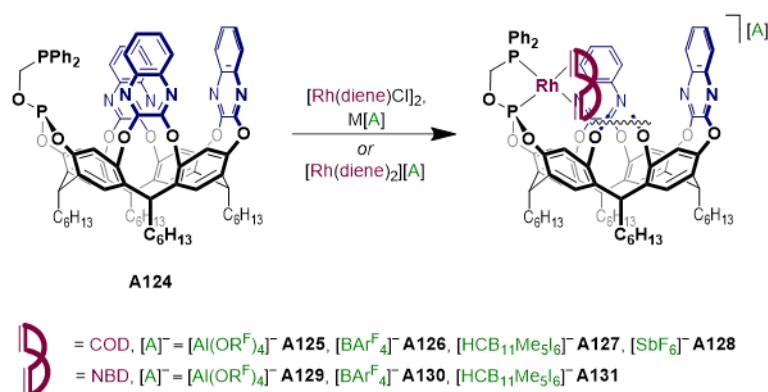

*Scheme 1.20. Gold-catalysed cyclisations reported by Echavarren, using ligands **A112-A123**.[130]*

The studies discussed here are some of the most detailed on the effects of catalyst and substrate confinement within a deep cavitand ligand on catalytic outcomes. Whilst the cavity effects are clearly complex, it can be seen that there is great potential for utilising deep cavitand-based ligands to influence chemo-, regio- and enantioselectivity in chemical transformations.

1.3.3. Rhodium Coordination Chemistry of a Cavitand-Based Ligand

The research discussed above has been heavily focussed on gold catalysis and understanding of the cavity effects has, in some cases, been complicated by the cleavage of a second wall, and addition of a second phosphorus donor (and, therefore, gold(I) nucleus), or oxidised phosphorus. As yet unpublished work in the Chaplin group has focused on expanding the applications of quinoxaline-walled resorcinarene ligands with the synthesis and rhodium coordination chemistry of a structurally related chelating phosphine-phosphite.[131]

The bespoke ligand **A124** possesses three quinoxaline walls, but, instead of a single phosphine donor as in the examples above, it possesses a pendant phosphine-phosphite, enabling chelation to a metal centre. The rhodium coordination chemistry of this ligand was investigated. A series of complexes were synthesised of the general formula [Rh(**A124**)(diene)][anion]. Two methods were used, the first being the reaction of **A124** with [Rh(diene)Cl]$_2$, in the presence of a halide abstracting agent, and the second being a substitution reaction between **A124** and [Rh(diene)$_2$][anion] (**Scheme 1.21**). The resulting diene complexes **A125**-**A131** were all well-characterised in solution and in the solid state.

= COD, [A]$^-$ = [Al(OR^F)$_4$]$^-$ **A125**, [BAr$^F_4$]$^-$ **A126**, [HCB$_{11}$Me$_5$I$_6$]$^-$ **A127**, [SbF$_6$]$^-$ **A128**
= NBD, [A]$^-$ = [Al(OR^F)$_4$]$^-$ **A129**, [BAr$^F_4$]$^-$ **A130**, [HCB$_{11}$Me$_5$I$_6$]$^-$ **A131**

*Scheme 1.21. Synthesis of rhodium(I) diene complexes **A125**-**A131**, using ligand **A124**.[131]*

Subsequent investigations focused on the removal of the diene, both in solution and in the solid state. Upon dissolution of [Al(OC(CF$_3$)$_3$)$_4$] salts **A125** and **A129** in a variety of solvents, the diene ligands were retained. However, dissolution in acetonitrile resulted in displacement of the diene and formation of acetonitrile complex **A132** (**Scheme 1.22**). Exposure of mesitylene solutions of **A125** and **A129** to an atmosphere of dihydrogen results in hydrogenation of the diene and displacement of the resultant alkane by mesitylene (**A133**, **Scheme 1.22**). Mesitylene is typically considered to be too large for a resorcinarene cavity[132,133] and significant structural distortion of the quinoxaline walls was apparent in the solid-state structure. Over time in mesitylene solution, a precipitate begins to form, which was assigned as dimeric complex **A134**. A similar diene hydrogenation and displacement process is observed in fluoroarene solution, giving fluorobenzene complex **A135** and 1,2-difluorobenzene complex **A136**. Hydrogenation of crystalline material of **A125**-**A131** was

also carried out, in an attempt to isolate a σ-alkane complex in the solid state. Despite a clear colour change from orange to red, complete loss of crystallinity was apparent upon attempted examination by X-ray diffraction. This concluded the investigation into the coordination chemistry of this ligand.
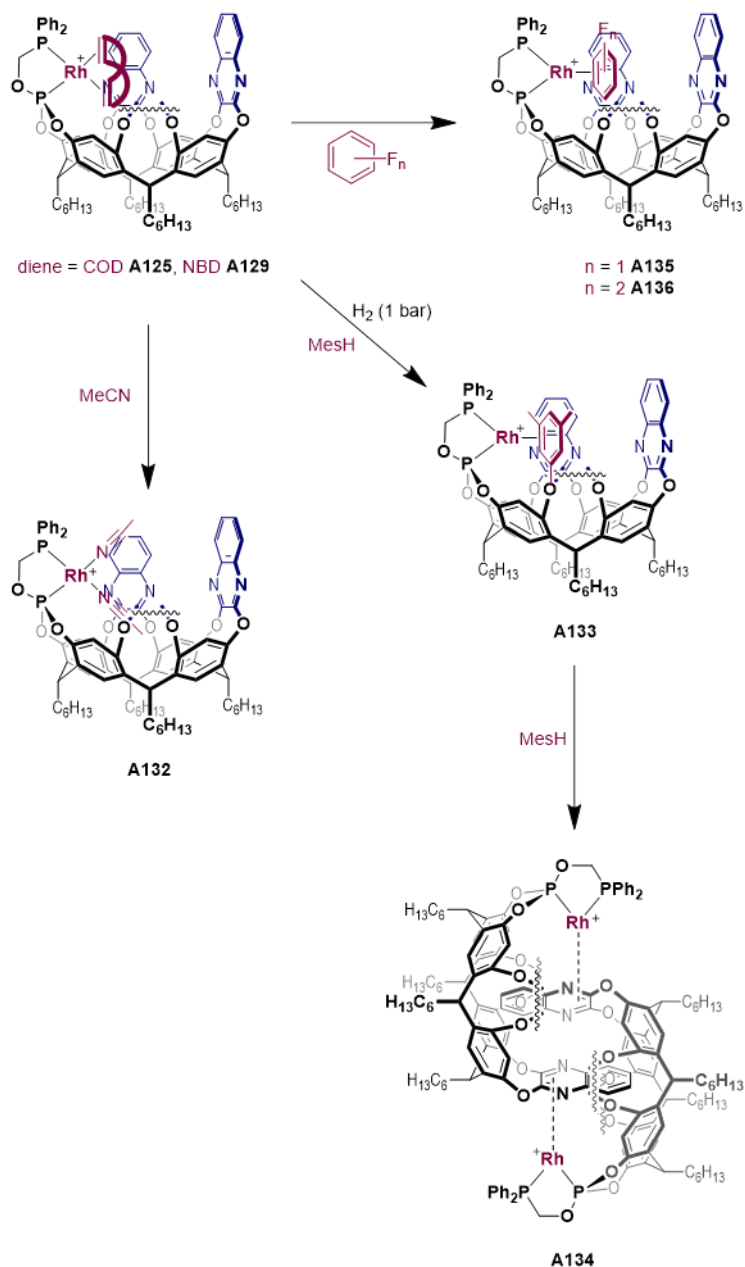
Scheme 1.22. *Reactivity of rhodium(I) diene complexes **A125** and **A129** with acetonitrile, mesitylene and fluoroarenes.[131] [Al(OC(CF₃)₃)₄] are omitted for clarity.*

A ligand of this nature provides opportunities for combining principles of primary coordination sphere ligand design with the confinement effects observed in host-guest chemistry. It is clear that there is potential for further investigation, and also for modification to the ligand scaffold that may allow for more exciting discoveries. As such, the use of a system such as this is a powerful strategy for rational catalyst design.

1.4. Aims and Objectives

The aim of this thesis is to demonstrate the concept of rational ligand design in both the primary and secondary coordination spheres. Three related systems have been investigated, where ligands have been chosen or bespoke systems have been created with specific applications in mind. These targets contribute to two major themes of modern organometallic chemistry: (i) investigating interactions between C-H bonds and group 9 metals and (ii) achieving regioselectivity in rhodium-catalysed hydroformylation.

Agostic interactions, in which an intramolecular C-H σ-bond is coordinated to a metal centre, are important intermediates in directed C-H activation and models for intermediates in intermolecular C-H activation. Given the lack of appreciable agostic interactions in 5-coordinate rhodium and iridium 2,2'-biphenyl complexes of PNP-^{t}Bu, PNP-Np is proposed to be a more suitable target for investigation, with longer and more flexible

M = Rh, Ir

PNP-Np

*neo*pentyl chains. The solution- and solid-state dynamics of these systems is presented, along with some reactivity.
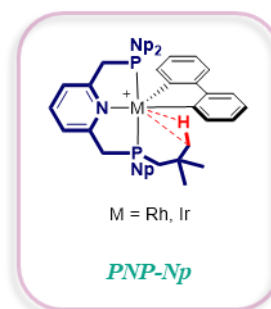
σ-Alkane complexes, in which an intermolecular C-H σ-bond is coordinated to a metal, are more difficult to isolate than complexes with agostic interactions. There have been no reports


Resorcinarene-derived PONP pincer
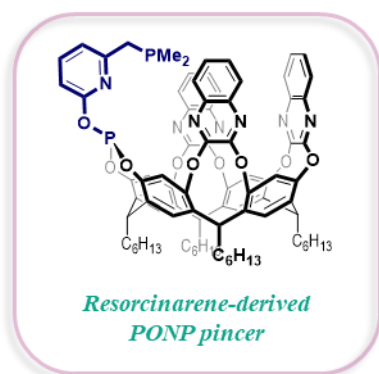
of a σ-alkane complex that can be fully characterised both in solution and in the solid state. Pincer ligands and stabilising microenvironments have been shown to be important factors in alkane binding. Inspired by this, and by cyclohexane binding in deep resorcinarene cavities, a pincer with an appended resorcinarene is targeted, where encapsulation of the alkane in the cavity could stabilise coordination to the metal centre.

Regioselective hydroformylation, enabling the synthesis of branched aldehydes, is of interest for fine chemical production. The use of supramolecular-inspired architectures to exert control over the secondary coordination sphere is an intriguing way to influence regioselectivity. With this in mind, a resorcinarene-based chelating phosphine-phosphite ligand, previously synthesised in the Chaplin group, is employed in the rhodium-catalysed hydroformylation of alkyl alkenes and compared to two model ligands, to investigate the effect of the cavitand on regioselectivity.

Resorcinarene-derived phosphine-phosphite ligand
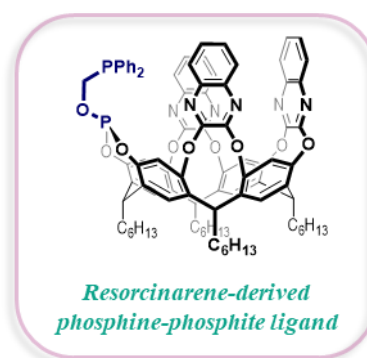
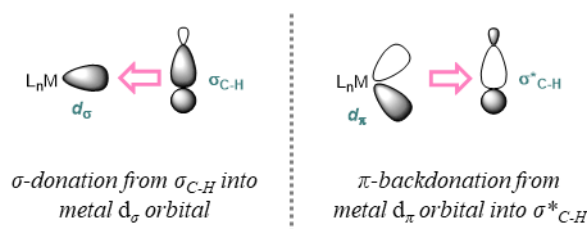## 2. Group 9 2,2'-Biphenyl Complexes of PNP-Np

In this chapter, an example of how modification of pincer ligand substituents can enable a bonding phenomenon to be studied is presented. It is hypothesised that the longer, flexible *neo*pentyl chains of the pincer ligand PNP-Np are more suitable for the adoption of agostic interactions than the *tert*-butyl groups of PNP-^{t}Bu. The M(I) carbonyl complexes of PNP-Np were synthesised and compared with those of PNP-^{t}Bu, in order to quantify the electronic differences between the two pincer ligands. Five-coordinate rhodium(III) and iridium(III) 2,2'-biphenyl complexes of PNP-Np were also synthesised, fully characterised and compared with previously reported PNP-^{t}Bu analogues. Solid- and solution-state dynamics were investigated by multinuclear, variable temperature NMR spectroscopy, XRD and ATR IR spectroscopy. Evidence for the formation of weak agostic interactions in the solid state is presented, although there is a lack of evidence for their persistence in solution on the NMR timescale across a range of temperatures. This is a different situation to that observed with the PNP-^{t}Bu analogues, which possess very weak agostic interactions in the solid state that are not observable by IR spectroscopy. Finally, the five-coordinate PNP-Np complexes are shown to react more readily with dihydrogen and carbon monoxide than the PNP-^{t}Bu analogues.

Displacement by CO · Solid-state agostics · Hydrogenolysis of 2,2'-biphenyl
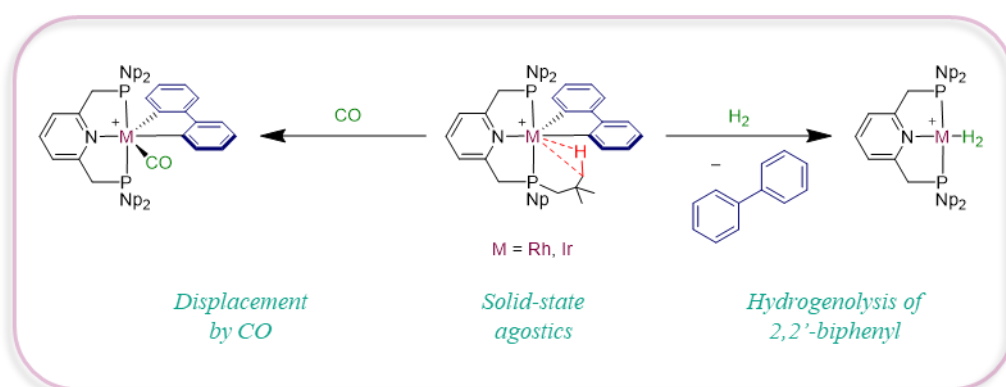
2.1. <u>Introduction</u>

2.1.1. <u>Agostic Interactions</u>

The ability to transform simple, unfunctionalised alkanes (easily obtainable from oil and natural gas) into higher value chemicals is a useful synthetic tool to both industrial and research chemists, alike. A better understanding of this process could ultimately be applied to the improved synthesis of fuels, drugs and the generation of useful chemical feedstocks. The activation of a C-H bond of an alkane by a transition metal is generally used to bring about this transformation, proceeding *via* an intermediate in which the C-H σ-bond is coordinated to the metal centre as a two-electron 'L' ligand (**Figure 2.1**).[134-143]

σ-donation from σ$_{C-H}$ into metal d$_σ$ orbital   *π-backdonation from metal d$_π$ orbital into σ*$_{C-H}$*

***Figure 2.1.** Electronic description of the bonding between a C-H bond of an alkane and an organometallic fragment 'L$_n$M'.*

These transient intermediates are known as σ-alkane complexes and are extremely difficult to isolate because of the poor ligating ability of the C-H bond: it is a strong, non-polar bond, with a low-lying HOMO and high energy LUMO. In addition to this, steric clashing between the alkyl substituent and ancillary ligands make complex formation energetically unfavourable.[144,145] This precludes investigation of these species and, ultimately, a greater understanding of the mechanism of transition metal-catalysed C-H activation. However, these complexes can be more easily studied when the C-H bond is tethered to the metal centre *via* a donor group (**Figure 2.2**). This is more entropically favourable as a result of the chelate effect and is known as an agostic interaction.[146-150] Complexes such as these are intermediates in intramolecular C-H activation. A requirement for the formation of such an interaction is an electronically and coordinatively unsaturated metal centre, allowing the agostic interaction to stabilise the metal centre at a vacant coordination site. The presence of an appropriate C-H bond, in close proximity to the metal centre, is also key.

Agostic Interaction   *σ-Alkane Complex*
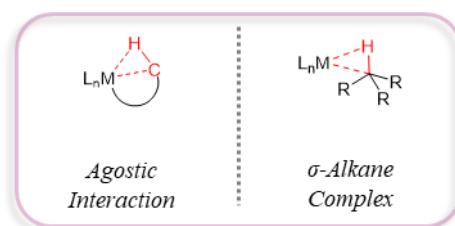
***Figure 2.2.** Intramolecular agostic interactions versus intermolecular σ-alkane complexes.*

In 1985, Crabtree and Holt constructed a reaction trajectory for the activation of a C-H bond by a metal centre (*i.e.* the reaction C-H + M → M-(H-C) → H-M-C), based on analysis of C-H-M geometries in examples of agostic interactions known at the time.[151] They demonstrated that as a C-H bond approaches a metal, it rotates such that the C-H vector points towards the metal at an angle of 130 °, decreasing to ~95 ° upon close approach. A significant lengthening of the bond also occurs, but only at very close approaches, as interaction with the metal increases (a result of backdonation into σ^*_{C-H}).[146,147] The end point of this trajectory is the C-H activated alkyl hydride product. Agostic interactions (and σ-alkane complexes) exist at some stage along this trajectory, between uncoordinated and oxidatively added to the metal. Weller has presented a series of solid-state rhodium σ-alkane complexes that are 'snapshots' along this continuum (**A137**-**A141**, **Figure 2.3**).[152,153] Starting from **A137**, in which a molecule of cyclooctane (COA) is encapsulated within the surrounding array of anions but not coordinated to the metal (but with two agostic interactions from the cyclohexyl substituents), moving on to **A138** which features an η^1-interaction, and finally the η^2-interactions observed in **A139**-**A141**. A decrease in the Rh-H-C angles are observed as backdonation from rhodium becomes more significant. These systems are discussed in more detail in **Section 3.1.3**.
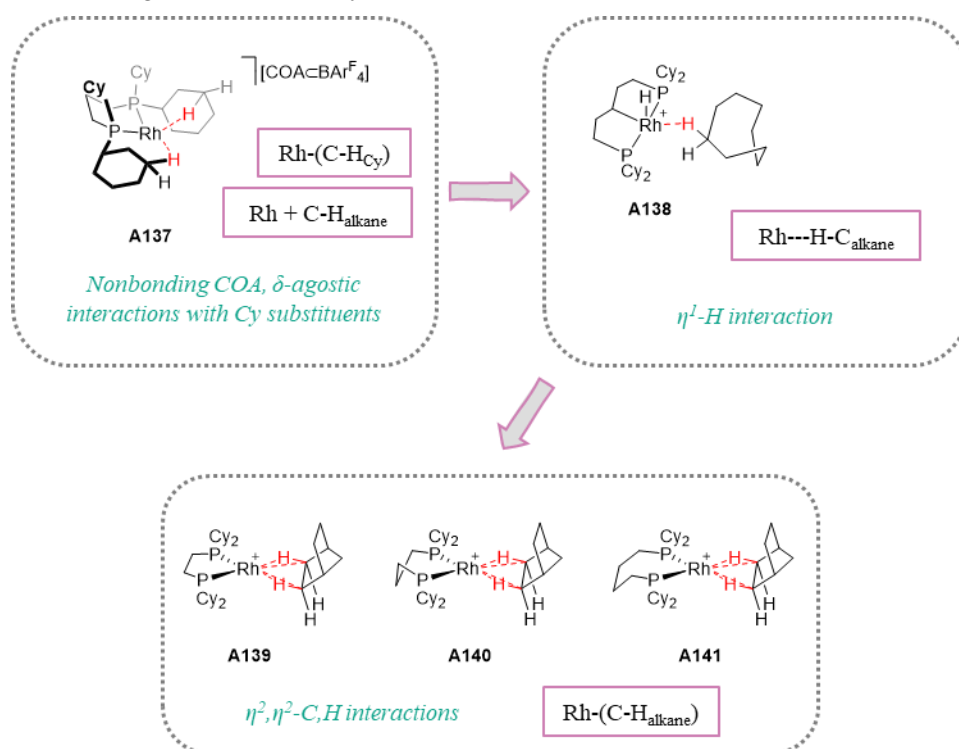
Figure 2.3. *Complexes **A137**-**A141**, reported by Weller, that represent snapshots along the Crabtree trajectory.[152,153] (BAr$^F_4$ = B[3,5-(CF$_3$)$_2$C$_6$H$_3$]$_4$).*

2.1.2. Agostic Interactions in Group 9 Complexes

There has been a wealth of reports of group 9 complexes displaying agostic interactions since they were formally identified and defined in 1983.[146] Of particular interest here are those featuring rhodium and iridium, as these metals have seen considerable application in C-H activation processes and so agostic interactions with these metals can be thought of as models for catalytic intermediates.[137-142,154]

A large number of the examples of rhodium and iridium complexes displaying agostic interactions feature an unsaturated metal centre in the M(III) oxidation state, with two *trans*-disposed L ligands, such as phosphines[155-159] or NHCs.[160-165] Others include Binor-*S* complexes (Binor-*S* = 1,2,4,5,6,8-dimetheno-*S*-indacene), in which the supporting alkyl phosphine engages in an γ-agostic interaction,[166-170] and dimeric rhodium(III) complexes with bridging agostics.[171-172]

Of particular relevance here is the use of the high *trans*-influence 2,2'-biphenyl (biph) ligand to synthesise coordinatively unsaturated M(III) complexes that display agostic interactions. 2,2'-Biphenyl is a strongly σ-donating ligand that is used in the stabilisation of low-coordinate metal centres. It is rigid and resistant to reductive elimination, and so can be considered as an organic protecting group. The low-coordinate complex *trans*-[Rh(P^{i}Pr$_3$)$_2$(biph)][BAr$^F_4$] (**A142**, **Figure 2.4**) is formed *via* η^6-π-coordination of biphenylene and subsequent C-C activation, and the solid-state structure provides evidence for a γ-agostic interaction with one *iso*-propyl C-H bond, and a weaker γ-agostic interaction with a C-H bond of the other phosphine.[173]

This result prompted the synthesis of a range of complexes of the formula *trans*-[M(PR$_3$)$_2$(biph)][BAr$^F_4$] (**A142**-**A149**).[174] Here, a more convenient synthetic route was used, involving ligand substitution in [Rh(dtbpm)(biph)Cl][175] (dtbpm = bis(di-*tert*-butylphosphino)methane) or [Ir(biph)(cod)Cl]$_2$[176,177] (cod = 1,5-cyclooctadiene), removing the need to activate the C-C bond of biphenylene. The resulting complexes displayed sawhorse geometries, with two vacant coordination sites at the M(III) centres. Complexes **A142**-**A147**, bearing trialkylphosphine ligands, all display agostic interactions in the solid state, as investigated by XRD. Whilst complexes **A142**-**A145** possess γ-agostic interactions, the more flexible *iso*-butyl groups in **A146** and **A147** enable the ligands to adopt δ-agostic interactions. Interestingly, the solid-state structures of the two triphenylphosphine complexes, **A148** and **A149**, both feature a molecule of dichloromethane occupying a vacant coordination site at the metal, with no stabilisation from an agostic interaction at the remaining vacant site. It was concluded that in this series of complexes, stronger agostic interactions are formed in the iridium complexes than in the rhodium congeners. With regards to the differing

phosphine substituents, the agostic strength decreases in the order: *iso*-butyl > cyclohexyl > *iso*-propyl > phenyl.

The biphenyl moiety has also been used in the Chaplin Group to investigate agostic interactions in a series of pincer-supported complexes. These five-coordinate, M(III) complexes are coordinatively unsaturated, bearing a vacant site *trans* to one of the M-C$_{aryl}$ bonds of the biphenyl ligand. Examples include complexes of a macrocyclic CNC pincer with *N*-heterocyclic carbene (NHC) donor groups of the formula [M(CNC-12)(biph)][BAr$^F_4$] (M = Rh, **A150**; Ir, **A151**).[178] In both cases, stabilising ε-agostic interactions were observed between the metal centres and the macrocyclic linker in the solid state, which were retained upon dissolution, leading to contortion of the macrocycle.

Using related macrocyclic ligands bearing phosphine donor groups, the complexes [M(pincer)(biph)][BAr$^F_4$] (M = Rh, pincer = PNP-14, **A152**; pincer = PONOP-14, **A153**;[179] M = Ir, pincer = PNP-14, **A154**[180]) were synthesised. These systems also display contortion of the macrocyclic chain, in order to accommodate weak γ-agostic interactions.

The analogous acyclic complexes **A155**-**A158** were also prepared, using the pincer ligands PNP-*t*Bu and PONOP-*t*Bu.[181] A notable feature shared by the solid-state structures of each of these complexes was the canting of a *tert*-butyl group towards the vacant coordination site at the metal centre. The short M···H–C contacts, combined with the reduced M-P-C$_{tBu}$ angles, appear to suggest the formation of weak agostic interactions between a *tert*-butyl C-H and the metal centre. For each ligand, these interactions would appear to be stronger in the iridium complexes, compared to the rhodium congeners, and stronger in the more donating PNP systems than in the PONOP systems. However, the presence of these agostic interactions was not detected by ATR IR spectroscopy. Taking these findings, together with NBO analysis, it was concluded that the short M---H–C contacts are better described as being a consequence of steric buttressing of biphenyl and the proximal *tert*-butyl substituent, leading to a yawing of the phosphine donor groups.

Despite the lack of appreciably strong agostic interactions in this system, they have been observed in complexes of the related pincer PNP-Np (Np = *neo*pentyl), in which the phosphine donor groups bear longer, more flexible *neo*pentyl chains (**Section 1.2.2**).[64] Analysis of the solid-state structure of dihydride complex **A50** indicated the presence of an agostic interaction between a methyl group and the vacant coordination site at iridium, conferring overall octahedral geometry and C$_1$ symmetry. The agostic is not persistent in solution on the NMR timescale, with the hydrides appearing as equivalent in the ^{1}H NMR spectrum, suggesting a C$_{2v}$-symmetric complex.

Inspired by this result, and the lack of any significant agostic interaction in **A155**-**A158**, complexes of the formula [M(PNP-Np)(biph)]$^+$ (M = Rh, Ir) were of interest. The synthesis of these would allow a comparison with the *tert*-butyl system, specifically, whether the presence

of an additional methylene unit in the alkyl substituents at phosphorus would be more suitable for the formation of stronger agostic interactions. Both *neo*pentyl and *tert*-butyl possess -C(CH$_3$)$_3$ groups, but the additional methylene unit places this steric bulk further away from the metal centre in complexes of PNP-Np. This should create a pocket at a low-coordinate metal centre, which, combined with the increased conformational flexibility of *neo*pentyl compared to *tert*-butyl (also a consequence of the additional methylene unit) led us to propose that agostic interactions may be observed in rhodium and iridium biphenyl complexes.

M = Rh, R = ^{i}Pr **A142**; Cy **A144**; ^{i}Bu **A146**; Ph **A148**
M = Ir, R = ^{i}Pr **A143**; Cy **A145**; ^{i}Bu **A147**; Ph **A149**

M = Rh **A150**; Ir **A151**

M = Rh, X = CH$_2$ **A152**
M = Rh, X = O **A153**
M = Ir, X = CH$_2$ **A154**

M = Rh, X = CH$_2$ **A155**
M = Rh, X = O **A156**
M = Ir, X = CH$_2$ **A157**
M = Ir, X = O **A158**

A50
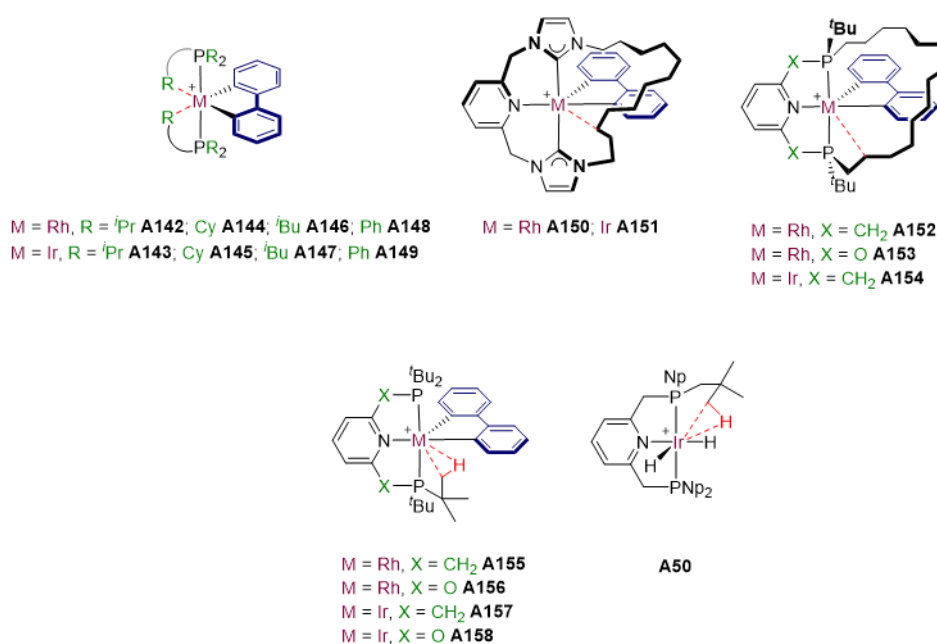
Figure 2.4. *Pincer-supported group 9 agostic complexes **A142**-**A158** and **A50**. Counterions are omitted for clarity ([BAr^F$_4$]$^−$ **A142**-**A158**, [BF$_4$]$^−$ **A50**).*[64,173,174,178-181]

2.2. Ligand Synthesis

PNP-Np was synthesised *via* a modification of the procedure described by Yamashita and Nozaki.[64] Firstly, di-*neo*pentylchlorophosphine was prepared by the Grignard reaction of *neo*pentylmagnesium chloride with trichlorophoshine (**Scheme 2.1**).[182] Distillation under reduced pressure gave pure di-*neo*pentylchlorophosphine in 54 % yield. Assignment was confirmed by ^{1}H and ^{31}P{^{1}H} NMR spectroscopy (δ_P 104.0).
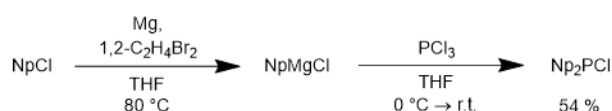
Scheme 2.1. Synthesis of Np$_2$PCl.[182]

Once di-*neo*pentylchlorophosphine had been prepared, 2,6-lutidine was then treated with *n*-butyllithium, in the presence of tetramethylethylenediamine (TMEDA), prior to introduction of the phosphine (**Scheme 2.2**). The resulting yellow residue contained PNP-Np as the major species, along with varying amounts of other phosphorus-containing species. In a deviation from the reported procedure, this product mixture was treated with borane dimethylsulfide complex to give the phosphine-borane adduct **1**, which was isolated by column chromatography in 65 % yield (**Scheme 2.2**). This technique has previously been used to great success within the group for the isolation of air-sensitive phosphine ligands.[177,183,184] The ^{31}P{^{1}H} NMR spectrum contains a single, broad resonance centred around 10.8 ppm and the ^{1}H NMR spectrum confirms the assignment of the product as the borane adduct **1**.

The deprotection method selected was that of refluxing compound **1** in neat diethylamine,[185,186] and the reaction was complete after 2 days. A white solid was obtained after the removal of volatiles, which was identified as PNP-Np by NMR spectroscopy, displaying a single resonance at −39.8 ppm in the ^{31}P{^{1}H} NMR spectrum. The ^{1}H and ^{13}C{^{1}H} NMR spectra also support the proposed structure and agree with the data reported by Yamashita and Nozaki.[64]
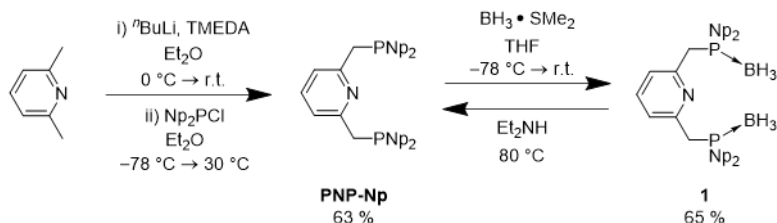

Scheme 2.2. Synthesis of PNP-Np, followed by borane protection, isolation of the phosphine-borane adduct and subsequent deprotection.

2.3. <u>M(I) Carbonyl Complexes of PNP-Np</u>

It has been shown that the donor strength of series of pincer ligands can be gauged by analysis of the carbonyl stretching frequencies of M(I) carbonyl complexes of the respective ligands.[187] It is assumed that PNP-Np will be a poorer electron donor than PNP-^{t}Bu, based on inductive effect considerations. The presence of three methyl groups on the carbon α- to the phosphorus in PNP-^{t}Bu has a positive inductive effect. The greater electronegativity of carbon, *cf.* hydrogen, results in a small negative dipole at carbon, which is ultimately relayed to the next carbon and to phosphorus, influencing the basicity of the lone pair. However, in PNP-Np, the carbon α- to phosphorus possesses only one alkyl group, with the three methyls being located further from phosphorus. As such, a smaller inducive effect is generated, and the lone pair at phosphorus is expected to be less basic than in PNP-^{t}Bu.

Square planar, 16-electron complexes of the formula [M(PNP-Np)(CO)][BAr$^F_4$] (M = Rh, **2**; Ir, **3**) were subsequently prepared, to experimentally gauge the electronic effect of changing the PNP *tert*-butyl substituents for *neo*pentyl. The synthesis of rhodium complex **2** was achieved by reaction of PNP-Np and [Rh(CO)$_2$Cl]$_2$ in the presence of Na[BAr$^F_4$] (**Scheme 2.3**). The product was isolated as a yellow solid in 73 % yield and was characterised by ^{1}H, ^{13}C{^{1}H} and ^{31}P{^{1}H} NMR spectroscopy (δ_P 17.4, $^1J_{RhP}$ = 121 Hz), IR spectroscopy, HR ESI-MS ([*M*]$^+$, 582.2489 (calcd 582.2495) *m/z*) and XRD. Bulk purity was established by elemental analysis. **Figure 2.5** shows the structure of complex **2**, along with key metrics. Two independent cations are present in the unit cell, both displaying slightly distorted square planar geometries. They possess P2-Rh1-P3 angles of 168.99(4) ° and 168.74(4) °, and N20-Rh1-C4 angles of 179.0(2) ° and 177.7(1) °, respectively. Solid-state analysis of the PNP-^{t}Bu analogue has been reported: Milstein's complex [Rh(PNP-^{t}Bu)(CO)][BF$_4$] (**A159**),[54] displays similar metrics, albeit with a marginally shorter Rh1-C4 bond (1.818(5) Å in **A159** *cf.* 1.845(4)/1.841(4) Å in **2**).
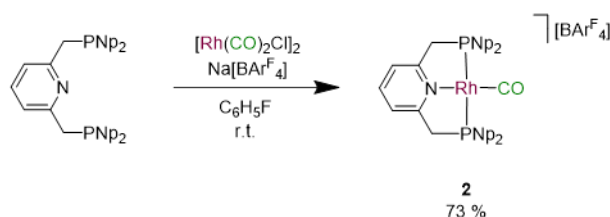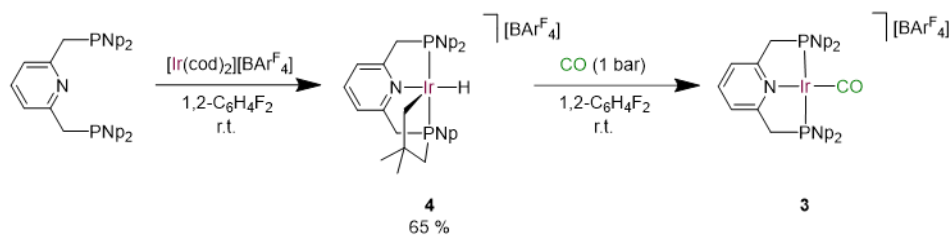

Scheme 2.3. *Synthesis of rhodium(I) carbonyl complex* **2**.
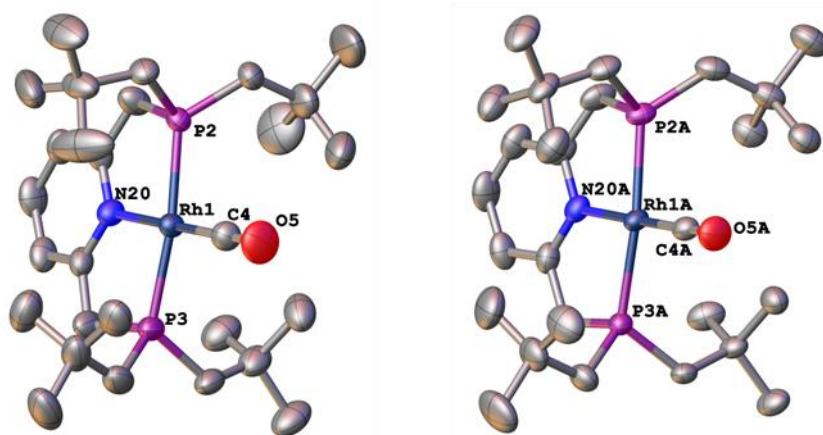
Figure 2.5. *Solid-state structures of the two independent cations of **2** (Z' = 2), determined at 150 K. Atomic displacement parameters are drawn at 50 % probability. Hydrogens and counterions are omitted for clarity. Selected bond distances (Å) and angles (°): Rh1-P2 2.291(1), Rh1-P3 2.293(1), Rh1-N20 2.096(3), Rh1-C4 1.845(4), P2-Rh1-P3 168.99(4), N20-Rh1-C4 179.0(2); Rh1A-P2A 2.293(1), Rh1A-P3A 2.297(1), Rh1A-N20A 2.095(3), Rh1A-C4A 1.841(4), P2A-Rh1A-P3A 168.74(4), N20A-Rh1A-C4A 177.7(1).*

A similar synthetic route to that used for **2** was also considered for the iridium(I) congener **3**, involving the use of Vaska's complex ([Ir(PPh$_3$)$_2$(CO)Cl]) in place of [Rh(CO)$_2$Cl]$_2$. However, related work in the Chaplin group has shown that reaction of the pincer ligand PONOP-Ar^F (Ar^F = 2-(CF$_3$)C$_6$H$_4$) with Vaska's complex, in the presence of Na[BAr$^F_4$], leads to the formation of a mixture of an iridium(I) carbonyl and an iridium(I) triphenylphosphine complex.[188] This route was, therefore, concluded to be unsuitable.

Instead, the method reported by Nozaki for the synthesis of [Ir(PNP-Np)(CO)][BF$_4$] (**A47**, **Section 1.2.2**) was implemented, starting from the reaction of PNP-Np with [Ir(cod)$_2$][BAr$^F_4$] to give the cyclometallated complex **4** (the [BAr$^F_4$] analogue of **A45**, **Figure 2.5**).[64] This was isolated as a red solid in 65 % yield and its assignment was supported by ^{1}H, ^{13}C{^{1}H} and ^{31}P{^{1}H} NMR spectroscopy, HR ESI-MS and XRD. The ^{31}P{^{1}H} NMR spectrum of **4** displays two resonances (δ_P 28.5, 18.5, *cf.* 29.0, 18.3 in **A45**) which exhibit coupling of 316 Hz, consistent with two inequivalent, *trans*-disposed phosphorus nuclei.[189,190] The presence of a characteristic hydride resonance (d$_H$ −16.82, *cf.* −16.87 in **A45**) is also apparent in the ^{1}H NMR spectrum. This hydride resonance appears as a triplet, displaying coupling to two almost equivalent phosphorus nuclei ($^2J_{PH}$ = 12 Hz). This is consistent with the literature.

Scheme 2.4. *Synthesis of iridium(I) carbonyl complex **3**, via cyclometallated complex **4**.*

This C-H activation of a *tert*-butyl group is evident in the solid-state structure of **4** (**Figure 2.6**), something which was not reported in the case of **A45**. The cyclometallated *neo*pentyl group can be clearly seen, with a covalent Ir1-C30 bond distance of 2.15(1) Å. The reduced Ir1-P2-C28 angle of 104.2(4) ° is also consistent with cyclometallation. A δ-agostic interaction between a methyl group and iridium occupies the vacant site *trans* to this, indicated by a short Ir1-C45 distance of 2.76 Å and an Ir1-P3-C43 angle of 110.2(4) °,[146,147,149] which is intermediate between those of the free *neo*pentyl groups and of the cyclometallated group. The absence of any ^{1}H NMR signals shifted to appreciably low frequency could suggest that this interaction is not persistent in solution on the NMR timescale. The complex displays distorted square pyramidal geometry and has a formal valence electron count of 16, although the adoption of the δ-agostic interaction confers overall octahedral geometry and satisfies the 18-electron rule (See **Appendix**). Another notable feature is the twisting of the pyridine ring out of the plane described by the donor groups (14.8(5) °), in order to accommodate the strain of the metallacycle.
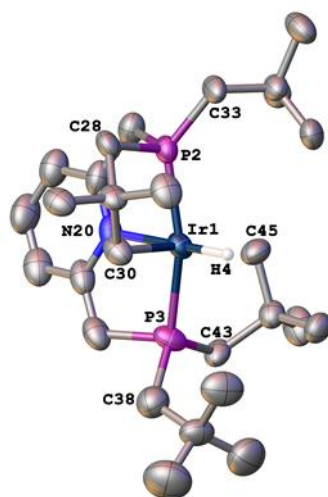
Figure 2.6. *Solid-state structure of **4**, determined at 150 K. Atomic displacement parameters are drawn at 50 % probability. Hydrogens (except H4) and counterion are omitted for clarity. The position of the hydride (H4) was restrained to 1.5 Å (based on complex **12**, see **Figure 2.15**). Selected bond distances (Å) and angles (°): Ir1-P2 2.271(2), Ir1-P3 2.271(2), Ir1-N20 2.17(1), Ir1-C30 2.15(1), Ir1-C45 2.76(1); P2-Ir1-P3 162.7(1), Ir1-P2-C28 104.2(4), Ir1-P2-C43 110.2(4), Ir1-P2-C33 133.7(4), Ir1-P3-C38 128.4(5).*

A solution of **4** in 1,2-difluorobenzene was then placed under 1 bar of carbon monoxide (**Scheme 2.4**). An immediate colour change of the solution from deep red to pale yellow was observed, indicating the formation of complex **3**. This was identified based upon *in situ* [1]H, ^{13}C{^{1}H} and ^{31}P{^{1}H} NMR spectroscopic data, alongside IR spectroscopic data and HR ESI-MS. However, complex **3** could not be separated from trace phosphorus-containing impurities. The data match that reported for **A47**, showing that the use of the [BAr$^F_4$]$^-$ anion has no significant effect on the complex.

The carbonyl stretching bands of these complexes in CH_2Cl_2 solution are shown in **Table 2.1** along with data for the PNP-^{t}Bu congeners **A31** and **A160**[184] and the literature value for **A47**.[64] It can be seen that for both PNP-Np complexes **2** and **3**, the carbonyl stretches appear at higher wavenumbers compared to their PNP-^{t}Bu analogues ($\Delta\nu_{CO} = 14$ cm^{-1}). This confirms the previous statement that PNP-Np is expected to be a poorer donor than PNP-^{t}Bu. Drawing conclusions about pincer donor strength based on carbonyl stretching frequencies is not necessarily straightforward,[7,8,187] but, given the agreement with theory, these values can be considered as acceptable validation for the difference in donor strengths of the two pincers.

Table 2.1. *Carbonyl stretching frequencies of PNP-Np complexes **2,3** and **A47**, and PNP-^{t}Bu complexes **A31** and **A160**, measured in CH_2Cl_2.*

Complex	ν_{CO} / cm^{-1}
[Rh(PNP-Np)(CO)][BAr$^F_4$] / **2**	2004
[Rh(PNP-^{t}Bu)(CO)][BAr$^F_4$] / **A31**	1990
[Ir(PNP-Np)(CO)][BAr$^F_4$] / **3**	1991
[Ir(PNP-Np)(CO)][BF$_4$] / **A47**	1986
[Ir(PNP-^{t}Bu)(CO)][BAr$^F_4$] / **A160**	1977

2.4. Synthesis of [M(PNP-Np)(biph)][BAr$^F_4$]

Initial attempts to synthesise the five-coordinate biphenyl complexes [M(PNP-Np)(biph)][BAr$^F_4$] (M = Rh, Ir) using the 'one-pot' procedure used for the synthesis of **A155** and **A157**,[181], involving reaction of the group 9 precursor, PNP-Np and Na[BAr$^F_4$], were not successful. Instead, a step-wise method was employed.[174,179,180,191,192] The six-coordinate chlorides [M(PNP-Np)(biph)Cl] (M = Rh, **5**; Ir, **6**) were prepared by heating fluorobenzene solutions of PNP-Np and the appropriate group 9 precursor to 85 °C for 18-24 hours (**Scheme 2.5**). Complexes **5** and **6** were obtained in reasonable yields (70 %, **5**; 64 %, **6**) and characterised by ^{1}H, ^{13}C{^{1}H} and ^{31}P{^{1}H} NMR spectroscopy, HR ESI-MS and XRD. Bulk purity was established by elemental analysis.
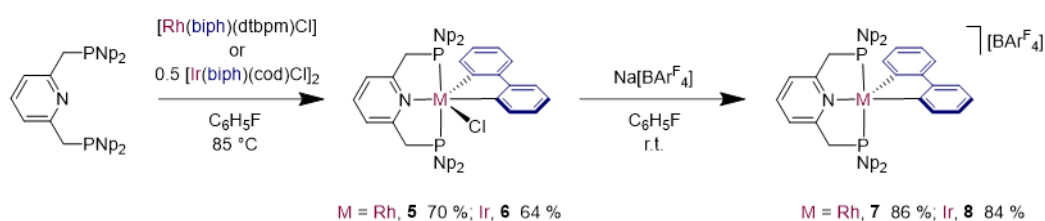
*Scheme 2.5. Synthesis of six-coordinate complexes **5** and **6**, followed by chloride abstraction to give five-coordinate complexes **7** and **8**.*

The ^{31}P{^{1}H} spectrum of complex **5** exhibits a doublet at 26.2 ppm ($^1J_{RhP}$ = 110 Hz), whilst that of complex **6** exhibits a singlet at 0.55 ppm (*cf.* −39.8, s, for free PNP-Np), both of which are consistent with two equivalent, metal-bound phosphorus nuclei. Analysis of the ^{1}H NMR spectra indicates the presence of two inequivalent *tert*-butyl groups. Consideration of the solid-state structures (*vide infra*), together with two-dimensional NOESY and ROESY NMR experiments, enables these to be assigned as lying above/under the chloride (CH$_3^{Cl}$) and above/under the biphenyl ring *cis* to nitrogen (CH$_3^{biph}$). With this knowledge, it is also possible to identify all eight individual biphenyl protons. The diastereotopic protons of the PNP methylene bridges can also be assigned as those on the side of the chloride (CH$_2^{Py-Cl}$) and those on the side of biphenyl (CH$_2^{Py-biph}$) (**Figure 2.7**). When two protons are attached to the same carbon, as in the pyridine and *neo*pentyl methylene groups of complexes **5** and **6**, depending on the symmetry of the molecule, they can be homotopic, enantiotopic or diastereotopic. Chemically identical, homotopic protons are related to each other by a plane of symmetry, such as a mirror plane or a C$_2$ rotation. If no such symmetry operation relates the two protons, they are enantio- or diastereotopic. In this case, they are diastereotopic: if one of these protons were to be replaced with deuterium, the resulting compounds would be diastereoisomers of each other. Consequently, these protons are magnetically inequivalent, giving rise to independent resonances and displaying geminal coupling to each other. The observation of this in the ^{1}H NMR spectra of complexes **5** and **6** (as characteristic sets of roofed doublets of virtual triplets), for both the pyridine and *neo*pentyl methylene protons, is confirmation.
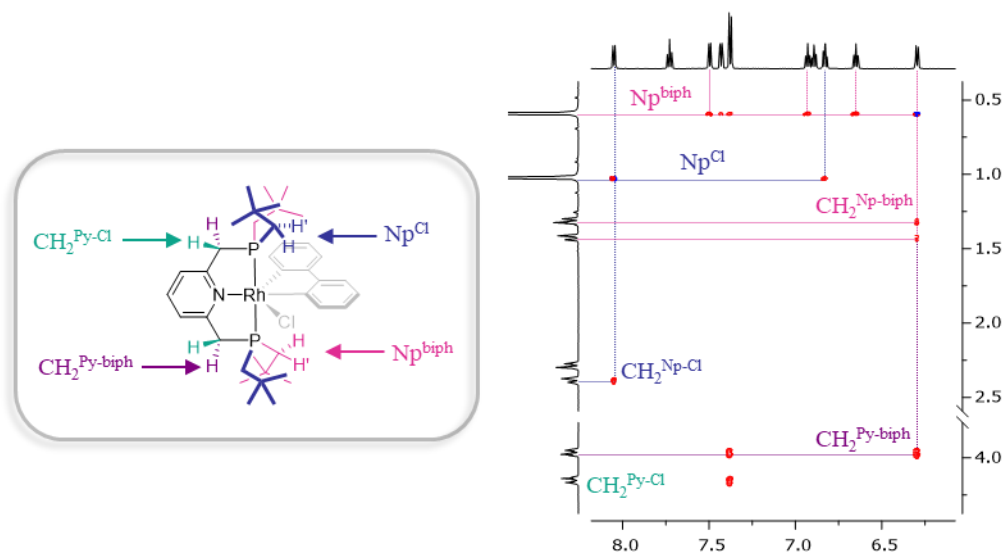
Figure 2.7. *Diagram based on the solid-state structure of complex **5** (left), showing the two* neo*pentyl and methylene linker environments, and a section of the 2D NOESY NMR spectrum of complex **5** (right, CD₂Cl₂, 600 MHz, 200 K), showing how the* tert-*butyl and methylene resonances were assigned based on their correlations with the biphenyl resonances.*

Single crystalline samples of **5** and **6**, suitable for analysis by X-ray diffraction, were obtained by slow diffusion of tetramethylsilane into fluorobenzene solutions at –30 °C. The solid-state structures are shown in **Figure 2.8**, with key bond metrics displayed in **Table 2.2**. Both complexes display distorted octahedral geometry about the metal centre. The N20-M1-C15 angles are near linear (176.40(9) ° in **5**, 176.58(9) ° in **6**), with more deviation evident in the P2-M1-P3 angles (164.33(3) ° in **5**, 164.03(3) ° in **6**), a consequence of the pincer bite angle. Torsion of the pyridine backbone is also displayed (17.5(1) ° and 17.6(1) ° from the plane described by the donor groups, respectively). The M1-C15 distances are 2.034(2) Å (**5**) and 2.053(2) Å (**6**), whilst the M1-C4 distances are marginally shorter, at 2.028(2) Å (**5**) and 2.040(2) Å (**6**), consistent with the nitrogen donor exerting a greater *trans* influence than chloride. The different positions of the *tert*-butyl groups, above/under one ring of the biphenyl ligand and above/under the chloride, can also be clearly seen. Taken together with the NOESY/ROESY NMR data (**Figure 2.7**), the spatial relationship between one pair of *tert*-butyls and the rear biphenyl ring is apparent, along with the proximity of the other pair of *tert*-butyls and two protons of the front biphenyl ring.
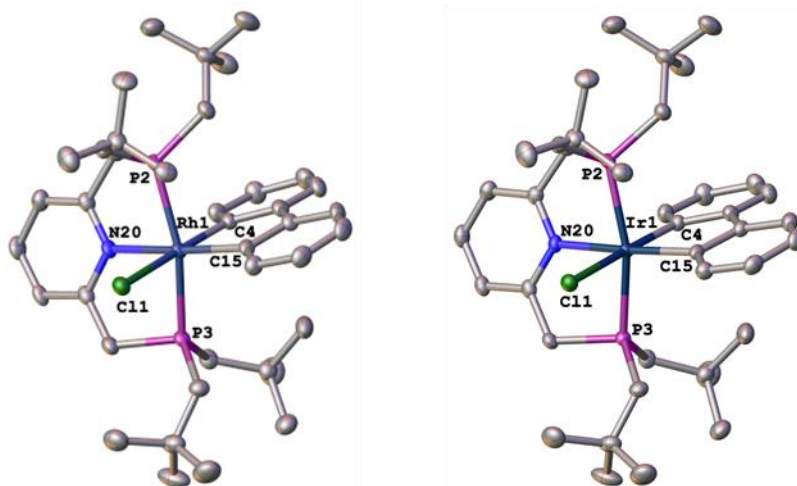
Figure 2.8. *Solid-state structures of rhodium(III) complex **5** (left) and iridium(III) complex **6** (right), determined at 150 K. Atomic displacement parameters are drawn at 50 % probability. Hydrogens and counterions are omitted for clarity.*

***Table 2.2.*** *Selected bond distances (Å) and angles (°) for complexes **5** and **6**.*

	5 (M=Rh)	**6 (M=Ir)**
M1-P2	2.3155(7)	2.3166(7)
M1-P3	2.3351(7)	2.3276(7)
M1-N20	2.150(2)	2.145(2)
M1-C4	2.028(2)	2.040(2)
M1-C15	2.034(2)	2.053(2)
M1-Cl1	2.5021(7)	2.4968(7)
P2-M1-P3	164.33(3)	164.03(3)
N20-M1-C15	176.40(9)	176.58(9)
C4-M1-Cl1	176.83(7)	176.36(7)

In order to obtain the five-coordinate complexes [M(PNP-Np)(biph)][BAr$^F_4$] (M = Rh, **7**; Ir, **8**), and ascertain whether they possess agostic interactions, fluorobenzene solutions of **5** and **6** were treated with Na[BAr$^F_4$] (**Scheme 2.5**). This led to the formation of desired products **7** and **8** in good yields (83-86 %). Both complexes were characterised by ^{1}H, ^{13}C{^{1}H} and ^{31}P{^{1}H} NMR spectroscopy, ATR IR spectroscopy, HR ESI-MS and XRD (**Section 2.5**). Bulk purity was established by elemental analysis.

The single, sharp ^{31}P{^{1}H} resonances of **7** and **8** are shifted from those of **5** and **6** by 3-11 ppm, confirming the presence of new species (δ_P 23.8, **7**; 11.2, **8**). The doublet of complex **7** exhibits ^{103}Rh-coupling of 110 Hz (as in **5**), consistent with a rhodium(III) centre. The ^{1}H NMR spectrum of **7** is significantly broadened at 298 K, allowing limited assignment, whilst that of compound **8** is considerably sharper. This is attributed to dynamic processes occurring at ambient temperature in solution, which are discussed in more detail in **Section 2.6**.

2.5. Solid-State Characterisation of [M(PNP-Np)(biph)][BAr$^F_4$]

Given the dynamic behaviour exhibited by these systems in solution, it was of interest to investigate their solid-state structures across a temperature range to gain more information. Both complexes are isomorphous, each possessing a molecule of dichloromethane and a molecule of tetramethylsilane in the unit cell. **Figure 2.9** shows the structures of complexes **7** and **8** (collected at 150 K) and key bond metrics are summarised in **Table 2.3** (final columns).
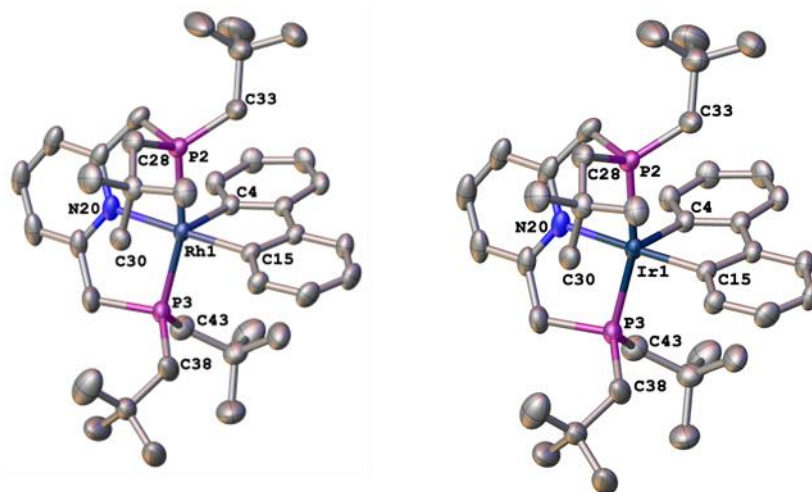
Figure 2.9. *Solid-state structures of five-coordinate biphenyl complexes **7** (left) and **8** (right), determined at 150K. Atomic displacement parameters are drawn at 50 % probability. Hydrogens, solvent and counterions are omitted for clarity.*

Both **7** and **8** adopt distorted square pyramidal geometries. However, in each case, one *tert*-butyl is canted towards the metal centre, as in PNP-*^{t}*Bu complexes **A155** and **A157**. If this is an indication of an agostic interaction, then these could be considered as distorted octahedral complexes. This is substantiated by M1-C30 distances that are slightly shorter than 3 Å (2.906(3), **7**; 2.842(4), **8**), and reduced M1-P2-C28 angles (110.5(1), **7**; 110.4(1), **8**).[146,147,149] Indeed, the M-C30 separations are shorter than the analogous separations observed in **A155** (3.025(3) Å) and **A157** (3.001(3) Å), which could imply a more substantial interaction. The P2-M1-P3 angles (163.42(3) °, **7**; 163.24(4) °, **8**) are smaller than those observed in the six-coordinate chlorides (164.33(3) °, **5**; 164.03(3) °, **6**), which could be a consequence of ligand yawing to accommodate the agostic interaction. However, the formation of δ-agostics (with the longer *neo*pentyl chains) should require less geometric distortion than the formation of γ-agostics (with *tert*-butyl groups) in the PNP-*^{t}*Bu systems, so significant ligand yawing is not necessarily to be expected. A disparity between the M1-C4 and M1-C15 bond lengths of 2.2(4) pm (**7**) and 3.0(5) pm (**8**) is noted, resulting from the stronger *trans* influence exerted by nitrogen compared to a weak agostic. Torsion of the pyridine backbone is observed, but to a lesser extent than in **7** than in **8**: 6.6(1) ° *cf.* 15.8(2). Interestingly, the PNP-Np complexes reported here that possess well-defined agostic interactions (**4** – *vide supra*, **12** – *vide infra*)

tend to exhibit greater twisting of the pyridine backbone than the complexes that do not possess agostics. This could indicate a stronger agostic interaction in iridium complex **8** than rhodium complex **7**, although this is speculative.

An interesting feature of the solid-state structures of PNP-*t*Bu complexes **A155** and **A157** is the disorder they display which has been attributed to conformational isomers with two different pincer binding modes. Across a temperature range of 75–250 K, it was concluded that the two pincer conformations are in dynamic equilibrium. A puckered, C_s-symmetric conformation (conferring overall C_s-symmetry on the complexes) is enthalpically favoured, but exclusively observed at 75 K. At higher temperatures, the entropically favoured, helical, C_2-symmetric conformation (conferring overall C_1-symmetry), becomes more important. However, complexes **7** and **8** do not appear to display this dynamic behaviour, adopting the helical binding and not exhibiting any disorder in the pincer backbone. This lack of contortion in the PNP backbone may be a consequence of steric effects: there is less steric clash between the *tert*-butyl groups and biphenyl in the more flexible PNP-Np system.

In order to investigate other solid-state dynamics that may be taking place in these PNP-Np systems, crystallographic data were also collected at 50 and 100 K for both complexes. A single crystal of each complex was investigated across the temperature range. **Table 2.3** highlights the key bond metrics at these temperatures.

Table 2.3. Selected bond distances (Å) and angles (°) for complexes 7 and 8 at 50, 100 and 150 K.

	7 (M = Rh)			**8** (M = Ir)		
	50 K	100 K	150 K	50 K	100 K	150 K
M1-P2	2.280(1)	2.2821(8)	2.2842(8)	2.292(1)	2.295(1)	2.294(1)
M1-P3	2.326(1)	2.3332(8)	2.3335(8)	2.324(1)	2.324(1)	2.326(1)
M1-N20	2.152(4)	2.156(2)	2.158(2)	2.146(4)	2.150(4)	2.149(3)
M1-C4	2.016(3)	2.012(2)	2.012(2)	2.025(5)	2.022(3)	2.026(3)
M1-C15	2.038(4)	2.035(2)	2.034(3)	2.050(4)	2.057(4)	2.056(4)
M1-C30	2.890(4)	2.887(3)	2.906(3)	2.822(5)	2.831(4)	2.842(4)
P2-M1-P3	163.17(5)	163.34(3)	163.42(3)	163.22(5)	163.25(4)	163.24(4)
N20-M1-C15	177.0(2)	177.16(9)	177.32(9)	176.4(2)	176.5(1)	176.6(1)
M1-P2-C28	110.7(2)	110.25(9)	110.5(1)	110.4(2)	110.3(1)	110.4(1)
M1-P2-C33	121.8(2)	121.49(9)	121.2(1)	120.9(2)	120.7(2)	120.5(2)
M1-P3-C38	115.4(2)	115.5(1)	115.8(1)	115.6(2)	115.8(2)	116.0(2)
M1-P3-C43	120.3(2)	120.54(9)	120.4(1)	119.7(2)	119.6(2)	119.5(2)

Analysis of the bond metrics of rhodium complex **7** indicates that the Rh1-C30 separation remains the same, within error, at 50 K and 100 K, but a slight increase of 1.9(4) pm is noted

when the temperature is increased to 150 K. However, the same conclusion cannot be drawn for iridium complex **8**: although a small increase in separation is seen at each temperature, these differences are not statistically significant. This slight lengthening of this M1-C30 separation with increasing temperature is not reflected in the M1-P2-C28 angles, which remain the same for each complex, within error. This observation is likely to be a consequence of the significant increase in the unit cell volumes across this temperature range (ΔV_{cell} = 160.93(13) Å^3, **7**; 162.00(11) Å^3, **8**).

Analysis of the ATR IR spectra of complexes **7** and **8** provides further support for the existence of weak agostic interactions in these complexes in the solid state. **Figure 2.10A** compares the ATR IR spectra of six-coordinate complex **5** with five-coordinate complex **7**. The broad signal centred around 2682 cm^{-1} falls within the range expected for an agostic interaction.[146,147] This is lower than a regular C-H stretch, indicative of an increased bond length as a result of coordination to the rhodium centre. The same feature is displayed by iridium(III) complex **8** (**Figure 2.10B**), where a broad signal centred around 2586 cm^{-1} is apparent. The lower frequency C-H stretch in the iridium system implies a stronger agostic interaction than in the rhodium system. Stronger metal-ligand bonding is expected in complexes of the heavier, third row metal and this observation is also a feature of biphenyl complexes **A142**-**A147** (**Figure 2.4**).[174]

It can, therefore, be concluded that these PNP-Np complexes behave differently to their PNP-*t*Bu analogues in the solid state, with no evidence for dynamic pincer binding modes in the structures of **7** and **8**. The M1-C30 distances they exhibit, of 2.906(3) Å and 2.842(4) Å, are shorter than those observed in the PNP-*t*Bu complexes and this, along with the additional corroboration provided by the ATR IR spectra, allows for a more conclusive assignment of agostic interactions in **7** and **8** in the solid state. These are, however, relatively weak, which is to be expected given their location with respect to the high *trans*-influencing biphenyl ligand.
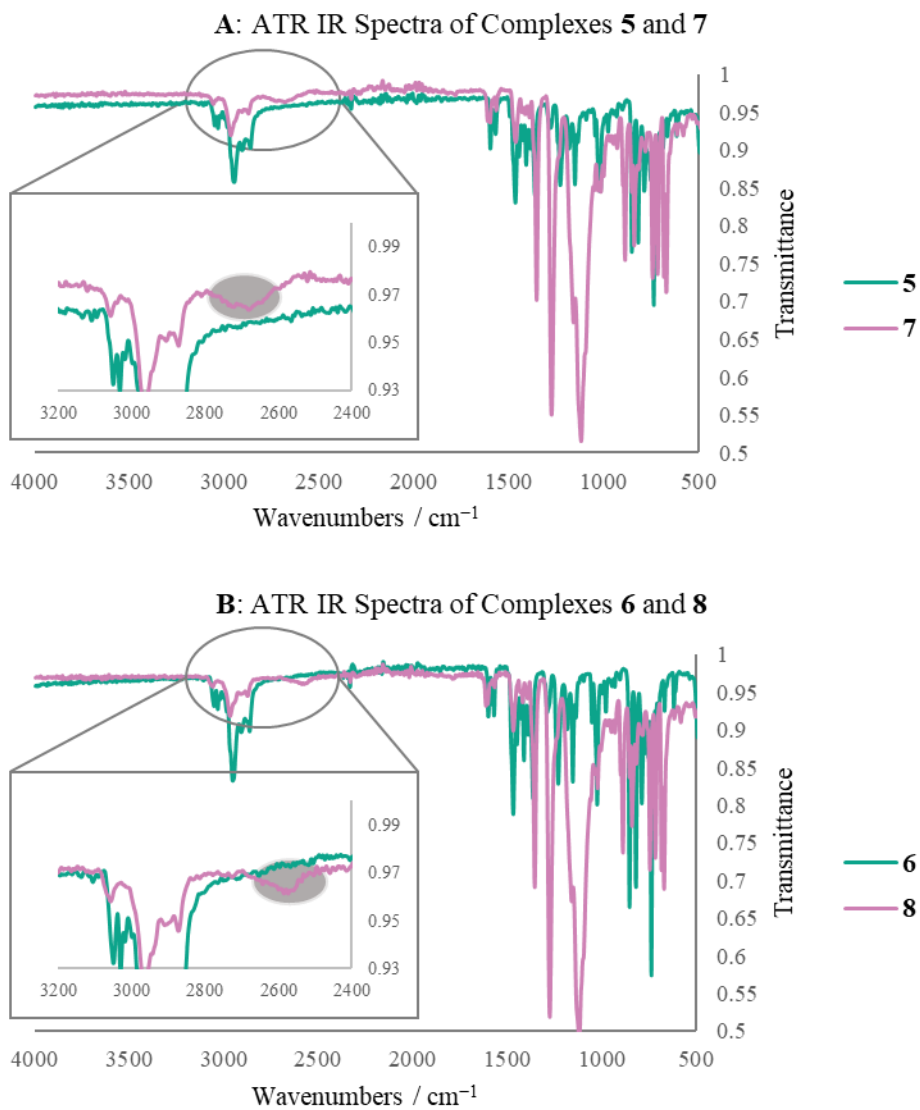
Figure 2.10A) *Stacked ATR IR spectra of rhodium(III) complexes **5** and **7**; **B)** stacked ATR IR spectra of iridium(III) complexes **6** and **8**, highlighting the low frequency agostic C-H bands.*

2.6. Solution-State Dynamics of [M(PNP-Np)(biph)][BAr$^F_4$]

The agostic interactions occupying the vacant coordination sites in **7** and **8** do not appear to be persistent on the NMR timescale in solution at ambient temperature, as inferred from the broadening observed in the ^{1}H NMR spectrum and the lack of signals shifted to an appreciably low frequency. The ^{1}H NMR spectrum of **7** displays significantly broadened biphenyl, methylene and *tert*-butyl resonances. Additionally, all the biphenyl carbons give rise to a single, broad resonance in the ^{13}C{^{1}H} NMR spectrum (*ca.* 127.4 ppm), as do the *neo*pentyl methylene resonances (*ca.* 33.2 ppm). Although exhibiting some broadening, the individual biphenyl resonances can be more easily resolved in the ^{1}H NMR spectrum of complex **8** and two distinct *tert*-butyl environments can be clearly seen.

These observations can be explained by the presence of two distinct dynamic processes taking place. Firstly, interchange between M-(H-C) interactions from the *tert*-butyl groups of the opposing phosphines likely occurs rapidly on the timescale of the experiment, conferring time-averaged C$_s$ symmetry, rather than the C$_1$-symmetric structure that exists in the solid-state, across the temperature range investigated. Secondly, rapid pseudorotation of the biphenyl ligand (a slower process than the agostic interchange) takes place on the NMR timescale, such that the complexes approach time-averaged C$_{2v}$ symmetry (**Scheme 2.6**) at ambient temperature. This process is also observed in the PNP-^{t}Bu complexes **A155** and **A157**.
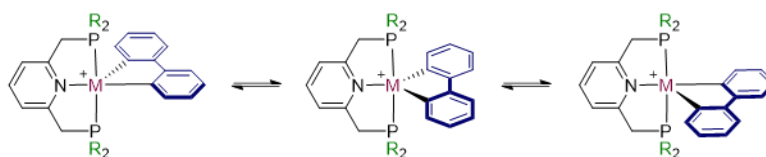
Scheme 2.6. Pseudorotation of biphenyl, between the two extremes of C$_s$ and C$_{2v}$ symmetry. R = ^{t}Bu, Np, M = Rh, Ir. [BAr$^F_4$]$^-$ counterions are omitted for clarity.

The dynamic behaviour exhibited by **7** and **8** (and the relatively high energy barriers found for biphenyl pseudorotation in **A155** and **A157**) led us to investigate them using variable temperature, multinuclear NMR spectroscopy in CD$_2$Cl$_2$ solution. **Figure 2.11** shows the ^{1}H NMR spectra of **7** and **8** between 185 K and 308 K (500 MHz). Full coalescence could not be achieved at 308 K and investigation into the temperature required to reach the fast exchange regime was limited by the boiling point of CD$_2$Cl$_2$. At 308 K, rhodium complex **7** is approaching time-averaged C$_{2v}$ symmetry on the NMR timescale, giving rise to a broader set of resonances than iridium complex **8**, in which the biphenyl, methylene and *tert*-butyl resonances are broadened but can still be resolved (*i.e.* resembling a C$_s$-symmetric complex). As the temperature is decreased to 185 K, de-coalescence begins to occur in the ^{1}H NMR spectra for both systems; the biphenyl rotation starts to freeze out, leading to a complex with pseudo-square pyramidal geometry that is approaching time-averaged C$_s$ symmetry. Even at

this low temperature, no low frequency signals were observed that could be attributed to an agostic interaction, indicating how rapid the agostic interchange is on the timescale of the experiment. Given that no dynamic pincer binding modes were observed in the solid state, it can be assumed that backbone puckering in solution would also be very rapid on the NMR timescale, even at low temperatures. Indeed, this was observed, as C_1 symmetry is not adopted by either complex at 185 K (arising from either backbone puckering or an agostic interaction).
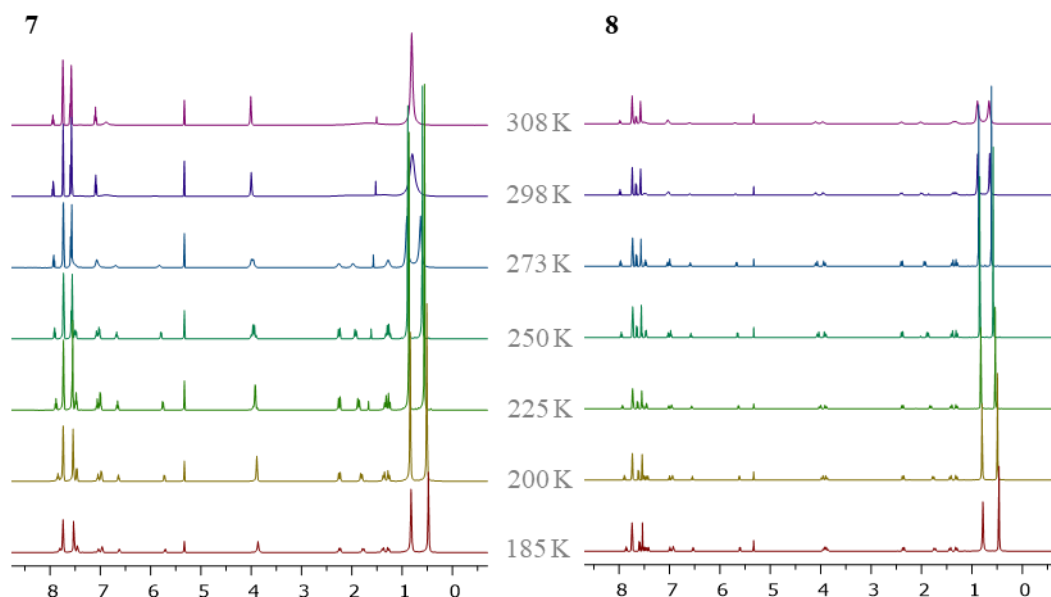
Figure 2.11. *Stacked variable temperature ^1H NMR spectra, collected between 185-308 K (CD$_2$Cl$_2$, 500 MHz), for complexes **7** (left) and **8** (right).*

Unfortunately, full de-coalescence could not be achieved within this temperature range. In order to determine the activation parameters for this pseudorotation, it was necessary to simulate the ^1H NMR spectra using gNMR.[193] **Figure 2.12** shows both the experimental and simulated spectra for the two complexes. Although similar values of $\Delta G^{\ddagger} = 58.2 \pm 0.4$ kJ mol^{-1} (**7**) and 61.1 ± 0.7 kJ mol^{-1} (**7**) were obtained, pseudorotation of biphenyl in rhodium complex **7** is slightly more facile, as expected based on the more broadened resonances at 298 K.[†] Compared with the PNP-^{t}Bu systems, complex **7** displays a higher barrier than **A155** (56 ± 1 kJ mol^{-1}), although this difference is small, whilst **8** displays the same barrier as **A157** (62 ± 1 kJ mol^{-1}), within error. Calculations on a truncated system where the phosphines possess methyl substituents suggest a significantly lower barrier to pseudorotation (21.2 kJ mol^{-1} **Rh**, 21.7 kJ mol^{-1} **Ir**), attributing the higher barriers in the PNP-^{t}Bu systems to the increased steric profile of the *tert*-butyls *cf.* methyl groups.[181] Given that **7** and **8** display similarly high

---

[†] gNMR simulations and $\Delta G^{\ddagger}$ calculations were performed by Dr Baptiste Leforestier, former PhD student, Chaplin group, University of Warwick.

barriers, the same may apply here, even though *neo*pentyl has more conformational freedom than *tert*-butyl.
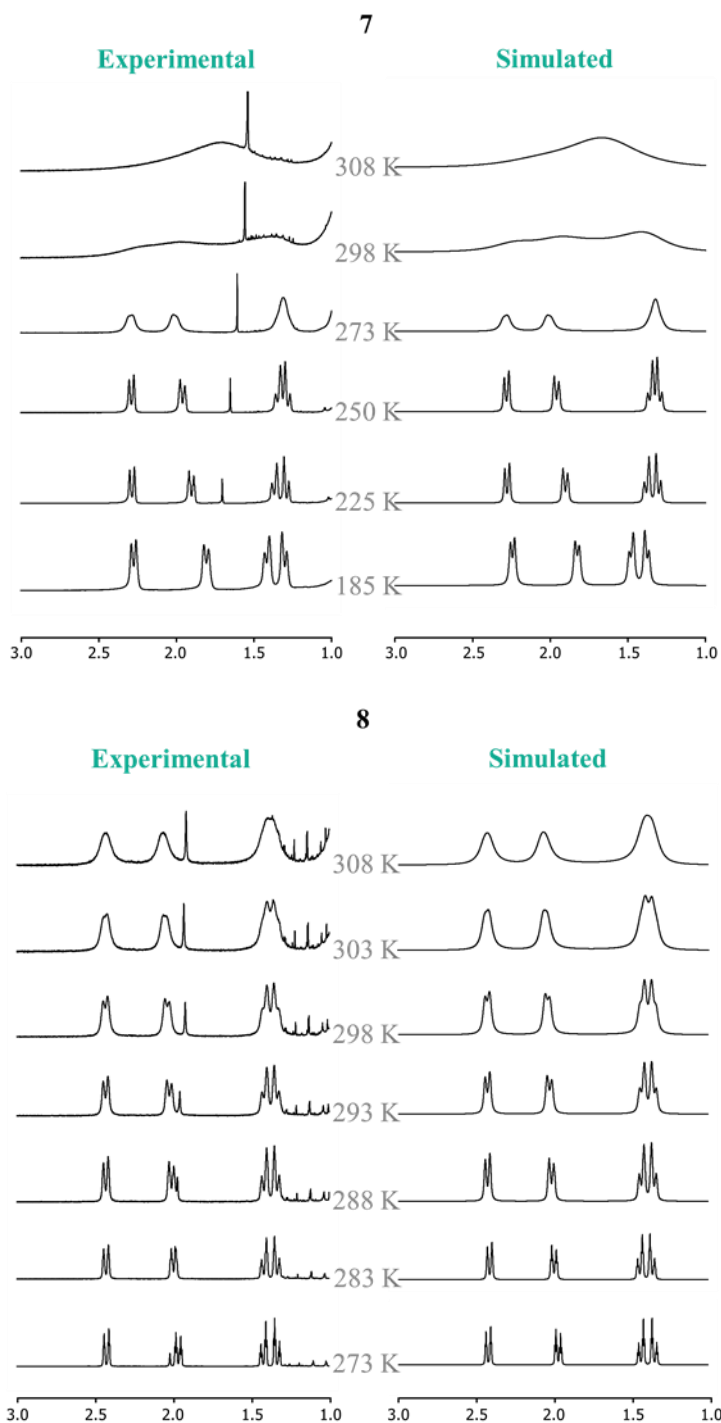
Figure 2.12. *Experimental (left) versus simulated (right) variable temperature ¹H NMR spectra (CD₂Cl₂, 500 MHz) for complexes **7** (top) and **8** (bottom).*

It can be seen from the stacked spectra of both complexes **7** and **8** that the lower frequency *tert*-butyl resonances (δ_H 0.48, **7**; 0.46, **8** at 185 K) display hindered rotation between 250 K

and 185 K. This hindered rotation about the C-C bond of one pair of *neo*pentyl chains is reminiscent of the hindered *tert*-butyl rotation observed in the PNP-*t*Bu systems **A155** and **A157**. Because of the lack of any signals notably shifted to an appreciably low frequency, it was concluded that this is less a consequence of a solution-persistent agostic interaction with this *tert*-butyl group, but is more likely a steric effect, resulting from its close proximity to the now restricted biphenyl ligand. The same may apply to these PNP-Np complexes. Moreover, the lower frequency *tert*-butyl group is assigned as that proximal to biphenyl by NOESY/ROESY experiments at 200 K, further supporting the conclusion that this hindered rotation arises from steric buttressing against biphenyl. By extension, the broadening of the higher frequency *tert*-butyl resonances could, therefore, be a result of the increased freedom of these groups, positioned over the vacant coordination site.

Analysis of the ^{31}P{^{1}H} NMR spectra (**Figure 2.13**) indicate only a small shift of 4 ppm (**7**) and 2 ppm (**8**) downfield with decreasing temperature, indicating that time-averaged C_1-symmetry is not conferred by an agostic interaction (or backbone puckering). However, noticeable broadening at 185 K is evident, in contrast to the PNP-*t*Bu systems, where sharp resonances are observed across the temperature range. This could be an early sign of the manifestation of an agostic interaction, although this is not supported by the other data.
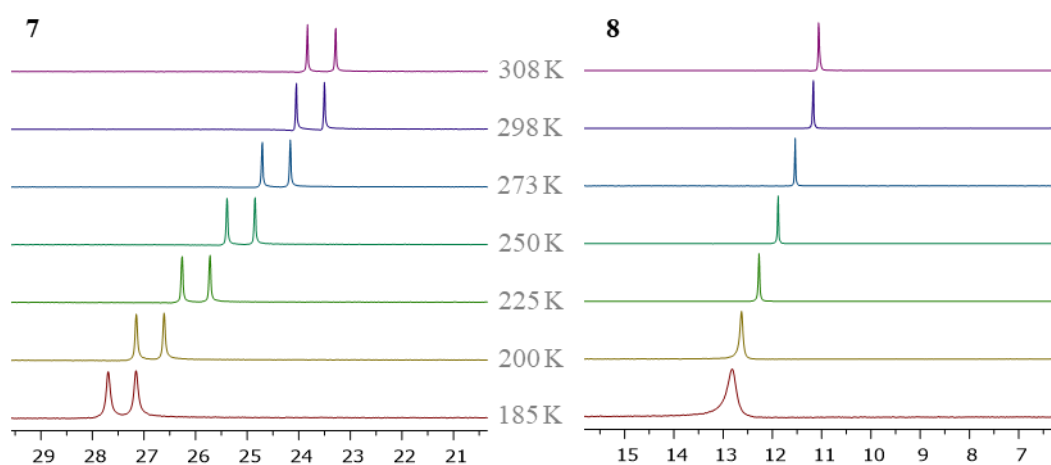
Figure 2.13. *Stacked variable temperature ^{31}P{^{1}H} NMR spectra, collected between 185-308 K (CD$_2$Cl$_2$, 202 MHz), for complexes **7** (left) and **8** (right).*

These findings would suggest that although there is convincing evidence for agostic interactions in the PNP-Np complexes in the solid state (*cf.* the PNP-*t*Bu complexes), there is no evidence to suggest that these are persistent in solution on the NMR timescale. The interchange between coordination of C-H bonds from the opposing phosphine donors is very rapid, even at the lower temperature limit of this experiment. Both pincer systems display similar solution-state dynamics, in which backbone puckering is also too rapid to be observed on the NMR timescale (even at low temperatures) and the vacant coordination site at the metal

is occupied by the dynamic biphenyl ligand in complexes approaching trigonal bipyramidal geometry. This pseudorotation is apparently more facile in the rhodium systems, with little differences observed between the PNP-^{t}Bu and PNP-Np systems. The fact that iridium complex **8** is likely to possess a stronger δ-agostic interaction may contribute to its higher activation energy barrier for biphenyl pseudorotation, although this is also exhibited by **A157**, which does not possess a significant agostic interaction.

The solution-state pseudorotation of the biphenyl ligand and the formation of agostic interactions stabilises these 16-electron M(III) d^6 complexes, allowing them to be isolated. Satisfaction of the 18-electron rule (see **Appendix**) can subsequently be achieved by additional coordination of two-electron donors (*vide infra*).

2.7. <u>Reactivity of [M(PNP-Np)(biph)][BAr$^F_4$]</u>

In order to prevent rotation of the biphenyl ligand and disrupt the agostic interactions observed in the solid state (and thereby satisfying the 18-electron rule), occupation of the vacant coordination site by a carbon monoxide ligand was pursued. This was also of interest to probe the electronic properties of these complexes. Unlike in the analogous PNP-^{t}Bu system, where only iridium complex **A157** reacted with carbon monoxide after 6 hours to give six-coordinate **A161** (**Scheme 2.7**), degassed 1,2-difluorobenzene solutions of both **7** and **8** immediately decolourised upon exposure to 1 bar of carbon monoxide at ambient temperature, and the formation of carbonyl complexes **9** and **10** was confirmed by ^{1}H, ^{13}C{^{1}H} and ^{31}P{^{1}H} NMR spectroscopy. Crystalline samples of **9** and **10** were obtained by slow diffusion of hexane into dichloromethane solutions at ambient temperature, enabling characterisation by XRD, and these complexes were additionally characterised by IR spectroscopy, HR ESI-MS and elemental analysis (**10** only). Both complexes were obtained in good yield (71 % **9**, 73 % **10**), although some dissociation of the carbonyl ligand in **9** was observed, leading to reformation of complex **7** (*vide infra*).

M = Rh, R = Np **7**
M = Ir, R = ^{t}Bu **A157**; Np **8**

M = Rh, R = Np **9** 71 %
M = Ir, R = ^{t}Bu **A161**; Np **10** 73 %
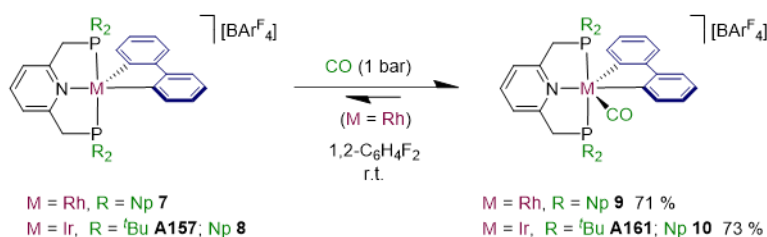
Scheme 2.7. Reaction of 5-coordinate complexes 7, 8 and A157 with carbon monoxide, to give the six-coordinate adducts 9, 10 and A161.[181]

The ^{31}P{^{1}H} spectra of both complexes exhibit single resonances (δ_P 23.2, d, $^1J_{RhP}$ = 97 Hz, **9**; −7.1, s, **10**), shifted to lower frequencies from those of the precursors (δ_P 23.8, d, $^1J_{RhP}$ = 97 Hz, **7**; 11.2, s, **8**). The ^{1}H NMR spectra are indicative of C$_s$-symmetric structures, consistent with their assignment as six-coordinate species. Analysis of the HR ESI-MS ([M −CO]$^+$, 706.3163 (calcd 706. 3172) *m/z*, **9**; [M]$^+$, 824.3691 (calcd 824.3698) *m/z*, **10**) indicated that carbonyl dissociation may be occurring in complex **9**, which could explain why the molecular ion of **7** is detected, whereas **10** is detected as the expected molecular ion. This would be consistent with a more weakly bound carbonyl ligand in **9**. In order to quantify this, a solution of **9** in 1,2-difluorobenzene was monitored for dissociation of carbonyl. The complex was stable in solution under 1 bar of carbon monoxide and showed no signs of decomposition over the course of two weeks when the atmosphere was replaced with argon. However, exposure of this complex to vacuum, or a dynamic atmosphere of argon for prolonged periods (as was required during the work-up and recrystallisation stages), leads to dissociation of the carbonyl. Complex **9** can be reformed by exposure of the mixture to 1 bar of carbon monoxide.

Figure 2.14 shows the solid-state structures of complexes **9** and **10**. Both suffer from significant crystallographic issues and so were only used to confirm connectivity, suggesting distorted octahedral geometries in both cases, with occupation of the vacant coordination site by a carbonyl ligand. This is fully consistent with the solution-state data.
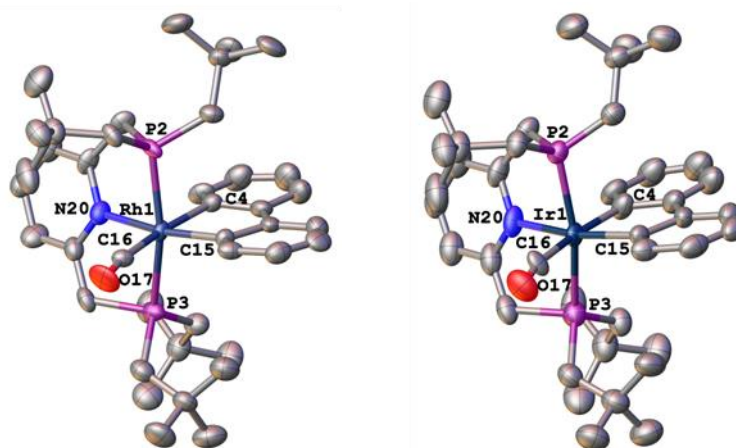
*Figure 2.14. Solid-state structures of **9** (left) and **10** (right), determined at 150 K. Atomic displacement parameters are drawn at 50 % probability. Hydrogens and counterions are omitted for clarity. Structures suffer from crystallographic issues and so are only used to confirm connectivity.*

Analysis of the IR spectra of **9** and **10** shows ν_{CO} to be higher than those reported for the M(I) analogues, consistent with formation of M(III) centres (**Table 2.4**). Unlike in the case of the M(I) carbonyls, the carbonyl stretching band of iridium complex **10** is almost identical to that reported for the PNP-^{t}Bu congener **A161** ($\Delta\nu_{CO} = 1$ cm^{-1}). This observation is in line with that of M(I) carbonyls displaying a more straightforward relationship with pincer donor strength than related M(III) carbonyls.[187] Rhodium complex **9** displays a much higher carbonyl stretching frequency than iridium complex **10** ($\Delta\nu_{CO} = 29$ cm^{-1}, *cf.* 13 cm^{-1} in the M(I) systems), further substantiating the conclusion that the carbonyl is more weakly bound in **9**.

*Table 2.4. Carbonyl stretching frequencies of M(III) complexes **9** and **10** versus M(I) complexes **2** and **3**, with PNP-^{t}Bu complexes **A160** and **A161** for comparison,[184] measured in CH$_2$Cl$_2$.*

Complex	ν_{CO} / cm^{-1}
[Ir(PNP-^{t}Bu)(CO)][BAr$^F_4$] / **A160**	1977
[Ir(PNP-^{t}Bu)(biph)(CO)][BAr$^F_4$] / **A161**	2028
[Rh(PNP-Np)(CO)][BAr$^F_4$] / **2**	2004
[Ir(PNP-Np)(CO)][BAr$^F_4$] / **3**	1991
[Rh(PNP-Np)(biph)(CO)][BAr$^F_4$] / **9**	2056
[Ir(PNP-Np)(biph)(CO)][BAr$^F_4$] / **10**	2027

The ease with which these carbonyl complexes are prepared, when compared with **A155** and **A157**, is interesting, given that PNP-Np is a poorer donor than PNP-^{t}Bu. This may result from the decrease in steric congestion at the metal centre, a result of the additional methylene unit present in *neo*pentyl but not *tert*-butyl.

In order to ascertain whether these systems could be used as a convenient starting point for further exploring the reactivity of PNP-Np, it was of interest to attempt hydrogenolysis of the biphenyl ligand. Attempts to react PNP-Np with precursors such as [Rh(cod)$_2$][BAr$^F_4$], [Rh(coe)$_2$Cl]$_2$, [Rh(PPh$_3$)$_3$Cl] and [Rh(C$_2$H$_4$)$_2$Cl]$_2$, to investigate the rhodium coordination chemistry of this relatively unexplored ligand, were inconclusive. Therefore, the removal of biphenyl and formation of hydride species was pursued.

A fluorobenzene solution of iridium complex **8** was placed under 1 bar of dihydrogen and heated to 80 °C for 16 hours (**Scheme 2.8**). Again, this reaction is more facile than for the PNP-^{t}Bu analogue **A157**. *In situ* NMR spectroscopic data of the completed reaction mixture suggest formation of complex **11**, displaying a single, broad hydride resonance (−23.04 ppm, fwhm = 142.2 Hz) and a broad ^{31}P resonance (7.9 ppm, fwhm = 96 Hz). The complex has been tentatively assigned as a classical dihydride with an additional coordinated dihydrogen molecule,[178] although a classical tetrahydride is also a possibility, given the high degree of fluxionality on the NMR timescale.[183] However, a fluxional process that results in all hydrides being equivalent may not necessarily proceed *via* a tetrahydride intermediate (*i.e.* σ-bond metathesis may be operating).[194] Upon degassing, the additional dihydrogen molecule dissociates and the dihydride complex **12** is formed. The ^{31}P resonance resolves into a triplet (8.15 ppm, $^1J_{PH}$ = 13 Hz), as does the hydride ^{1}H resonance (−23.09 ppm, $^1J_{PH}$ = 14 Hz). Complex **12** was isolated and characterised by ^{1}H, ^{13}C{^{1}H} and ^{31}P{^{1}H} NMR and IR spectroscopy, HR ESI-MS and XRD. The data are consistent with those reported for [BF$_4$]$^-$ analogue **A50**.[64]
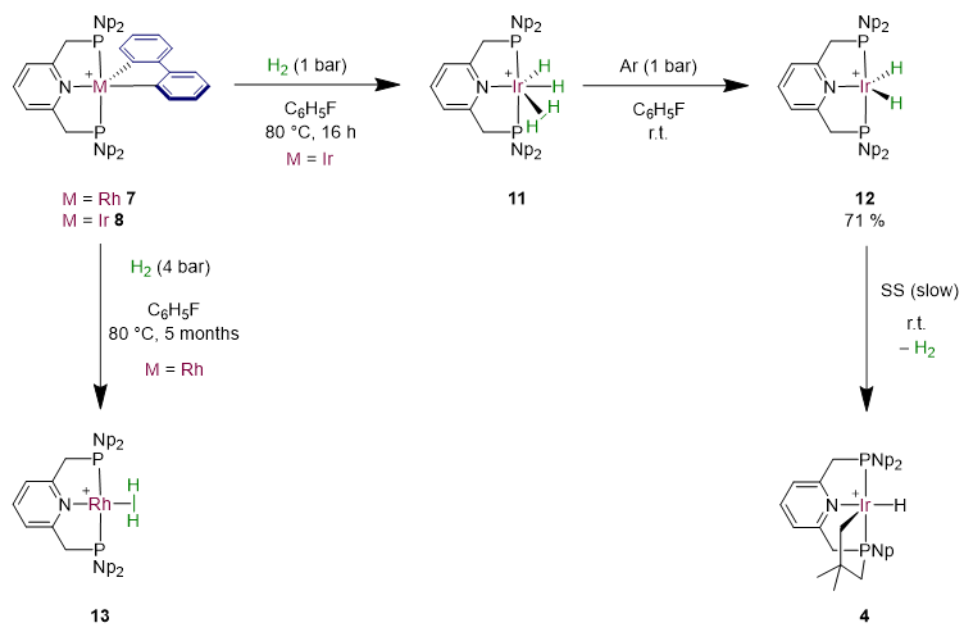
Scheme 2.8. *Hydrogenolysis of biphenyl in complexes 7 and 8, to give dihydride 12 (M = Ir) and dihydrogen complex 13 (M = Rh). [BAR$^F_4$]$^-$ counterions are omitted for clarity.*

Characteristic NMR spectroscopic features include a single ^{31}P resonance at 9.2 ppm (as in **A50**) and the hydride resonance, which appears as a doublet in the ^{1}H NMR spectrum (δ_H −23.05, ^{1}J$_{PH}$ = 14 Hz, *cf.* −23.19, ^{1}J$_{PH}$ = 14 Hz for **A50**). Single crystals of complex **12** were obtained from slow diffusion of hexane into a fluorobenzene solution. It was found to crystallise with one molecule of fluorobenzene and half a molecule of hexane in the unit cell, and the solid-state structure is shown in **Figure 2.15**. As expected, the distorted square pyramidal structure is very similar to that reported by Yamashita and Nozaki for the [BF$_4$]$^-$ analogue, **A50**. As seen in the majority of complexes discussed here, the pyridine backbone exhibits a torsion angle of 16.1(1) ° from the plane defined by the donor groups. Again, a δ-agostic interaction stabilises this formally 16-electron complex and this is evident by the short Ir1-C30 contact of 2.739(3) Å (*cf.* 2.729 and 2.828 Å for the reported two independent cations of **A50**) and the reduced Ir1-P2-C28 angle of 108.13(8). [146,147,149] This is further substantiated by a weak, broad signal in the ATR IR spectrum around 2588 cm^{-1}, corresponding to this agostic interaction. In addition to the data collected above, a T_1 NMR experiment was also performed: T_1 = 851 ms (298 K, 600 MHz), confirming the assignment of **12** as a classical dihydride complex. [195] This is analogous to the reactivity demonstrated by PNP-^{t}Bu complex **A157**. Interestingly, complex **12** was found to slowly evolve dihydrogen in the solid-state, reforming cyclometallated complex **4** (~10 % after 7 months). Placing a fluorobenzene solution of this mixture back under one bar of dihydrogen reformed complex **12** after 16 hours, analogous to Yamashita and Nozaki's procedure for the formation of **A50** from **A45**.
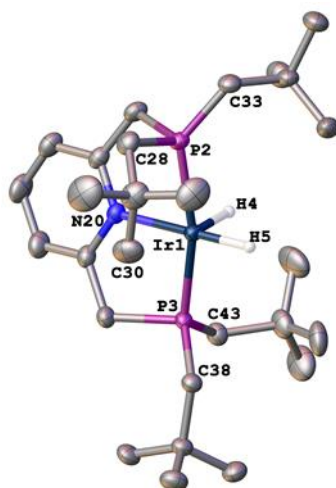
Figure 2.15. *Solid-state structure of dihydride **12**, determined at 150 K. Atomic displacement parameters are drawn at 50 % probability. Hydrogens (except H4 and H5), solvent and counterions are omitted for clarity. The positions of the hydrides (H4 and H5) have been freely refined. Selected bond distances (Å) and (°): Ir1-P2 2.2774(8), Ir1-P3 2.2861(8), Ir1-N20 2.140(2), Ir1-H4 1.46(3), Ir1-H5 1.52(3), Ir1-C30 2.739(3); P2-Ir1-P3 164.84(3), N20-Ir1-H5 176(1), Ir1-P2-C28 108.13(8), Ir1-P2-C33 132.34(8), Ir1-P3-C38 115.41(7), Ir1-P3-C43 120.68(8).*

Where hydrogenolysis of biphenyl in rhodium complex **A155** was not possible, heating a fluorobenzene solution of **7** at 80 °C resulted in a very slow reaction. The solution was periodically freeze-pump-thaw degassed and backfilled with 4 bar of dihydrogen over 5 months. The reaction stalled at around 90 % completion and was analysed by ^{1}H and ^{31}P{^{1}H} NMR spectroscopy *in situ*. A new doublet in the ^{31}P{^{1}H} spectrum, at 16.4 ppm ($^1J_{RhP} = 120$ Hz), is seen, alongside a hydride in the ^{1}H spectrum at −11.00 ppm (dm, $^1J_{RhH} = 29$ Hz). It is proposed that this is a molecular dihydrogen complex (**13**, **Scheme 2.8**), as with macrocyclic PNP-14 systems **A152** and **A153** (**Figure 2.4**).[179] Although speculative, LR ESI-MS data indicates the presence of 14-electron fragment "[Rh(PNP-Np)]$^+$", alongside its dinitrogen and acetonitrile adducts, as the major components, suggesting the dihydrogen molecule is weakly bound. This fragment is also observed alongside the molecular ion in HR ESI-MS. Attempts to characterise complex **13** in CD$_2$Cl$_2$ resulted in a third, rhodium-coupled ^{31}P{^{1}H} NMR resonance growing in, with a new hydride resonance, displaying complex multiplicity, in the ^{1}H NMR spectrum. After four days, decomposition to an intractable mixture occurred, with no evidence for complex **13** remaining. This is attributed to activation of CD$_2$Cl$_2$, also observed for the related PNP-^{t}Bu complex **A33** (**Section 1.2.2**).[57] However, unlike **A33**, exposure of this product mixture to dihydrogen does not reform dihydrogen complex **13**.

These observations contribute to the known reactivity of PNP-Np but were not pursued any further as iridium complexes **12**/**A50** can be prepared more easily from the cyclometallated precursors **3**/**A45** and the procedure by which rhodium complex **13** is formed is not a viable synthetic route.

2.8. <u>Summary and Conclusions</u>

The overarching aim of this study was to apply the principles of ligand design to the pursuit of agostic interactions in five-coordinate biphenyl complexes. Analysis was conducted on the role played by the pincer ligand and, in particular, the *tert*-butyl substituents, in the previously reported PNP-*t*Bu complexes. This, along with the lack of conclusive evidence for agostic formation in these complexes, led us to consider how the system could be modified to encourage the formation of stronger agostics. PNP-Np was suggested as an alternative pincer ligand: it was hypothesised that the increased flexibility of *neo*pentyl (*cf. tert*-butyl) may allow for the formation of agostic interactions in its coordinatively unsaturated group 9 complexes.

This was, indeed, borne out in the observation of short M-C contacts (<3 Å) and reduced M-P-C angles, which indicate stronger agostic interactions than are implied by the bond metrics of the respective PNP-*t*Bu systems. This is further supported by the observation of broad C-H stretches in the ATR IR spectra at reduced wavenumbers. The lower frequency C-H stretch in the iridium system suggests a stronger agostic interaction in this complex. These bands were notably absent from the IR spectra of the PNP-*t*Bu complexes, and allow us to conclude that in this case, the interesting geometric features are not just a consequence of steric buttressing.

Despite the evidence for a stronger agostic interaction in the solid state, the PNP-Np and PNP-*t*Bu systems behave similarly in solution, displaying dynamics attributed to pseudorotation of the biphenyl ligand on the NMR timescale, along with rotation of unhindered *tert*-butyl groups. From this, it can be inferred that (on the NMR timescale at the temperatures investigated) interchange between agostic interactions from the opposing phosphorus donors is extremely rapid, conferring time-averaged C_s symmetry (when the biphenyl rotation is frozen out). The onset of decoalescence of the time-averaged resonances (a consequence of biphenyl pseudorotation) occurs at a higher temperature in the iridium system, which may be a consequence of the stronger agostic interaction in this complex.

In contrast to the *tert*-butyl analogues, the M(III) carbonyl complexes of PNP-Np were easily prepared. Moreover, synthesis of the iridium(III) dihydride was relatively easy to achieve *via* biphenyl hydrogenolysis, and significant conversion to the (albeit unstable) rhodium(I) dihydrogen complex was observed. This is interesting given that analysis of the carbonyl stretching frequencies of M(I) carbonyls of PNP-Np and PNP-*t*Bu (M = rhodium, iridium) suggest that PNP-Np is a poorer donor. This difference in reactivity between may be a consequence of the steric differences between the pincer ligands.

The results presented here highlight the importance of considering principles of ligand design when attempting to investigate weak interactions, such as agostics. They also demonstrate the versatility of pincer ligands and how the fine-tuning of substituents can allow

for subtle changes in the reactivity of their complexes. The group 9 coordination chemistry of PNP-^{t}Bu has, at this point, been very thoroughly investigated. The promising results obtained here suggest that there is potential for further comparison of the chemistry of these two pincer ligands, if the difficulties in exploring the rhodium chemistry of PNP-Np can be overcome. It would also be interesting to attempt the synthesis of as-yet unreported PONOP-Np, so additional comparisons can be made and a greater understanding of the effect of the additional methylene unit on the formation of agostic interactions in these complexes could be gathered. Finally, further work in this area could include DFT analysis, such as NBO or QTAIM analysis, of the bonding situations in the five-coordinate biphenyl complexes, to gain more information about the agostic interactions discussed here.

3. Synthesis of a Cavitand-Derived Pincer Ligand

The synthesis of a σ-alkane complex which is stable enough to be characterised in both the solid state and solution, remains a key challenge in organometallic chemistry. Inspired by Diederich's reports of resorcinarene alkane binding, Weller's solid-state σ-alkane complexes that are stabilised through interactions with the microenvironment, and Brookhart's seminal pincer-supported σ-methane complex, a resorcinarene-derived pincer ligand was designed. This should provide rigidity and stability at a metal centre, whilst enabling alkane encapsulation within the metal coordination sphere. This chapter describes the development and implementation of a synthetic route to this new ligand, along with characterisation of intermediate species and details of the challenges that were overcome during this process. Some initial coordination chemistry was also performed, leading to the formation of a Rh(I) carbonyl complex and a tentatively assigned Rh(III) carbonyl dichloride.
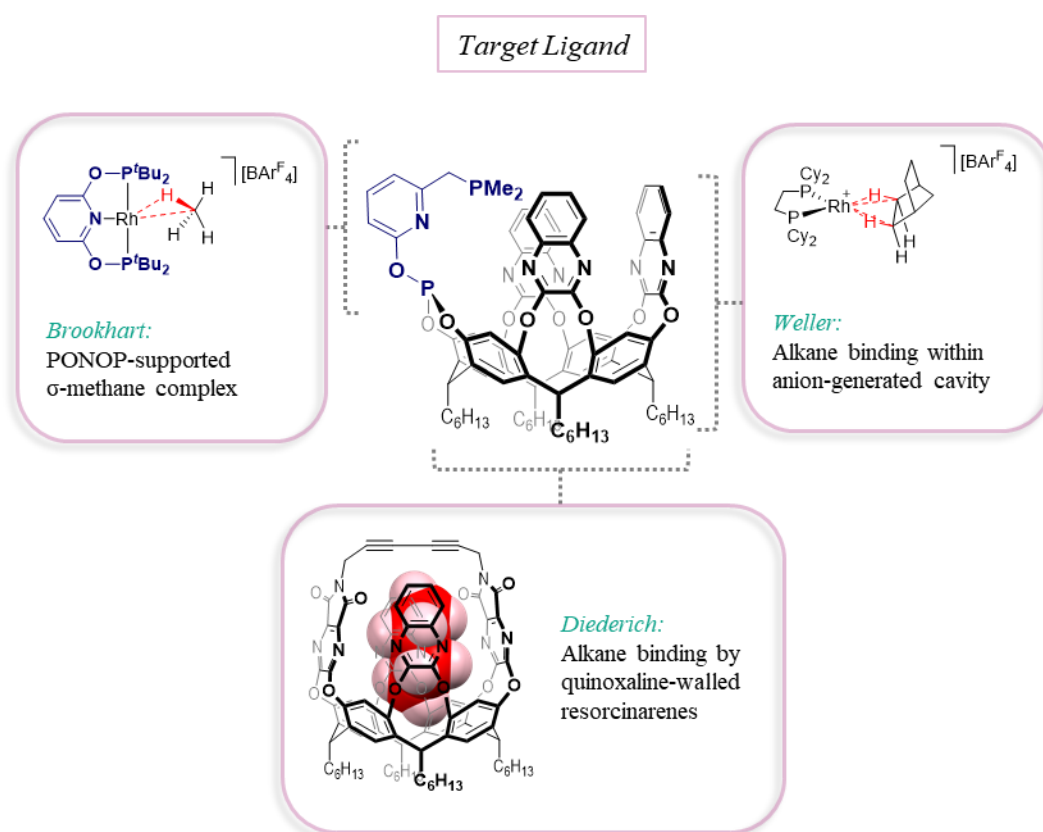
3.1. Introduction

3.1.1. σ-Alkane Complexes

As discussed in **Section 2.1.1**, the ability to selectively functionalise a hydrocarbon *via* transition metal-catalysed C-H activation, is an incredibly important process, with a wide range of current and potential applications.[138] The intermediate C-H-ligated species can be studied in the form of intramolecular, agostic interactions, but isolation of a complex in which an intermolecular C-H bond interacts with the metal centre (a σ-alkane complex) is harder to achieve.[134-137,140,144,145] Attempts to study σ-alkane complexes in solution have been hampered by their instability. The low temperatures required, and the short lifetimes of these alkane complexes (because of the tendency of the alkane to be displaced by solvent, or undergo C-H activation) is problematic, hindering characterisation using techniques that generally require higher temperatures and long data collection times.

The first σ-alkane complexes to be reported were synthesised, albeit unintentionally, in low temperature matrix isolation experiments. In these experiments, transition metal carbonyl complexes were subjected to photolysis in varying matrices,[196] including noble gases and alkanes, to generate and observe coordinatively unsaturated species.[197-205] From these initial reports, photolysis experiments in alkane solutions[203,206-226] and in the gas phase[227-229] were also performed. The majority of these complexes were identified by shifts of the carbonyl bands in their IR or UV-visible spectra, suggesting consumption of the starting complex and formation of a new species in which the vacant coordination site has been occupied by alkane. Later developments included reports of ^{1}H and ^{13}C NMR spectroscopic evidence for σ-alkane complexes, enabling the M-(H-C) interaction to be directly confirmed.[214,216,220-226,230,231]

3.1.2. Characterisation of σ-Alkane Complexes in Solution

The NMR spectroscopic investigations into σ-alkane complexes in solution include complexes **A162-A166**, reported by Geftakis, Ball and Hill (**Figure 3.1**).[216,225,226]
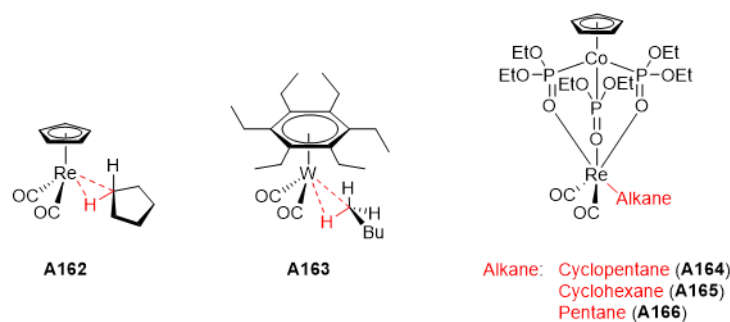
Figure 3.1. *Selected examples of σ-alkane complexes studied by NMR spectroscopy.[216,225,226]*

However, despite the numerous reports of σ-alkane complexes in solution, a well-characterised complex of the simplest alkane, methane, remained elusive. Brookhart and co-workers were able to fill in this gap, using a different strategy. Here, protonation of the methyl ligand of complex **A167** generates methane in the metal coordination sphere, to give the relatively long-lived σ-methane complex **A168** (**Scheme 3.1**).[232] Prior to this, protonation of the iridium congener instead gave a methyl hydride complex.[233] Site exchange of the hydride and methyl protons indicated that dynamic reductive elimination and C-H activation processes must be occurring, necessarily proceeding *via* a σ-alkane complex. C-H activation is less favoured in the rhodium system, allowing the alkane complex to be observed.
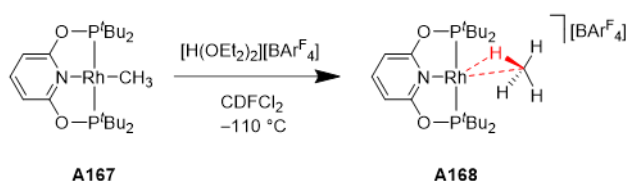
Scheme 3.1. *Protonation of a methyl ligand to generate σ-methane complex **A168**.[232]*

NMR characterisation of the ^{13}C-labelled complex revealed a significantly shielded ^{13}C NMR resonance (when compared with the starting complex and the iridium methyl hydride system) at −41.7 ppm, suggesting a C-H σ-interaction with the metal centre. The quintet multiplicity displayed a $^1J_{CH}$ coupling constant of 124 Hz, suggesting that the protons are in rapid exchange. Whilst the iridium methyl hydride cation also displays a quintet ^{13}C resonance for the methyl carbon, this has a much smaller coupling constant. The value of 124 Hz is similar to that recorded for free methane in CDFCl$_2$ solution (125 Hz). Upon proton decoupling, the ^{13}C{^{1}H} NMR signal collapses to a broad singlet, with no resolvable rhodium or phosphorus coupling, suggesting a weak interaction between the methane carbon and the metal fragment. In the ^{1}H NMR spectrum, a broad doublet at −0.86 ppm ($^1J_{RhH}$ = 6.3 Hz) correlates to the labelled methane carbon. This data supports the assignment of a methane complex in which a C-H bond is bound to rhodium, and the structure was further supported by DFT calculations.

This methodology was then extended to include the corresponding ethane complex, with protonation of **A169** yielding **A170** (**Scheme 3.2**).[234] However, **A170** was found to be less stable than **A168**, a result of the larger steric profile of ethane compared to methane. The *tert*-butyl groups of the pincer phosphines create a small binding pocket at rhodium, into which methane fits well. However, the extra methyl group of ethane clashes with the *tert*-butyl substituents. The NMR spectroscopic data support the assignment of this compound as a σ-ethane complex. In a series of VT experiments, the ^{13}C signals broaden on warming, indicative of chain walking of the metal fragment between the two carbons. The structure of this complex was further substantiated by DFT calculations.
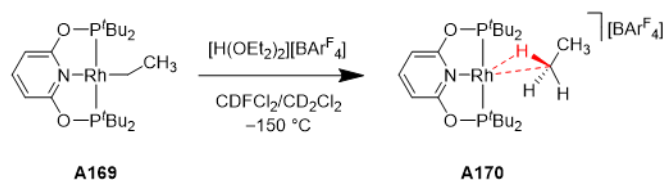
*Scheme 3.2. Protonation of an ethyl ligand to generate the more unstable σ-ethyl complex **A170**.[234]*

Brookhart's system is important in the context of this chapter, forming a key part of the strategy employed in the design of the new ligand (see **Section 3.2**). However, it should be noted that a series of group 8 σ-methane complexes were reported by Ball and co-workers in 2022.[135,136] Here, the complexes [M(Cp)(CO)$_3$][Al(OC(CF$_3$)$_3$)$_4$] (M = Fe **A171**, Ru **A172**, Os **A173**, Cp = cyclopentadienyl, **Figure 3.2**) were irradiated at −90 °C in HFP solution (HFP = 111,333-hexafluoropropane), in the presence of methane, to form the corresponding methane complexes. The first of these, osmium complex **A173**,[135] was shown to be stable for 13.5 hours at -90 °C. This makes it the most stable σ-methane complex so far reported. The analogous **A171** and **A172** were only persistent under continuous irradiation.

M = Fe (**A171**)
Ru (**A172**)
Os (**A173**)
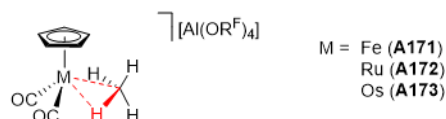
*Figure 3.2. σ-Methane complexes **A171-A173**, reported by Ball.[135,136] OR^F = OC(CF$_3$)$_3$.*

This method is akin to that described earlier in this section, unlike Brookhart's method of generating methane in the metal coordination sphere. The methyl protonation methodology is relatively simple by comparison, and still marks a significant development in the field. The PONOP-^{t}Bu framework appears to be suitable for stabilising bound alkanes at rhodium. Pincer ligands, such as this, are particularly useful because of their robust nature. The rigid backbone often allows their complexes to withstand higher temperatures and pressures than related complexes and the large steric profile covers a considerable part of the metal coordination sphere.[36-43] This gives control over vacant sites - a particularly useful feature in this case. In addition to this, a rigid pincer is thought to be more suitable for stabilising a metal at the entrance to a resorcinarene cavity.

3.1.3. Characterisation of σ-Alkane Complexes in the Solid State

Prior to 2012, there were only limited examples of alkanes residing within the coordination sphere of a metal, such as an iron(II) porphyrin in which a molecule of heptane is encapsulated.[237] This interaction could not be probed in detail due to crystallographic disorder. Other examples involve coordination at a uranium centre[238] and alkane-iron(II) interactions within a metal-organic framework.[239] However, in recent years, significant developments have occurred, which have changed the way the synthesis of σ-alkane complexes is approached.

Weller has reported a new method of single-crystal-to-single-crystal (SC-SC) hydrogenation, enabling rhodium(I) diene complexes $[Rh(L_2)(diene)][BAr^F_4]$ (($BAr^F_4 = B[3,5-(CF_3)_2C_6H_3]_4$) to be transformed into the corresponding alkane complexes in the solid state (exemplified in **Scheme 3.3**, with the hydrogenation of **A174** to give **A175**).[240-257] The benefit of using this method is that it allows for the synthesis of crystalline material, enabling detailed structural analysis to be undertaken and making them some of the most fully characterised σ-alkane complexes to date. It has also been proved to be a very versatile method, leading to the development of the field of solid-state organometallic (SMOM) chemistry.
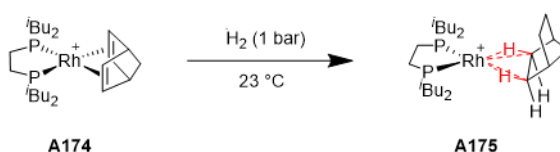
*Scheme 3.3. Solid-state hydrogenation of [Rh(L₂)(diene)][BAr^F₄] (e.g. **A174**) to give the corresponding alkane complex (e.g. **A175**). Here, L₂ = ^iBu₂P-(CH₂)₂-P^iBu₂, diene = norbornadiene/NBD.[240] [BAr^F₄]⁻ counterions are omitted for clarity.*

Figure 3.3 shows the range of σ-alkane complexes that have been synthesised *via* this method, with variation of the phosphine backbone length (and, therefore, bite angle, **A139**-**A141**, **A176**),[152,241] phosphine substituents (**A184**-**A186**)[241,247] and anion.[241,248] Complexes of other alkanes (of varying stability) were synthesised, including cyclooctane (COA, **A138**),[152] pentane (**A177**),[244] *iso*-butane (**A178**), cyclohexane (**A179**),[250] propane (**A180**), 2-methylbutane (**A181**), hexane (**A182**) and 3-methylpentane (**A183**).[255] Other interesting examples include a cobalt complex (**A187**)[252] and an air-stable complex with a polymer interface.[253] These alkane complexes can undergo processes such as H/D exchange,[245,246,249,250,256] acceptorless dehydrogenation[250,255] and ligand exchange.[242,246] Some are effective catalysts for the isomerisation of 1-butene to *cis-* and *trans*-2-butene, *via* displacement of the bound alkane, under industrially relevant conditions.[246,249,251,254]

In all of these examples, the key to the stability (*i.e.* the exclusion of solvent, which prevents alkane displacement) and the reactivity displayed by these complexes is a result of the extended environment around the rhodium cation. In the majority of cases, the $[BAr^F_4]^-$ anions are arranged in a pseudo-octahedral arrangement (in some cases this takes the form of a bi-capped square prism), with the alkane sitting in a cleft defined by two aryl faces of the anion. This provides a tertiary periodic molecular framework and a secondary microenvironment around the cationic fragment. Encapsulation of the alkane within this environment (and the metal coordination sphere) allows for the formation of stabilising non-covalent interactions (NCIs), such as van der Waals interactions, non-classical $C-H^{\delta+}$---$F^{\delta-}$-C hydrogen-bonds and C-H---C interactions, which support the primary Rh-H-C interactions. Weller has concluded that the stability of σ-alkane complexes depends upon

several factors: (i) the strength of the Rh-H-C interactions, (ii) the presence NCIs with the secondary microenvironment (iii) how the alkane fits into the binding pocket and (iv) the tertiary, periodic crystal structure. This environment is important as it allows long range order to be maintained, whilst providing the necessary flexibility at the coordination site. The trifluoromethyl groups also provide hydrophobic pathways through the lattice. This relationship of the ligand with the primary, secondary and tertiary environments is reminiscent of metalloenzyme catalysis.[254] It was demonstrated that NCIs with the secondary microenvironment can influence the orientation and regioselectivity of alkane binding,[249,254] and that the microenvironment is flexible enough to allow structural change, such as rotation, of both the organic[241] and cationic[247] fragments upon hydrogenation.
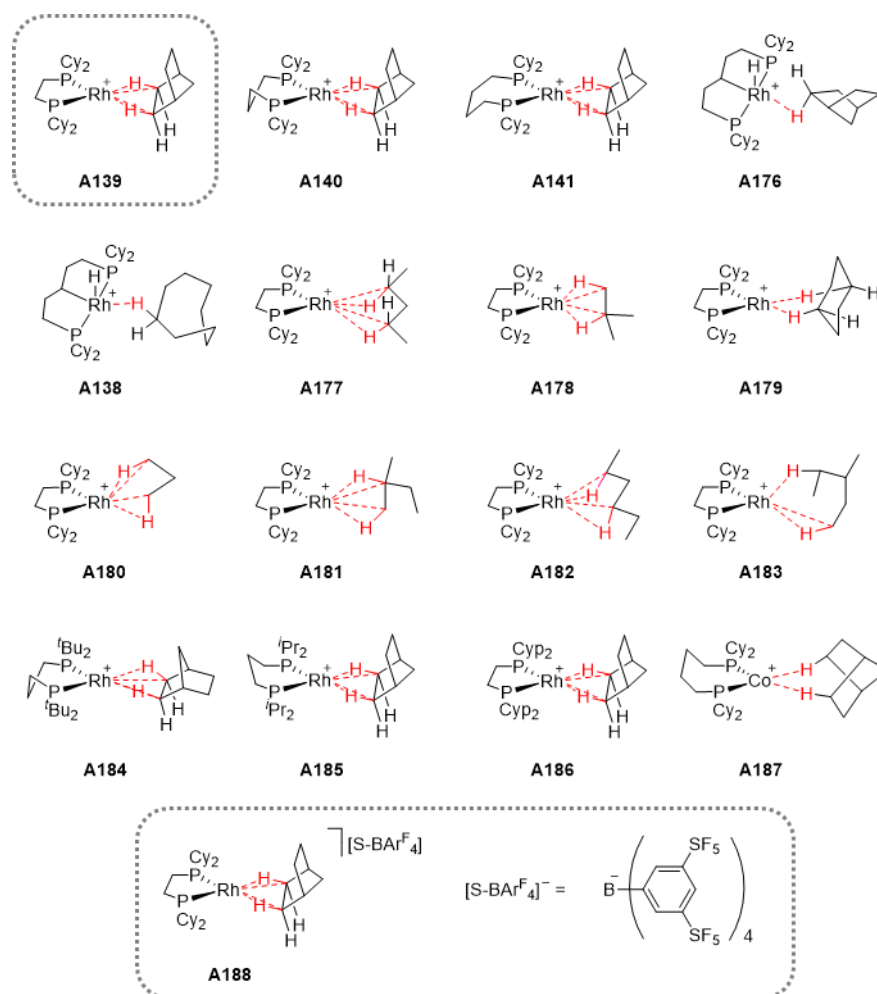
Figure 3.3. *Solid-state -alkane complexes reported by Weller.[240-257] The most stable systems, **A139** and **A188** are highlighted. [BAr^F_4]^- counterions (in **A138-A141**, **A176-A187**) are omitted for clarity.*

Detailed computational investigations have been carried out to support these experimental findings.[153] Treatment of the isolated cation does not reproduce experimental results as well as when periodic DFT calculations are carried out, taking into account the extended NCI, lattice and packing effects. This confirms that these considerations are necessary to explain the relative stabilities of the complexes and the different alkane binding modes adopted, along

with any reactivity that is displayed. In addition to this, NBO calculations were carried out on a range of systems, which indicate that C-H σ-donation into *trans*-σ*$_{(Rh-P)}$ makes a more significant contribution to alkane bonding than back-donation from a rhodium lone pair (in a $d_π$ orbital) or *cis*-σ$_{(Rh–P)}$ bonding orbital to σ*$_{(C-H)}$.

The σ-alkane complexes reported by Weller show impressive stability when compared to previous examples and microenvironment considerations are likely to have a major impact on the design and synthesis of alkane complexes in the future. However, none of the complexes reported retain the alkane ligand upon dissolution, with a solvent molecule typically displacing the weakly bound alkane. In the most recent development, complex **A188** (**Figure 3.3**) was reported, in which a new weakly-coordinating anion, [S-BAr$^F_4$]$^−$ (S-BAr$^F_4$ = B[3,5-(SF$_5$)$_2$C$_6$H$_3$]$_4$), is utilised.[257] This complex displays higher thermal stability than **A139** and can be suspended in pentane without decomposing for 2 hours. This was attributed to the increased number of C-H$^{δ+}$---F$^{δ−}$-C hydrogen-bonds formed as a result of the different anion and represents a step closer to the exciting prospect of a stable, soluble σ-alkane complex.

3.1.4. Outlook

The series of complexes discussed above are some of the most stable and well-characterised σ-alkane complexes reported to date. The SC-SC solid-state hydrogenation methodology is clearly a useful route to alkane complexes, which can be applied to many variations of the original system. The cavity provided by the [BAr$^F_4$]$^−$ counterion around the vacant coordination site at rhodium is believed to be responsible for the stabilisation of alkanes within the metal coordination sphere and any attempts to synthesise a σ-alkane complex need to take the influence of the extended secondary environment into account. However, attempts to characterise these complexes in solution resulted in displacement of the alkane. The synthesis of an alkane complex that can be characterised in the solid state and also in solution is, therefore, an important challenge and this forms the core aim of the present proposal.

3.2. Ligand Design Rationale

To address the outstanding issue of retention of the C-H σ-interaction upon dissolution of the complex, it is proposed that the stabilising secondary microenvironment could be provided by a permanent, well-defined cavity around the metal centre. This could take the form of a cavitand, and so host-guest interactions would be responsible for stabilising the metal-alkane interaction, as opposed to weak NCIs with a counterion-created cavity, over which there is little synthetic control. Tethering this cavity to a chelating ligand would ensure that the metal centre permanently retains a confined secondary coordination sphere. It was this idea that led to the proposal to design a ligand framework that incorporates a permanent cavity in the form of a resorcinarene.

Resorcinarene was chosen as the basis for this new ligand because of the potential for molecular encapsulation, along with the ease with which aromatic walls (such as quinoxaline) can be added to deepen the cavity, and also cleaved upon treatment with nucleophiles (*e.g.* catechol). Donating groups can then be introduced, so that the cavitand can be accommodated into a ligand framework (**Scheme 3.4**).[127,258] The ability of functionalised resorcinarenes to bind small guest organic molecules has been well investigated.[113] Of relevance here are the investigations of alkane encapsulation within deep-cavity resorcinarenes.[133,259-264]
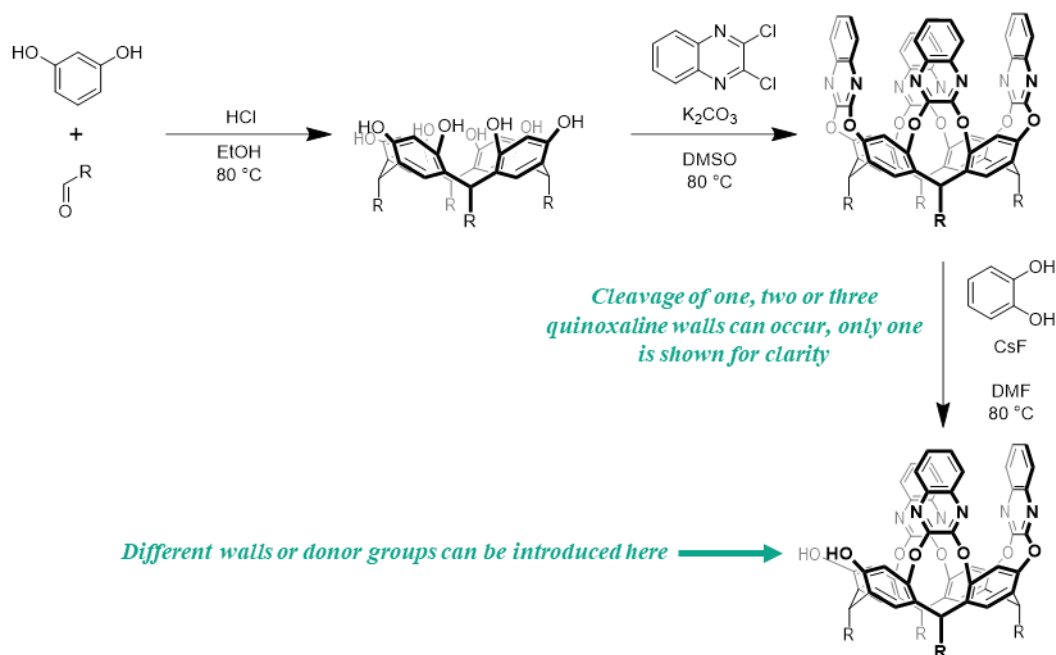
Scheme 3.4. Generalised scheme showing the synthesis of resorcinarene via *the acid catalysed condensation of resorcinol and an aldehyde, followed by introduction of the quinoxaline walls[258] and subsequent nucleophilic cleavage to enable structural modification of the cavitand.[127]*

Diederich has reported resorcinarene-based 'molecular baskets', functionalised with two quinoxaline and two diazaphthalimide walls, the latter of which were bridged by an alkynyl (**A189**-**A190**, **Figure 3.4**)[133,261] or a *para*-xylyl (**A191**-**A193**)[262,263] chain. The bridging of two

trans-disposed walls is beneficial as it enforces a 'vase' conformation, preventing the walls from opening outwards and forming the more open 'kite' conformation. The bridge also caps the cavity, preventing formation of the self-inclusion complexes seen in **Section 1.3.3**.[131] The resulting molecular baskets were shown to bind cycloalkanes in solution. A series of alkanes were investigated, with cyclohexane having the greatest binding strength. The poly(ethylene glycol) substituents of **A193** increase its water solubility, enabling binding studies to be carried out in aqueous media. Alkane encapsulation was inferred from the significant shielding of the ^{1}H NMR signals by the quinoxaline π-cloud. This is also responsible for stabilising the complex, as C-H---π interactions occur between the alkane and the quinoxaline walls. The guests could subsequently be released by protonation: the quinoxaline nitrogens experience repulsion when protonated, and so the walls open out and release the alkane.
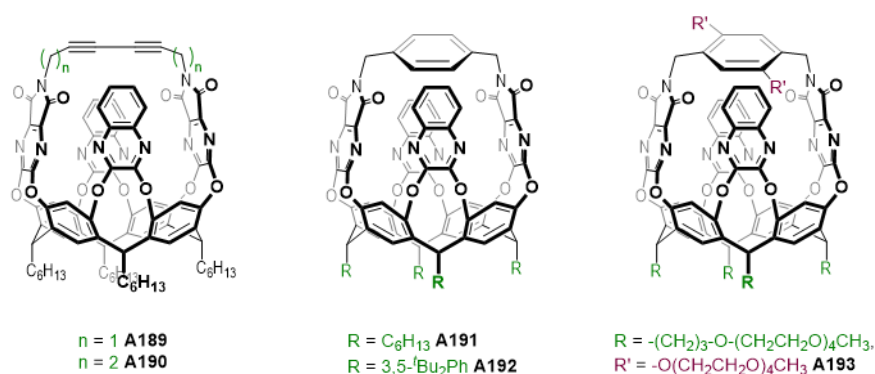
Figure 3.4. Molecular baskets A189-A193, reported by Diederich and investigated in cycloalkane binding studies.[133,261-263]

Alkane binding by substituted resorcinarenes has also been investigated in the Chaplin group.[264] Bisquinoxaline-walled resorcinarenes **A194**-**A196** (**Figure 3.5**) were synthesised and found to bind cyclohexane, when bulky (*i.e.* a poor guest) mesitylene-d_{12} was used as a solvent. The results from Diederich and Chaplin provide a precedent for alkane encapsulation by functionalised resorcinarenes. Inspired by this, a quinoxaline-walled resorcinarene was chosen to provide the well-defined cavity of the new ligand and act as a host for alkanes within a metal coordination sphere.
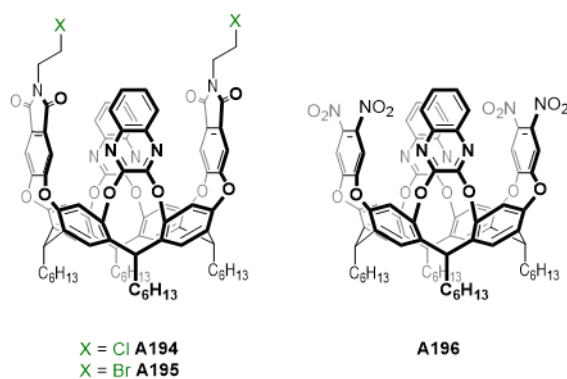
Figure 3.5. Substituted resorcinarenes A194-A196 investigated in cyclohexane binding studies.[264]

Previous work carried out within the Chaplin Group developed this idea, installing a chelating phosphine-phosphite to the upper rim of a functionalised resorcinarene (**Section 1.3.3**).[131] As previously discussed, synthesis of a series of diene complexes was achieved and the SC-SC hydrogenation method, pioneered by Weller, was applied to these. Although there was evidence for hydrogenation of the diene, characterisation of the resulting complexes was hindered by weak diffraction, potentially a consequence of the flexibility of the system.

With this information in mind, Brookhart's σ-methane complex (one of the most stable and well characterised solution-state alkane complexes) was also considered. The stability of this complex was attributed to the rigidity and robustness that the PONOP pincer ligand imposes upon the complex. It was therefore posited that if a pincer could be appended to the resorcinarene cavity, this may allow for the synthesis of rigid, stable alkane complexes, in which the metal centre is held at the entrance of the resorcinarene cavity. There is precedent for the incorporation of pincer ligands into supramolecular frameworks, including Miller's crown ether pincers (**A81-A86**, **Section 1.2.3**)[74-81] and pincers that form part of a macrocycle,[265-267] such as **A150-A154** (**Section 2.1.2**).[178-180] However, none of these feature a pincer placed above a deep cavity.

Combining these ideas, ligand **14** ('Rc-PONP') was conceived. The key features of this ligand are (i) the resorcinarene cavity (ii) the PONP pincer component, based on pyridine as it removes the requirement for a C-H activation step prior to coordination and with asymmetric 'arms' (for synthetic convenience – see **Section 3.3**) and (iii) the dimethylphosphino group, a steric requirement as larger alkyl groups would clash with the walls of the cavitand. The proposed retrosynthesis is shown in **Scheme 3.5**. Presented in this chapter is the development of this synthetic route, along with the hurdles that were overcome during this process. Characterisation data of intermediate compounds is discussed and evidence for the synthesis of ligand **14** provided. Some initial coordination chemistry of ligand **14** is also explored.
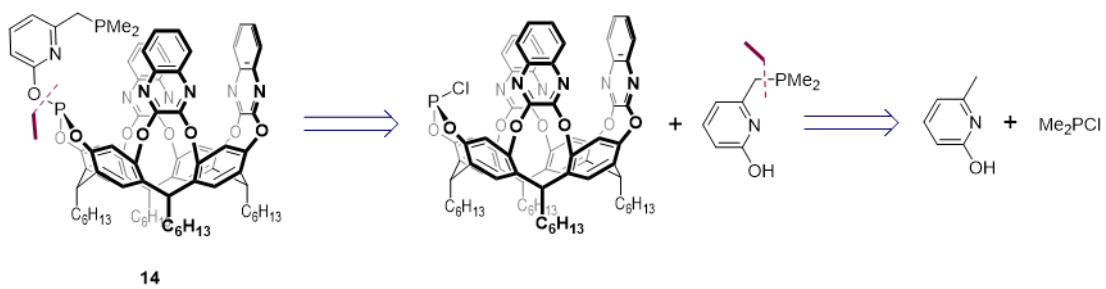
Scheme 3.5. *Proposed retrosynthesis of target ligand* **14**.

3.3. Ligand Synthesis

3.3.1. Installation of the Dimethylphosphino- Moiety
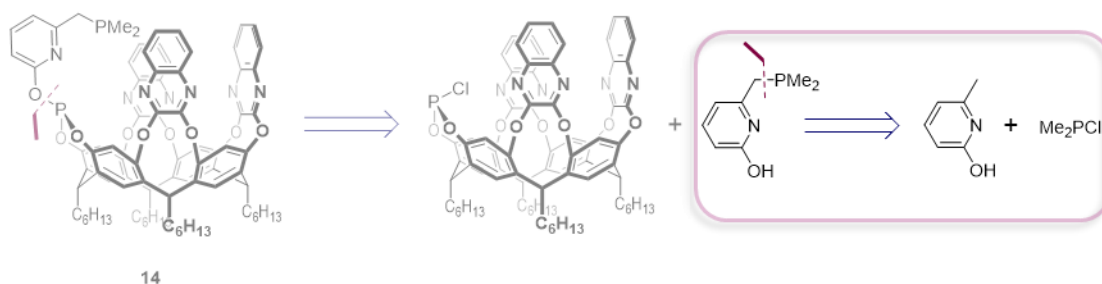
Scheme 3.6. *Proposed retrosynthesis of the PONP component of **14**: installation of the dimethylphosphino- moiety to the pyridine scaffold.*

In order to synthesise this asymmetric pincer ligand, a different method to those typically used for symmetric PNP-type pincers was required. A new synthetic route, starting from 2-hydroxy-6-methylpyridine (**15**), was proposed, based on the retrosynthetic approach shown in **Scheme 3.6**. It was necessary to protect the hydroxyl group as a silyl ether before deprotonation of the methyl group could be undertaken. Heating compound **15** with tri-*iso*-propylsilyl chloride to reflux, in the presence of triethylamine, for 1 hour proceeded to give the new silyl ether **16** as a pale yellow oil in 86 % yield (**Scheme 3.7**). This was characterised on the basis of ^{1}H and ^{13}C{^{1}H} spectroscopy. Notable spectroscopic features include the loss of the broad hydroxyl resonance at δ_H 13.21-13.41 and the presence of a septet (δ_H 1.42, $^3J_{HH}$ = 7.4 Hz) and doublet (δ_H 1.13, $^3J_{HH}$ = 7.9 Hz), corresponding to the tri-*iso*-propyl groups.
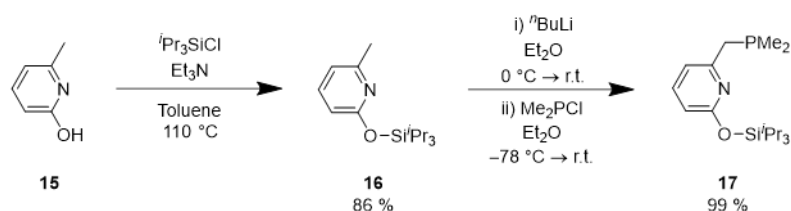
Scheme 3.7. *Protection of the hydroxyl group to give silyl ether **16**, followed by deprotonation of the methyl group and introduction of the dimethylphosphino group to give **17**.*

With this compound in hand, deprotonation of the methyl group using *n*-butyllithium, followed by introduction of dimethylphosphine chloride, was attempted. The lithiation step was initially carried out in the presence of TMEDA (tetramethylethylenediamine) at 0 °C before warming to ambient temperature. A solution of dimethylphosphine chloride was subsequently transferred onto the lithiated mixture at −78 °C (Method A). Following work-up, analysis of the ^{31}P{^{1}H} NMR spectroscopic data for this reaction highlighted the presence of two phosphorus-containing species, δ_P −45.2 (major, ~90 %) and −41.0 (minor, ~10 %). It was proposed that the major product is the desired product **17**, whilst the minor product, displaying spectroscopic and chemical similarities to **17**, is the disubstituted compound **18**.

The following explanation has been proposed to explain the formation of byproduct **18**: when the product **17** is formed alongside unreacted lithiated intermediate **19**, a second deprotonation can occur, giving a second lithiated species **20**. This in turn reacts with dimethylphosphine chloride to give the disubstituted phosphine **18** (**Scheme 3.8**).
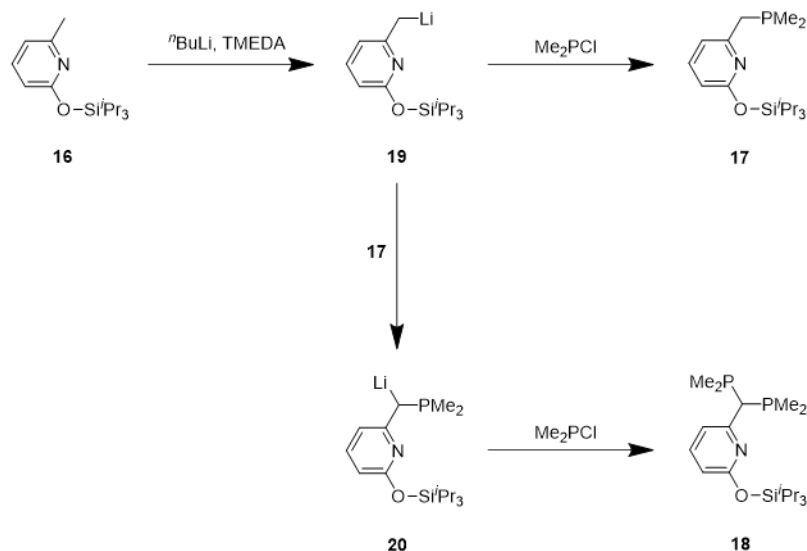
Scheme 3.8. Reaction of compound 16 with ⁿBuLi and the possible side reaction occurring, giving rise to compound 18.

To provide further evidence for this proposal, the sulfur protected compounds **21** and **22** were synthesised, by reaction of the crude **17**/**18** mixture with an excess of S_8 (**Scheme 3.9**). As expected, the $^{31}P\{^{1}H\}$ NMR spectrum of the resulting mixture displayed two signals in a 1:0.4 ratio (δ_P 36.1, 41.3). HR ESI-MS analysis of this mixture confirms the presence of both **21** and **22**.
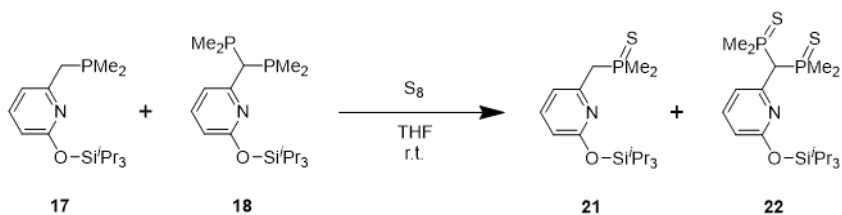
Scheme 3.9. Synthesis of sulfur-protected compounds 21 and 22.

With this possible reaction pathway in mind, several modifications to the original procedure were made. Firstly, the lithiation of compound **16** was carried out in the absence of TMEDA, in an attempt to make a second deprotonation step harder to achieve. Secondly, the organolithium intermediate **19** was then transferred onto the dimethylchlorophosphine solution (the opposite way to the previous attempt), preventing formation of a high concentration of product **17** alongside **19** until the reaction was nearing completion. Only at this point is formation of **18** most likely to occur, given the high concentration of **17** compared to dimethylchlorophosphine. This method was successful in giving compound **17** as the

product, allowing it to be characterised by ^{1}H, ^{13}C{^{1}H} and ^{31}P{^{1}H} NMR spectroscopy and HR ESI-MS.

3.3.2. Coordination Chemistry of Compound **17**

At this point, it was of interest to investigate the coordination chemistry of compound **17**, in order to obtain crystalline material that could be analysed by single crystal X-ray diffraction. This would provide further support for the assignment of compound **17** as the expected intermediate in the synthetic route to target ligand **14**. Reaction of compound **17** with one equivalent of [Rh(cod)$_2$][BAr$^F_4$] (cod = 1,5-cyclooctadiene) gave a 1:1 mixture of two rhodium-bound phosphine species after one hour (δ_P 24.2, $^1J_{RhP}$ = 147 Hz and 39.1, $^1J_{RhP}$ = 167 Hz). After 18 hours, only the resonance at 24.2 ppm remained. This compound was assigned as the cod complex **23** (**Scheme 3.10**) and characterised by ^{1}H, ^{13}C{^{1}H} and ^{31}P{^{1}H} NMR spectroscopy, HR ESI-MS and XRD.
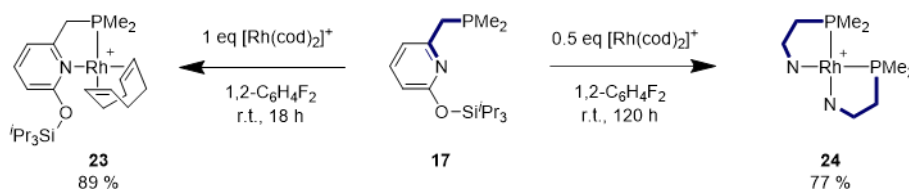
*Scheme 3.10. Reaction of compound **17** with [Rh(cod)$_2$][BAr$^F_4$] to give complexes **23** and **24**. [BAr$^F_4$]$^-$ counterions are omitted for clarity. Pyridine backbone has been simplified in complex **24** for clarity.*

The intermediate species giving rise to the resonance at 39.1 ppm was tentatively assigned as complex **24**, in which both cod ligands have been substituted. In order to investigate this, the reaction of compound **17** with half an equivalent of [Rh(cod)$_2$][BAr$^F_4$] was attempted. As observed previously, after one hour a 1:1 mixture of the same two species was observed. This gradually converted to a single species, δ_P 39.1, after 5 days at room temperature. Again, this was fully characterised by ^{1}H, ^{13}C{^{1}H} and ^{31}P{^{1}H} NMR spectroscopy, HR ESI-MS and XRD and these data support the assignment of this species as complex **24** (**Scheme 3.10**).

The solid-state structures of **23** and **24** are depicted in **Figure 3.6**. Complex **23** was found to crystallise with three independent cations in the unit cell, one of which is displayed. The structure suffers from significant crystallographic issues and so reliable metrics cannot be obtained. However, distorted square planar geometry is observed, with the presence of the cod ligand evident. Complex **24** again displays distorted square planar geometry. The solid-state structure confirms the *cis*-arrangement of the two phosphine donors. Whilst the Rh-P bond lengths are the same within error, the Rh1-N40 separation is slightly larger than the Rh1-N20 separation (1.1(3) pm). Steric buttressing of the adjacent bulky tri-*iso*-propylsilyl groups is evident in the large N20-Rh1-N40 angle of 102.30(6) °.
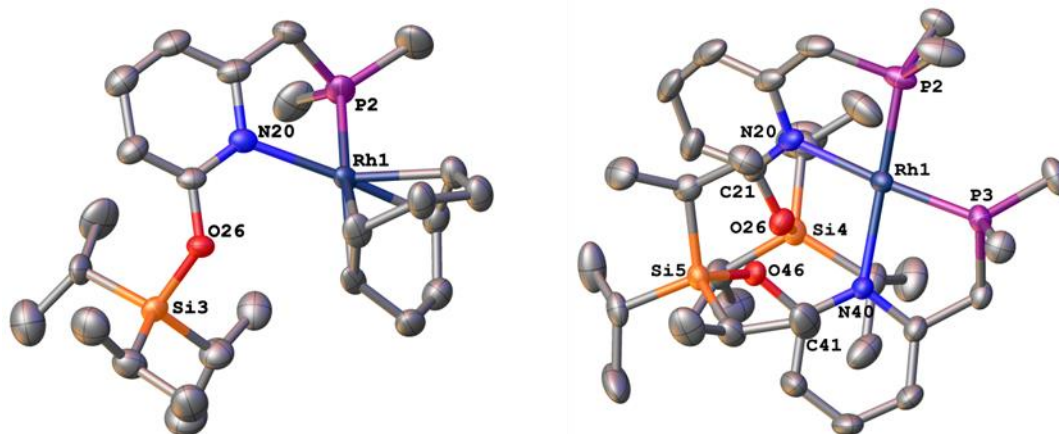
Figure 3.6. Solid-state structures of the one of the independent cations of **23** (Z' = 3, left) and **24** (right), determined at 150 K. Atomic displacement parameters are drawn at 50 % probability. Hydrogens and counterion are omitted for clarity. **23** suffers from crystallographic issues and so is only used to confirm connectivity. Selected bond distances (Å) and angles (°) for **24**: Rh1-P2 2.1723(7), Rh1-P3 2.1736(7), Rh1-N20 2.167(2), Rh1-N40 2.178(2); P3-Rh1-N20 171.13(5), P2-Rh1-N40 170.88(5).

In an attempt to construct ligand **14** using the rhodium centre as a template, a THF solution of complex **23** with treated with TBAF (tetrabutylammonium fluoride) to deprotect the silyl ether. Complete conversion to a new species was observed in the $^{31}P\{^1H\}$ NMR spectrum of the reaction mixture. This contained two inequivalent phosphorus nuclei, both displaying rhodium coupling and *cis* phosphorus coupling to each other. This product was not characterised further, as it would appear that even when starting from the mono-ligated complex **23**, a bis-ligated product is formed, which is not useful with respect to the synthesis of ligand **14**. This synthetic route was not pursued any further.

3.3.3. Installation of the Resorcinarene Moiety
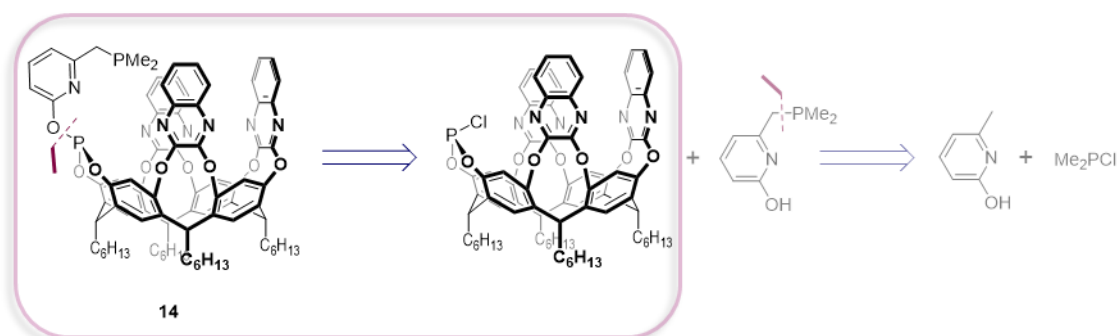
Scheme 3.11. Proposed retrosynthesis for the installation of the resorcinarene moiety.

Returning to the planned synthetic route, and with compound **17** now in hand, it was necessary to deprotect the silyl ether, before the resorcinarene could be introduced (**Scheme 3.11**). As above, TBAF was chosen for this purpose, followed by an aqueous work-up (**Scheme 3.12**). Compound **25** could not, however, be isolated from residual tri-*iso*-propyl fluoride and ammonium salts. A decision was then made to borane protect **25** to facilitate purification

(outlined in **Section 2.2** for the purification of PNP-Np) and so the phosphine-borane adduct **26** was synthesised from **25** *in situ* (**Scheme 3.12**). Fortunately, this could be recrystallised *via* slow diffusion of hexane into a THF solution of **26**. The air-stable product was characterised by ^{1}H, ^{11}B{^{1}H}, ^{13}C{^{1}H} and ^{31}P{^{1}H} NMR spectroscopy, ATR IR spectroscopy, HR ESI-MS and XRD. Compound **26** is likely to be tautomeric, existing as both the 2-pyridone and 2-hydroxypyridine structures, but analysis of the solid-state structure (**Figure 3.7**) indicates that the C21-O26 separation of 1.255(2) Å more closely resembles that of a double bond (this is shorter that the C21-O26 and C41-O46 bond distances of 1.343(2) Å and 1.341(2) Å, respectively, observed in **24**). The disparity between the C21-C22/C23-C24 bond lengths (1.426(2)/1.409(2) Å) and the C22-C23/C24-C25 bond lengths (1.365(2)/1.359(2) Å) suggests a disruption to the aromaticity in the pyridine backbone. This conclusion is further substantiated by the presence of a carbonyl stretching band at 1640 cm^{-1} in the ATR IR spectrum. It is, therefore, concluded that **26** exists in the 2-pyridone form in the solid state and is represented schematically as such.

Deprotection of the phosphine was then achieved by heating compound **26** to reflux in diethylamine for five days (**Scheme 3.12**). Following work-up, compound **25** was obtained as an analytically pure material in good yield (77 %) and characterised by ^{1}H, ^{13}C{^{1}H} and ^{31}P{^{1}H} NMR spectroscopy and HR ESI-MS.
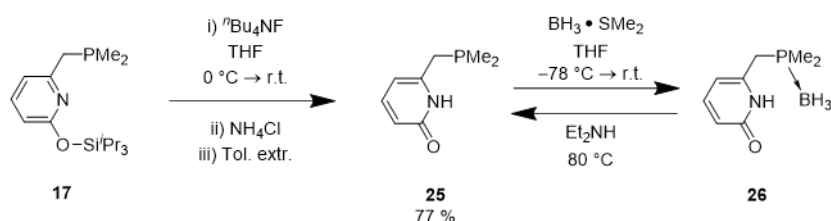
*Scheme 3.12. Desilylation of **17** to give **25**, followed by borane protection, isolation of the phosphine-borane adduct **26** and subsequent deprotection.*
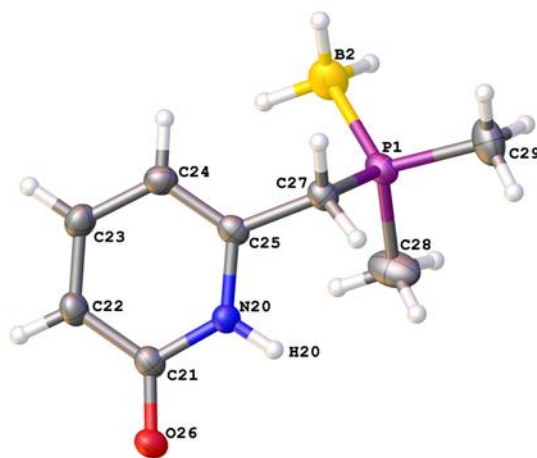
*Figure 3.7. Solid-state structure of **26**, determined at 150 K. Atomic displacement parameters are drawn at 50 % probability. Selected bond distances (Å): P1-B2 1.902(2), C21-O26 1.255(2), N20-C21 1.371(2), C21-C22 1.426(2), C22-C23 1.365(2), C23-C24 1.409(2, C24-C25 1.359(2), N20-C25 1.371(2).*

The final step in this synthetic route was the installation of the resorcinarene. Compound **25** was treated with potassium hexamethyldisilylamide (KHMDS) prior to the addition of a THF solution of the chlorophosphite **A197** (**Scheme 3.13**). Despite convincing ^{1}H and ^{31}P{^{1}H} NMR spectroscopic evidence for the synthesis of the desired compound **14**, isolation of this species was not possible. Although being the major product formed, it was always observed in the presence of a second species, along with trace amounts of other impurities. The ^{31}P{^{1}H} NMR spectrum of this product mixture displays two major singlet resonances: δ_P 135.6 and −46.0 (**Figure 3.8A**). These are in the regions expected for phosphite and phosphine groups, respectively, and integrate approximately as 1:1. The minor product appears to also display two singlet resonances: δ_P 134.9 and 37.2. Based on the latter, the minor product was tentatively assigned as compound **27**, in which the dimethylphosphino group has been oxidised. Repeated synthesis of **14** always led to the formation of **27** in varying degrees and despite scrutiny of the experimental procedure, this by-product could not be eliminated.
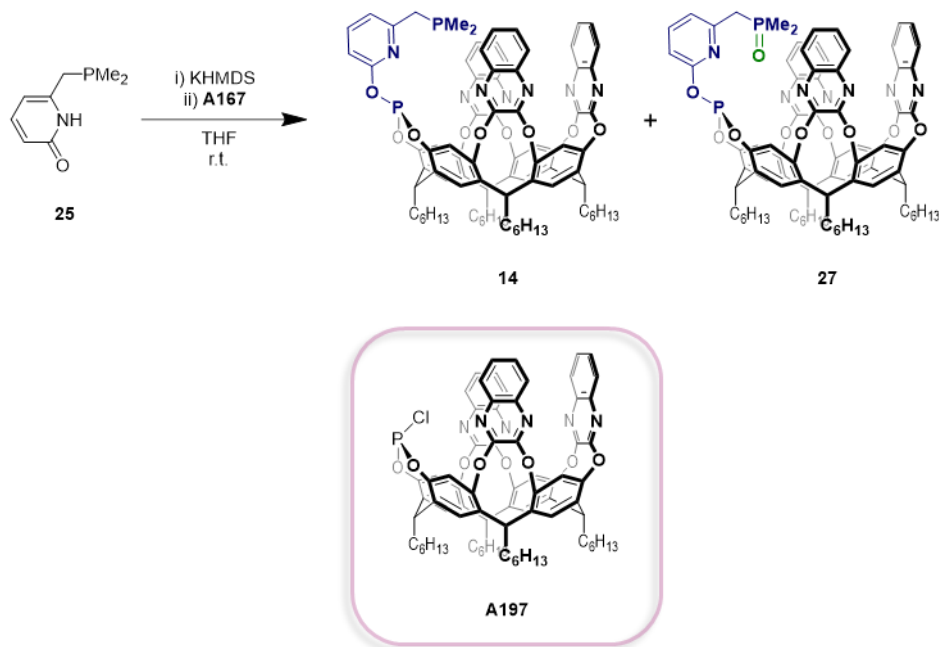
Scheme 3.13. *Deprotonation of **25** and reaction with **A197**, giving ligand **14** alongside a side-product, assigned as phosphine oxide **27**.*

Isolation attempts *via* extraction, washing or recrystallisation were hampered by the high solubility of **14** in a variety of solvents and so ^{1}H, ^{13}C{^{1}H} and ^{31}P{^{1}H} NMR characterisation was performed *in situ*. Although the presence of at least two resorcinarene-containing species resulted in broad, overlapping resonances in the alkyl and aromatic regions, useful structural information could still be extracted from this data. **Figure 3.8B** shows a section of the ^{1}H NMR spectrum, with some of the key resonances highlighted. Connectivity was determined with the aid of COSY, HSQC and HMBC experiments. Crucially, the 2-Py ^{13}C{^{1}H} resonance displays two-bond phosphorus coupling (δ_C 160.8, d, $^2J_{PC}$ = 6 Hz), confirming that installation

of the resorcinarene fragment has occurred in the expected position. The resonances arising from the methyl groups (δ_H 0.87, d, $^2J_{PH}$ = 4 Hz; δ_C 13.6, d, $^1J_{PC}$ = 16 Hz) would suggest that they are positioned above the cavity, as predicted, and do not reside within the cavity as this would be accompanied by an upfield shift in the respective resonances.[113] Multiple resonances were observed between −2.65 and 0.33 ppm, likely resulting from the encapsulation of solvent molecule(s) within the resorcinarene cavity. Analysis of the product mixture by HR ESI-MS provides further support for the assignment of this major species as ligand **14**, with observation of the [*M-O+Na*]$^+$ cation.
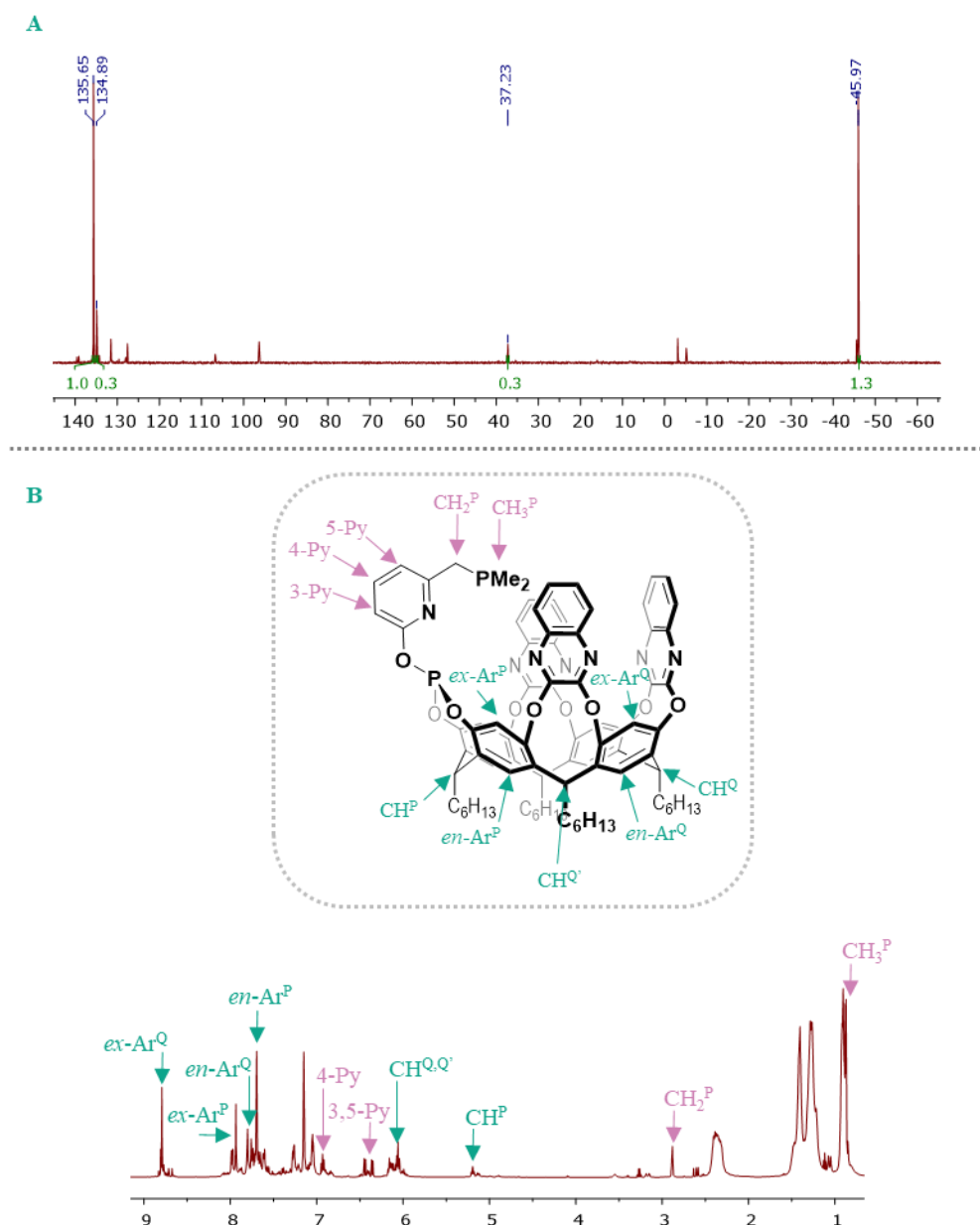
Figure 3.8A) *$^{31}P\{^1H\}$ NMR spectrum of crude **14** (C_6D_6, 162 MHz, 298 K); **B**) a section of the ^1H NMR spectrum of crude **14** (C_6D_6, 500 MHz, 298 K).*

Ligand **14** appears to be stable in C_6D_6 solution for at least 96 hours. It was observed that some samples, when left in solution overnight, became pale pink, orange or even dark red in one

case, with no discernible changes observed by NMR. This has been attributed to the presence of trace unidentified impurities in the samples and not to degradation of the major component.

To provide further evidence for this product assignment, the **14**/**27** mixture was treated with methyl iodide, in order to methylate the phosphine phosphorus in **14**, giving **28** (**Scheme 3.14**). Precipitation of a white solid occurred almost immediately and the reaction was monitored by $^{31}P\{^1H\}$ NMR spectroscopy. After 16 hours, the resonances corresponding to ligand **14** had disappeared, leaving only those assigned to **27**. The white solid was isolated and characterised as **28** (in ~86 % purity) by ^1H, $^{13}C\{^1H\}$ and $^{31}P\{^1H\}$ NMR spectroscopy in THF-d_8. The $^2J_{PH}$ value for the CH_3^P protons (δ_H 2.03) of 15 Hz is larger than that observed in **14** (4 Hz), consistent with reduced electron density at the phosphorus centre.[189] This resonance integrates to 9 against the resorcinarene CH^Q resonance (δ_H 5.87), consistent with the presence of three methyl groups in **28**. HR ESI-MS also confirmed the presence of the $[M]^+$ cation. The filtrate was also analysed by ^1H, $^{13}C\{^1H\}$ and $^{31}P\{^1H\}$ NMR spectroscopy, allowing the tentatively assigned oxide **27** to be characterised. Again, the $^2J_{PH}$ values for the CH_2^P and CH_3^P protons (17 and 13 Hz, respectively) are larger than those observed in **14** (3 and 4 Hz) - this is likely to result from the presence of electronegative oxygen. In both compounds **27** and **28**, the noticeable increase in $^1J_{PC}$ from **14** suggests that the phosphine lone pair has been lost.[189]
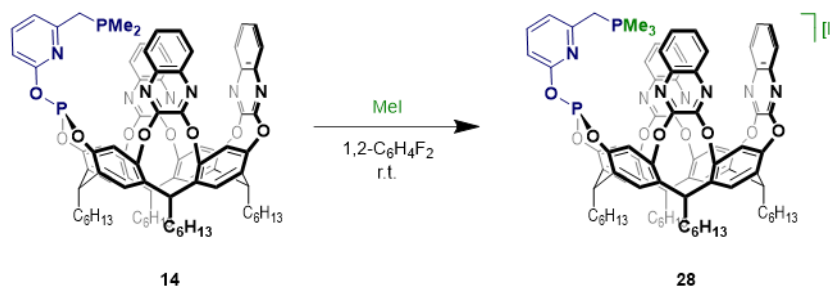
Scheme 3.14. Reaction of 14 with methyl iodide, to give iodide salt 28.

Because of the difficulties encountered in isolating **14**, and the non-trivial synthesis of the precursor **A197**, a parallel investigation into model complex **29** was also undertaken. Treatment of compound **25** with $^tBu_2PCl$, in the presence of KHMDS, initially appeared promising (**Scheme 3.15**). *In situ* analysis of the THF solution revealed the presence of two major resonances in the $^{31}P\{^1H\}$ NMR spectrum (δ_P 152.1; −45.0). This resembles the results observed in the synthesis of **14**, however, subsequent manipulation of the sample resulted in significant degradation to an intractable mixture.
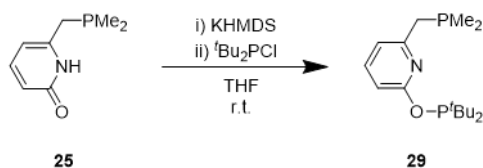
Scheme 3.15. Preparation of model PONP ligand 29.

Given these results, it would appear that the PONP pincer backbone is potentially unstable. In particular, it would seem that problems arise when the precursor **25** is treated with KHMDS and reacted with a chlorophosphite or chlorophosphine. A search of the literature found no examples of pincer ligands possessing this PONP backbone for comparison, although some related systems were found. For example, there are some complexes bearing ligands with a PONX framework (**A198**-**A200**, **Figure 3.9**),[268-270] however, a key difference between these systems and ligand **13** is the lack of any methylene protons adjacent to the pyridine. The most structurally similar examples include the POCP systems **A201**, reported by Eberhard,[271] and **A202**, reported by Goldman.[272] These are reported to have straightforward syntheses, although it is noted that some of the ligands are used as crude oils, without further purification.[272]

A ruthenium complex bearing a NONP ligand was reported by Milstein and co-workers (**A203**), along with PNN congeners.[273] Here, deprotonation of the methylene bridge, in order to achieve dearomatisation of the pyridine ring, was carried out on complexes of each ligand. This mode of reactivity is more common in PNP-type systems because pyridine is more easily dearomatised than the benzene ring in PCP systems.[274] In the case of **A203**, degradation to an intractable mixture of compounds was observed upon treatment with KO^{t}Bu. The authors speculate that this is due to the presence of oxygen, directly attached to pyridine, which increases the electron density of the system when compared to the PNN complexes. The effect of this is that the deprotonated complex is destabilised and so decomposition is observed. It is proposed that a similar situation may be occurring when ligand **14** is synthesised. If there is unreacted KHMDS present alongside newly formed **14**, perhaps dearomatisation and subsequent decomposition occurs in a similar manner, to some extent. This could explain the pink (and sometimes deep red) colouration of many of the solutions of PONP compounds synthesised here. Phosphite decomposition has been reported, giving various phosphine-oxides (among other decomposition products),[275-277] and this may well be the origin of the oxygen required to form phosphine oxide **27** in the reaction mixture.
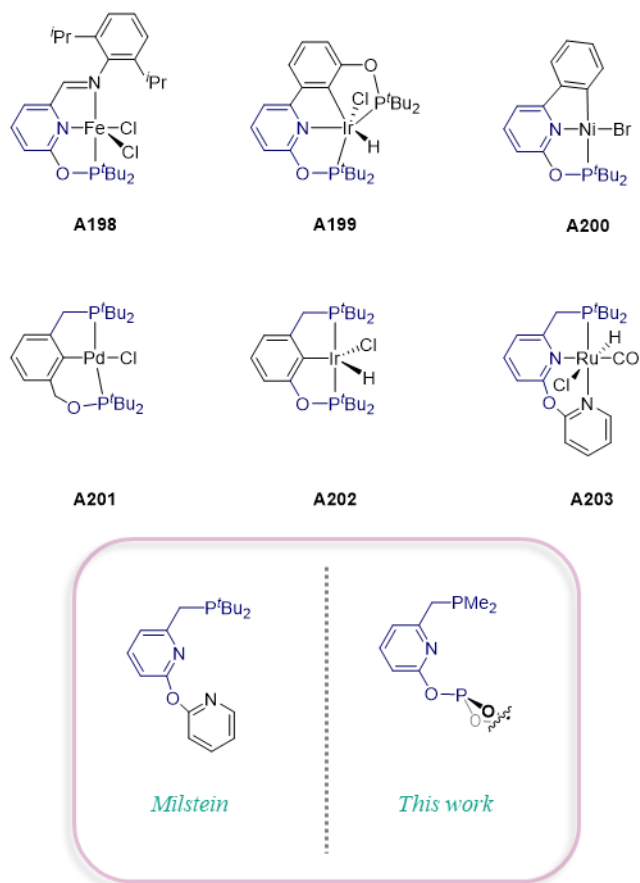
Figure 3.9. *Reported complexes bearing pincer ligands that are structurally related to **14**: PONX complexes **A198**-**A200**,[268-270] POCP complexes **A201** and **A202**[271,272] and NONP complex **A203**.[273]*

3.4. <u>Coordination Chemistry</u>

3.4.1. <u>Reaction with Wilkinson's Catalyst</u>

Given the decomposition observed in the systems above, a new procedure was proposed, involving synthesis of the phosphine-borane adduct of the PONP pincer, with a later deprotection step. To test the viability of this method, compound **26** was treated with Np_2PCl, in the presence of KHMDS, to form model system **30**. Following work-up, a pink solution was obtained, containing a major species, as found by $^{31}P\{^1H\}$ NMR spectroscopy (δ_P 125.1; 6.4-8.4, m). This was assigned as adduct **30** by *in situ* ^1H, $^{11}B\{^1H\}$ and $^{31}P\{^1H\}$ NMR spectroscopy, and strategies to deprotect the phosphine were subsequently employed. As in the case of adduct **26**, heating to reflux in diethylamine was attempted. The reaction was monitored by $^{31}P\{^1H\}$ NMR spectroscopy, but only reached completion after 216 hours and did not proceed cleanly. A different method was, therefore, proposed. By reacting **30** with [Rh(PPh_3)_3Cl] (Wilkinson's catalyst), liberation of triphenylphosphine and triphenylphosphine-borane should occur, giving rhodium(I) complex **31** (**Scheme 3.16**). This complex was identified on the basis of ^1H and $^{31}P\{^1H\}$ NMR spectroscopy and characterised *in situ*. The ^1H NMR spectrum contained trace impurities, but three new $^{31}P\{^1H\}$ NMR resonances were observed. Those at 178.3 and 11.4 ppm display *trans*-phosphorus coupling ($^2J_{PP}$ = 317 Hz), assigned to the phosphinite and phosphine groups, respectively, and both resonances display *cis*-phosphorus coupling to the resonance at 41.6 ppm ($^2J_{PP}$ = 31, 44 Hz), assigned to triphenylphosphine. Salt metathesis of the outer-sphere chloride with $Na[BAr^F_4]$ was then undertaken, giving a new species, **32**, which was characterised by ^1H and $^{31}P\{^1H\}$ NMR spectroscopy (the lack of appreciable differences in the $^{31}P\{^1H\}$ NMR resonances with this transformation would suggest that the chloride of **31** is outer-sphere). Crystals suitable for X-ray diffraction were obtained via slow diffusion of hexane into a 1,2-difluorobenzene solution of **32**, confirming this structural assignment (**Figure 3.10**). The complex displays distorted square planar geometry with three different Rh-P bond distances: Rh1-P2 2.2524(5) Å, Rh1-P3 2.2885(6) Å and Rh1-P4 2.2502(5) Å.

Given the success of this method, phosphine-borane **26** was instead treated with **A197** to give **33** (the borane protected analogue of **14**, **Scheme 3.17**). In this case, however, no reaction with Wilkinson's catalyst was observed by $^{31}P\{^1H\}$ NMR spectroscopy after heating at 80 °C for 48 hours. As a result, this alternative route was not considered any further and it was concluded that the original synthesis was the best option for obtaining a complex of ligand **14**.
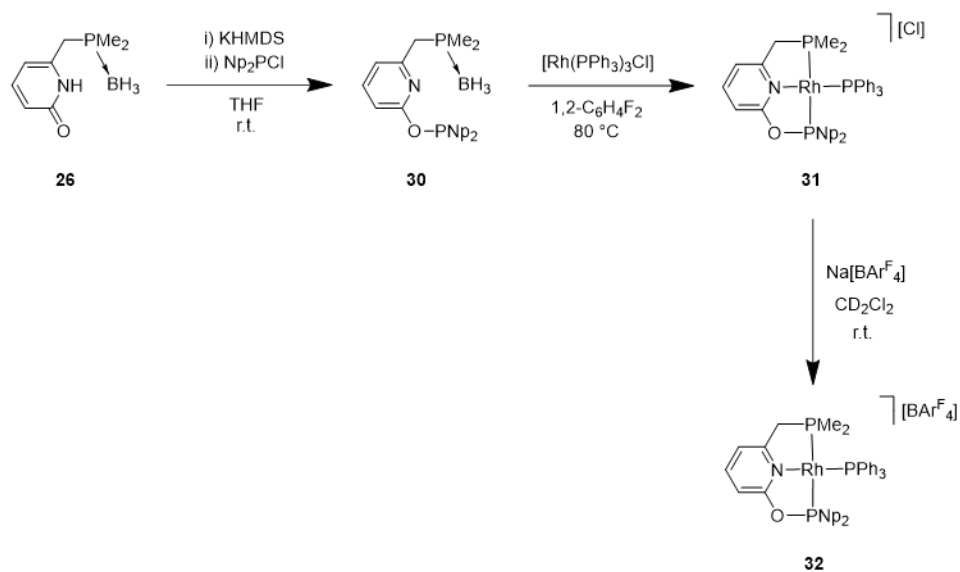
Scheme 3.16. *Synthesis of model phosphine-borane adduct **30**, followed by reaction with Wilkinson's catalyst to give **31** and salt metathesis to give **32**.*
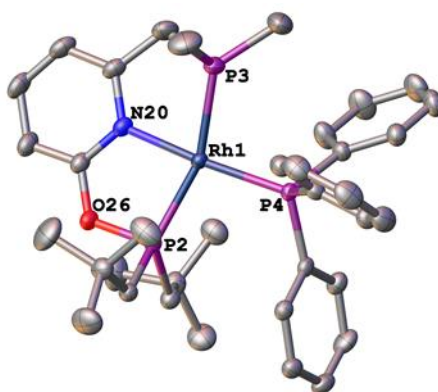
Figure 3.10. *Solid-state structure of **32**, determined at 150 K. Atomic displacement parameters are drawn at 50 % probability. Selected bond distances (Å) and angles (°): Rh1-P2 2.2524(5), Rh1-P3 2.2885(6), Rh1-P4 2.2502(5), Rh1-N20 2.085(1); N20-Rh1-P4 169.93(5), P3-Rh1-P2 160.13(2).*
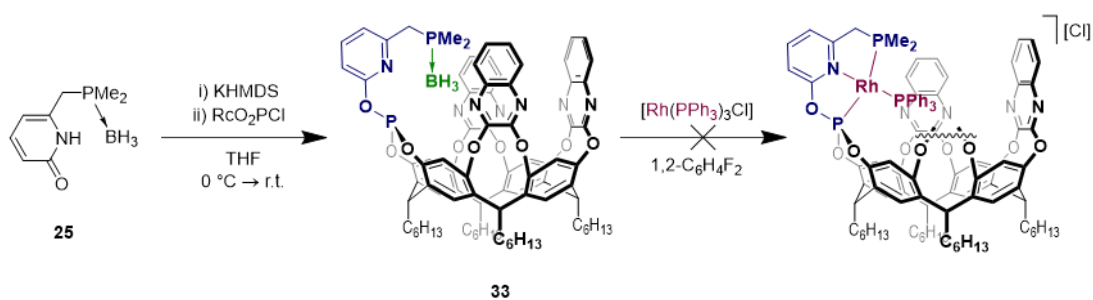
Scheme 3.17. *Synthesis of phosphine-borane adduct **33**, which did not react with Wilkinson's catalyst in the same manner as **30**.*

3.4.2. Synthesis of a Rh(I) Carbonyl Complex

Unable to isolate a pure sample of ligand **14**, its coordination chemistry was investigated *in situ* with the objective of generating an isolable metal complex. To this end, synthesis of a Rh(I) carbonyl derivative was targeted, using $[Rh(CO)_2Cl]_2$ as the precursor. The success of this method was demonstrated in **Section 2.3**, with the synthesis of $[Rh(PNP-Np)(CO)][BAr^F_4]$ (**2**), and further corroborated when the method was applied to the synthesis of the known complex $[Rh(PONOP-^tBu)(CO)][BAr^F_4]$ (**A32**, **Scheme 3.18**). A solution of pincer ligand, rhodium dimer and $Na[BAr^F_4]$ in fluorobenzene was stirred for 2 hours, giving a single species in 84 % yield, which was characterised by ^1H, $^{13}C\{^1H\}$ and $^{31}P\{^1H\}$ NMR spectroscopy, ATR IR spectroscopy and HR ESI-MS. This data matches that reported in the literature for **A32**,[57] confirming the viability of this method for the synthesis of Rh(I) carbonyls of pincer complexes.
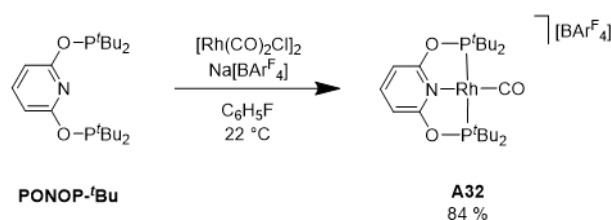
Scheme 3.18. Synthesis of A32[57] using $[Rh(CO)_2Cl]_2$ as a precursor.

The analogous complex of **14** was then synthesised, pairing the cationic fragment with either the $[BAr^F_4]$ (**34**) or $[Al(OC(CF_3)_3)_4]$ (**35**) weakly coordinating anions (in the latter case, $Li[Al(OC(CF_3)_3)_4]$ was used as the halide abstracting agent, **Scheme 3.19**). The $[HCB_{11}Me_5I_6]$ analogue **36** was also synthesised, using an alternative method in which **14** was treated with $[Rh(nbd)][HCB_{11}Me_5I_6]$, before being placed under an atmosphere of CO *in situ*. All three complexes **34**-**36** were isolated as impure orange or yellow solids.
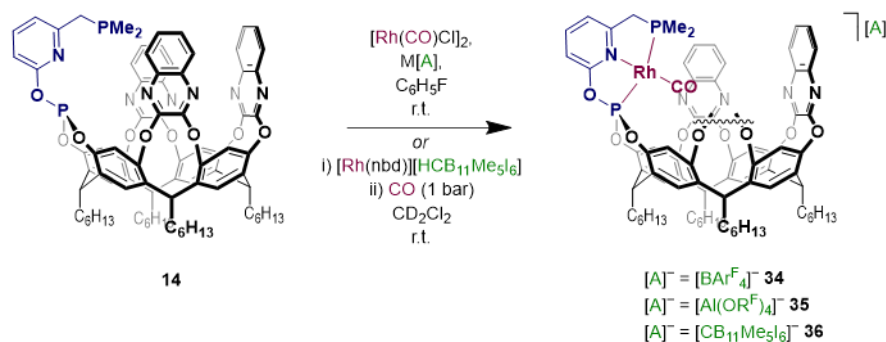
Scheme 3.19. Synthesis of rhodium(I) carbonyl complexes 34-36, via two different methods.
$OR^F = OC(CF_3)_3$.

In all three cases, analysis by $^{31}P\{^1H\}$ NMR spectroscopy revealed complete consumption of the ligand and major impurity, along with the generation of two complexes, based on the presence of four new, anion-independent, resonances in the $^{31}P\{^1H\}$ NMR spectra. Two of

these resonances display *trans*-phosphorus coupling to each other, along with coupling to a rhodium(I) centre (δ_P 155.3-156.7, dd, $^2J_{PP}$ = 428-431 Hz, $^1J_{RhP}$ = 207 Hz; 17.2-17.9, dd, $^1J_{RhP}$ = 122-123 Hz). These are attributed to the target complexes **34**-**36**, in which two inequivalent, *trans*-disposed phosphorus nuclei would be expected. The remaining two signals most likely arise from the presence of phosphine oxide **27** in the reaction mixture, leading to the formation of species **37**-**39** in which only the phosphite moiety is bound to rhodium (δ_P 151.8-152.5, d, $^1J_{RhP}$ = 270-276 Hz), with the phosphine oxide either remaining uncoordinated or coordinated to rhodium through oxygen[278] (δ_P 61.3-61.8, s). The magnitude of the rhodium-phosphorus coupling would suggest that this is also a rhodium(I) complex.

Analysis of the ^{1}H and ^{13}C{^{1}H} NMR spectra is again hampered by the presence of multiple resorcinarene-containing species, although the key resonances can be identified (assignment of the individual quinoxaline protons is not possible, and the broad hexyl methylene resonances are complex). In all three cases, the pyridine backbone, methylene bridge and dimethylphosphino protons can be assigned, along with those belonging to the resorcinarene backbone. Whilst the spectra of **34** and **35** are largely independent of the anion, there are noticeable differences in that of **36**. This may be due to interactions between the iodine atoms of the carborane and the quinoxaline walls. These are known to be flexible and so a distortion upon interaction with the anion is not unlikely, resulting in changes to the NMR shifts of various protons. Interaction of the iodine atoms with the rhodium centre is also a possibility. Complex **35** provides the best NMR data (this was synthesised on a larger scale and so preparation of a more concentrated NMR sample was possible), allowing key resonances belonging to the by-product **38** to be identified.

Although weak, the ^{13}C{^{1}H} NMR spectra of complexes **34**-**36** can be assigned with the aid of HSQC and HMBC experiments and corroborate the structural assignments. However, resonances corresponding to the carbonyl carbon are noticeably absent. This is likely a result of the weakness of the samples, combined with the coupling experienced by this carbon to two inequivalent phosphorus nuclei and rhodium, resulting in significant broadening, such that the signals are hard to resolve. Therefore, ATR IR spectroscopy must be relied upon to confirm the presence of the carbonyl ligand. Indeed, two C=O stretches are observed for each compound mixture, suggesting the presence of more than one bound carbonyl. Given the significant difference in intensities of these two bands, the most intense peak was attributed to the major product. All three spectra are relatively similar. [BAr$^F_4$] salts **34/37** display a broad major band at 2032 cm^{-1}, along with a minor band at 2087 cm^{-1} (attributed to **37**). This pattern is repeated for [Al(OC(CF$_3$)$_3$)$_4$] salts **35/38**, although shifted to slightly higher wavenumbers (2036, 2113 cm^{-1}). [HCB$_{11}$Me$_5$I$_6$] system **36/39** more closely resembles the [BAr$^F_4$] system (2030, 2089 cm^{-1}). The small variations in these results would suggest that the electronics of these solid-state systems are not independent of the anion.

The presence of major and minor carbonyl stretching bands in the ATR IR spectra of these complexes would suggest that the by-products are also rhodium(I) carbonyl complexes. If the oxidised ligand **27** coordinates to rhodium through oxygen, then the structure proposed in **Figure 3.11A** would be expected. If the phosphine oxide remains uncoordinated, the remaining coordination site may be occupied by a solvent molecule, or perhaps by formation of a self-inclusion complex. A fluorobenzene complex of the related resorcinarene-based phosphine-phosphite **A124** (**Section 1.3.3**) is known,[131] characterised by a ^{19}F resonance of -116.96 ppm. No such resonance can be found in the ^{19}F NMR spectrum of the **35/38** mixture, suggesting that formation of a self-inclusion complex is more likely. There is also precedent for this behaviour (**A134**), and a structure resembling that shown in **Figure 3.11B** could be envisaged. These proposed structures are purely speculative without further structural information, although the higher frequency carbonyl stretches of **37**-**39** imply reduced electron density at rhodium, consistent with the presence of a weaker donor (*cf.* -PMe$_2$) at the third coordination site. This lends support to these two proposals.
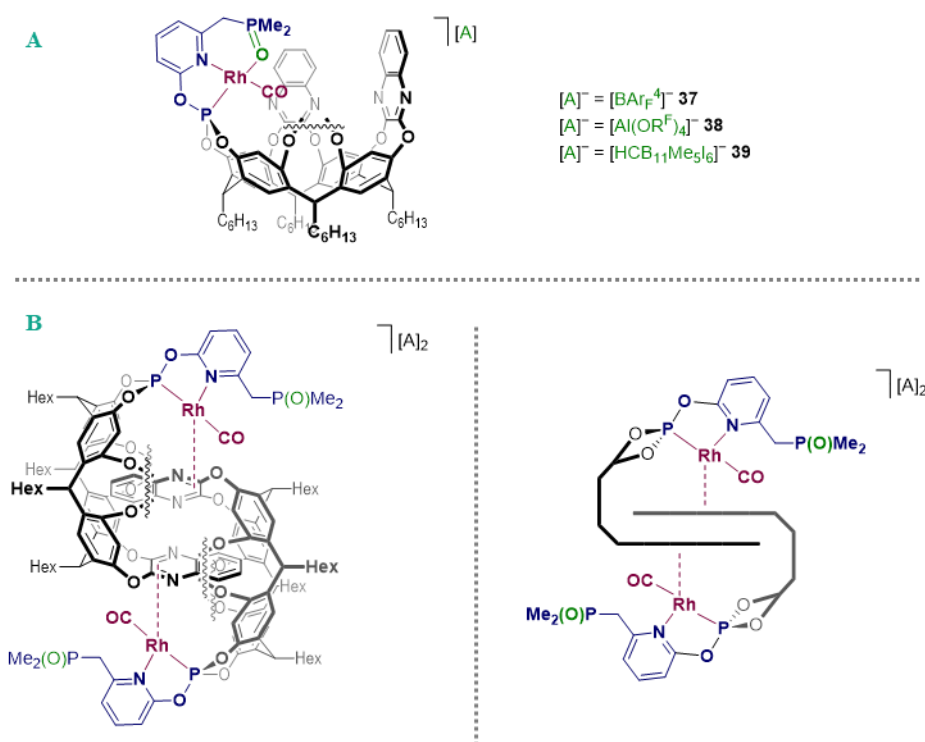
Figure 3.11. Proposed structures for the side-products 35-37, featuring A) the phosphine oxide coordinated to rhodium[278] or B) a self-inclusion complex and uncoordinated phosphine oxide.[131]

Unfortunately, all attempts to recrystallise complexes **34**-**36**, or the corresponding by-products **37**-**39**, produced crystals that were too small or too weakly diffracting, preventing more conclusive identification. HR ESI-MS does, however, confirm the presence of the $[M]^+$ cation as the major signal in all three product mixtures. The "[Rh(**27**)(CO)]"$^+$ fragment was also identified in the **34**/**37** mixture, consistent with both proposed structures.

3.4.3. Attempted Synthesis of a Rh(III) Carbonyl Dichloride

Having obtained evidence to support the formation of 16-electron rhodium(I) complexes **34**-**36** (and side-products **37**-**39**), it was of interest to synthesise the corresponding 18-electron rhodium(III) carbonyl dichlorides, to see if these provided an opportunity for isolation of a single species and to extend the coordination chemistry of this new ligand. Reaction of the model complex **A32** with PhICl$_2$ was attempted (**Scheme 3.20**), but showed limited conversion by ^{31}P{^{1}H} NMR spectroscopy, after 2 hours, to two new species. Neither of these suggest the formation of the rhodium(III) oxidative addition product, probably due to the steric bulk of the *tert*-butyl groups and the fact that PONOP is a poorer choice of ligand for stabilising a rhodium(III) complex due to its weaker donor capabilities, *cf.* PNP.
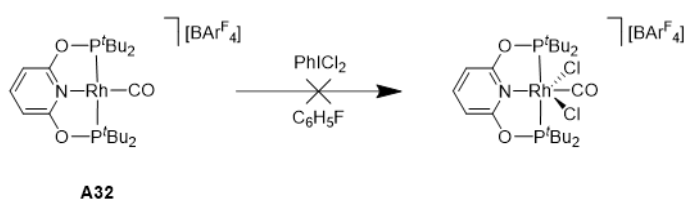
Scheme 3.20. *Attempted reaction of A32 with PhICl$_2$.*

However, when complexes **34** and **35** were reacted with PhICl$_2$ under the same conditions, complete conversion to two new rhodium(III) species, **40** and **41**, was observed (**Scheme 3.21**). Analysis of the ^{31}P{^{1}H} NMR spectra of these complexes shows two signals displaying *trans*-phosphorus coupling, along with smaller rhodium coupling than was observed in **34** and **35** (δ_P 113.9-114.2, dd, $^2J_{PP}$ = 664-666 Hz, $^1J_{RhP}$ = 121 Hz; 41.6-41.8, dd, $^1J_{RhP}$ = 75 Hz). These data are consistent with the assignment of **40** and **41** as rhodium(III) carbonyl dichlorides. [Al(OC(CF$_3$)$_3$)$_4$] salt **35** was accompanied by a minor product (**43**) arising from the presence of side-product **38**: the phosphite resonance in the ^{31}P{^{1}H} NMR spectrum displays rhodium coupling (δ_P 94.4, d, $^1J_{RhP}$ = 162 Hz) whilst the phosphine oxide resonance does not (δ_P 63.1, s). [BAr$^F_4$] salt **34** appeared to be the only phosphorus-containing species after work up, but two species were observed when the reaction was monitored *in situ* and so this is likely to just be a consequence of the weak NMR sample and it is thought that the analogous side-product, **42**, is also present. Again, analysis of the ^{1}H and ^{13}C{^{1}H} NMR spectra for these compounds is challenging.
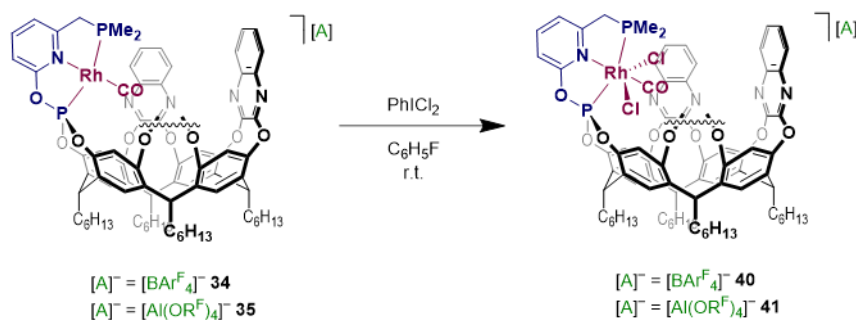
Scheme 3.21. Reaction of 34 and 35 with PhICl₂ to give 40 and 41.

ATR IR spectroscopy of these two product mixtures again highlights the presence of two carbonyl stretching bands. As above, the most intense peak was attributed to the major product. The data are summarised in **Table 3.1** and compared with those of the respective rhodium(I) carbonyls. The side-products **42** and **43** give rise to higher frequency stretches than **40** and **41**, consistent with the replacement of the phosphine with a weaker donor. The stretching frequencies of [BAR$^F_4$] salts **34/37** and **40/42** are surprisingly similar, albeit the major band of **40** is narrower. However, [Al(OC(CF$_3$)$_3$)$_4$] salts **41/43** exhibit bands that are shifted to slightly lower wavenumbers than **35/38**. These results are difficult to explain without further insight, as the rhodium(III) complexes would be expected to give higher frequency carbonyl stretches than the rhodium(I) complexes. However, it is now known that IR stretching frequencies of carbonyl ligands in transition metal complexes cannot always be rationalised by the Dewar-Chatt-Duncanson model alone.[279-281] The position of the carbonyl ligands of **40-43**, within the resorcinarene cavity, could explain why these systems do not follow the expected trends. The quinoxaline π-cloud may generate a local electric field within the cavity that affects carbonyl bonding.

Table 3.1. ATR IR carbonyl stretching frequencies of rhodium(I) carbonyls 34, 35, 37 and 36, and rhodium(III) carbonyls 40-43 (with the minor product in parentheses).

Complex	v_{CO} / cm^{-1}
[Rh(**13**)(CO)][BAr$^F_4$] / **34**, (**37**)	2032 (br), (2087)
[Rh(**13**)(CO)(Cl)$_2$][BAr$^F_4$] / **40**, (**42**)	2019, (2089)
[Rh(**13**)(CO)][Al(OC(CF$_3$)$_3$)$_4$] / **35**, (**38**)	2036, (2113)
[Rh(**13**)(CO)(Cl)$_2$][Al(OC(CF$_3$)$_3$)$_4$] / **41**, (**43**)	2030, (2095)

With this ^{1}H, ^{13}C{^{1}H} and ^{31}P{^{1}H} NMR and IR spectroscopic data alone, complexes **40** and **41** (along with **42** and **43**) cannot be assigned unambiguously. Attempts to recrystallise any of these complexes were unsuccessful and ESI-MS does not provide any evidence for the existence of the proposed products. These assignments, therefore, remain tentative.

3.5. <u>Summary and Conclusions</u>

In this chapter, a new synthetic route to an asymmetric pincer ligand, featuring both non-equivalent linkers and donor groups, was devised and carried out. Despite encountering some issues during this multi-step synthesis, most of these were addressed satisfactorily. Intermediate species were well characterised and, crucially, there is evidence, provided by ^{1}H, ^{13}C{^{1}H} and ^{31}P{^{1}H} NMR spectroscopy, HR ESI-MS and by further reactivity with MeI and [Rh(CO)$_2$Cl]$_2$, to suggest that the target ligand has been synthesised *via* this route. A notable outstanding experiment, which could not be carried out within the timeframe of this project, is the deliberate oxidation of ligand **14**, to further confirm the assignment of by-product **27** as the phosphine oxide.

Some initial coordination chemistry was performed; however, characterisation of these complexes is limited by the lack of any solid-state structures. Despite many attempts to recrystallise these samples, single crystals suitable for X-ray diffraction were not obtained. The air sensitivity of these samples limited the crystallisation techniques that could be applied.

The overarching aim of this chapter – to determine whether this system enables the synthesis and full characterisation of a σ-alkane complex, has not yet been achieved and it was not possible, within this timeframe, to investigate the alkane binding ability of rhodium complexes of this ligand. Key outstanding experiments include the pursuit of a σ-alkane complex, such as *via* the synthesis of rhodium alkene complexes, which would subsequently allow the solid-state hydrogenation methodology to be investigated. **Scheme 3.22** highlights some potential approaches that could be explored to progress towards this goal.

In order for this to be achieved, purer samples of ligand **14** would be required and it is unlikely that this is possible using this synthetic methodology. It is proposed that the final step, involving addition of the resorcinarene precursor as a chlorophosphite, is the most problematic as this step leads to a mixture of products (possibly a result of decomposition). For investigations into this system to continue, this issue needs to be addressed. The use of a weaker base could be investigated, such as triethylamine, that wouldn't result in pyridine dearomatisation. Other synthetic routes to asymmetric pincers have been reported,[282] although many of these are not compatible with the differing phosphorus donor groups in ligand **14**. The dimethylphosphino moiety is also problematic as it requires installation *via* dimethylphosphine chloride, limiting the choice of synthetic route. An answer to this could be to modify this donor group – perhaps by investigating the effect of introducing greater steric bulk at the top of the resorcinarene cavity, or by changing the nature of the group entirely (*e.g.* amines, carbenes, imines, phosphaalkenes could be worth investigating). By changing the nature of the linker on this arm (*i.e.* not a methylene group), or by methylating the linker, this could also prevent decomposition of the ligand (**Figure 3.12**).
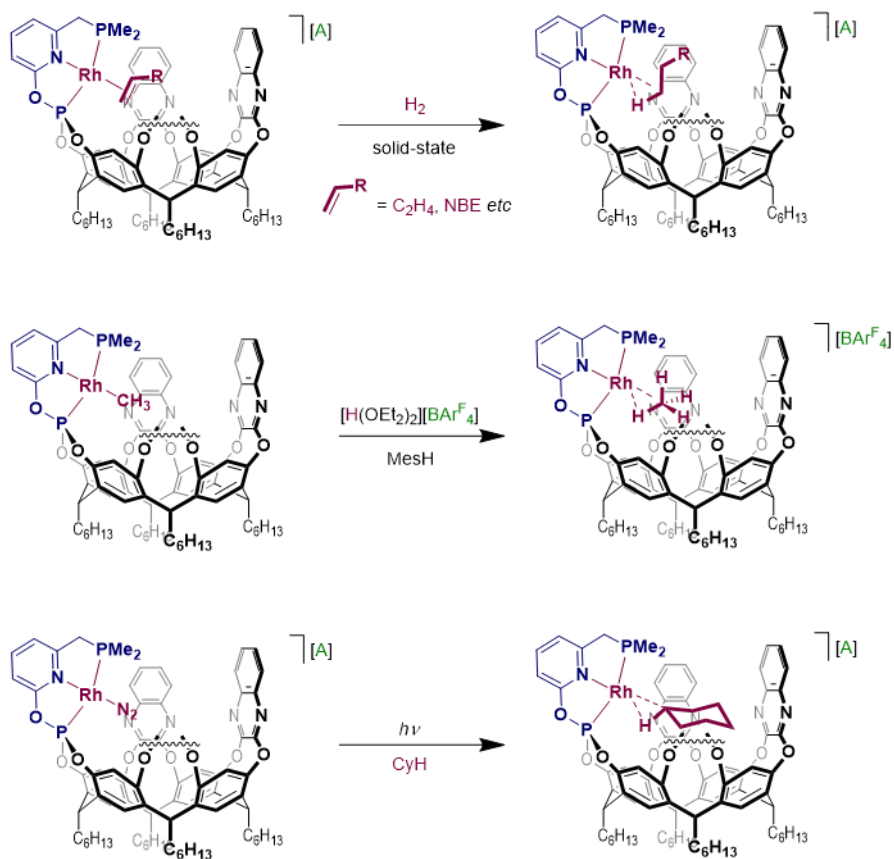
Scheme 3.22. *Potential routes to a σ-alkane complex, stabilised by ligand **14**, that could be explored in the future.*
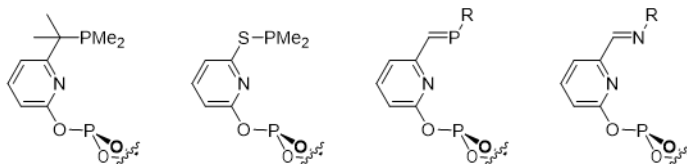
Figure 3.12. *Potential modifications to the pincer backbone that would block the major decomposition pathway.*

Thus, there are many potential ways in which the system and the synthetic methodology used in this work could be varied and this should form the basis for any future investigations.

4. Rhodium-Catalysed Hydroformylation With a Cavitand-Derived Phosphine-Phosphite Ligand

In seeking to achieve branched-selective hydroformylation, a resorcinarene-derived, chelating phosphine-phosphite (**A124**) was investigated as a ligand in the rhodium-catalysed hydroformylation of unfunctionalised, linear alkenes. It was hypothesised that conducting catalysis within the cavity would proceed with high regioselectivity. This ligand has been compared to two model chelating ligands: dppe, known for its poor activity and selectivity in hydroformylation, and (S_{ax},S,S)-BOBPHOS, which currently gives the highest branched selectivity in the hydroformylation of 1-hexene (75 %). The synthesis and characterisation of pre-catalysts of each ligand (L_2) of the formula [Rh(L_2)(acac)] is reported – these are then employed in the hydroformylation of alkyl alkenes. Whilst dppe performs as expected and (S_{ax},S,S)-BOBPHOS results in consistently high branched selectivity in the hydroformylation of 1-hexene, 1-heptene and 1-octene, selectivity with the resorcinarene-based ligand **A124** increases with olefin chain length, up to a maximum of 85 % in the hydroformylation of 1-octene. The effect of the cavity is discussed, aided by *in situ* characterisation of a hydride intermediate by ^{1}H and ^{31}P NMR spectroscopy.
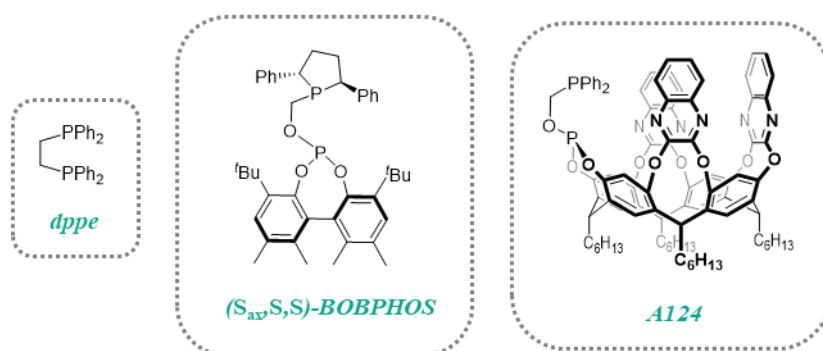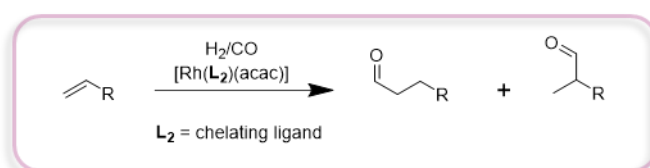
4.1. Introduction

4.1.1. Rhodium-Catalysed Hydroformylation

Hydroformylation is the formation of aldehyde products from alkenes, following the addition of syngas (a mixture of dihydrogen and carbon monoxide) in the presence of a catalyst.[283-287] It is an important strategy in green chemistry due to the atom economy of the transformation. A mixture of linear and branched aldehydes will typically be formed (except in the case of symmetrical alkenes), depending on the regioselectivity of the addition (**Scheme 4.1**). In the case of the branched aldehydes, chiral centres are formed, giving rise to the possibility for asymmetric transformations. The mixture of products can be further complicated by alkene isomerisation, leading to the production of other branched aldehydes, and alkene hydrogenation can also occur under the reaction conditions. As a result, many investigations seek to find ways in which chemo- and regioselectivity can be influenced by factors such as catalyst design and reaction conditions. There is a wealth of literature surrounding the issue of linear-selective aldehyde synthesis because of the importance of these products to various industries.[284,287] However, high selectivity for branched aldehydes has not been as thoroughly pursued until recently, with a growing demand for these compounds in organic synthesis and fine chemical production. The ability to selectively produce branched aldehyde products from unbiased alkenes is now an important goal.[288,289]
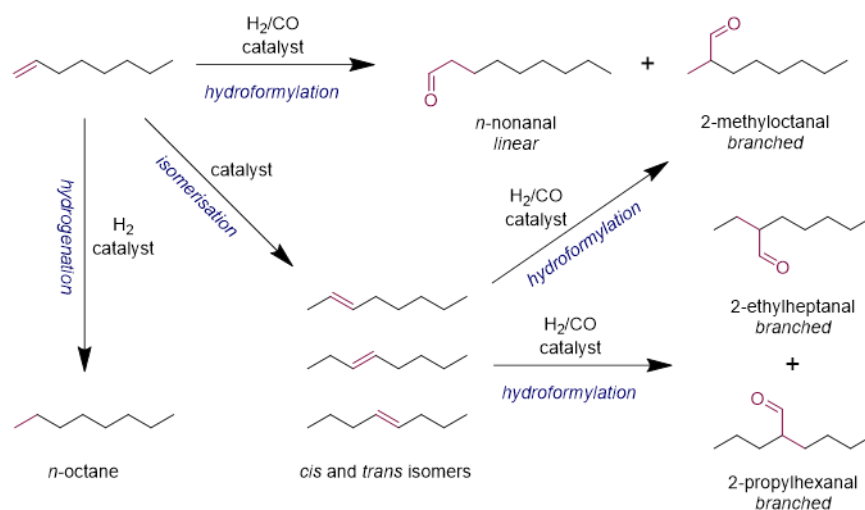
Scheme 4.1. *Hydroformylation of 1-octene and the other reactions that can potentially occur under catalytic conditions, resulting in a mixture of alkane, alkene and aldehyde products.*[284]

In industrial hydroformylation processes, cobalt and rhodium catalysts are used, with rhodium-based systems more widely studied in academia.[284,285,287] Heck and Breslow proposed a mechanism for cobalt-catalysed hydroformylation,[290] which Wilkinson later extended to more superior rhodium catalysts that required less forcing conditions.[291-300] It is generally still considered to be applicable: the active species being a rhodium hydride (**II**, **Scheme 4.2**),

formed from the rhodium phosphine acetylacetonate (acac) complex (**I**). Coordination of the olefin (**IV**), followed by 1,2-migratory insertion into the M-H bond leads to formation of an alkyl species (**V-VI**). It is here that divergent pathways become apparent: insertion into the M-H bond can proceed to give linear or branched alkyl intermediates, depending on the regioselectivity of addition. 1,1-Migratory insertion of a carbonyl ligand into the M-C bond affords acyl species (**VII-IX**) which undergoes hydrogenolysis to yield the aldehyde products. Catalyst deactivation can occur by the formation of inactive dimers and carbonyl clusters.
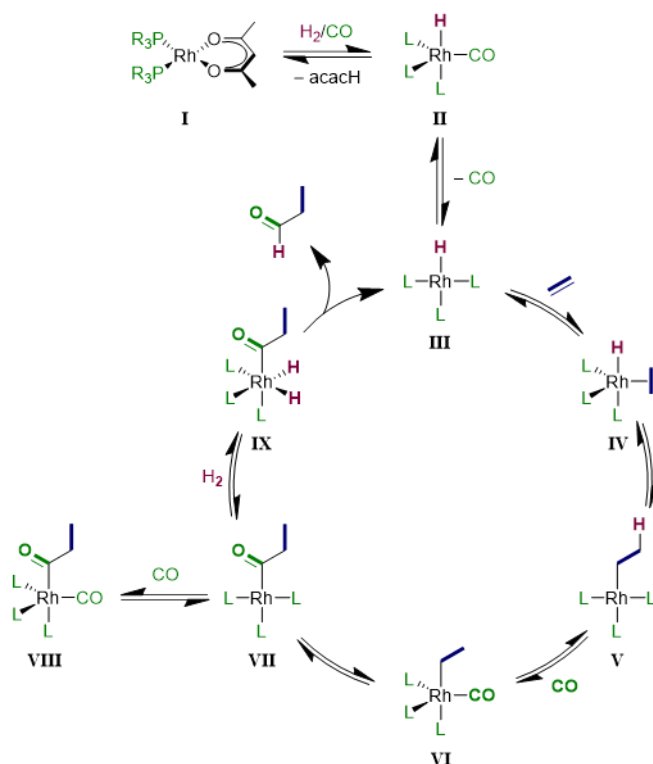
Scheme 4.2. *General catalytic cycle for the hydroformylation of alkenes, using [Rh(L$_2$)(acac)] as a pre-catalyst. L represents either a trivalent phosphorus (PR$_3$) or carbonyl ligand.*

This mechanism has been well-substantiated. Detailed DFT analysis was performed on systems containing phosphines, phosphites and NHCs,[301] concluding that the rate determining step could be altered by changing the electronics of the ligand. Mono- and bis-ligated triphenylphosphine complexes were also studied computationally by de Bruin and Reek, where the mono-ligated system displayed higher activity.[302] Experimental techniques used to characterise intermediates and catalyst resting states have included *in situ* high pressure IR spectroscopy,[95,303-309] but carbonyl stretches only provide limited structural information. ^{31}P NMR spectroscopy is more useful,[305,309-311] however, mass transfer limitations mean that analysis of a reaction mixture inside a high pressure NMR tube does not necessarily provide an accurate reflection of how the system behaves in an autoclave.[312] In the last few years, *operando* FlowNMR spectroscopy has become a useful technique, enabling detailed, quantitative insight into catalytic systems.[313-315] Hintermair has highlighted the potential of

this technique to gain deep mechanistic understanding, with thorough investigations into catalyst activation/deactivation and turnover speciation under typical reaction conditions, in both triphenylphosphine-[316,317] and phosphite-ligated processes.[318] A combination of ^{1}H, [31]P{[1]H} and selective excitation ^{1}H experiments, along with two-dimensional correlation experiments, enabled on-cycle rhodium-phosphine/phosphite intermediates to be characterised and quantified during catalyst activation and turnover.

These studies all highlight that hydroformylation is very sensitive to reaction conditions, the steric and electronic properties of the ligands used and even the nature of the substrate, making mechanistic analysis challenging. Changes to any of these factors can result in a change in reaction rate (and the rate determining step), with different intermediate species being invoked. Shown in **Scheme 4.2** is a very simplified and generic view of the mechanism by which rhodium-catalysed hydroformylation occurs. Here, 'L' can represent either a phosphorus-based ligand or a carbonyl. For bidentate ligands, one equivalent of ligand per rhodium centre is to be expected but the situation is more complex for monodentate ligands, with the number of bound ligands dependent upon factors such as their steric bulk and the number of equivalents used, and interconversion between a range of phosphorus/carbonyl-ligated species occurring. Bidentate ligands will be considered here, as they impart stability at the rhodium centre, reducing the number of possible on-cycle species and providing more control over the metal coordination sphere during turnover. This is beneficial for enhancing the regioselectivity of the catalyst.

4.1.2. Hybrid Phosphine-Phosphite Ligands

A considerable proportion of the hydroformylation literature features trivalent phosphorus-ligated rhodium systems, such as phosphines and phosphite complexes.[284-287] π-Acidic phosphites are of particular interest as these typically lead to an increase in rate: the reduction in electron density at the metal results in more facile dissociation of carbonyl.[318] Bidentate ligands are also widely used as the chelate effect is employed to reduce ligand dissociation, ultimately leading to a more selective catalyst (albeit showing lower activities compared to monoligated systems).[302] In particular, chelating ligands with larger natural bite angles were found to be the most effective.[14,17,319-326] Whilst diphosphine and diphosphite systems are common, those comprising of both phosphine and phosphite donors have received less attention in the past (and are generally only reported in asymmetric hydroformylation).[327-330] These mixed systems are of interest because of the potential for fine tuning the steric and electronic properties of the ligand, which can have a significant impact upon catalysis.

A seminal example is the use of binaphthol-derived ligands **A204**-**A208** (**Figure 4.1**). Takaya and Nozaki demonstrated that rhodium complexes of these displayed high enantio- and (branched) regioselectivities in the hydroformylation of aryl alkenes, functionalised

olefins and styrenes. The selectivities were, however, much lower for unfunctionalised olefins.[331-335]
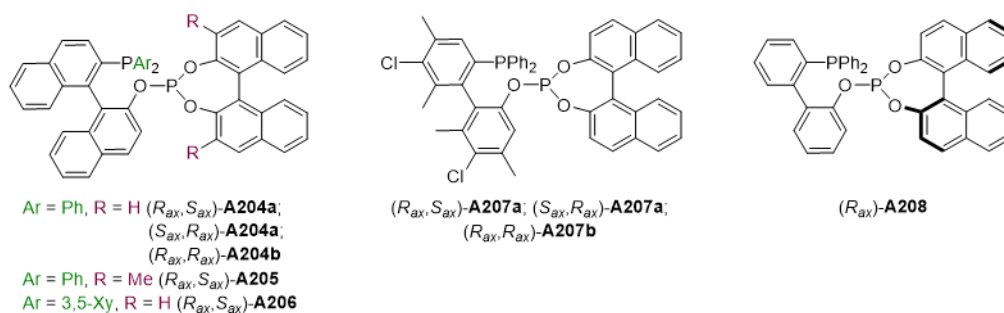
Figure 4.1. *Binaphthol-derived ligands* **A204-A208***, employed in the asymmetric hydroformylation of various substrates by Takaya and Nozaki.[331-335]Xy = xylyl, 'a/b' notation denotes diastereoisomers.*

Ligands based on a "R_2P-$(CH_2)_n$-O-PO_2" backbone have also been reported and are summarised in **Figure 4.2A**.[336-341] In the majority of these examples, enantioselectivity was the main interest, although good branched selectivity was observed in many cases. However, the most common substrate used was styrene, which has an inherent preference for the branched aldehyde product because of the vinyl stabilisation of the rhodium-alkyl intermediate. Other biased olefins were also used, with no reports of unsubstituted, straight-chain olefins showing good regioselectivity for the branched product.

The most relevant result with this type of ligand comes from the group of Clarke.[309,342-346] Features of two good asymmetric hydroformylation ligands were combined in (S_{ax},S,S)-BOBPHOS (**Figure 4.2B**) and high regioselectivity (71-91 %) for the branched product was observed across a range of substrates. Crucially, hydroformylation of 1-hexene, at 15 °C for 46 hours, produced 2-methylhexanal with 75 % selectivity.[342] Extremely good selectivities were also observed with vinyl arenes (>80 % in some cases, with 86-90 % *ee*)[343] An investigation of the structure-activity relationship of ligands **A224**-**A229** in propene hydroformylation has recently been carried out, where rational modifications to the ligand backbone enabled the design of a catalyst that is highly selective (75 %) for *iso*butanal synthesis.[345,346]

Mechanistic studies were performed to explain these results, combining high pressure IR and NMR studies, kinetic profiling, deuterium-labelling and DFT studies.[309] This enabled the conclusion to be drawn that the branched selectivity is determined early on in the catalytic cycle, likely a consequence of the irreversibility of alkene insertion to form rhodium alkyl intermediates (thus preventing isomerisation between the linear and branched species). Attractive C-H---π non-covalent interactions (NCIs) in an early transition state for C-H bond formation on the linear pathway, along with steric buttressing of the alkene against a phenyl group, disfavoured the rotation necessary for onward reaction, leading to a predominantly branched pathway. The authors have suggested that attempts to design a branched selective

hydroformylation catalyst need to incorporate an open site for the formation of branched alkyl/acyl intermediates, whilst also considering ways in which the linear pathway could be disfavoured. This could arise from steric factors, or because of the presence of NCIs that influence transition state energies, as demonstrated here. A way in which this could be achieved is the incorporation of a supramolecular component to the system, where NCIs between catalyst and substrate in the secondary coordination sphere can provide additional control over the outcomes of catalysis.
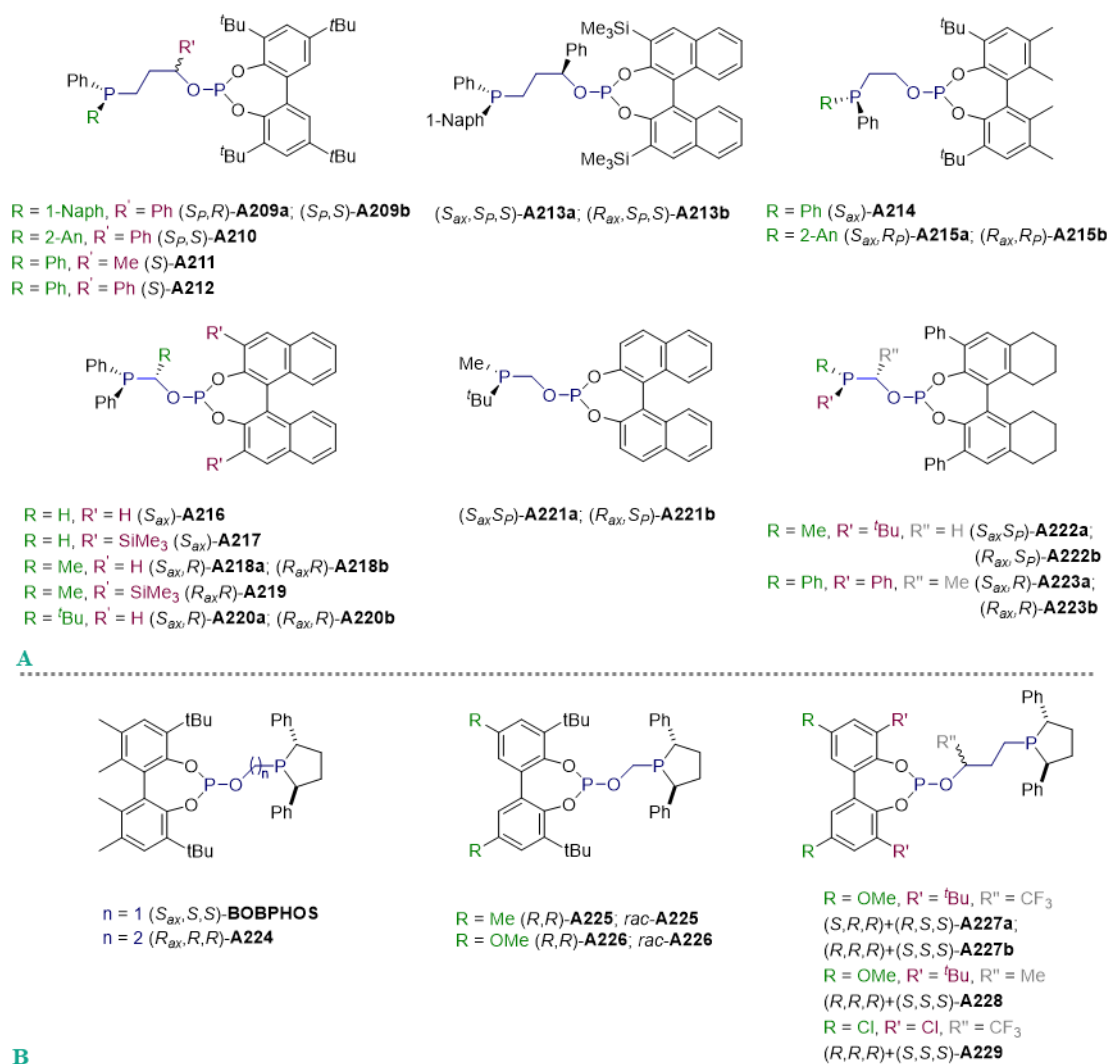
Figure 4.2. *Hydroformylation ligands possessing a "R_2P-$(CH_2)_n$-O-PO_2" backbone. **A**) Ligands reported by van Leeuwen (**A209-A213**),[336] Peruzzini and Pizzano (**A214, A215**),[337] Faraone (**A216, A217**)[338] and Vidal Ferran (**A218-A223**);[339-341] **B**) ligands reported by Clarke ((S_{ax},S,S)-**BOBPHOS**, **A224-A229**).[309,342-346] Where axial chirality is not described, the biphenyl scaffold does not show atropisomerism. Naph = naphthyl, An = anisyl.*

4.1.3. Hydroformylation in a Confined Space

Building on the principles introduced in **Section 1.3**, the use of supramolecular ligand architectures and secondary interactions to control the regioselectivity of hydroformylation is of considerable current interest.[20,27,305,347] A seminal example is the zinc porphyrin-based capsule **A96** reported by Reek (**Figure 4.3**, **Section 1.3.1**).[91-97] Notable branched selectivity across a range of alkenes was observed (53-62 %), making this one of the most branched selective systems to date. Good regioselectivity in the hydroformylation of internal olefins was also observed. This results from NCIs between the porphyrin units - formation of branched species results in little perturbation of these NCIs as there is little distortion of the capsule. However, formation of linear species requires more significant distortion and, therefore, an associated energy penalty.[94]
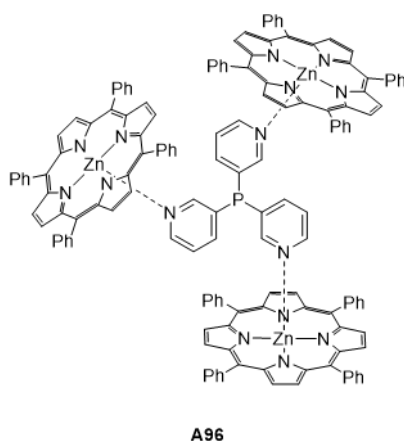
*Figure 4.3. Ligand-templated zinc porphyrin capsule **A96** reported by Reek.[91-97]*

As an extension of work in the Chaplin group using resorcinarene-derived ligands (**Section 1.3.3** and **Chapter 3**), their application in hydroformylation was of interest.[348] Ligands based on cyclodextrin,[349-355] calixarene and resorcinarene scaffolds have been reported, although it is the last two groups that are more prevalent.

In 1998, Kollár found that the lower rim-functionalised tetraphosphines and phosphinities **A230** and **A231** (**Figure 4.4**) gave good branched selectivities in the hydroformylation of styrene (up to 93 %).[356] However, an issue with functionalisation of the lower rim is that the metal is placed underneath the cavity rather than inside it. The vacant coordination site is, subsequently, located on the opposite side to the cavity, and as such, coordination of the olefin and the subsequent hydride migration step can become controlled by the sterics of the phosphorus substituents rather than the cavity. This can result in high linear selectivities, or little selectivity at all.[357-365]
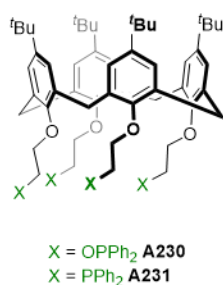
Figure 4.4. Lower rim-functionalised calixarene ligands A230 and A231 employed in rhodium-catalysed hydroformylation by Kollár.[356]

Examples of upper rim-functionalisation include the phosphine-functionalised calixarenes reported by Harvey (**A232**-**A237**, **Figure 4.5**).[366] Reaction with transition metal precursors led to the formation of dimeric species, even when the phosphine groups were located on neighboring aromatic rings as in **A235**-**A237**. Moderate linear selectivity (63-65 %) was observed in the hydroformylation of 1-hexene, along with good branched selectivity for substituted olefins such as styrene and vinyl acetate (> 90 %).

An unusual example of an upper rim-functionalised cavitand ligand is the calix-fused phosphole **A238**, reported by Sémeril.[367] The lone pair on phosphorus is directed into the cavity, placing the rhodium centre above the cavity during catalysis. Again, excellent regioselectivity for the branched product (95-97 %) was observed in the hydroformylation of vinyl arenes. Sémeril also synthesised the diphosphite ligands **A239** and **A240**, are based on calixarene and resorcinarene backbones, respectively.[368] A rhodium chelate complex was observed in the case of calixarene **A239**, but resorcinarene **A240** formed a dimer because of the greater distance between the phosphite donors. High branched selectivities (51->99 %), and moderate enantioselectivities (up to 89 %), were observed in the hydroformylation of vinyl arenes.
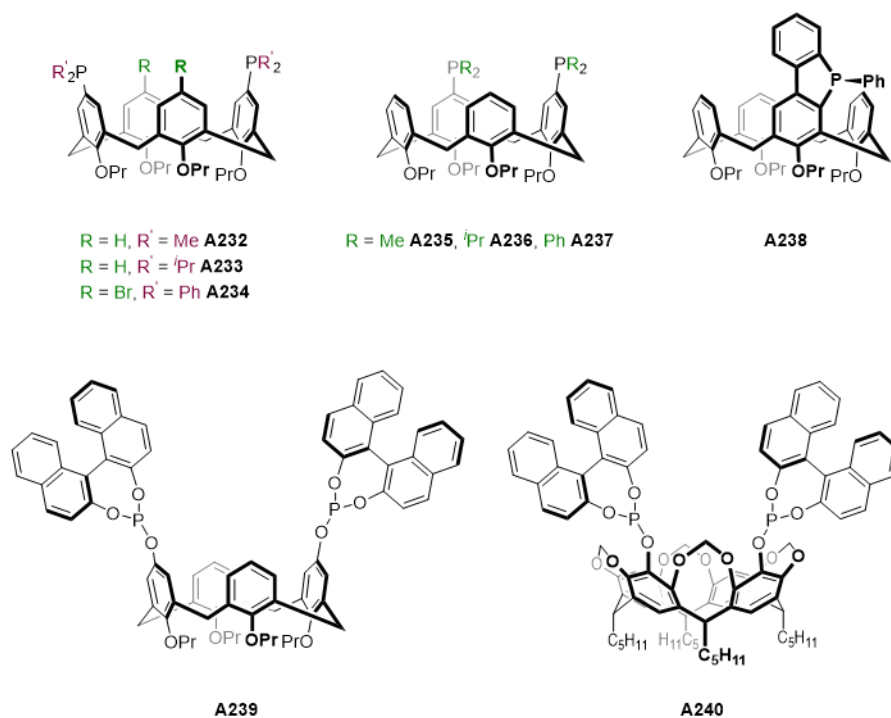
Figure 4.5. *Selected examples of lower-rim functionalised cavitand ligands employed in rhodium-catalysed hydroformylation.*[366-368]

Overall, these systems do not display particularly remarkable cavity effects. It is possible that the dimer formation observed in some cases, along with the flexibility of the cavitand, reduces regioselectivity. The strategy of incorporating a cavitand into a ligand framework does have potential for achieving branched selective hydroformylation, but there is room for improvement in terms of ligand design, allowing the full potential of the cavitand to be utilised. The use of a deep cavitand, with the donor groups embedded in one of the walls, is likely to place the metal centre just inside a well-defined confined space, ensuring the cavity plays a role in catalysis. Iwasawa and Sémeril have recently reported on the hydroformylation of styrene using ligands that fit this description.[125] Resorcinarene-based ligands **A106**, **A241** and **A242** (**Figure 4.6**, **Section 1.3.2**) were investigated to probe the effect of the number and positioning of the quinoxaline walls on catalysis. To the best of our knowledge, these, along with **A240**, remain the only resorcinarene-derived ligands investigated in rhodium-catalysed hydroformylation. Key observations made here include the high branched selectivity displayed by all three ligands. *Cis*-walled **A242** displayed a branched to linear (b/l) ratio that remained constant with increasing P/Rh ratio, but both **A106** and **A241** behave similarly, with branched selectivity increasing with the P/Rh ratio, likely to be due to mono-ligation in these systems. In each case, linear selectivity increased with temperature. The reduced confinement provided by a *cis*-walled cavitand appears to be less important here than in the gold(I) chemistry of these ligands (**Section 1.3.2**).
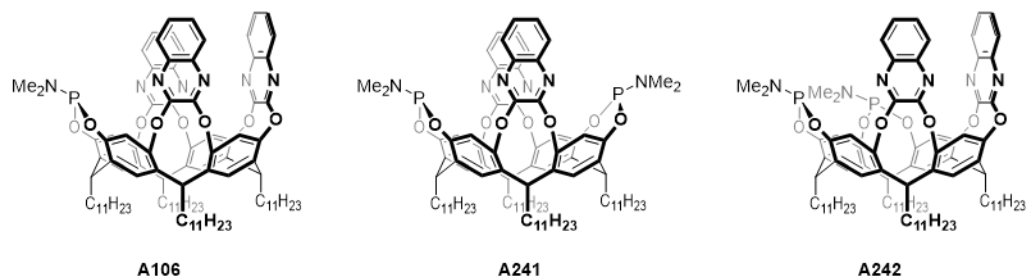
Figure 4.6. Deep cavitand ligands investigated by Iwasawa and Sémeril.[125]

The lack of data relating to straight-chain, terminal olefins is unhelpful in assessing the impact of confinement upon regioselectivity. We propose that by functionalising the upper rim of a deep cavity resorcinarene with a pendant chelate, dimer formation could be avoided. Moreover, the metal centre will reside inside the well-defined confined space. This should ensure that confinement plays a role in catalysis. Given that the phosphine-phosphite ligand **A124** (**Figure 4.7**, **Section 1.3.3**) possesses these features,[131] along with the beneficial electronic differences in its donor groups, and inspired by the fact that it has a similar backbone to (S_{ax},S,S)-BOBPHOS, it's application in the rhodium-catalysed hydroformylation of terminal olefins was of particular interest.
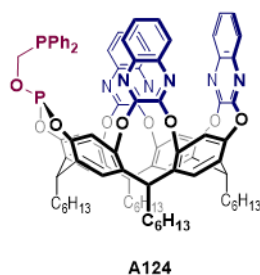
*Figure 4.7. Resorcinarene-derived chelating ligand **A124**, previously synthesised in the Chaplin group.[131]*

4.2. A Resorcinarene-Based Chelating Phosphine-Phosphite Ligand

4.2.1. Ligand Synthesis

The synthetic route to the resorcinarene-derived ligand **A124** has previously been developed within the Chaplin group.[131] Following the procedure outlined in **Section 3.2**, *tris*-walled resorcinarene **A243** was synthesised.[127,258] In a modification of the procedure described by Iwasawa,[117] a phosphoramidite moiety was subsequently introduced to form **A244**, which was converted into chlorophosphite **A197** following treatment with hydrochloric acid. Finally, this was treated with (hydroxymethyl)diphenylphosphine, in the presence of base, to give the desired ligand **A124**.
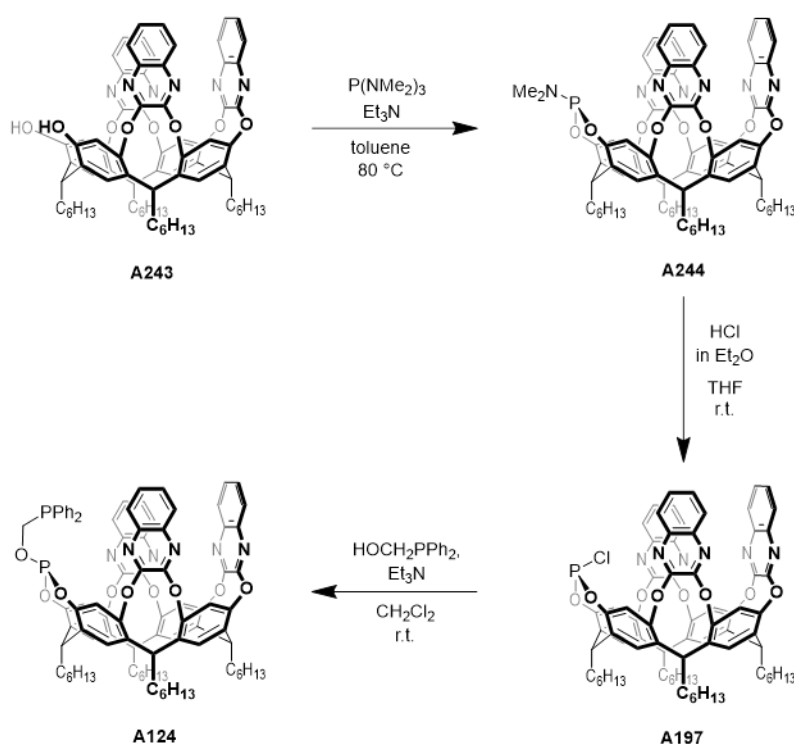
Scheme 4.3. *Synthesis of resorcinarene-derived phosphine-phosphite A124.[131]*

4.2.2. Synthesis and Characterisation of Acetylacetonate Complexes

In order to probe the effect of the cavity upon hydroformylation, two non-supramolecular model ligands were chosen with which to compare the resorcinarene system against. 1,2-Bis(diphenylphosphino)ethane (dppe) was chosen as it has a small steric profile, is known to display poor activity and selectivity in rhodium-catalysed hydroformylation, and is readily available.[18,284,322] In addition to this, (S_{ax},S,S)-BOBPHOS was chosen because of the high selectivity shown in the hydroformylation of 1-hexene. It was predicted that this system would maintain this selectivity with increasing olefin chain length, whilst **A124** may display size selectivity. All three of these ligands display small natural bite angles (the observed bite angles

in [PdCl$_2$L$_2$] complexes of dppe[369] and (S_{ax},S,S)-BOBPHOS[309] are 85.82(7) ° and 86.13(9) °, respectively). Ligands with larger natural bite angles lead to a catalyst with the ligand bound in an equatorial-equatorial fashion, ultimately giving higher proportions of linear product.[370] Could the use of a smaller bite angle chelate (which would result in equatorial-axial binding) promote branched product formation?

For the purposes of this study, the acac complexes of the three ligands: dppe, (S_{ax},S,S)-BOBPHOS and **A124** were synthesised and characterised, prior to be being trialled as hydroformylation pre-catalysts (an alternative strategy involves the pressurising of a solution of [Rh(CO)$_2$(acac)] and ligand with syngas, to form the pre-catalyst *in situ*). The complexes **44**-**46** were prepared *via* a substitution reaction of the appropriate ligand with [Rh(CO)$_2$(acac)] at ambient temperature (**Scheme 4.4**) and isolated in good yield (70 % **44**, 73 % **45**, 80 % **46**). Although dppe complex **44** has been previously reported, only ^{31}P{^{1}H} and ^{13}C{^{1}H} NMR shifts were given.[371] Full ^{1}H, ^{13}C{^{1}H} and ^{31}P{^{1}H} NMR data was, therefore, obtained, with the value of δ_P 70.2 (d, $^1J_{RhP}$ = 193 Hz) being consistent with the literature. Single crystals suitable for X-ray diffraction were obtained by slow diffusion of hexane into a fluorobenzene solution at ambient temperature and the crystal structure is displayed in **Figure 4.8**.
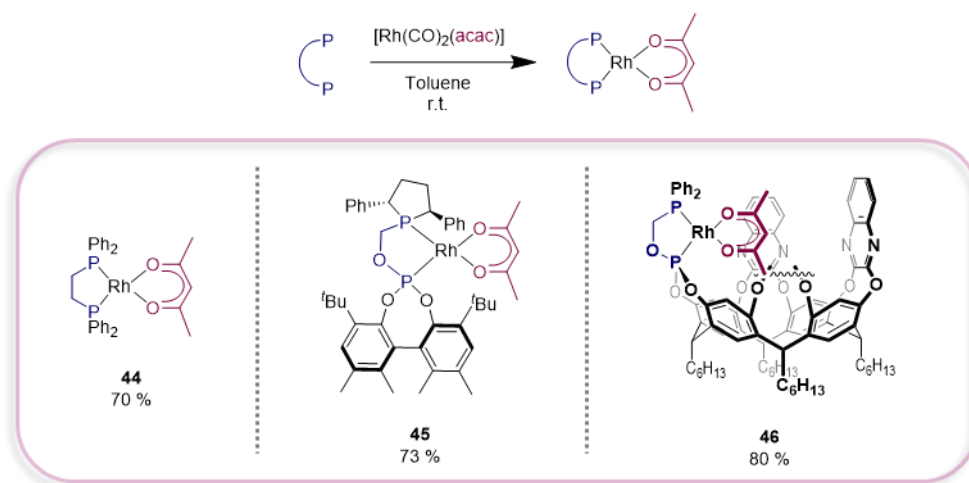
Scheme 4.4. Synthesis of pre-catalysts 44-46.
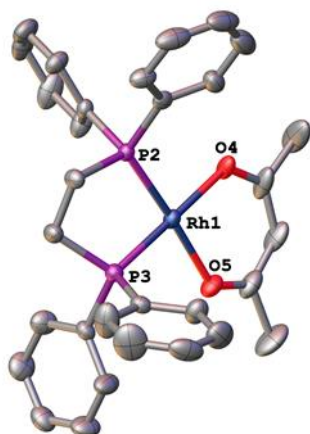
***Figure 4.8.** Solid-state structure of complex **44**, determined at 150 K. Atomic displacement parameters are drawn at 50 % probability. Hydrogens are omitted for clarity. Selected bond distances (Å) and angles (°): Rh1-P2 2.181(1), Rh1-P3 2.179(1), Rh1-O4 2.080(3), Rh1-O5 2.072(3); P2-Rh1-P3 84.85(4), P2-Rh1-O4 95.0(1), P3-Rh1-O5 91.4(1), O4-Rh1-O5 88.8(1), P2-Rh1-O5 176.2(1), P3-Rh1-O4 178.9(1).*

Despite extensive investigations by Clarke and co-workers,[342-344,346] complex **45** has not previously been isolated. Key spectroscopic features include resonances in the ^{31}P{^{1}H} NMR spectrum, corresponding to the phosphite and phosphine moieties: δ_P 164.80 (dd, $^2J_{PP}$ = 318, $^1J_{RhP}$ = 72), 113.3 (dd, $^2J_{PP}$ = 192, $^1J_{RhP}$ = 72). Complex **45** was characterised by ^{1}H, ^{13}C{^{1}H} and ^{31}P{^{1}H} NMR spectroscopy, HR ESI-MS and elemental analysis. XRD was used to confirm connectivity and the structure is shown in **Figure 4.9**.
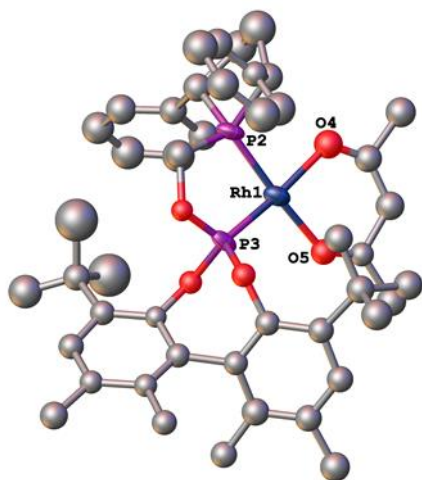
***Figure 4.9.** Solid-state structure of complex **45**, determined at 150 K. Atomic displacement parameters are drawn at 50 % probability. Rhodium and phosphorus atoms were refined anisotropically, all others were refined isotropically. Hydrogens are omitted for clarity. Structure suffers from crystallographic issues and so is only used to confirm connectivity.*

Finally, complex **46** was characterised by ^{1}H, ^{13}C{^{1}H} and ^{31}P{^{1}H} NMR spectroscopy and bulk purity was established by elemental analysis. The ^{31}P{^{1}H} NMR spectrum also displayed resonances corresponding to the phosphine and phosphite moieties: δ_P 160.8 (dd, $^1J_{RhP}$ = 305 Hz, $^2J_{PP}$ = 79 Hz), 76.6 (dd, $^1J_{RhP}$ = 181.6, $^2J_{PP}$ = 79 Hz). A notable feature of this complex is the acac protons, which experience significant shielding (δ_H 0.94, CH; −0.01, −2.75, CH$_3$),

helping to confirm the structural assignment that places the acac ligand within the resorcinarene cavity. The same feature is noted for the rhodium(I) diene complexes presented in **Section 1.3.3**. The most shielded resonance is assigned to that which resides deeper in the cavity (*en*-CH$_3$), whilst the highest frequency signal corresponds to the methyl group pointing towards the top of the cavity (*ex*-CH$_3$). The same observation can be made in the ^{13}C{^{1}H} NMR spectrum, but to a lesser extent: the acac ^{13}C{^{1}H} resonances in **46** are all 1-7 ppm lower than those in complexes **44** and **45**. This observation is promising as it would suggest that any rhodium species formed during catalysis will be influenced by the cavity. Attempts to obtain single crystals suitable for X-ray diffraction were not successful, and so *in lieu* of a solid-state structure, that of rhodium(I) NBD complex **A131** (**Section 1.3.3**, NBD = norbornadiene) was inspected, instead.[131] **Figure 4.10** highlights that the organometallic fragment resides within the cavity defined by the quinoxaline walls, and it is this feature that led us to conclude that this could be a suitable candidate for the selective hydroformylation of alkyl olefins.
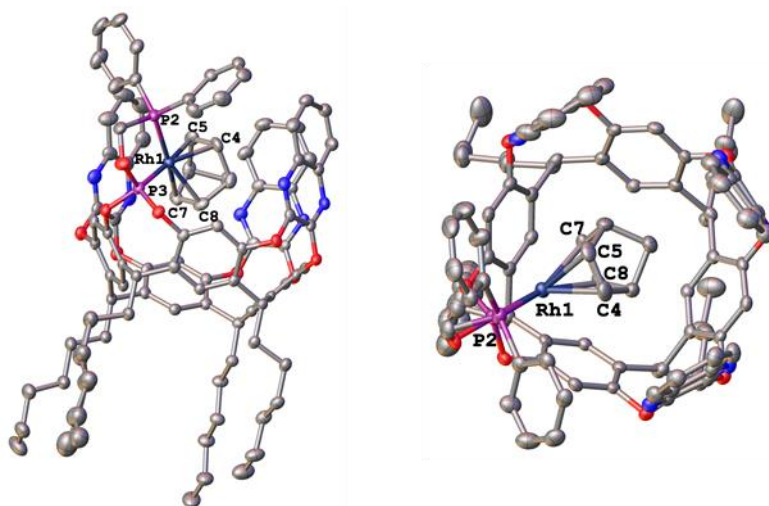
Figure 4.10. *Different views of the solid-state structure of **A131**, determined at 150 K, showing the placement of the organometallic fragment within the quinoxaline-defined cavity.[131] Thermal ellipsoids are drawn at 50 % probability. Hydrogens and counterion are omitted for clarity. P2-Rh1-P3 82.16(4) °*

4.3. Hydroformylation Catalysis

With the three pre-catalysts **44**-**46** in hand, hydroformylation of the terminal, unbiased alkenes 1-hexene, 1-heptene and 1-octene was pursued. Prior to analysis of the resorcinarene and (S_{ax},S,S)-BOBPHOS systems, conditions were optimised using the model dppe system (pre-catalyst **44**).[‡]

This optimisation was informed by a standard hydroformylation procedure that has been developed in the Pringle group, based upon collective knowledge and experience in carrying out hydroformylation experiments. It involves the activation of a solution of 0.012 mmol of pre-catalyst in 1.5 mL of toluene at the chosen reaction temperature and under 10 bar of 1:1 H_2/CO mixture for 30 minutes, before addition of substrate (using a substrate/Rh ratio of 400) at 20 bar of 1:1 H_2/CO. A standard reaction time is 30 minutes, at which point the reaction is quenched and an aliquot is taken for analysis by NMR spectroscopy. These conditions form a convenient starting point, from which modifications can be investigated if necessary. For example, various temperatures and reaction times can be explored. In this case, a conversion of ~30 % was targeted. This is desirable if b/l is to be investigated and compared across several ligands, because at higher conversions, olefin isomerisation becomes more significant. This subsequently results in hydroformylation of the internal olefins produced, complicating analysis of the product distribution. At much lower conversions, the error in the measurements will be greater.

Given the poor conversion displayed by pre-catalyst **44** after 30 minutes (**Table 4.1**: entries **1**-**2**), a reaction time of 1.5 hours was chosen and hydroformylation of 1-hexene with complex **44** was investigated at 50, 60 and 70 °C. The results are shown in **Table 4.1** (entries **3**-**8**). Duplicate runs were conducted to ensure consistency in the conversion and b/l ratio. A temperature of 60 °C (at this longer reaction time) gave a suitable conversion for analysis of the product distribution, as shown in entries **5** and **6**. These conditions were subsequently used in the hydroformylation of 1-heptene and 1-octene (**Table 4.1**: entries **9**-**12**) without further screening.

The b/l ratio decreases slightly with increasing temperature, a phenomenon which is commonly observed in hydroformylation. This is due to a combination of a shift in the equilibrium for rhodium-alkyl formation at higher temperatures and the fact that the activation energy of hydrogenolysis of the linear acyl group is higher than that for the branched acyl group, and so the rate constant has a stronger temperature dependence.[372] However, the system remains consistently unselective (b/l = 0.41-0.43, 29-30 %) at 60 °C across all substrates

---

[‡] Initial optimisation was performed by Dr Rebekah J. Jeans, Pringle Group, University of Bristol.

(**Figure 4.11**). These results are in line with the lack of selectivity previously observed when dppe is used as a ligand in hydroformylation. [18,284,322]

Table 4.1. *Rhodium-catalysed hydroformylation using complex pre-catalyst **44** (dppe).[a]*

Entry	Substrate	Temp / °C	Total conversion / %[b]	b/l[b]	Branched selectivity / %
1[c]	1-hexene	60	7.8	0.44	30
2[c]	1-hexene	60	7.3	0.46	32
3	1-hexene	50	4.6	0.54	35
4	1-hexene	50	5.6	0.50	33
5	1-hexene	60	24.8	0.41	29
6	1-hexene	60	29.5	0.41	29
7	1-hexene	70	67.3	0.39	28
8	1-hexene	70	64.5	0.39	28
9	1-heptene	60	16.8	0.46	32
10	1-heptene	60	25.4	0.42	30
11	1-octene	60	29.8	0.41	29
12	1-octene	60	25.9	0.43	30

[a] **44** (0.012 mmol/0.25 mol%), toluene (1.5 mL), activation for 30 min at 10 bar H_2/CO; 1-hexene (0.60 mL)/1-heptene (0.68 mL)/1-octene (0.75 mL) in toluene (1 mL), products obtained after reaction for 1.5h at 20 bar H_2/CO.
[b] Product distribution determined by ^{1}H NMR spectroscopy (see **6.4.5**).
[c] Products obtained after reaction for 30 min.

Attention was then turned to (S_{ax},S,S)-BOBPHOS complex **45**. Given the literature precedents for this ligand's role in hydroformylation,[342-344,346] **45** was expected to be more active than **44**. As before, a reaction time of 30 minutes was initially investigated, using the optimal temperature of 60 °C, as determined above, for consistency. Although slightly lower overall, the conversions achieved across all three susbtrates were still deemed suitable and so the reaction time and temperature were not screened further. The results obtained with this system are summarised in **Table 4.2**.[§]

[§] Catalysis with complex **45** was performed by Dr Rebekah J. Jeans.

Entry	Substrate	Total conversion / %[b]	b/l[b]	Branched selectivity / %
1	1-hexene	22.1	2.30	70
2	1-hexene	16.6	2.30	70
3	1-heptene	18.6	2.22	69
4	1-heptene	14.3	2.25	69
5	1-octene	21.1	2.23	69
6	1-octene	21.2	2.19	69

[a] **45** (0.012 mmol/0.25 mol%), toluene (1.5 mL), activation for 30 min at 10 bar H_2/CO; 1-hexene (0.60 mL)/1-heptene (0.68 mL)/1-octene (0.75 mL) in toluene (1 mL), products obtained after reaction for 30 min in toluene at 60 °C and 20 bar H_2/CO.
[b] Product distribution determined by ^1H NMR spectroscopy (see **6.4.5**).

Consistent with the literature, pre-catalyst **45** shows a high b/l ratio across all the substrates (**Figure 4.11**), although the value of 2.30 is lower than the reported value of 3.0 (in the hydroformylation of 1-hexene). This difference is not unexpected, as it has already been stated that hydroformylation is very sensitive to the conditions applied and those used in this study are different to those used in the literature (5 bar H_2/CO, 16 °C, 46 h).[342]

In order to guage the activity of novel pre-catalyst **46**, hydroformylation of 1-hexene was examined after 1.5 hours at 60 °C (the conditions found to be suitable with pre-catalyst **44**, using dppe as a ligand). A very high conversion of 93.1 % was obtained (**Table 4.3**: entry **1**), indicating that the resorcinarene-based **46** forms a much more active system than dppe complex **44**. Therefore, hydroformylation of 1-hexene was investigated at 50, 60 and 70 °C, with the standard reaction time of 30 minutes. The results of these runs are shown in **Table 4.3** (entries **2**-**6**). As seen with complex **44**, the same decrease in branched selectivity was observed with increasing temperature.

Table 4.3. Rhodium-catalysed hydroformylation using complex pre-catalyst *46 (A124)*.[a]

Entry	Substrate	Temp / °C	Total conversion / %[b]	b/l[b]	Branched selectivity / %
1[c]	1-hexene	60	93.1	0.97	49
2	1-hexene	50	18.3	1.06	51
3	1-hexene	50	18.1	1.07	52
4	1-hexene	60	57.9	0.92	48
5	1-hexene	60	55.9	0.93	48
6	1-hexene	70	90.5	0.85	46
7	1-hexene	70	88.2	0.86	46
8	1-heptene	60	24.7	2.51	72
9	1-heptene	60	30.3	2.45	71
10	1-octene	60	21.8	6.07	86
11	1-octene	60	23.6	5.66	85

[a] *46* (0.012 mmol/0.25 mol%), toluene (1.5 mL), activation for 30 min at 10 bar H_2/CO; 1-hexene (0.60 mL)/1-heptene (0.68 mL)/1-octene (0.75 mL) in toluene (1 mL), products obtained after reaction for 30 min at 20 bar H_2/CO.
[b] Product distribution determined by ^{1}H NMR spectroscopy (see **6.4.5**).
[c] Products obtained after reaction for 1.5 h.

The initial results obtained using 1-hexene as a substrate are promising, showing the system to be more selective than the dppe-ligated system (**Table 4.3**: entries **4**-**5**, 48 % *cf.* 29 %). However, this is less selective than the (S_{ax},*S*,*S*)-BOBPHOS-ligated system (75 % literature value,[342] 69 % under our conditions). Lower temperatures may have resulted in higher selectivities, but it is likely that this would have required further adjustments to the reaction time and it was not considered worthwhile investigating this further at this stage, given the time and material constraints.

Attention was, instead, turned to the longer-chain substrates. Interestingly, hydroformylation of 1-heptene results in higher branched selectivity (**Table 4.3**, entries **8**-**9**, 71 %). These values are more comparable with (S_{ax},*S*,*S*)-BOBPHOS. The highest b/l ratio occurs when the olefin chain length is increased further: hydroformylation of 1-octene gives an average branched selectivity of 85 % (**Table 4.3**, entries **10**-**11**; **Figure 4.11**). This is higher than the 62 % achieved by Reek with a rhodium catalyst based on porphyrin capsule **A96**.[92] Initial interpretation of these results potentially points towards a degree of size-selectivity taking place, with the longer alkyl chain of the branched octyl rhodium intermediate interacting favourably with the cavitand and, therefore, preferentially following the branched pathway over the linear one. For the shorter-chain olefins, this effect would be less pronounced, resulting in lower selectivities. Another interesting feature is that the conversion after 30 minutes decreases with increasing chain length, from 57 % to 23 %. This could be

explained in terms of sterics: it is easier for the shorter-chain 1-hexene to reach the rhodium centre, embedded in the cavity, than the bulkier 1-octene.
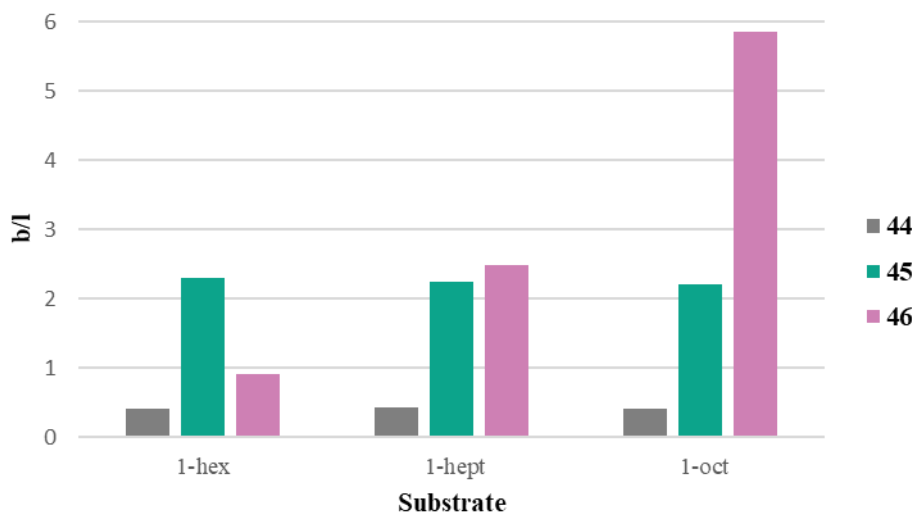
***Figure 4.11.** Bar chart showing the branched to linear ratio (b/l) for the pre-catalysts employed in the hydroformylation of 1-hexene, 1-heptene and 1-octene (**44**:dppe, **45**:(S$_{ax}$,S,S)-BOBPHOS, **46**:A124).*

It is also worth noting that while **46** results in greater isomerisation than **44** and **45** at these low conversions (2-hexene: 1.22 % **44**, 1.25 % **45**, 4.13 % **46**; 2-heptene: 0 **44**, 0.968 % **45**, 2.96 % **46**; 2-octene: 1.46 % **44**, 0.959 % **45**, 1.38 % **46**), this still only forms a minor component of the overall mixture. No evidence for further isomerisation to the 3-alkenes was observed in any case. **Scheme 4.5** shows the possible aldehyde products that could arise from hydroformylation of these alkenes. Hydroformylation of terminal alkenes would lead to the production of linear **I** and branched **II**, whereas hydroformylation of internal alkenes would lead to the production of branched aldehydesof types **II** and **III**. The presence of **II** and **III**, originating from internal alkenes, can increase the branched aldehyde product total. A recent study by Abolhasani reports impressive selectivities for branched aldehyde products of up to 94 % (b/l = 16.7) in the hydroformylation of 1-octene using a fluorophosphate ligand, but this relies on modification of conditions to encourage isomerisation to internal octenes, with subsequent hydroformylation, producing a mixture of branched aldehyde products.[373] However, in our three systems, an aldehyde possessing structure **III** (specifically, 2-ethylpentanal) was only ever observed with resorcinarene-based pre-catalyst **46**, when conversion reached 88 % or higher (**Table 4.3**: entries **1**, **6** and **7**). This indicates that hydroformylation of internal alkenes is more challenging for these systems. It is, therefore, most likely that the origin of branched aldehydes **II** is primarily the formation of 2-alkyl rhodium intermediates from 1-alkenes, rather than hydroformylation of isomerised alkenes. This gives further support to the theory that it is the presence of the deep cavity that influences the regioselectivity in hydroformylation using pre-catalyst **46**.
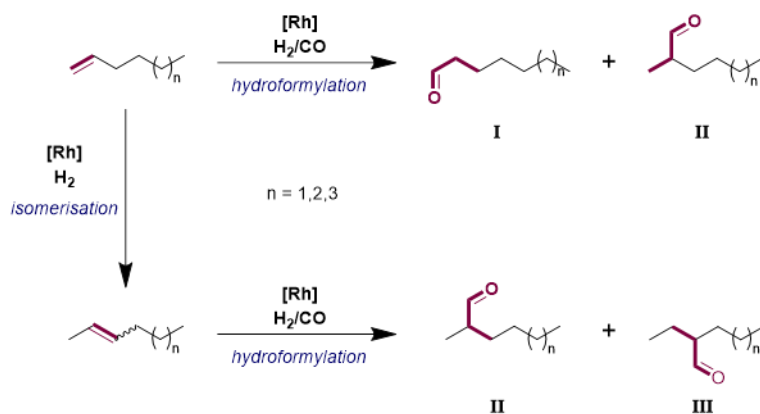
Scheme 4.5. *Possible alkene and aldehyde products that could arise from the hydroformylation of 1-hexene, 1-heptene and 1-octene under these conditions.*

One final point to note is that in many studies, an excess of ligand is used (*i.e.* a higher ligand to rhodium ratio than 1). This is particularly important where monodentate ligands are used as dissociation can occur, but this is less of a concern when bidentate ligands are used, as the resulting complex is stabilised *via* the chelate effect. Additionally, this is likely to be less of an issue in the context of this work as the reaction mixtures were analysed at lower conversions, before any significant decomposition could take effect. Because of the activation procedure used here, where the pre-catalyst was pre-formed prior to activation, introduction of an excess of ligand was less straightforward. This method was, however, tested with dppe system **44**, using an additional equivalent of dppe in the reaction mixture alongside pre-formed **44**. Following the standard protocol, an increased b/l of 1.10 (52 %) was observed. This was accompanied by a significant reduction in activity, with conversion dropping to 4.59 %. It was concluded that this additional equivalent of ligand inhibits catalysis and so was not investigated for the other two systems.

A discussion of the error asscoaited with NMR integration should be included here. Signal to noise ratio can be an issue, although it was deemed acceptable in these cases. If the pulse delay used to obain these spectra is too short compared to the T_1 relaxation rates of the protons, the spectra can become saturated, resulting in inaccurate integrations. The pulse delay used here was 1 s, and although greater accuracy can be achieved if a longer pulse delay is used (between 5-10 s), the error associated with this is not huge. Errors arising from saturation effects can be larger when comparing protons in different environments, as these will have different T_1 values. This may apply to this work, as integrations of aldehyde and alkene protons were compared to determine conversion. Another potential error source is line-shape considerations and ensuring that the integrations are carried out over a sufficient frequency range. In this case, the multiplets (and accompanying ^{13}C satellites) of interest were broad and given the intensity differences between, for example, excess unreacted alkene and the small amounts of isomerised alkene, error may have been introduced here. Finally, the

presence of ^{13}C satellites which potentially overlap with other resonances may have introduced error to the integrations, in particular when determing the amount of alkene isomerisation taking place, as a result of the proximity of the two resonances and the intensity issues discussed previously. ^{13}C decoupling can remove this issue, but also introduces inaccuriacies from Nuclear Overhauser Effects (which can distort peak intensities).[374]

Overall, these issues can lead to a small amount of error in data based upon NMR integrations. However, this error is not huge and conclusions can still be drawn from this data. The errors discussed above are likely to impact the calculated conversions and degrees of isomerisation more than the b/l ratios, and it is these last parameters that are of greatest interest here. If more accurate values are desired, the results could be reinforced by GC-MS analysis, a useful technique for accurately determining component quantities. However, the results obtained with pre-catalysts **44** and **45** show a high degree of consistency and literature agreement, whilst the trend displayed by pre-catalyst **46** is clearly significant enough to be unimpacted by the small error sources discussed here.

4.4. <u>NMR Spectroscopic Investigations</u>

With the resorcinarene-based system **46** showing such promising results in hydroformylation catalysis under the conditions applied above, it was of interest to examine the active species using high pressure ^{1}H and ^{31}P NMR spectroscopy. In **Section 4.1.1**, it was stated that the active hydroformylation catalyst is a trigonal bipyramidal hydrido carbonyl species, in which the strong, σ-donating hydride occupies an axial position.[375] With a bidentate ligand, steric considerations mean that one equivalent of this ligand, along with two carbonyls, are expected to be coordinated to rhodium. For a hybrid chelate there are three possible binding modes: an axial-axial mode, the phosphine coordinated axially and the phosphite equatorially, or the phosphite coordinated axially and the phosphine equatorially. It is the latter two (equatorial-axial) binding modes that are observed for smaller bite angle ligands. The aim of these NMR investigations was, firstly, to provide information on whether the resorcinarene-based ligand was indeed coordinated to rhodium during catalysis (and so is responsible for the impressive branched selectivity that is observed in the hydroformylation of 1-octene) and, secondly, to determine the binding mode of ligand **A124**. This is important as an equatorially-bound phosphite moiety would place the hydride ligand inside the cavity during catalysis (**47**, **Figure 4.12**), whereas an axially-bound phosphite would place the hydride pointing towards the top of the cavity (**48**).
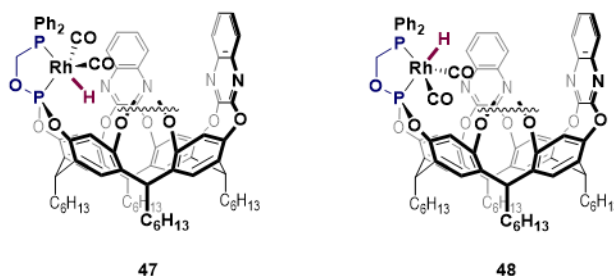
*Figure 4.12. Possible structures of the active rhodium(I) hydrido carbonyl species, with ligand **A124** bound in an equatorial-axial fashion.*

A solution of 0.0091 mmol of complex **46** in 1.5 mL of toluene was activated under 20 bar 1:1 H_2/CO in a 10 mL reactor for two days at ambient temperature. A 500 μL aliquot of this reaction mixture was then transferred to an NMR tube and analysed under ambient conditions.** Significant conversion to a major new rhodium-bound species, along with other minor phosphorus-containing species, was observed by ^{31}P{^{1}H} NMR spectroscopy. This major product was assigned as hydrido carbonyl complex **47** (**Scheme 4.6**) with the two new resonances both displaying coupling to each other: δ$_P$ 181.1 (dd, $^1J_{RhP}$ = 225 Hz, $^2J_{PP}$ = 43 Hz),

---

** NMR investigations were performed by Dr Rebekah J. Jeans.

68.6 (dd, $^1J_{RhP}$ = 99 Hz). These were attributed to the phosphite and phosphine groups, respectively, with the coupling constant of 43 Hz confirming the *cis*-relationship between them. The ^1H NMR spectrum displays a hydride resonance at −9.99 ppm. It appears as a doublet of doublets of doublets ($^2J_{PH}$ = 108 Hz, $^2J_{PH}$ = 22 Hz, $^1J_{RhH}$ = 7 Hz), coupling to rhodium and to the two inequivalent phosphorus nuclei. This coupling between the hydride ligand and the phosphorus nuclei was also observed in a ^1H-^{31}P HMBC experiment, confirming connectivity. In order to confirm that coordination of ligand **A124** takes place as described in situation **47** (rather than as in **48**), $^1H\{^{31}P\}$ experiments were conducted with selective decoupling of each phosphorus resonance. With decoupling of the phosphite resonance (δ_P 181.1), the hydride resonance collapses to a doublet of doublets, with the loss of the smaller, *cis*-phosphorus coupling ($^2J_{PH}$ = 22 Hz). With decoupling of the phosphine resonance (δ_P 68.6), the hydride again collapses to a doublet of doublets, this time with the loss of the larger, *trans*-phosphorus coupling ($^2J_{PH}$ = 108 Hz). These data suggest that a single, static species is present, as opposed to two rapidly interconverting isomers, and it can be concluded that the phosphite is coordinated equatorially (*cis* to the hydride) and the phosphine axially (*trans* to the hydride) - *i.e.* the situation represented by complex **47**.

The values of the coupling constants can also provide structural information. The large differences between the $^2J_{PH}$ values also indicate the presence of a single, static structure, as rapid interconversion of two isomers on the NMR timescale would give rise to intermediate coupling constants.[376] The *cis* $^2J_{PH}$ value of 22 Hz is slightly larger than expected for a trigonal bipyramidal complex, but this is more likely a consequence of distortion from the ideal coordination geometry, brought about by steric congestion and the small bite angle of **A124**.[337] Indeed, this value is similar to those observed in [Rh(PO-P)(CO)$_2$H] complexes, where 'PO-P' is a small bite angle phosphine-phosphite ligand (**Table 4.4**).[309,340] Van Leeuwen has concluded that a $^2J_{PH}$ value of ~102 Hz is consistent with a complex possessing axial phosphine and hydride ligands, whilst a smaller value (~2 Hz in the case of a larger bite angle PO-P ligand) suggests an equatorially-bound phosphite and axial hydride, giving further support to the structural assignment of intermediate **47**. Furthermore, the value of $^1J_{RhH}$ serves to confirm the equatorial-axial binding of **A124**, because the value would be much smaller (<4 Hz) if a carbonyl was coordinated *trans* to the hydride, rather than a phosphine or phosphite.[336]

Table 4.4. $^2J_{PH}$ *coupling constants for complexes of the formula [Rh(L₂)(CO)H], where L₂ is the small bite angle ligands **A124**, (S_ax,S,S)-BOBPHOS[309] and (S_ax,R)-**A223a**,[340] with the larger bite angle (S_p,S)-**A209b** included for comparison (**Figure 4.2A**).[336]*

Ligand	$^2J_{PH}(cis)$ / Hz	$^2J_{PH}(trans)$ Hz
A124	22	108
(S_ax,S,S)-BOBPHOS	23	116
(S_ax,R)-**A223a**	26	111
(S_p,S)-**A209b**	<2	102

This coordination mode, with the phosphine in the axial position and the phosphite in the equatorial position, is widely observed in complexes of hybrid phosphine-phosphite ligands (including (S_ax,S,S)-BOBPHOS),[309,336,337,340] reinforcing the theory that the less electron donating donor resides in an equatorial position in trigonal bipyramidal d^8 complexes.[375,377] The convincing evidence for the formation of hydrido carbonyl complex **47** is important as it can be concluded that the hydride resides within the cavity. Subsequent migratory insertion of the alkene to form rhodium(I) alkyl isomers **49** and **50** (

Scheme 4.6) will, therefore, place the alkyl chain deep within the cavity, rather than directed out of the cavity (the isomeric acyl complexes **51** and **52** will necessarily possess the same feature).

Repetition of this experiment under 10 bar of 1:1 H_2/CO in a pressure valved NMR tube was also undertaken.[††] However, heating at 50 °C for 1 hour did not lead to significant conversion to the hydride species. This is likely due to mass transfer limitations in the NMR tube compared to the autoclave. After heating for 72 hours, conversion to the same hydride species, **47**, was observed, along with evidence of catalyst decomposition. $^{31}P\{^1H\}$ NMR spectra were collected at 298, 273, 253 and 236 K, displaying little variation, although some broadening of the phosphite resonance was observed at 236 K (**Figure 4.13**). This is not significant enough to suggest rapid interconversion between two isomers on the NMR timescale, supporting the conclusion drawn above that a static species is present. Interestingly, a small decrease in the phosphine-rhodium coupling is observed with decreasing temperature (−4 Hz), alongside an increase in phosphite-rhodium coupling (+5 Hz). The phosphine-phosphite coupling is constant across the temperature range.

Figure 4.13. Variable temperature $^{31}P\{^1H\}$ NMR spectroscopy of the activated mixture containing complex 47.
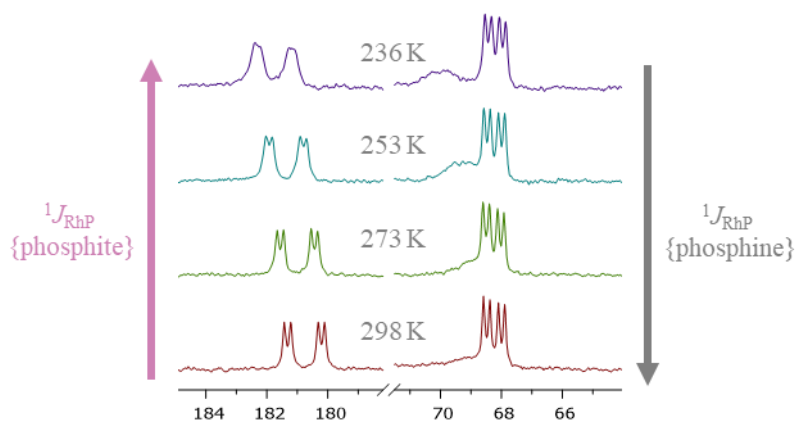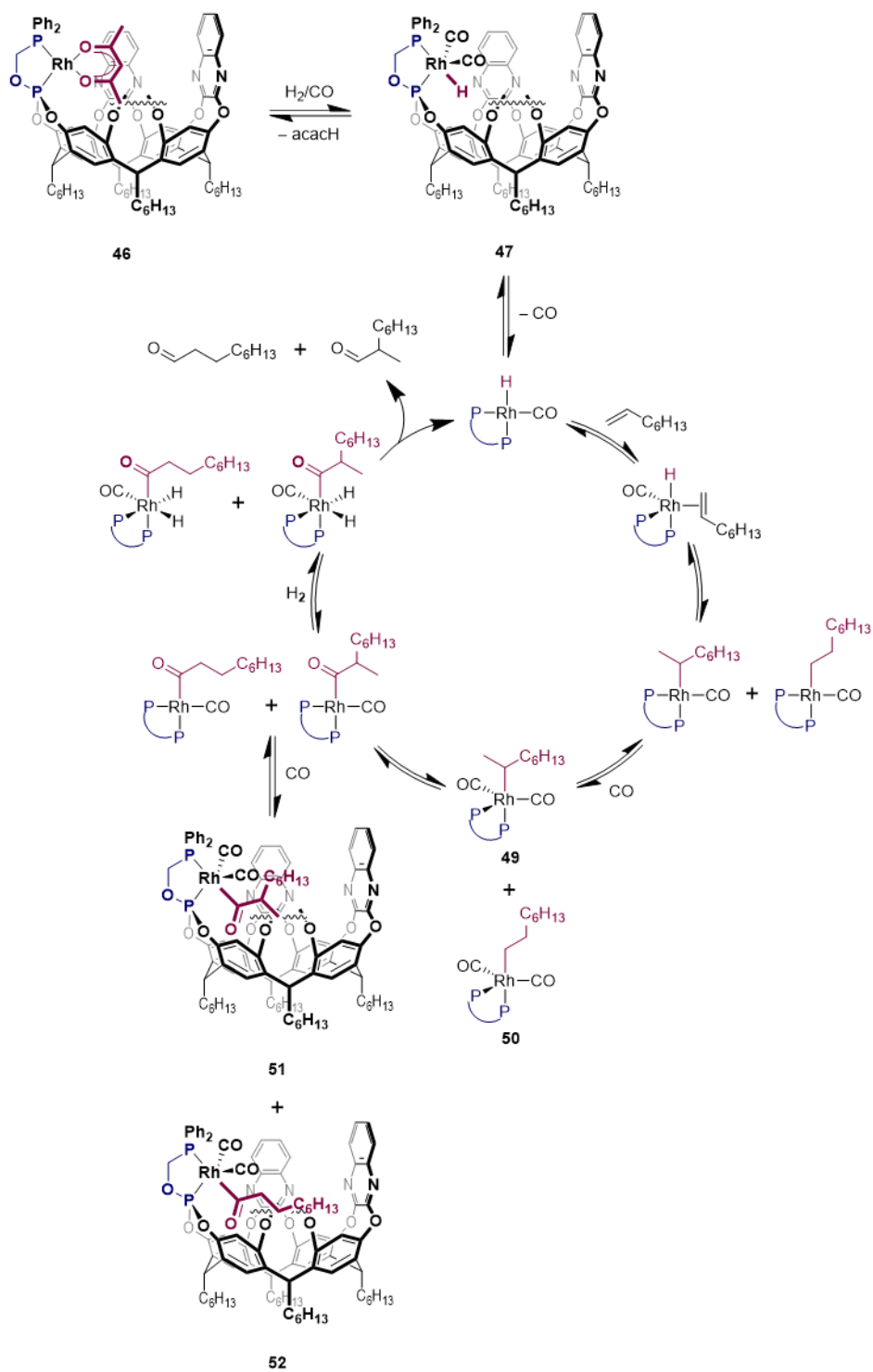
Scheme 4.6. *Putative cycle for the hydroformylation of 1-octene using pre-catalyst **46**. Where the resorcinarene cavity is drawn in full, the species have been observed. Other species are postulated based on the catalytic cycle presented in **4.1.1**.*

To this activated mixture was added 1-octene (chosen because the highest selectivity was observed with this substrate), in order to obtain evidence for the acyl complexes **51** and **52**. This was carried out under an atmosphere of 6 bar of ^{13}CO, enabling identification of the intermediate species based on the presence of ^{13}C-labelled carbonyl ligands. This system suffered from incomplete activation and subsequent catalyst decomposition, resulting in only a small amount of conversion and, subsequently, weak signals. Notably, disappearance of the hydride resonance is apparent in the ^{1}H NMR spectrum. Furthermore, in the ^{13}C{^{1}H} NMR spectrum, two resonances can be seen in the region expected for acyl carbons: δ_C 238.6 (dd, $^2J_{PC}$ = 119 Hz, $^1J_{RhC}$ = 19 Hz), 231.9 (dd, $^2J_{PC}$ = 126 Hz, $^1J_{RhC}$ = 17 Hz). It is postulated that the *cis* carbon-phosphorus couplings, along with *cis* carbon-carbon couplings, would be small and this could explain why they are not observed here. The geometry of **51** and **52** has been assumed based upon the bite angle of the ligand, the geometry adopted by complex **47** and the fact that if **A124** was coordinated equatorially, with a carbonyl *trans* to the acyl group, $^2J_{CC}$ would not be as large as 119-126 Hz. These values are more indicative of *trans* carbon-phosphorus coupling. In high pressure NMR hydroformylations such as this, the structures of intermediate species can typically be confirmed by analysis of the resonances arising from the ^{13}C-labelled carbonyl ligands in the region ~185-195 ppm. However, in this case, this region is obscured by a broad hump, making conclusive structural analysis challenging, and so these results cannot be taken as reliable evidence for the existence of **51** and **52**, as they are represented in **Scheme 4.6**.

Given the ^{1}H and ^{31}P NMR spectroscopic evidence for the active species **47**, along with the very tentative assignment of rhodium acyl intermediates **51** and **52**, the high regioselectivity with increasing alkene chain length can be attributed to the cavity effects of ligand **A124**. The structures of **51** and **52** depicted in **Scheme 4.6.** highlight how steric considerations could explain the results obtained here. The formation of the linear alkyl chain would require significant buckling to be accommodated by the cavity, and so is likely to be sterically disfavoured. This would become more important with increasing alkene size, explaining why the highest b/l was observed in the hydroformylation of 1-octene.

In addition to this, C-H---π interactions are known to play a role in the formation of inclusion complexes, particularly in terms of alkane binding in deep-cavity resorcinarenes.[113,378] In **Section 3.2**, the ability of resorcinarenes to bind small molecules such as alkanes was discussed.[133,259-264] The hydrophobic interior of the resorcinarene cavity is electron rich, offering a concave surface that can induce folding of the substrate and binding *via* C-H---π interactions.[379,380,381] The entropic penalty of alkyl chain folding is, therefore, likely to be offset by the formation of NCIs with the cavity interior and this should also be taken into account when formation of the rhodium alkyl species **49** and **50** is considered. Intermediates along the branched pathway may involve enhanced C-H---π interactions with

the quinoxaline walls, potentially favouring this pathway over the linear one. DFT investigations into the hydroformylation of propene using bidentate phosphines have shown that for small bite angle ligands with differing electronics, the regioselectivity is determined by the relative energies of the transition states for the hydride migration step (*i.e.* the formation of the rhodium alkyl species), and not by isomerisation of the resulting alkyl intermediates, because of the slow rate of *β*-hydride elimination in these systems.[377] Therefore, it is proposed that the branched selectivity displayed by the resorcinarene-based system is a result of formation of **50** being more disfavoured, rather than significant isomerisation between **49** and **50** occurring. The size-selectivity demonstrated here is also potentially due to the larger 2-octyl forming stronger C-H---π interactions than the smaller 2-heptyl or 2-hexyl groups, formed with the shorter-chain alkenes. More detailed investigation, such as computational analysis of these systems, is required to substantiate these claims.

4.5. Summary and Conclusions

In conclusion, the results presented in this chapter show that resorcinarene-based ligand **A124** has potential in the regioselective hydroformylation of alkyl alkenes. Although the hydroformylation of 1-hexene proceeded with lower branched selectivity than that obtained by Clarke, the selectivity was noticeably greater when 1-heptene was used as a substrate. Most interestingly, hydroformylation of 1-octene proceeds to give 2-methyloctanal with 85 % selectivity. To the best of our knowledge, this is one of the highest selectivities obtained in the hydroformylation of 1-octene, with the only better system relying on alkene isomerisation to provide high proportions of a mixture of branched aldehyde products. This increase in selectivity with substrate chain length is proposed to result from a combination of steric effects (disfavouring the linear pathway) and enhanced C-H---π interactions between the intermediate 2-octyl rhodium complex and the quinoxaline walls of the cavitand (favouring the branched pathway). The smaller substrates show reduced selectivity because of the reduced steric demands and potentially because weaker non-covalent interactions are formed, so there is less energetic preference for the branched pathway over the linear pathway. The increase in selectivity that is observed with increasing chain length is accompanied by a decrease in reaction rate, likely to be a steric effect of the bulkier 1-octene entering the cavity to access the rhodium centre.

This work highlights the benefits of rational design of catalytic systems: by analysing features of systems reported in the literature, a novel pre-catalyst was designed that possessed features that were expected to offer an improvement. The results obtained so far would suggest that the deep cavity does enable catalysis to occur within it, and cavity effects are likely to be responsible for the selectivity observed. Furthermore, the pendant chelate on the upper rim of the resorcinarene results in a robust catalyst that does not appear to suffer significantly from ligand dissociation. The small bite angle and electronic differences between the phosphine and phosphite donors are also likely to have impacted the behaviour of pre-catalyst **45**.

Initial mechanistic investigation using high pressure ^{1}H and ^{31}P NMR spectroscopy has confirmed the presence, and geometry, of the intermediate trigonal bipyramidal rhodium hydride – the active species. There is also evidence for the generation of two rhodium acyl complexes (expected on-cycle intermediates). It would be useful to gain more mechanistic insight into this system – the data for these complexes is somewhat inconclusive and it would be of interest to look for evidence of other catalytically-relevant species in the reaction mixture, to gain a deeper understanding of this process. Initially, addition of 1-octene to a sample of fully activated complex **47** should be carried out to provide more useful information.

Another area that warrants further investigation is the effect of varying reaction conditions on the selectivity displayed by pre-catalyst **46**. The effect of increasing the

equivalents of ligand was only investigated with the dppe system **44**; what would be the effect of increasing the ratio of resorcinarene-based ligand to rhodium? Would this allow the high selectivity be maintained at higher conversions, or under more industrially relevant conditions, by increasing catalyst stability?

To further gauge the effect of the deep cavity upon catalysis, related ligands in which the quinoxaline walls are replaced with pyrazine walls, or no walls, could be synthesised, in the manner reported by Iwasawa in the gold(I) catalysis of a resorcinarene-based phosphoramidite (**Section 1.3.2**). This would enable the hypothesis that C-H---π interactions with the quinoxaline groups are responsible for favouring the branched reaction pathway to be tested.

Computational investigation would also give greater insight into the mechanism by which this selectivity arises; in particular, NCI plots of the rhodium alkyl and acyl intermediates would allow stronger conclusions about the interaction of the substrate with the cavitand to be drawn.

Finally, it may be of interest to introduce a stereocenter to the pendant chelate, so that asymmetric, branched-selective hydroformylation could be pursued. Overall, these initial results are very promising and there is much potential for further investigation of this system.

5. **Concluding Remarks**

In this thesis, ligand design strategies were applied to three key targets: i) the investigation of agostic interactions in 2,2-biphenyl complexes of rhodium and iridium; ii) the synthesis of a ligand framework with the potential to stabilise a σ-alkane complex in the solid state and in solution; and iii) regioselectivity control in hydroformylation *via* the secondary coordination sphere. To pursue these targets, the literature was critically assessed to identify key features that should be incorporated into the proposed systems and where previous studies could be improved upon.

Building on a report from the Chaplin group that complexes of the formula $[M(PNP-^tBu)(biph)][BAr^F_4]$ (M = Rh, Ir) do not show appreciable agostic interactions in the solid state, the lesser-known PNP-Np was investigated. The coordination chemistry of this pincer has been extended and includes the $[M(PNP-Np)(biph)][BAr^F_4]$ complexes. As predicted, stronger agostic interactions were formed in these complexes than in the PNP-^{t}Bu analogues. This is likely to result from the additional methylene unit possessed by *neo*pentyl, resulting in the formation of δ-agostics (as opposed to γ-agostics) and resulting in less steric buttressing between the *tert*-butyls and biphenyl. This provides an example of how modification of the primary coordination sphere can influence reactivity.

Various literature reports were drawn upon to design a system that could be used to investigate σ-alkane complex stability in the solid state and in solution. By incorporating a pincer component (inspired by Brookhart's $[Rh(PONOP-^tBu)(CH_4)][BAr^F_4]$) and a resorcinarene (inspired by Diederich's reports of cyclohexane binding in deep cavity resorcinarenes and Weller's solid-state σ-alkane complexes that are stabilised by a well-defined microenvironment), a target ligand was designed. Although the overall objective was not achieved (the ligand could not be isolated) this work provides a promising new ligand design strategy, as potential shortcomings were identified and improvements suggested.

The final objective was inspired by the intriguing strategy of combining supramolecular chemistry and classic organometallic chemistry to exert control over the secondary coordination sphere. Branched-selective hydroformylation is an important strategy in organic synthesis and by employing a resorcinarene-derived chelating ligand, previously developed in the Chaplin group, high regioselectivity was observed for the branched product in the rhodium-catalysed hydroformylation of 1-octene. The size-selectivity displayed by this system, along with NMR investigations, suggest that cavity effects are responsible for this exciting result, and further investigation into this system is of significant interest.

In conclusion, this thesis has demonstrated ways in which the principles of rational ligand design can be drawn upon to develop systems with desired features and reactivity.

6. <u>Experimental</u>

6.1. <u>General Considerations</u>

6.1.1. <u>General Practices</u>

All manipulations were performed under an atmosphere of Ar using Schlenk and glove box techniques, unless otherwise stated. Glassware was oven dried at 150 °C overnight and flame-dried under vacuum prior to use. Molecular sieves were activated by heating at 300 °C *in vacuo* overnight.

6.1.2. <u>Gases</u>

Ar, CO and syngas were purchased from BOC and used as received. H_2 was purchased from BOC and dried by passage through a stainless-steel column of activated 3 Å molecular sieves prior to use. N_2 was obtained from the in-house supply and used as received.

6.1.3. <u>Solvents</u>

C_6H_5F and 1,2-$C_6H_4F_2$ were purchased from Fluorochem and dried over neutral Al_2O_3 for 4 hours, over CaH overnight, vacuum-distilled, freeze-pump-thaw degassed and dried over two batches of 3 Å molecular sieves. Anhydrous solvents were purchased from Acros Organics or Sigma-Aldrich, freeze-pump-thaw degassed and stored over 3 Å molecular sieves, except in the following cases: 'dry' Et_2O and dioxane were dried over Na and benzophenone overnight, vacuum-distilled, freeze-pump-thaw-degassed and stored over 3 Å molecular sieves; $SiMe_4$ was dried over Na overnight, vacuum-distilled, freeze-pump-thaw degassed and stored over a K mirror; Et_2NH was dried over CaH overnight, vacuum-distilled and freeze-pump-thaw degassed prior to use; toluene used in hydroformylations was purified using a solvent purification system and stored over 3 Å molecular sieves. Solvents handled under N_2 were used as received. $CDCl_3$ was purchased from Sigma-Aldrich and used as received. Other deuterated solvents were purchased from Goss Scientific. CD_2Cl_2 was freeze-pump-thaw degassed and stored over 3 Å molecular sieves, C_6D_6 and THF-d_8 were dried over Na overnight, vacuum-distilled and stored over a K mirror,

6.1.4. <u>Reagents</u>

[Rh(CO)$_2$Cl]$_2$,[382] [Ir(cod)$_2$][BAr$^F_4$],[383] [Rh(dtbpm)(biph)Cl],[175] [Ir(biph)(cod)Cl]$_2$,[176] Na[BAr$^F_4$],[384] [Rh(cod)$_2$][BAr$^F_4$],[385] Rh(PPh$_3$)$_3$Cl],[386] Li[Al(OC(CF$_3$)$_3$)$_4$],[387] and PhICl$_2$[388] were prepared according to literature procedures. [Rh(nbd)][HCB$_{11}$Me$_5$I$_6$] was prepared based on a modification of the literature procedure for [Rh(cod)$_2$][BAr$^F_4$].[385] All other reagents were commercial. 2,6-Lutidine and TMEDA were dried over Na and benzophenone overnight, vacuum-distilled, freeze-pump-thaw-degassed and stored over 3 Å molecular sieves.

$BH_3 \cdot SMe_2$ was freeze-pump-thaw-degassed prior to use. Et_3N was dried over CaH overnight, vacuum-distilled and freeze-pump-thaw degassed prior to use. 1-hexene, 1-heptene and 1-octene were filtered through Al_2O_3 prior to use. All other reagents were used as received, degassing prior to use if necessary.

6.1.5. Analytical Techniques

NMR spectra for product characterisation purposes were recorded on Bruker spectrometers (300-600 MHz) under Ar at 298 K, unless otherwise stated. Chemical shifts are quoted in ppm and coupling constants (J) in Hz. Abbreviations used are: singlet (s), doublet (d), triplet (t), quartet (q), septet (sept), multiplet (m), broad (br), very broad (vbr), virtual triplet (vt) and apparent triplet (app. t). Very broad signals are quoted with an associated line width (fwhm) in Hz. Virtual triplet coupling constants are reported as the separation between the first and second lines. Apparent triplet coupling constants are reported as one J-value (the separation between the first and second line), representing the two independent, but equivalent J-values. Where 'HSQC' or 'HMBC' is quoted, signals cannot be located in $^{13}C\{^1H\}$ spectra, but correlations can be observed in the respective 2D spectra. Where integrations are excluded, the data is not of sufficient quality to provide reliable values. NMR spectra recorded in *proteo* solvent were recorded using an internal capillary of C_6D_6, unless otherwise stated. ^1H NMR spectra recorded in C_6H_5F were referenced using the highest intensity peak of the lowest frequency fluoroarene multiplet (δ_H 6.865). ^1H NMR spectra recorded in 1,2-$C_6H_4F_2$ were referenced using the highest intensity peak of the highest frequency fluoroarene multiplet (δ_H 6.865). Spectra are otherwise referenced to an external standard. HR ESI-MS were recorded on a Bruker Maxis Plus instrument, LR ESI-MS were recorded on an Agilent 6130B single Quad instrument. Infrared spectra were recorded on a Perkin-Elmer Spectrum 100 or a Jasco FT-IR-4700 spectrometer using a KBr transmission cell in CH_2Cl_2. Microanalyses were performed by Elemental Microanalysis Ltd.

6.2. <u>Experimental Data for Chapter 2</u>

6.2.1. <u>Synthesis of Np$_2$PCl</u>
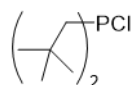
A suspension of magnesium turnings (1.32 g, 53.4 mmol) and 1,2-C$_2$H$_4$Br$_2$ (0.24 mL, 2.8 mmol) in THF (30 mL) was heated to reflux for 20 hours. This was allowed to cool to ambient temperature prior to the dropwise addition of NpCl (5.77 mL, 46.9 mmol). The resulting brown mixture was stirred at ambient temperature for 30 minutes and then at reflux for 22 hours. This was allowed to cool to ambient temperature and the solids left to settle out. The Grignard reagent was then filtered onto PCl$_3$ (1.6 mL, 19 mmol) in THF (5 mL) at 0 °C. An orange solution began to form, turning brown upon completion, with precipitation of white magnesium salts. The slurry was slowly stirred for 18 hours and filtered. Magnesium salts were washed with THF (3 x 10 mL) and the washings were combined with the dark orange solution. Dioxane was added (1 mL) to encourage further precipitation of magnesium salts and the solution was filtered again. Solvent was removed by distillation at ambient pressure. Phosphine was purified *via* vacuum distillation (24 °C, 1.68 x 10^{-2} mbar). Yield: 2.1 g (10 mmol, 54 %). Data are consistent with the literature.[182]

^{1}H NMR (C$_6$D$_6$, 300 MHz): δ 2.03 (d, $^2J_{HH}$ = 14.7, 1H, $CH_2{}^{Np}$), 1.49 (dd, $^2J_{HH}$ = 14.7, $^2J_{PH}$ = 5, 1H, CH_2), 0.98 (s, 9H, CH_3).
^{31}P{^{1}H} NMR (C$_6$D$_6$, 121 MHz): δ 104.0 (s).

6.2.2. <u>Synthesis of Crude PNP-Np</u>
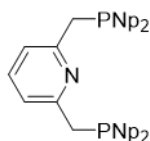
(impure)

A solution of 2,6-lutidine (0.20 mL, 1.7 mmol) and TMEDA (0.55 mL, 3.7 mmol) in Et$_2$O (10 mL) was cooled to 0 °C and ^{n}BuLi (1.6 M in hexanes, 2.5 mL) was added dropwise. The colourless solution immediately turned orange and was stirred at ambient temperature for 21 hours. Solution was then cooled to −78 °C and a solution of Np$_2$PCl (3.78 mmol) in Et$_2$O (10 mL) was added dropwise. Solution turned yellow with precipitation of a white solid and was heated at 30 °C for 92 hours. Yellow solution was filtered and volatiles removed under reduced pressure to give a yellow residue. Crude yield: 0.88 g.

6.2.3. Borane Protection of PNP-Np, **1**
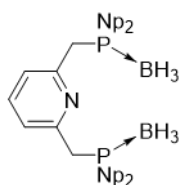
A solution of crude PNP-Np (0.88 g) in THF (15 mL) was cooled to −78 °C and BH$_3$·SMe$_2$ (0.41 mL, 4.3 mmol) was added. The resulting mixture was stirred at ambient temperature for 30 minutes before quenching with saturated aqueous NH$_4$Cl (20 mL). The organic portion was extracted, dried over MgSO$_4$ and filtered. Volatiles were removed under reduced pressure to give a white solid which was purified *via* column chromatography (70 % CH$_2$Cl$_2$, 30 % hexane, R_F 0.45). Yield: 0.53 g (1.1 mmol, 65 %).

^{1}H NMR (CDCl$_3$, 500 MHz): δ 7.59 (t, $^3J_{HH}$ = 7.7, 1H, *4-Py*), 7.12 (d, $^3J_{HH}$ = 7.6, 2H, *3,5-Py*), 3.19 (d, $^2J_{PH}$ = 10, 4H, *CH$_2^{Py}$*), 1.87 (dd, $^2J_{HH}$ = 14.9, $^2J_{PH}$ = 12, 4H, *CH$_2^{Np}$*), 1.47-1.63 (m, 4H, *CH$_2^{Np}$*), 1.12 (s, 48H, *CH$_3$*), 0.49-0.90 (br, 6H, *BH$_3$*).

^{11}B{^{1}H} NMR (CDCl$_3$, 96 MHz): δ −35.6 (br s).

^{13}C{^{1}H} NMR (CDCl$_3$, 126 MHz): δ 154.5 (dd, $^2J_{PC}$ = 8, $^4J_{PC}$ = 2, *2,6-Py*), 137.0 (s, *4-Py*), 123.6 (vt, J_{PC} = 5, *3,5-Py*), 39.6 (d, $^1J_{PC}$ = 28, *CH$_2^{Np}$*), 38.8 (d, $^1J_{PC}$ = 30, *CH$_2^{Py}$*), 32.6 (s, *C^{tBu}*), 31.8 (d, $^3J_{PC}$ = 6, *CH$_3$*).

^{31}P{^{1}H} NMR (CDCl$_3$, 162 MHz): δ 10.7 (br s).

HR ESI-MS (positive ion, 4 kV): 502.4050, [*M+Na*]$^+$ (calcd 502.4054) *m/z*.

6.2.4. Deprotection of **1**
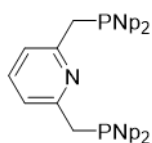
(pure)

Purified adduct **1** (0.310 g, 0.647 mmol) was suspended in Et$_2$NH (10 mL) and heated to reflux for 52 hours. Volatiles were removed under reduced pressure to give a white solid. Pentane was added (2 mL) and removed under reduced pressure to form an azeotrope with any remaining Et$_2$NH. The product was extracted into toluene (5 mL) and washed with degassed H$_2$O (5 mL). The organic portion was extracted *via* cannula, dried over degassed MgSO$_4$ and filtered *via* cannula. Volatiles were removed under reduced pressure to give a white solid. Yield 0.184 g (0.408 mmol, 63 %). Data are consistent with the literature.[64]

1H NMR (C$_6$D$_6$, 500 MHz): δ 7.06 (t, $^3J_{HH}$ = 7.7, 1H, *4-Py*), 6.78 (d, $^3J_{HH}$ = 7.6, 2H, *3,5-Py*), 2.95 (d, $^2J_{PH}$ = 2, 4H, *CH$_2$^{Py}*), 1.76 (dd, $^2J_{HH}$ = 14, $^2J_{PH}$ = 4, 4H, *CH$_2$^{Np}*), 1.28 (dd, $^2J_{HH}$ = 14, $^2J_{PH}$ = 3, 4H, *CH$_2$^{Np}*), 1.04 (s, 34H, *CH$_3$*).

13C{1H} NMR (C$_6$D$_6$, 126 MHz): δ 159.6 (d, $^2J_{PC}$ = 4, *2,6-Py*), 136.4 (s, *4-Py*), 121.2 (dd, $^3J_{PC}$ = 5, $^5J_{PC}$ = 2, *3,5-Py*), 45.4 (d, $^1J_{PC}$ = 18, *CH$_2$^{Np}*), 41.0 (d, $^1J_{PC}$ = 18, *CH$_2$^{Py}*), 32.3 (d, $^2J_{PC}$ = 15, *C^{tBu}*), 31.7 (d, $^3J_{PC}$ = 9, *CH$_3$*).

31P{1H} NMR (C$_6$D$_6$, 162 MHz): δ −39.8 (s).

HR ESI-MS (positive ion, 4 kV): 452.3559, [*M*+H]$^+$ (calcd 452.3570) *m/z*.

6.2.5. Synthesis of [Rh(PNP-Np)(CO)][BAr$^F_4$], 2
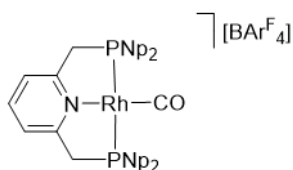
A solution of PNP-Np (12.1 mg, 26.8 μmol) in C$_6$H$_5$F (500 μL) was transferred onto [Rh(CO)$_2$Cl]$_2$ (5.3 mg, 14 μmol) and Na[BAr$^F_4$] (27.0 mg, 30.5 μmol) in an NMR tube fitted with a J Young's valve and agitated for 30 minutes. The yellow solution was filtered and volatiles were removed under reduced pressure to give a yellow residue. This was washed with hexane (0.5 mL), filtered and dried. The resulting solid was extracted into CH$_2$Cl$_2$, filtered and volatiles removed under reduced pressure to yield a yellow solid. Yield: 28.4 mg (19.6 μmol, 73 %). Single crystals suitable for X-ray diffraction were obtained by slow diffusion of hexane into a CD$_2$Cl$_2$ solution at ambient temperature.

1H NMR (CD$_2$Cl$_2$, 500 MHz): δ 7.77 (t, $^3J_{HH}$ = 7.8, 1H, *4-Py*), 7.72-7.75 (m, 8H, o-*Ar^F*), 7.57 (s, 4H, p-*Ar^F*), 7.39 (d, $^3J_{HH}$ = 7.8, 2H, *3,5-Py*), 3.86 (vt, J_{PC} = 9, 4H, *CH$_2$^{Py}*), 2.10 (dvt, $^2J_{HH}$ = 14.8, J_{PH} = 6, 4H, *CH$_2$^{Np}*), 2.02 (dm, $^2J_{HH}$ = 14.8, 4H, *CH$_2$^{Np}*), 1.18 (s, 34H, *CH$_3$*).

13C{1H} NMR (CD$_2$Cl$_2$, 126 MHz): δ 193.8 (dt, $^1J_{RhC}$ = 71, $^2J_{PC}$ = 15, *CO*), 163.1-163.2 (m, *2,6-Py*), 162.6 (q, $^1J_{CB}$ = 50, i-*Ar^F*), 141.4 (s, *4-Py*), 135.6 (s, o-*Ar^F*), 129.7 (qq, $^2J_{FC}$ = 32, $^3J_{CB}$ = 3, m-*Ar^F*), 125.4 (q, $^1J_{FC}$ = 272, *CF$_3$*), 123.1 (vt, J_{PC} = 11, *3,5-Py*), 118.3 (sept, $^3J_{FC}$ = 4, p-*Ar^F*), 46.6 (vtd, J_{PC} = 25, $^2J_{RhC}$ = 1, *CH$_2$^{Np}*), 45.9 (vt, J_{PC} = 23, *CH$_2$^{Py}*), 32.4 (s, *C^{tBu}*), 32.3 (vt, J_{PC} = 6, *CH$_3$*).

31P{1H} NMR (CD$_2$Cl$_2$, 162 MHz): δ 17.4 (d, $^1J_{RhP}$ = 121).

ATR IR: ν$_{CO}$ 2011 cm^{-1}.

IR (CH$_2$Cl$_2$): ν$_{CO}$ 2004 cm^{-1}.

HR ESI-MS (positive ion, 4 kV): 582.2489, [*M*]$^+$ (calcd 582.2495) *m/z*.

Anal. Calcd for C$_{71}$H$_{71}$BF$_{24}$NP$_2$Rh (1569.98 g mol^{-1}): C, 49.85; H, 4.39; N, 0.97; Found: C, 50.08; H, 4.32; N, 0.98.

6.2.6. Synthesis of [Ir(PNP-Np')H][BArF4], **4**
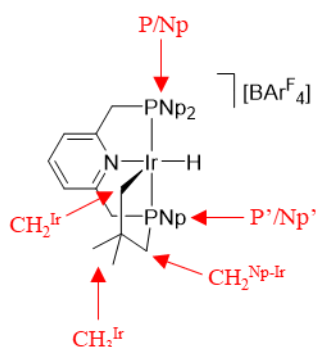
In a modification of the procedure reported by Yamashita and Nozaki, PNP-Np (20.1 mg, 44.5 μmol) and [Ir(cod)$_2$][BAr$^F_4$] (57.0 mg, 44.8 μmol) were dissolved in 1,2-C$_6$H$_4$F$_2$ (10 mL) and the red solution was stirred at ambient temperature for 30 minutes. Volatiles were removed under reduced pressure to give a deep red residue. This was washed with hexane (5 mL), filtered and dried to give a pale red solid. Yield 43.9 mg (29.1 μmol, 65 %). Data are consistent with the literature.[64] Single crystals suitable for X-ray diffraction were obtained by slow diffusion of hexane into a C$_6$H$_5$F solution at ambient temperature.

^{1}H NMR (CD$_2$Cl$_2$, 500 MHz): δ 7.18 (t, $^3J_{HH}$ = 7.8, 1H, *4-Py*), 7.71-7.76 (m, 9H, o-*Ar^F*), 7.56 (s, 3H, p-*Ar^F*), 7.52 (d, $^3J_{HH}$ = 7.7, 2H, *3,5-Py*), 4.06-4.15 (m, 1H, *CH$_2^{Py}$*), 3.80-3.96 (m, 2H, *CH$_2^{Py}$*), 3.56 (dd, $^2J_{HH}$ = 17.1, $^2J_{PH}$ = 8, 1H, *CH$_2^{Py}$*), 2.64-2.73 (m, 1H, *CH$_2^{Ir}$*), 2.38-2.55 (m, 2H, *CH$_2^{Np'}$ + CH$_2^{Np}$*), 2.15-2.29 (m, 2H, *CH$_2^{Np}$*), 2.07 (dd, $^2J_{HH}$ = 14.9, $^2J_{PH}$ = 6, 1H, *CH$_2^{Np}$*), 1.75 (dd, $^2J_{HH}$ = 14.4, $^2J_{PH}$ = 11, 1H, *CH$_2^{Np'}$*), 1.61 (dd, $^2J_{HH}$ = 13.6, $^2J_{PH}$ = 8, 1H, *CH$_2^{Np-Ir}$*), 1.24 (s, 9H, *CH$_3$*), 1.18 (s, 10H, *CH$_3$*), 1.06 (s, 3H, *CH$_3^{Ir}$*), 1.02 (s, 3H, *CH$_3$*), 0.82-0.93 (m, 2H, *CH$_2^{Ir}$ + CH$_2^{Np-Ir}$*), 0.39 (s, 9H, *CH$_3$'*), −16.80 (t, $^2J_{PH}$ = 12, 1H, *Ir-H*).

^{13}C{^{1}H} NMR (CD$_2$Cl$_2$, 126 MHz): δ 162.6 (q, $^1J_{CB}$ = 50, i-*Ar^F*), 161.0 (s, *2-Py*), 160.5 (s, *6-Py*), 139.4 (s, *4-Py*), 135.6 (s, o-*Ar^F*), 129.7 (qq, $^2J_{FC}$ = 31, $^3J_{CB}$ = 3, m-*Ar^F*), 125.4 (q, $^1J_{FC}$ = 272, *CF$_3$*), 123.7 (d, $^3J_{PH}$ = 10, *3/5-Py*), 123.2 (d, $^3J_{PH}$ = 9, *5/3-Py*), 118.3 (sept, $^3J_{FC}$ = 4, p-*Ar^F*), 48.8 (d, $^1J_{PH}$ = 23, *CH$_2^{Np'}$*), 47.6 (d, $^1J_{PH}$ = 28, *CH$_2^{Py}$*), 46.9 (d, $^1J_{PH}$ = 30, *CH$_2^{Py}$*), 41.5 (dm, $^1J_{PH}$ = 22, *CH$_2^{Np}$*), 40.9 (dm, $^1J_{PH}$ = 23, *CH$_2^{Np}$*), 40.4 (d, $^1J_{PH}$ = 34, *CH$_2^{Np-Ir}$*), 34.5 (s, *C$^{tBu'}$*), 33.6 (s, *C^{tBu}*), 32.7 (s, *C^{tBu}*), 32.0 (d, $^3J_{PH}$ = 6, *CH$_3$*), 31.7 (d, $^3J_{PH}$ = 7, *CH$_3$*), 30.0 (d, $^3J_{PH}$ = 7, *CH$_3$'*), 29.4 (d, $^3J_{PH}$ = 4, *CH$_3^{Ir}$*), 28.2 (d, $^3J_{PH}$ = 18, *CH$_3^{Ir}$*), 20.4 (s, *CH$_2^{Ir}$*).

^{31}P{^{1}H} NMR (CD$_2$Cl$_2$, 162 MHz): δ 28.5 (d, $^2J_{PP}$ = 316, *P'*), 18.5 (d, $^2J_{PP}$ = 316, *P*).

HR ESI-MS (positive ion, 4 kV): 644.3115, [*M*]$^+$ (calcd 644.3122) *m/z*.

6.2.7. Synthesis of [Ir(PNP-Np)(CO)][BArF4], **3**
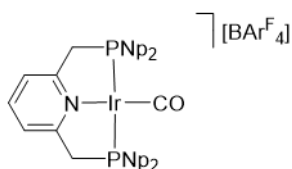
In a modification of the procedure reported by Yamashita and Nozaki, a solution of **4** (8.0 mg, 5.3 μmol) in 1,2-C$_6$H$_4$F$_2$ (500 μL) was prepared in an NMR tube fitted with a J Young's valve. This was freeze-pump-thaw degassed and placed under 1 bar of CO and gently shaken at ambient temperature. An immediate colour change from red to pale yellow was observed. Volatiles were removed under reduced pressure to give a yellow solid which was washed with hexane (0.5 mL) and dried *in vacuo*. This compound was synthesised in ~93 % purity (by ^{31}P{^{1}H} NMR) alongside minor unidentified impurities and could not be isolated. Data are consistent with the literature.[64]

^{1}H NMR (CD$_2$Cl$_2$, 500 MHz, selected data): δ 7.88 (t, $^3J_{HH}$ = 7.7, 1H, *4-Py*, 1H), 7.73 (s, 10H, o-*Ar^F*), 7.57 (s, 5H, p-*Ar^F*), 7.50 (d, $^3J_{HH}$ = 7.8, 2H, *3,5-Py*), 3.95 (vt, J_{PH} = 9, 4H, *CH$_2$^{Py}*), 2.24 (dvt, $^2J_{HH}$ = 14.9, J_{PH} = 8, 5H, *CH$_2$^{Np}*), 2.17 (dvt, $^2J_{HH}$ = 14.9, J_{PH} = 7, 5H, *CH$_2$^{Np}*), 1.18 (s, 41H, *CH$_3$*).

^{13}C{^{1}H} NMR (CD$_2$Cl$_2$, 126 MHz, selected data): δ 180.7 (t, $^2J_{PC}$ = 9, *CO*), 165.0 (vt, J_{PC} = 10, *2,6-Py*), 162.6 (q, $^1J_{CB}$ = 50, i-*Ar^F*), 141.6 (s, *4-Py*), 135.6 (s, o-*Ar^F*), 129.7 (qq, $^2J_{FC}$ = 32, $^3J_{CB}$ = 3, m-*Ar^F*), 125.3 (q, $^1J_{FC}$ = 272, *CF$_3$*), 122.9 (vt, J_{PC} = 11, *3,5-Py*), 118.3 (sept, $^3J_{FC}$ = 4, p-*Ar^F*), 47.0 (vt, J_{PC} = 28, *CH$_2$^{Py}*), 46.6 (vt, J_{PC} = 31, *CH$_2$^{Np}*), 32.45 (s, *C^{tBu}*), 32.37 (vt, J_{PC} = 6, *CH$_3$*).

^{31}P{^{1}H} NMR (CD$_2$Cl$_2$, 162 MHz, selected data): δ 13.59 (s).

ATR IR: ν_{CO} 1997 cm^{-1}.

IR (CH$_2$Cl$_2$): ν_{CO} 1991 cm^{-1}.

HR ESI-MS (positive ion, 4 kV): 672.3070, [*M*]$^+$ (calcd 672.3071) *m/z*.

6.2.8. Synthesis of [Rh(PNP-Np)(biph)Cl], **5**
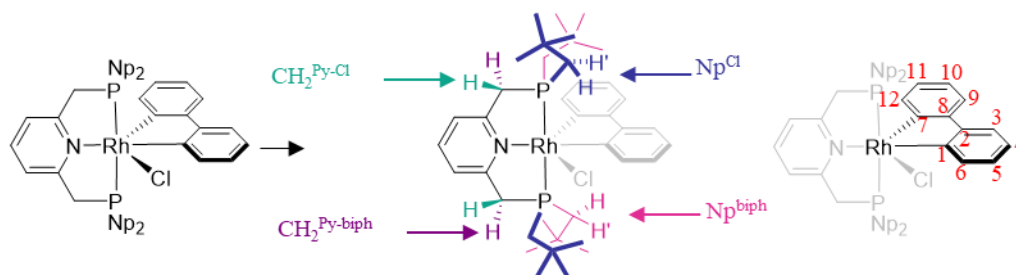
NMR assignments of PNP-Np biphenyl complexes are based on this system

PNP-Np (111.0 mg, 0.246 mmol) and [Rh(biph)(dtbpm)Cl] (146.3 mg, 0.246 mmol) were suspended in C_6H_5F (10 mL) and heated to reflux for 18 hours. Volatiles were removed under reduced pressure to give an orange residue which was extracted into CH_2Cl_2 (10 mL). Volatiles were removed under reduced pressure and the resulting orange residue was washed with pentane (3 x 5 mL), filtered and dried *in vacuo* to give a white solid. Yield: 128.6 mg (0.173 mmol, 70 %). Single crystals suitable for X-ray diffraction were obtained by slow diffusion of $SiMe_4$ into a CH_2Cl_2 solution at −30 °C.

^{1}H NMR (CD_2Cl_2, 600 MHz): δ 8.05 (d, $^3J_{HH}$ = 7.5, 1H, *6-biph*), 7.73 (t, $^3J_{HH}$ = 7.8, 1H, *4-Py*), 7.50 (dd, $^3J_{HH}$ = 7.6, $^4J_{HH}$ = 1.5, 1H, *9-biph*), 7.43 (dd, $^3J_{HH}$ = 7.5, $^4J_{HH}$ = 1.5, 1H, *3-biph*), 7.38 (d, $^3J_{HH}$ = 7.8, 2H, *3,5-Py*), 6.93 (t, $^3J_{HH}$ = 7.3, 1H, *10-biph*), 6.89 (t, $^3J_{HH}$ = 7.3, 1H, *4-biph*), 6.83 (td, $^3J_{HH}$ = 7.3, $^4J_{HH}$ = 1.5, 1H, *5-biph*), 6.65 (td, $^3J_{HH}$ = 7.4, $^4J_{HH}$ = 1.5, 1H, *11-biph*), 6.30 (d, $^3J_{HH}$ = 7.5, 1H, *12-biph*), 4.15 (dvt, $^2J_{HH}$ = 16.1, J_{PH} = 9, 2H, CH_2^{Py-Cl}), 3.96 (dvt, $^2J_{HH}$ = 16.1, J_{PH} = 8, 2H, $CH_2^{Py-biph}$), 2.38 (dvt, $^2J_{HH}$ = 14.7, J_{PH} = 7, 2H, CH_2^{Np-Cl}), 2.29 (dvt, $^2J_{HH}$ = 14.6, J_{PH} = 6, 2H, $CH_2^{Np-Cl'}$), 1.43 (d, $^2J_{HH}$ = 15.4, 2H, $CH_2^{Np-biph'}$), 1.31 (dvt, $^2J_{HH}$ = 15.5, J_{PH} = 6, 2H, $CH_2^{Np-biph}$), 1.02 (s, 18H, CH_3^{Cl}), 0.59 (s, 18H, CH_3^{biph}).

^{13}C{^{1}H} NMR (CD_2Cl_2, 126 MHz): δ 166.8 (dt, $^1J_{RhC}$ = 35, $^2J_{PC}$ = 9, *7-biph*), 166.1 (dt, $^1J_{RhC}$ = 30, $^2J_{PC}$ = 9, *1-biph*), 160.7 (vt, J_{PC} = 7, *2,6-Py*), 155.5 (d, $^2J_{RhC}$ = 1, *8-biph*), 152.3 (d, $^2J_{RhC}$ = 2, *2-biph*), 138.3 (s, *6-biph*), 137.8 (s, *4-Py*), 134.1 (vt, J_{PC} = 3, *12-biph*), 125.6 (s, *11-biph*), 124.9 (s, *5-biph*), 123.0 (s, *10-biph*), 122.0 (vt, J_{PC} = 10, *3,5-Py*), 121.7 (s, *4-biph*), 121.1 (s, *9-biph*), 119.7 (s, *3-biph*), 43.8 (vt, J_{PC} = 22, CH_2^{Py}), 38.3 (vt, J_{PC} = 18, CH_2^{Np-Cl}), 34.0 (vtd, J_{PC} = 16, $^2J_{RhC}$ = 3, $CH_2^{Np-biph}$), 32.9 (vt, J_{PC} = 6, CH_3^{Cl}), 32.6 (vt, J_{PC} = 6, C^{tBu-Cl}), 32.4-32.5 (m, $C^{tBu-biph}$), 32.4 (vt, J_{PC} = 5, CH_3^{biph}).

^{31}P{^{1}H} NMR (CD_2Cl_2, 162 MHz): δ 26.2 (d, $^1J_{RhP}$ = 110).

HR ESI-MS (positive ion, 4 kV): 706.3166, [*M-Cl*]$^+$ (calcd 706.3172) *m/z*.

Anal. Calcd for $C_{39}H_{59}ClNP_2Rh$ (742.21 g mol^{-1}): C, 63.11; H, 8.01; N, 1.89; Found: C, 63.39; H, 7.88; N, 1.79.

6.2.9. Synthesis of [Ir(PNP-Np)(biph)Cl], **6**
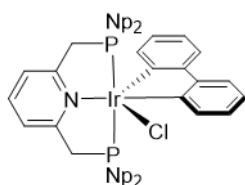
PNP-Np (108.3 mg, 0.240 mmol) and [Ir(biph)(cod)Cl]$_2$ (93.7 mg, 0.0960 mmol) were suspended in C_6H_5F (10 mL) and heated to reflux for 24 hours, giving a yellow solution. Volatiles were removed under reduced pressure to give a yellow residue which was washed

with pentane (3 x 5 mL), filtered and dried *in vacuo* to give a pale yellow solid. Yield: 127 mg (0.153 mmol, 64 %). Single crystals suitable for X-ray diffraction were obtained by slow diffusion of hexane into a C_6H_5F solution −30 °C.

^{1}H NMR (CD$_2$Cl$_2$, 500 MHz): δ 7.92 (d, $^3J_{HH}$ = 7.4, 1H, *6-biph*), 7.77 (t, $^3J_{HH}$ = 7.8, 1H, *4-Py*), 7.47 (dd, $^3J_{HH}$ = 7.6, $^4J_{HH}$ = 1.5, 1H, *9-biph*), 7.42 (d, $^3J_{HH}$ = 7.8, 2H, *3,5-Py*), 7.41 (dd, $^3J_{HH}$ = 7.5, $^4J_{HH}$ = 1.4, 1H, *3-biph*), 6.89 (t, $^3J_{HH}$ = 7.3, 1H, *10-biph*), 6.85 (t, $^3J_{HH}$ = 7.2, 1H, *4-biph*), 6.79 (td, $^3J_{HH}$ = 7.3, $^4J_{HH}$ = 1.5, 1H, *5-biph*), 6.58 (td, $^3J_{HH}$ = 7.3, $^4J_{HH}$ = 1.5, 1H, *11-biph*), 6.27 (d, $^3J_{HH}$ = 7.4, 1H, *12-biph*), 4.10 (dvt, $^2J_{HH}$ = 16.2, J_{PH} = 9, 2H, *CH$_2^{Py-Cl}$*), 4.00 (dvt, $^2J_{HH}$ = 16.1, J_{PH} = 9, 2H, *CH$_2^{Py-biph}$*), 2.40 (dvt, $^2J_{HH}$ = 14.7, J_{PH} = 7, 2H, *CH$_2^{Np-Cl}$*), 2.26 (dvt, $^2J_{HH}$ = 14.7, J_{PH} = 7, 2H, *CH$_2^{Np-Cl'}$*), 1.51 (dvt, $^2J_{HH}$ = 15.4, J_{PH} = 5, 2H, *CH$_2^{Np-biph}$*), 1.33 (dvt, $^2J_{HH}$ = 15.3, J_{PH} = 7, 2H, *CH$_2^{Np-biph'}$*), 1.02 (s, 19H, *CH$_3^{Cl}$*), 0.59 (s, 18H, *CH$_3^{biph}$*).

^{13}C{^{1}H} NMR (CD$_2$Cl$_2$, 126 MHz): δ 162.1 (vt, J_{PC} = 6, *2,6-Py*), 156.5 (s, *8-biph*), 153.6 (s, *2-biph*), 146.0 (t, $^2J_{PC}$ = 7, *1-biph*), 145.4 (t, $^2J_{PC}$ = 7, *7-biph*), 137.99 (s, *4-Py*), 137.02 (s, *6-biph*), 132.4 (s, *12-biph*), 125.7 (s, *11-biph*), 125.2 (s, *5-biph*), 122.4 (s, *10-biph*), 121.7 (vt, J_{PC} = 9, *3,5-Py*), 121.1 (s, *4-biph*), 121.0 (s, *9-biph*), 119.7 (s, *3-biph*), 44.0 (vt, J_{PC} = 27, *CH$_2^{Py}$*), 37.2 (vt, J_{PC} = 23, *CH$_2^{Np-Cl}$*), 32.8 (vt, J_{PC} = 6, *CH$_3^{Cl}$*), 32.7 (s, *CH$_2^{Np-biph}$*), 32.6 (s, *C^{tBu-Cl}*), 32.4 (vt, J_{PC} = 6, *C$^{tBu-biph}$*), 32.3 (vt, J_{PC} = 6, *CH$_3^{biph}$*).

^{31}P{^{1}H} NMR (CD$_2$Cl$_2$, 162 MHz): δ 0.55 (s).

HR ESI-MS (positive ion, 4 kV): 796.3743, [*M-Cl*]$^+$ (calcd 796.3749) *m/z*.

Anal. Calcd for C$_{39}$H$_{59}$ClNIrP$_2$ (831.52 g mol^{-1}): C, 56.33; H, 7.15; N, 1.68; Found: C, 56.02; H, 7.12; N, 1.64.

6.2.10. <u>Synthesis of [Rh(PNP-Np)(biph)][BAr$^F_4$], **7**</u>
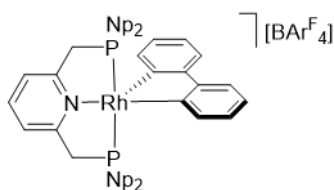
Complex **5** (94.4 mg, 0.127 mmol) and Na[BAr$^F_4$] (113.5 mg, 0.128 mmol) were dissolved in C_6H_5F (10 mL) and stirred at ambient temperature for 30 minutes. The resulting suspension was filtered and volatiles were removed under reduced pressure to give a yellow solid. This was washed with pentane (5 mL), filtered and dried *in vacuo*. Yield: 172 mg (0.109 mmol, 86 %). Single crystals suitable for X-ray diffraction were obtained by slow diffusion of SiMe$_4$ into a CH$_2$Cl$_2$ solution at −30 °C.

¹H NMR (CD$_2$Cl$_2$, 298 K, 600 MHz): δ 7.92 (t, $^3J_{HH}$ = 7.9, 1H, *4-Py*), 7.74-7.78 (m, 9H, o-*Ar^F*), 7.56-7.60 (m, 8H, p-*Ar^F* + *3,5-Py* + *biph*), 7.09 (t, $^3J_{HH}$ = 7.4, 2H, *biph*), 6.88 (vbr, fwhm = 101 Hz, 2H, 5.92 (vbr, fwhm = 170 Hz, 1H, *biph*), 4.00 (s, 4H, *CH$_2^{Py}$*), 1.96 (vbr, fwhm = 368 Hz, 1H, *CH$_2^{Np}$*), 1.39 (vbr, fwhm = 174 Hz, 1H, *CH$_2^{Np}$*), 0.49-1.04 (br s, 40H, *CH$_3$*).

¹³C{¹H} NMR (CD$_2$Cl$_2$, 298 K, 151 MHz): δ 162.7 (q, $^1J_{CB}$ = 50, i-*Ar^F*), 161.0 (vt, J_{PC} = 6, *2,6-Py*), 141.1 (s, *4-Py*), 135.6 (s, o-*Ar^F*), 129.8 (qq, $^2J_{FC}$ = 32, $^3J_{CB}$ = 3, m-*Ar^F*), 127.3-127.5 (br s, *biph*), 125.5 (q, $^1J_{FC}$ = 272, *CF$_3$*), 124.3 (vt, J_{PC} = 10, *3,5-Py*), 118.3 (sept, $^3J_{FC}$ = 4, p-*Ar^F*), 44.1 (vt, J_{PC} = 22, *CH$_2^{Py}$*), 33.1-33.4 (br s, *CH$_2^{Np}$*), 32.4 (s, *CH$_3$*).

¹H NMR (CD$_2$Cl$_2$, 200 K, 500 MHz): δ 7.85 (t, $^3J_{HH}$ = 7.8, 1H, *4-Py*), 7.69-7.79 (m, 8H, o-*Ar^F*), 7.50-7.59 (m, 7H, p-*Ar^F* + *3,5-Py* + *3-biph*), 7.43-7.49 (m, 2H, *6-biph* + *9-biph*), 7.05 (t, $^3J_{HH}$ = 7.4, 1H, *4-biph*), 6.93-7.01 (m, 2H, *5-biph* + *10-biph*), 6.64 (t, $^3J_{HH}$ = 7.6, 1H, *11-biph*), 5.72 (d, $^3J_{HH}$ = 7.9, 1H, *12-biph*), 3.89 (vt, J_{PH} = 8, 4H, *CH$_2^{Py}$*), 2.24 (d, $^2J_{HH}$ = 15.1, 2H, *CH$_2^{Np-□}$*), 1.80 (dvt, $^2J_{HH}$ = 15.2, J_{PH} = 7, 2H, *CH$_2^{Np-□'}$*), 1.37 (dvt, $^2J_{HH}$ = 15.4, J_{PH} = 7, 2H, *CH$_2^{Np-biph'}$*), 1.27 (dvt, $^2J_{HH}$ = 15.3, J_{PH} = 5, 2H, *CH$_2^{Np-biph}$*), 0.84 (s, 19H, *CH$_3^{□}$*), 0.50 (s, 18H, *CH$_3^{biph}$*).

¹³C{¹H} NMR (CD$_2$Cl$_2$, 200 K, 126 MHz): δ 161.0-162.6 (m, i-*Ar^F* + *7-biph*), 159.3 (s, *2,6-Py*), 157.2 (dm, $^1J_{RhC}$ = 43, *1-biph*), 152.0 (s, *8-biph*), 148.7 (s, *2-biph*), 140.2 (s, *4-Py*), 135.1 (s, *6-biph*), 134.6 (s, o-*Ar^F*), 129.2 (d, $^2J_{RhC}$ = 2, *12-biph*), 128.5 (qm, $^2J_{FC}$ = 31, m-*Ar^F*), 126.8 (s, *11-biph*), 125.7 (s, *5-biph*), 124.4 (q, $^1J_{FC}$ = 272, *CF$_3$*), 124.2 (s, *10-biph*), 123.6-123.8 (m, *3,5-Py*), 122.7 (s, *4-biph*), 121.8 (s, *9-biph*), 120.8 (s, *3-biph*), 117.4-117.6 (m, p-*Ar^F*), 42.6 (vt, J_{PC} = 24, *CH$_2^{Py}$*), 40.7 (vt, J_{PC} = 17, *CH$_2^{Np-□}$*), 34.5 (vt, J_{PC} = 21, *CH$_2^{Np-biph}$*), 33.4 (s, *C^{tBu}*), 31.9 (s, *C^{tBu}*), 31.3 (s, *CH$_3^{□}$*), 31.1 (s, *CH$_3^{biph}$*).

³¹P{¹H} NMR (CD$_2$Cl$_2$, 298 K, 162 MHz): δ 23.8 (d, $^1J_{RhP}$ = 110).

ATR IR: ν$_{CH}$ ~2682 cm^{-1} (broad).

HR ESI-MS (positive ion, 4 kV): 706.3166, [*M*]$^+$ (calcd 706.3172) *m/z*.

Anal. Calcd for C$_{71}$H$_{71}$BF$_{24}$NP$_2$Rh (1569.98 g mol^{-1}): C, 54.32; H, 4.56; N, 0.89; Found: C, 54.67; H, 4.49; N, 0.92.

6.2.11. Synthesis of [Ir(PNP-Np)(biph)][BAr$^F_4$], **8**
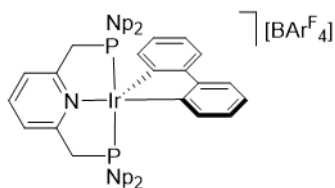
Complex **6** (106.4 mg, 0.128 mmol) and Na[BAr$^F_4$] (124.1 mg, 0.140 mmol) were dissolved in C$_6$H$_5$F (10 mL) and stirred at ambient temperature for 1 hour. The resulting suspension was

filtered and volatiles removed under reduced pressure to give an orange solid. This was washed with pentane (5 mL), filtered and dried *in vacuo*. Yield: 177.3 mg (1.07 mmol, 84 %). Single crystals suitable for X-ray diffraction were obtained by slow diffusion of SiMe$_4$ into a CH$_2$Cl$_2$ solution at −30 °C.

^{1}H NMR (CD$_2$Cl$_2$, 298 K, 600 MHz): δ 7.99 (t, $^3J_{HH}$ = 7.9, 1H, *4-Py*), 7.72-7.77 (m, 9H, o-*Ar^F*), 7.67 (d, $^3J_{HH}$ = 7.9, 2H, *3,5-Py*), 7.57 (s, 5H, p-*Ar^F* + *3/6-biph*), 7.48-7.53 (m, 1H, *6/3-biph*), 7.44-7.48 (m, 1H, *9-biph*), 6.98-7.10 (m, 3H, *4,5,10-biph*), 6.60 (s, 1H, *11-biph*), 5.69 (s, 1H, *12-biph*), 4.11 (d, $^2J_{HH}$ = 17.2, 2H, *CH$_2$^{Py}*), 3.94 (d, $^2J_{HH}$ = 17.5, 2H, *CH$_2$^{Py}*), 2.40 (d, $^2J_{HH}$ = 15.1, 2H, *CH$_2$^{Np}*), 2.00 (d, $^2J_{HH}$ = 15.1, 2H, *CH$_2$^{Np}*), 1.38 (d, $^2J_{HH}$ = 15.8, 2H, *CH$_2$^{Np}*), 1.31 (d, $^2J_{HH}$ = 15.8, 2H, *CH$_2$^{Np}*), 0.89 (s, 19H, *CH$_3$$^{\square}$*), 0.65 (s, 21H, *CH$_3$^{biph}*).

^{13}C{^{1}H} NMR (CD$_2$Cl$_2$, 298 K, 151 MHz): δ 162.6 (q, $^1J_{CB}$ = 50, i-*Ar^F*), 162.3 (vt, J_{PC} = 5, *2,6-Py*), 152.9 (br s, *8-biph*), 150.6 (br s, *2-biph*), 143.2 (br s, *1,7-biph*), 140.5 (s, *4-Py*), 136.2 (s, *9-biph*), 135.6 (s, o-*Ar^F*), 129.7 (qq, $^2J_{FC}$ = 32, $^3J_{CB}$ = 3 Hz, m-*Ar^F*), 127.7 (s, *10-biph*), 127.6 (s, *12-biph*), 126.9 (s, *11-biph*), 125.4 (q, $^1J_{FC}$ = 272, *CF$_3$*), 125.4 (s, *4/5-biph*), 124.1 (vt, J_{PC} = 10, *3,5-Py*), 123.6 (s, *5/4-biph*), 122.4 (s, *3/6-biph*), 121.9 (s, *6/3-biph*), 118.3 (sept, $^3J_{FC}$ = 4, p-*Ar^F*), 44.7 (vt, J_{PC} = 28, *CH$_2$^{Py}*), 44.0 (br s, *CH$_2$$^{Np-\square}$*), 35.1 (br s, *CH$_2$$^{Np-biph}$*), 34.3 (s, *C^{tBu}*), 32.7 (s, *C^{tBu}*), 32.4 (s, *CH$_3$$^{\square}$*), 32.1 (s, *CH$_3$^{biph}*).

^{1}H NMR (CD$_2$Cl$_2$, 200 K, 500 MHz): δ 7.89 (t, $^3J_{HH}$ = 7.9, 1H, *4-Py*), 7.70-7.77 (m, 8H, o-*Ar^F*), 7.61 (d, $^3J_{HH}$ = 7.9, 2H, *3,5-Py*), 7.54 (s, 4H, p-*Ar^F*), 7.51 (d, $^3J_{HH}$ = 7.7, 1H, *3-biph*), 7.47 (d, $^3J_{HH}$ = 7.4, 1H, *6-biph*), 7.43 (d, $^3J_{HH}$ = 7.6, 1H, *9-biph*), 7.00 (t, $^3J_{HH}$ = 7.4, 1H, *4-biph*), 6.90-6.96 (m, *5-biph* + *10-biph*), 6.54 (t, $^3J_{HH}$ = 7.5, 1H, *11-biph*), 5.61 (d, $^3J_{HH}$ = 7.8, 1H, *12-biph*), 3.97 (dvt, $^2J_{HH}$ = 16.9, J_{PH} = 9, 2H, *CH$_2$$^{Py-biph}$*), 3.88 (dvt, $^2J_{HH}$ = 16.9, J_{PH} = 8, 2H, *CH$_2$$^{Py-\square}$*), 2.37 (d, $^2J_{HH}$ = 15.4, 2H, *CH$_2$$^{Np-\square}$*), 1.76 (dvt, $^2J_{HH}$ = 15.4, J_{PH} = 8, 2H, *CH$_2$$^{Np-\square'}$*), 1.43 (dvt, $^2J_{HH}$ = 15.4, J_{PH} = 7, 2H, *CH$_2$$^{Np-biph}$*), 1.31 (dvt, $^2J_{HH}$ = 15.3, J_{PH} = 6, 2H, *CH$_2$$^{Np-biph'}$*), 0.80 (s, 18H, *CH$_3$$^{\square}$*), 0.49 (s, 18H, *CH$_3$^{biph}*).

^{13}C{^{1}H} NMR (CD$_2$Cl$_2$, 200 K, 126 MHz): δ 161.8 (q, $^1J_{CB}$ = 50, i-*Ar^F*), 160.4 (s, *2,6-Py*), 152.0 (s, *8-biph*), 149.9 (s, *2-biph*), 143.4 (t, $^2J_{PC}$ = 6, *7-biph*), 139.7 (s, *4-Py*), 136.0 (s, *6-biph*), 134.6 (s, o-*Ar^F*), 132.2 (vt, J_{PC} = 14, *1-biph*), 128.6 (qq, $^2J_{FC}$ = 32, $^3J_{CB}$ = 3, m-*Ar^F*), 127.1 (s, *12-biph*), 126.5 (s, *5-biph*), 126.1 (s, *11-biph*), 124.4 (q, $^1J_{FC}$ = 273, *CF$_3$*), 124.0 (s, *10-biph*), 123.6 (vt, J_{PC} = 9, *3,5-Py*), 122.1 (s, *4-biph*), 121.2 (s, *9-biph*), 120.7 (s, *3-biph*), 117.4-117.6 (m, p-*Ar^F*), 43.2 (vt, J_{PC} = 30, *CH$_2$^{Py}*), 41.4 (vt, J_{PC} = 23, *CH$_2$$^{Np-\square}$*), 34.2 (s, *C^{tBu}*), 33.2 (vt, J_{PC} = 23, *CH$_2$$^{Np-biph}$*), 31.6 (vt, J_{PC} = 4, *C^{tBu}*), 31.0 (s, *CH$_3$*).

^{31}P{^{1}H} NMR (CD$_2$Cl$_2$, 298 K, 162 MHz): δ 11.2 (s).

ATR IR: v$_{CH}$ ~2586 cm^{-1} (broad).

HR ESI-MS (positive ion, 4 kV): 796.3755, [*M*]$^+$ (calcd 796.3749) *m/z*.

Anal. Calcd for $C_{71}H_{71}BF_{24}IrNP_2$ (1659.29 g mol^{-1}): C, 51.39; H, 4.31; N, 0.84; Found: C, 51.52; H, 4.19; N, 0.87.

6.2.12. Variable Tempearture NMR Experiments

NMR tubes fitted with J Young's valves were loaded with compound **7** or **8** (10 µmol) in CD2Cl2 (500 µL). Solution state dynamics were investigated by ^{1}H (500 MHz) and ^{31}P{^{1}H} (202 MHz) NMR spectroscopy. Samples were equilibrated at each temperature for 5 minutes. Dynamics were also simulated using gNMR,[193] with reference line widths and values of J_{PH} fixed following analysis of low temperature data (**Table 6.1**). Activation parameters were determined using the equation $\Delta G^{\ddagger} = RT [23.760 + \ln(T/k_{exchange})]$; reported values and errors are based on a statistical analysis of at least 3 different temperature points.

Table 6.1. *Exchange rates for biphenyl ligand in complexes* **7** *and* **8** *at various temperatures, as determined by gNMR simulations.*[193]

Complex	Rate of Exchange / s^{-1}									
	225	250	273	278	283	288	293	298	303	308
7	0.4	6	68	-	-	-	575	-	-	1145
8	-	-	-	-	5	10	19	36	67	120

6.2.13. Synthesis of [Rh(PNP-Np)(biph)(CO)][BAr$^F_4$], **9**
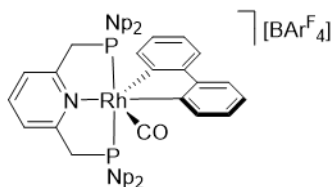
A 20 mM solution of **7** (15.7 mg, 10.0 µmol) in 1,2-C$_6$H$_4$F$_2$ (500 µL) was prepared in an NMR tube fitted with a J Young's valve. This was freeze-pump-thaw degassed and placed under 1 bar of CO and gently shaken at ambient temperature. An immediate colour change from yellow to colourless was observed. The solution was subsequently freeze-pump-thaw degassed and placed back under Ar. Recrystallisation by slow diffusion of hexane into the 1,2-C$_6$H$_4$F$_2$ solution afforded colourless crystals. Yield: 11.4 mg (7.13 µmol, 71 %). Single crystals suitable for X-ray diffraction were obtained by slow diffusion of hexane into a 1,2-C$_6$H$_4$F$_2$ solution at ambient temperature.

^{1}H NMR (CD$_2$Cl$_2$, 500 MHz): δ 7.96 (t, $^3J_{HH}$ = 7.9, 1H, *4-Py*), 7.70-7.76 (m, 10H, o-*Ar^F* + *9-biph*), 7.65 (d, $^3J_{HH}$ = 7.7, 1H, *3-biph*), 7.58-7.63 (m, 3H, *3,5-Py* + *6-biph*), 7.57 (s, 4H, p-*Ar^F*), 7.18 (t, $^3J_{HH}$ = 7.4, 1H, *10-biph*), 7.13 (t, $^3J_{HH}$ = 7.4, 1H, *4-biph*), 7.00 (td, $^3J_{HH}$ = 7.4, $^4J_{HH}$ = 1.5, 1H, *5-biph*), 6.88 (t, $^3J_{HH}$ = 7.4, 1H, *11-biph*), 5.97 (d, $^3J_{HH}$ = 7.6, 1H, *12-biph*),

4.39 (dvt, $^2J_{HH}$ = 17.3, J_{PH} = 10, 2H, $CH_2^{Py-biph}$), 3.81 (dvt, $^2J_{HH}$ = 17.3, J_{PH} = 7, 2H, CH_2^{Py-CO}), 2.55 (d, $^2J_{HH}$ = 15.2, 2H, CH_2^{Np-CO}), 2.18 (d, $^2J_{HH}$ = 15.4, $CH_2^{Np-CO'}$), 1.30 (dvt, $^2J_{HH}$ = 16.0, J_{PH} = 6, 2H, $CH_2^{Np-biph}$), 1.20 (dvt, $^2J_{HH}$ = 15.9, J_{PH} = 7, 2H, $CH_2^{Np-biph'}$), 1.01 (s, 17H, CH_3^{CO}), 0.71 (s, 19H, CH_3^{biph}).

^{13}C{^{1}H} NMR (CD$_2$Cl$_2$, 126 MHz): δ 190.1 (dt, $^1J_{RhC}$ = 44, $^2J_{PC}$ = 9, *CO*), 166.4 (dt, $^1J_{RhC}$ = 26, $^2J_{PC}$ = 9, *7-biph*), 162.6 (q, $^1J_{CB}$ = 50, i-*Ar^F*), 159.7 (vt, J_{PC} = 5, *2,6-Py*), 155.4 (dt, $^1J_{RhC}$ = 29, $^2J_{PC}$ = 7, *1-biph*), 153.6 (s, *8-biph*), 151.7 (s, *2-biph*), 141.2 (s, *4-Py*), 139.4 (s, *6-biph*), 135.6 (s, o-*Ar^F*), 132.7 (vt, J_{PC} = 4, *12-biph*), 129.7 (qq, $^2J_{FC}$ = 32, $^3J_{CB}$ = 3, m-*Ar^F*), 128.1-128.2 (m, *5,11-biph*), 126.6 (s, *10-biph*), 125.4 (q, $^1J_{FC}$ = 272, *CF$_3$*), 125.1 (s, *4-biph*), 124.2 (vt, J_{PC} = 10, *3,5-Py*), 123.5 (s, *9-biph*), 123.1 (s, *3-biph*), 118.3 (sept, $^3J_{FC}$ = 4, p-*Ar^F*), 45.3 (vt, J_{PC} = 21, $CH_2^{Np-biph}$), 44.6 (vt, J_{PC} = 24, CH_2^{Py}), 34.3 (vtd, J_{PC} = 19, $^2J_{RhC}$ = 2, CH_2^{Np-CO}), 33.8 (vt, J_{PC} = 8, C^{tBu}), 33.1 (s, C^{tBu}), 32.7 (vt, J_{PC} = 6, CH_3^{CO}), 32.2 (vt, J_{PC} = 6, CH_3^{biph}).

^{31}P{^{1}H} NMR (CD$_2$Cl$_2$, 162 MHz): δ 23.2 (d, $^1J_{RhP}$ = 97).

ATR IR: v_{CO} 2058 cm^{-1}.

IR (CH$_2$Cl$_2$): v_{CO} 2056 cm^{-1}.

HR ESI-MS (positive ion, 4 kV): 706.3163, [*M-CO*]$^+$ (calcd 706. 3172) *m/z*.

6.2.14. Synthesis of [Ir(PNP-Np)(biph)(CO)][BAr$^F_4$], **10**
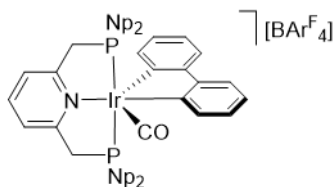
A 20 mM solution of **8** (16.6 mg, 10.0 μmol) in 1,2-C$_6$H$_4$F$_2$ (500 μL) was prepared in an NMR tube fitted with a J Young's valve. This was freeze-pump-thaw degassed and placed under 1 bar of CO and gently shaken at ambient temperature. An immediate colour change from yellow to colourless was observed. The solution was subsequently freeze-pump-thaw degassed and placed back under Ar. Recrystallisation by slow diffusion of hexane into the 1,2-C$_6$H$_4$F$_2$ solution afforded colourless crystals. Yield: 12.4 mg (7.34 μmol, 73 %). Single crystals suitable for X-ray diffraction were obtained by slow diffusion of hexane into a 1,2-C$_6$H$_4$F$_2$ solution at ambient temperature.

^{1}H NMR (CD$_2$Cl$_2$, 500 MHz): δ 8.01 (t, $^3J_{HH}$ = 7.9, 1H, *4-Py*), 7.71-7.77 (m, 10H, o-*Ar^F* + *9-biph*), 7.68 (d, $^3J_{HH}$ = 8.0, 3H, *3,5-Py + 6-biph*), 7.65 (dd, $^3J_{HH}$ = 7.8, $^4J_{HH}$ = 1.5, 1H, *3-biph*), 7.57 (s, 4H, p-*Ar^F*), 7.19 (td, $^3J_{HH}$ = 7.5, $^4J_{HH}$ = 1.3, 1H, *10-biph*), 7.10 (t, $^3J_{HH}$ = 7.5, 1H, *4-biph*), 6.96 (td, $^3J_{HH}$ = 7.4, $^4J_{HH}$ = 1.5, 1H, *5-biph*), 6.89 (td, $^3J_{HH}$ = 7.4, $^4J_{HH}$ = 1.4, 1H,

11-biph), 5.90 (dd, $^3J_{HH}$ = 7.5, $^4J_{HH}$ = 1.4, 1H, *12-biph*), 4.59 (dvt, $^2J_{HH}$ = 17.4, J_{PH} = 10, 2H, $CH_2^{Py\text{-}biph}$), 3.90 (dvt, $^2J_{HH}$ = 17.3, J_{PH} = 8, 2H, $CH_2^{Py\text{-}CO}$), 2.71 (dvt, $^2J_{HH}$ = 15.1, J_{PH} = 5, 2H, $CH_2^{Np\text{-}CO}$), 2.32 (dvt, $^2J_{HH}$ = 15.2, J_{PH} = 6, 2H, $CH_2^{Np\text{-}CO'}$), 1.38 (dvt, $^2J_{HH}$ = 16.1, J_{PH} = 6, 2H, $CH_2^{Np\text{-}biph}$), 1.22 (dvt, $^2J_{HH}$ = 15.9, J_{PH} = 8, 2H, $CH_2^{Np\text{-}biph'}$), 1.01 (s, 21H, CH_3^{CO}), 0.70 (s, 21H, CH_3^{biph}).

^{13}C{^{1}H} NMR (CD$_2$Cl$_2$, 126 MHz): δ 177.9 (t, $^2J_{PC}$ = 7, *CO*), 162.6 (q, $^1J_{CB}$ = 50, i-*Ar^F*), 161.5 (vt, J_{PC} = 4, *2,6-Py*), 154.8 (s, *8-biph*), 153.2 (vt, J_{PC} = 20, *7-biph*), 151.7 (s, *2-biph*), 141.4 (s, *4-Py*), 139.0 (s, *6-biph*), 135.6 (s, o-*Ar^F*), 134.9 (vt, J_{PC} = 12, *1-biph*), 132.2 (vt, J_{PC} = 4, *12-biph*), 129.7 (qq, $^2J_{FC}$ = 32, $^3J_{CB}$ = 3, m-*Ar^F*), 128.6 (s, *5-biph*), 128.2 (s, *11-biph*), 126.8 (s, *10-biph*), 125.4 (q, $^1J_{FC}$ = 272, *CF$_3$*), 124.9 (s, *4-biph*), 123.9 (vt, J_{PC} = 9, *3,5-Py*), 123.6 (s, *9-biph*), 122.9 (s, *3-biph*), 118.3 (sept, $^3J_{FC}$ = 4, p-*Ar^F*), 45.7 (vt, J_{PC} = 29, CH_2^{Py}), 44.4 (vt, J_{PC} = 26, $CH_2^{Np\text{-}CO}$), 33.4 (vt, J_{PC} = 7, *C^{tBu}*), 32.99-33.04 (m, *C^{tBu}*), 33.0 (vt, J_{PC} = 25, $CH_2^{Np\text{-}biph}$), 32.6 (vt, J_{PC} = 6, CH_3^{CO}), 32.2 (vt, J_{PC} = 6, CH_3^{biph}).

^{31}P{^{1}H} NMR (CD$_2$Cl$_2$, 162 MHz): δ −7. 1 (s).

ATR IR: $ν_{CO}$ 2028 cm^{-1}.

IR (CH$_2$Cl$_2$): $ν_{CO}$ 2027 cm^{-1}.

HR ESI-MS (positive ion, 4 kV): 824.3691, [*M*]$^+$ (calcd 824.3698) *m/z.*

Anal. Calcd for C$_{72}$H$_{71}$BF$_{24}$IrNOP$_2$ (1687.30 g mol^{-1}): C, 51.25; H, 4.24; N, 0.83; Found: C, 51.10; H, 4.10; N, 0.82.

6.2.15. <u>NMR Experiment to Monitor the Decomposition of **9**</u>
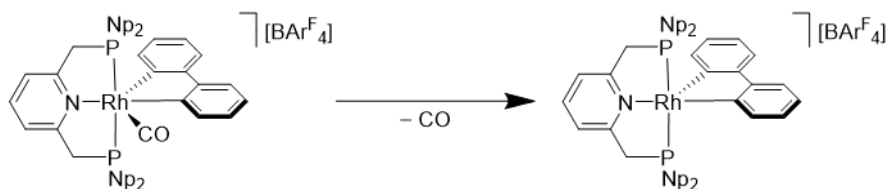
A 20 mM solution of **9** (15.7 mg, 10.0 μmol) in 1,2-C$_6$H$_4$F$_2$ (500 μL) was prepared in an NMR tube fitted with a J Young's valve. This was freeze-pump-thaw degassed and placed under 1 bar of CO and gently shaken at ambient temperature. An immediate colour change from yellow to colourless was observed. Tube was agitated at ambient temperature for 24 hours with no signs of decomposition. The solution was freeze-pump-thaw degassed and the atmosphere replaced with Ar (1 bar). Tube was agitated at ambient temperature for 2 weeks with no signs of decomposition. Volatiles were removed under reduced pressure and resulting white solid was dried *in vacuo*, before being redissolved in 1,2-C$_6$H$_4$F$_2$ (500 μL). A trace amount of **7** could be detected by ^{31}P{^{1}H} NMR spectroscopy. This exposure to vacuum and redissolving in 1,2-C$_6$H$_4$F$_2$ process was repeated another four times, leading to the formation of ~1 % **7** by ^{31}P{^{1}H} NMR spectroscopy.

^{31}**P{^{1}H} NMR** (1,2-C$_6$H$_4$F$_2$, 162 MHz): δ 23.5 (d, $^1J_{RhP}$ = 110, **7**), 22.5 (d, $^1J_{RhP}$ = 96, **8**).

6.2.16. Hydrogenolysis of **7**
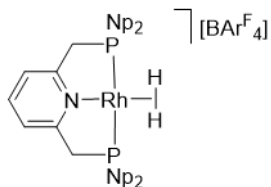
A solution of **7** (13.1 mg, 8.34 μmol) in C$_6$H$_5$F (500 μL) was prepared in an NMR tube fitted with a J Young's valve. This was freeze-pump-thaw degassed and placed under 4 bar of H$_2$. The solution was heated at 80 °C for 5 months: after 3 months, solution was freeze-pump-thaw degassed and the atmosphere replaced with H$_2$ (4 bar). This was repeated again after 4 months. At 5 months, reaction had reached ~90 % completion (by ^{31}P{^{1}H} NMR spectroscopy) and was analysed *in situ*, under 4 bar of H$_2$.

^{1}**H NMR** (C$_6$H$_5$F, 500 MHz, *selected data*): δ 8.30 (s, o-*Ar^F*), 7.61 (s, p-*Ar^F*), 7.47 (d, $^3J_{HH}$ = 7.6, *3,5-Py*), 7.27 (t, $^3J_{HH}$ = 7.6, *4-Py*), 3.26 (vt, J_{PH} = 8, *CH$_2^{Py}$*), 1.62 (dvt, $^2J_{HH}$ = 14.8, J_{PH} = 6, *CH$_2^{Np}$*), 1.52 (dvt, $^2J_{HH}$ = 14.8, J_{PH} = 7, *CH$_2^{Np}$*), 1.37 (s, *CH$_3$*), 1.00 (s, *CH$_3$*), −11.00 (dm, $^1J_{RhH}$ = 28.9, *Rh-(H$_2$)*).

^{31}**P{^{1}H} NMR** (C$_6$H$_5$F, 162 MHz, *selected data*): δ 16.4 (d, $^1J_{RhP}$ = 120).

^{31}**P{^{1}H} NMR** (CD$_2$Cl$_2$, 162 MHz, *selected data*): δ 18.1 (d, $^1J_{RhP}$ = 120).

HR ESI-MS (positive ion, 4 kV): 556.2698, [*M*]$^+$ (calcd 556.2703); 554.2545, [*M−H$_2$*]$^+$ (calcd 554.2546) *m/z*.

6.2.17. Hydrogenolysis of **8**
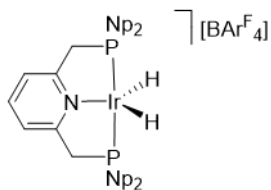
A 20 mM solution of **8** (16.6 mg, 10.0 μmol) in C$_6$H$_5$F (500 μL) was prepared in an NMR tube fitted with a J Young's valve. This was freeze-pump-thaw degassed and placed under 1 bar of H$_2$. The solution was heated at 80 °C for 16 hours before volatiles were removed under reduced pressure. The pale yellow solid was washed with hexane (3 x 1 mL) and dried *in vacuo*. Recrystallisation by slow diffusion of hexane into a C$_6$H$_5$F solution afforded colourless crystals. Yield: 10.7 mg (7.09 μmol, 71 %).

¹H NMR (CD$_2$Cl$_2$, 500 MHz): δ 7.79 (t, $^3J_{HH}$ = 7.8, 1H, *4-Py*), 7.73 (s, 9H, o-*Ar^F*), 7.57 (s, 4H, p-*Ar^F*), 7.48 (d, $^3J_{HH}$ = 7.8, 2H, *3,5-Py*), 3.84 (vt, J_{PH} = 8, 4H, *CH$_2^{Py}$*), 2.23 (dvt, $^2J_{HH}$ = 14.7, J_{PH} = 7, 5H, *CH$_2^{Np}$*), 1.94 (dvt, $^2J_{HH}$ = 14.8, J_{PH} = 7, 5H, *CH$_2^{Np}$*), 0.97 (s, 39H, *CH$_3$*), −23.05 (t, $^2J_{PH}$ = 14, 2H, *Ir-H*).

¹³C{¹H} NMR (CD$_2$Cl$_2$, 126 MHz): δ 162.6 q, $^1J_{CB}$ = 50, i-*Ar^F*), 161.7 (vt, J_{PH} = 6, *2,6-Py*), 139.5 (s, *4-Py*), 135.6 (s, o-*Ar^F*), 129.7 (qq, $^2J_{FC}$ = 32, $^3J_{CB}$ = 3, m-*Ar^F*), 125.3 (q, $^1J_{FC}$ = 272, *CF$_3$*), 122.7 (vt, J_{PH} = 10, *3,5-Py*), 118.3 (sept, $^3J_{FC}$ = 4, p-*Ar^F*), 49.6 (vt, J_{PH} = 29, *CH$_2^{Py}$*), 45.9 (vt, J_{PH} = 29, *CH$_2^{Np}$*), 33.2 (s, *C^{tBu}*), 31.5 (vt, J_{PH} = 7, *CH$_3$*).

³¹P{¹H} NMR (CD$_2$Cl$_2$, 162 MHz): δ 9.2 (t, $^2J_{PH}$ = 13).

ATR IR: ν_{CH} ~2588 cm^{-1} (broad), ν_{IrH} 2148 cm^{-1}.

HR ESI-MS (positive ion, 4 kV): 646.3290, [*M*]$^+$ (calcd 646.3278) *m/z*.

6.3. Experimental Data for Chapter 3

6.3.1. Synthesis of 2-(^{i}Pr$_3$SiO)-6-(CH$_3$)-C$_5$H$_3$N, **16**
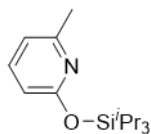
2-Hydroxy-6-methylpyridine (**15**) (2.00 g, 18.3 mmol) was suspended in toluene (20 mL) and triethylamine (2.8 mL, 20 mmol) was added. Mixture was heated at reflux to give a brown solution. Tri(*iso*-propyl)silyl chloride (3.9 mL, 18 mmol) was added and solution was heated at reflux for 1 hour. Solution was filtered and solvent was removed under reduced pressure to give an oil, which was extracted into hexane. Solvent was removed under reduced pressure to give a yellow oil. Yield: 4.2 g (16 mmol, 86 %).

^{1}H NMR (CD$_2$Cl$_2$, 500 MHz): δ 7.46 (app. t, J_{HH} = 7.7, 1H, *4-Py*), 6.72 (d, $^3J_{HH}$ = 7.3, 1H, *5-Py*), 6.51 (d, $^3J_{HH}$ = 8.1, 1H, *3-Py*), 2.38 (s, 3H, *CH$_3$*), 1.42 (sept, $^3J_{HH}$ = 7.5, 3H, *CH^{iPr}*), 1.13 (d, $^3J_{HH}$ = 7.9, 23H, *CH$_3$^{iPr}*).

^{13}C{^{1}H} NMR (CD$_2$Cl$_2$, 126 MHz): δ 162.9 (s, *2-Py*), 157.2 (s, *6-Py*), 139.8 (s, *4-Py*), 116.4 (s, *5-Py*), 109.6 (s, *3-Py*), 24.4 (s, *CH$_3$*), 18.8 (s, *CH$_3$^{iPr}*), 13.4 (s, *CH^{iPr}*).

6.3.2. Synthesis of 2-(^{i}Pr$_3$SiO)-6-(CH$_2$(PMe$_2$))-C$_5$H$_3$N, **17** (Method A)
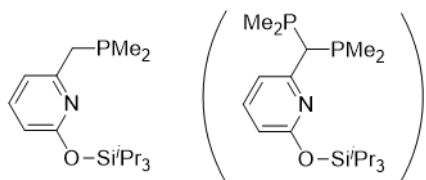
Compound **16** (2.54 g, 9.57 mmol) and TMEDA (1.43 mL, 9.57 mmol) were dissolved in dry Et$_2$O (20 mL) to give a yellow solution. This was cooled to 0 °C and ^{n}BuLi (1.6 M in hexanes, 5.98 mL) was added dropwise. The solution turned orange and was stirred at ambient temperature for 24 hours. A solution of Me$_2$PCl (0.83 mL, 10 mmol) in Et$_2$O (10 mL) was added slowly at −78 °C and the mixture was stirred at ambient temperature for 18 hours, lightening and with precipitation of a pale yellow solid. Volatiles were removed under reduced pressure to give a yellow oil. This was extracted into pentane, filtered and dried to give an orange oil. Crude yield: 3.0 g.

^{31}P{^{1}H} NMR (C$_6$D$_6$, 202 MHz, *selected data*): δ −41.1-−40.9 (m, *18*), −45.4-−45.1 (m, *17*).

6.3.3. Synthesis of 2-(^{i}Pr$_3$SiO)-6-(CH$_2$(P(=S)Me$_2$))-C$_5$H$_3$N, **21**, and 2-(^{i}Pr$_3$SiO)-6-(CH(P(=S)Me$_2$)$_2$)-C$_5$H$_3$N, **22**
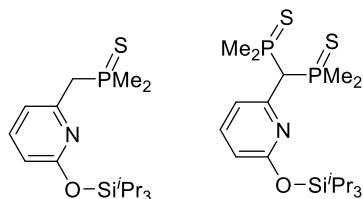
An NMR tube fitted with a J Young's valve was loaded with crude **17**/**18** mixture (43.8 mg) and THF (500 μL). This was transferred onto S$_8$ (86.0 mg, 0.335 mmol) in a separate NMR tube and agitated at ambient temperature for 24 hours. The yellow suspension was filtered and dried to give a yellow solid.

^{31}P{^{1}H} NMR (CDCl$_3$, 122 MHz): δ 41.3 (s, **22**), 36.1 (s, **21**).

HR ESI-MS (positive ion, 4 kV): 380.1604, [*M(21)+Na*]$^+$ (calcd 380.1604); 472.1445, [*M(22)+Na*]$^+$ (calcd 472.1453) *m/z*.

6.3.4. Synthesis of 2-(^{i}Pr$_3$SiO)-6-(CH$_2$(PMe$_2$))-C$_5$H$_3$N, **17** (Method B)
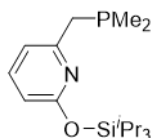
Compound **16** (5.43 g, 20.4 mmol) was dissolved in dry Et$_2$O (30 mL) to give a yellow solution. This was cooled to 0 °C and ^{n}BuLi (1.6 M in hexanes, 12.8 mL) was added dropwise. The solution turned red and was stirred at ambient temperature for 22 hours. The lithiated solution was then transferred onto a solution of Me$_2$PCl (1.97 g, 20.4 mmol) in Et$_2$O (10 mL) at −78 °C. The mixture was stirred at ambient temperature for 19.5 hours, lightening and with precipitation of a pale yellow solid. This was filtered, left to stand for 17 hours to allow for further precipitation and filtered. Solvent was removed under reduced pressure, yielding an orange oil. Yield: 6.60 g (20.3 mmol, 99 %).

^{1}H NMR (C$_6$D$_6$, 600 MHz): δ 7.04 (app. t, J_{HH} = 7.7, 1H, *4-Py*), 6.45 (d, $^{3}J_{HH}$ = 8.1, 1H, *3-Py*), 6.43 (d, $^{3}J_{HH}$ = 7.3, 1H, *5-Py*), 2.65 (s, 2H, *CH$_2$^{P}*), 1.53 (sept, $^{3}J_{HH}$ = 7.5, 3H, *CH^{iPr}*), 1.22 (d, $^{3}J_{HH}$ = 7.5, 20H, *CH$_3$^{iPr}*), 0.82 (d, $^{2}J_{PH}$ = 4, 6H, *CH$_3$^{P}*).

^{13}C{^{1}H} NMR (C$_6$D$_6$, 151 MHz): δ 163.2 (s, *2-Py*), 157.7 (d, $^{2}J_{PC}$ = 3, *6-Py*), 139.7 (s, *4-Py*), 116.9 (d, $^{3}J_{PC}$ = 5, *5-Py*), 110.0 (s, *3-Py*), 41.7 (d, $^{1}J_{PC}$ = 17, *CH$_2$^{P}*), 19.1 (s, *CH$_3$^{iPr}*), 14.4 (d, $^{1}J_{PC}$ = 16, *CH$_3$^{P}*), 13.6 (s, *CH^{iPr}*).

^{31}P{^{1}H} NMR (C$_6$D$_6$, 243 MHz): δ −45.2 (s).

HR ESI-MS (positive ion, 4 kV): 326.2058, $[M+H]^+$ (calcd 326.2064) *m/z*.

6.3.5. Synthesis of $[Rh(\mathbf{15})(cod)][BAr^F_4]$, **23**
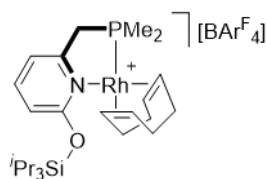
A 20 mM solution of **17** in 1,2-$C_6H_4F_2$ was prepared and 500 μL was transferred to an NMR tube fitted with a J Young's valve and loaded with $[Rh(cod)_2][BAr^F_4]$ (11.8 mg, 9.98 μmol). The orange solution was agitated for 18 hours. The solvent was then removed under reduced pressure and the resulting yellow solid was washed with hexane, filtered and dried *in vacuo*. Yield: 12.4 mg (8.86 μmol, 89 %).

^{1}H NMR (CD$_2$Cl$_2$, 500 MHz): δ 7.78 (app. t, J_{HH} = 7.9, 1H, *4-Py*), 7.73 (s, 10H, *o-Ar^F*), 7.57 (s, 4H, p-*Ar^F*), 7.16 (d, $^3J_{HH}$ = 7.4, 1H, *5-Py*), 6.79 (d, $^3J_{HH}$ = 8.3, 1H, *3-Py*), 5.64-5.71 (m, 2H, *CH^{cod}*), 4.02-4.08 (m, 2H, *CH^{cod}*), 3.67 (d, $^2J_{PH}$ = 10, 2H, *CH$_2$^{P}*), 2.39-2.49 (m, 2H, *CH$_2$^{cod}*), 2.22-2.32 (m, 5H, *CH$_2$^{cod}*), 2.08-2.16 (m, 2H, *CH$_2$^{cod}*), 1.40 (sept, $^3J_{HH}$ = 7.4, 3H, *CH^{iPr}*), 1.29 (d, $^2J_{PH}$ = 10, 7H, *CH$_3$^{P}*), 1.17 (d, $^3J_{HH}$ = 7.5, 20H, *CH$_3$^{iPr}*).

^{13}C{^{1}H} NMR (CD$_2$Cl$_2$, 126 MHz): δ 165.5 (s, *2-Py*), 162.6 (q, $^1J_{CB}$ = 50, i-*Ar^F*), 158.5 (d, $^2J_{PC}$ = 3, *6-Py*), 143.5 (s, *4-Py*), 135.6 (s, o-*Ar^F*), 129.7 (qq, $^2J_{FC}$ = 32, $^3J_{CB}$ = 3, m-*Ar^F*), 125.4 (q, $^1J_{FC}$ = 272, *CF$_3$*), 119.0 (d, $^3J_{PC}$ = 9, *5-Py*), 118.3 (sept, $^3J_{FC}$ = 4, p-*Ar^F*), 113.7 (s, *3-Py*), 106.7 (dd, J_{RhC} = 10, J_{PC} = 6, *CH^{cod}*), 74.0 (d, J_{RhC} = 13, *CH^{cod}*), 41.6 (d, $^1J_{PC}$ = 28, *CH$_2$^{P}*), 33.2 (d, J_{RhC} = 3, *CH$_2$^{cod}*), 29.0 (s, *CH$_2$^{cod}*), 18.3 (s, *CH$_3$^{iPr}*), 13.6 (s, *CH^{iPr}*), 11.3 (dd, $^1J_{PC}$ = 27, $^2J_{RhC}$ = 2, *CH$_3$^{P}*).

^{31}P{^{1}H} NMR (CD$_2$Cl$_2$, 162 MHz): δ 25.1 (d, $^1J_{RhP}$ = 148).

HR ESI-MS (positive ion, 4 kV): 536.1970, $[M]^+$ (calcd 536.1979) *m/z*.

6.3.6. Synthesis of $[Rh(\mathbf{15})_2][BAr^F_4]$, **24**
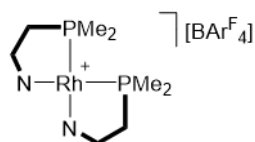
A 20 mM solution of **17** in 1,2-$C_6H_4F_2$ was prepared and 500 μL was transferred to an NMR tube fitted with a J Young's valve and loaded with $[Rh(cod)_2][BAr^F_4]$ (5.8 mg, 4.9 μmol). The yellow solution was agitated for 120 hours. The solvent was then removed under reduced pressure and the resulting orange solid was washed with hexane, filtered and dried *in vacuo*. Yield: 6.1 mg (3.8 μmol, 77 %).

¹H NMR (CD₂Cl₂, 500 MHz): δ 7.73 (s, 8H, *o-ArF*), 7.64 (app. t, J_{HH} = 7.8, 1H, *4-Py*), 7.57 (s, 3H, *p-ArF*), 7.12 (d, $^3J_{HH}$ = 7.4, 1H, *5-Py*), 6.66 (d, $^3J_{HH}$ = 8.2, 1H, *3-Py*), 3.68 (dt, $^2J_{HH}$ = 16.2, $^2J_{PH}$ = 4, 1H, *CH₂P*), 3.26 (dt, $^2J_{HH}$ = 15.7, $^2J_{PH}$ = 8, 1H, *CH₂P*), 1.57-1.60 (m, 3H, *CH₃P*), 1.22-1.25 (m, 4H, *CH₃P*), 1.17 (d, $^3J_{HH}$ = 7.4, 10H, *CH₃iPr*), 0.89 (sept, $^3J_{HH}$ = 7.3, 4H, *CHiPr*), 0.80 (d, $^3J_{HH}$ = 7.3, 11H, *CH₃iPr*).

¹³C{¹H} NMR (CD₂Cl₂, 126 MHz): δ 165.2 (s, *2-Py*), 162.6 (q, $^1J_{CB}$ = 50, *i-ArF*), 158.8 (s, *6-Py*), 140.9 (s, *4-Py*), 135.6 (s, *o-ArF*), 129.7 (qq, $^2J_{FC}$ = 32, $^3J_{CB}$ = 3, *m-ArF*), 125.4 (q, $^1J_{FC}$ = 272, *CF₃*), 118.3 (sept, $^3J_{FC}$ = 4, *p-ArF*), 117.8 (t, $^3J_{PC}$ = 5, *5-Py*), 113.3 (s, *3-Py*), 44.5 (d, $^1J_{PC}$ = 14, *CH₂P*), 44.4 (d, $^1J_{PC}$ = 14, *CH₂P*), 18.7 (s, *CH₃iPr*), 18.3 (s, *CH₃iPr*), 17.3-17.7 (m, *CH₃P*), 16.1-16.3 (m, *CH₃P*), 13.9 (s, *CHiPr*).

³¹P{¹H} NMR (CD₂Cl₂, 162 MHz): δ 40.0 (d, $^1J_{RhP}$ = 167).

6.3.7. Synthesis of 2-O-6-(CH₂(PMe₂))-C₅H₄N, **25**
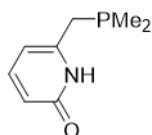
(impure)

A solution of **17** (0.671 g, 2.06 mmol) in THF (10 mL) was cooled to 0 °C. TBAF (1 M in THF, 2.3 mL) was added and the solution was stirred at 0 °C for 10 minutes, turning pale yellow. This warmed to ambient temperature and stirred for a further hour. The reaction was quenched with saturated aqueous NH₄Cl (10 mL). The organic portion was extracted into toluene (10 mL) and separated. The solution was dried over MgSO₄ and solvent was removed under reduced pressure to give a yellow residue. Crude yield: 0.54 g.

6.3.8. Synthesis of 2-O-6-(CH₂(P(BH₃)Me₂))-C₅H₄N, **26**
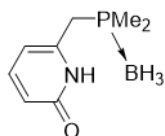
Crude **25** (0.54 g) was dissolved in THF (10 mL) and cooled to −78 °C. BH₃•SMe₂ (0.60 mL, 6.3 mmol) was added and the solution was stirred at −78 °C for 5 minutes. Solution was then stirred at ambient temperature for a further 10 minutes. Saturated aqueous NH₄Cl was added (10 mL) and the organic portion was separated. This was dried over MgSO₄ and the solvent was removed under reduced pressure to give an air-stable, fine, white solid. This was purified by slow diffusion of hexane into a THF solution at ambient temperature. Yield: 0.30 g, 1.6

mmol. Single crystals suitable for X-ray diffraction were obtained by slow diffusion of hexane into a THF solution at ambient temperature.

^{1}H NMR (CDCl$_3$, 500 MHz): δ 7.48 (dd, $^3J_{HH}$ = 9.1, 6.9, 1H, *4-Py*), 6.52 (d, $^3J_{HH}$ = 9.1, 1H, *3-Py*), 6.26 (dd, $^3J_{HH}$ = 7.0, $^4J_{PH}$ = 2, 1H, *5-Py*), 3.10 (d, $^2J_{PH}$ = 11, 2H, *CH$_2$^{P}*), 1.38 (d, $^2J_{PH}$ = 10, 6H, *CH$_3$^{P}*), 0.06-0.93 (br m, *BH$_3$*).

^{11}B{^{1}H} NMR (CDCl$_3$, 96 MHz): δ −38.1 (d, $^1J_{PB}$ = 59).

^{13}C{^{1}H} NMR (CDCl$_3$, 151 MHz): δ 165.8 (s, *2-Py*), 142.5 (d, $^4J_{PC}$ = 3, *4-Py*), 141.8 (d, $^2J_{PC}$ = 7, *6-Py*), 118.0 (d, J_{PC} = 3, *3-Py*), 108.8 (d, $^3J_{PC}$ = 5, *5-Py*), 32.0 (d, $^1J_{PC}$ = 29, *CH$_2$^{P}*), 11.2 (d, $^1J_{PC}$ = 36, *CH$_3$^{P}*).

^{31}P{^{1}H} NMR (CDCl$_3$, 243 MHz): δ 8.0-9.6 (br m).

ATR IR: ν$_{CO}$ 1640 cm^{-1}.

HR ESI-MS (positive ion, 4 kV): 389.1864, [*M$_2$+Na*]$^+$ (calcd 389.1867) *m/z*.

6.3.9. Deprotection of **26**
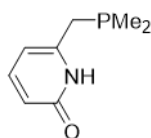
(pure)

Compound **26** (0.30 g, 1.6 mmol) was suspended in Et$_2$NH (10 mL) and stirred at 80 °C for 120 hours. Volatiles were removed under reduced pressure to give a white solid. Pentane was added (2 mL) and removed under reduced pressure to form an azeotrope with any remaining Et$_2$NH. Solid was dried *in vacuo*. Yield: 0.27 g, (1.6 mmol, 77 %).

^{1}H NMR (C$_6$D$_6$, 500 MHz): δ 13.79 (br s, 1H, *NH*), 6.79 (dd, $^3J_{HH}$ = 9.1, 6.9, 1H, *4-Py*), 6.38 (d, $^3J_{HH}$ = 9.1, 1H, *3-Py*), 5.52 (d, $^3J_{HH}$ = 6.8, 1H, *5-Py*), 2.52 (d, $^2J_{PH}$ = 2, 2H, *CH$_2$^{P}*), 0.80 (d, $^2J_{PH}$ = 4, 6H, *CH$_3$^{P}*).

^{13}C{^{1}H} NMR (C$_6$D$_6$, 126 MHz): δ 166.9 (s, *2-Py*), 147.6 (d, $^2J_{PC}$ = 2, *6-Py*), 141.9 (s, *4-Py*), 117.0 (d, $^5J_{PC}$ = 2, *3-Py*), 106.0 (d, $^3J_{PC}$ = 6, *5-Py*), 35.1 (d, $^1J_{PC}$ = 21, *CH$_2$^{P}*), 13.7 (d, $^1J_{PC}$ = 17, *CH$_3$^{P}*).
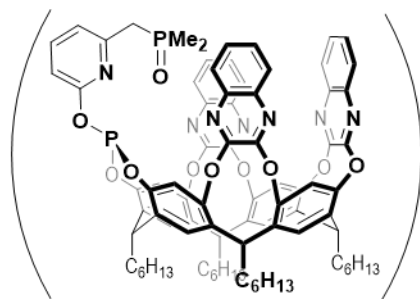
^{31}P{^{1}H} NMR (C$_6$D$_6$, 162 MHz): δ −44.1 (s).

HR ESI-MS (positive ion, 4 kV): 361.1205, [*M$_2$+Na*]$^+$ (calcd 361.1205) *m/z*.

6.3.10. Synthesis of Rc-PONP-Me$_2$, **14**
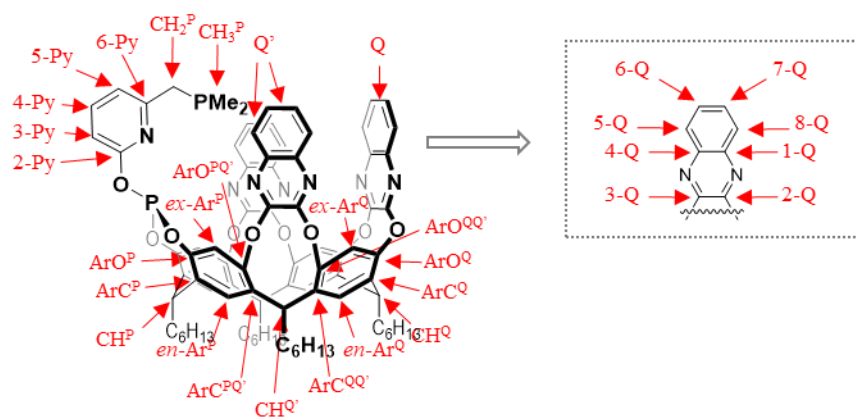
Hex: CH$_3^{hex}$, 5-CH$_2$, 4-CH$_2$, 3-CH$_2$, 2-CH$_2$, 1-CH$_2$

NMR assignments of resorcinarene PONP compounds are based on this system

A suspension of **25** (19.5 mg, 0.115 mmol) and KHMDS (23.0 mg, 0.115 mmol) in THF was stirred at ambient temperature for 1 hour. The suspension was then transferred onto chlorophosphite **A197** (146.0 mg, 0.1153 mmol) and stirred for a further hour. A small amount of hexane was added to precipitate salts and the reaction mixture was filtered. Volatiles were removed under reduced pressure to give a cream solid, which was extracted into Et$_2$O and dried. Crude yield: 143 mg.

^{1}H NMR (C$_6$D$_6$, 500 MHz, *selected data*): δ 8.79 (s, ex-*Ar^Q*), 7.96-8.00 (m, *5-8-Q/Q'*), 7.93 (s, ex-*Ar^P*), 7.80 (s, en-*Ar^Q*), 7.73-7.77 (m, *5-8-Q/Q'*), 7.69 (s, en-*Ar^P*), 7.59-7.63 (m, *5-8-Q/Q'*), 7.25-7.29 (m, *5-8-Q/Q'*), 7.02-7.07 (m, *5-8-Q/Q'*), 6.93 (app. t, J_{HH} = 7.8, 1H, *4-Py*), 6.44 (d, $^3J_{HH}$ = 8.1, 1H, *3-Py*), 6.36 (d, $^3J_{HH}$ = 7.4, 1H, *5-Py*), 6.17 (t, $^3J_{HH}$ = 8.2, 1H, *CH^Q*), 6.06 (t, $^3J_{HH}$ = 8.0, 2H, *CH$^{Q'}$*), 5.19 (t, $^3J_{HH}$ = 7.9, 1H, *CH^P*), 2.88 (d, $^2J_{PH}$ = 3, *CH$_2^P$*), 2.16-2.49 (m, *1-CH$_2$*), 1.15-1.56 (br m, *CH$_2$*), 0.87 d, $^2J_{PH}$ = 4, *CH$_3^P$*), 0.72-0.98 (br m, *CH$_3^{hex}$*).
^{13}C{^{1}H} NMR (C$_6$D$_6$, 126 MHz, *selected data*): δ 160.8 (d, $^2J_{PC}$ = 6, *2-Py*), 157.0 (s, *6-Py*), 153.4-154.3 (*ArO$^{Q,QQ,PQ'}$* + *2-3-Q/Q'*), 148.6 (d, $^2J_{PC}$ = 7, *ArO^P*), 141.2 (s, *1/4-Q/Q'*), 140.94 (s, *1/4-Q/Q'*), 140.88 (s, *1/4-Q/Q'*), 140.1 (s, *4-Py*), 139.2 (d, $^3J_{PH}$ = 2, *ArC^P*), 137.5 (s, *ArC$^{PQ'/QQ'}$*), 137.3 (s, *ArC$^{PQ'/QQ'}$*), 136.7 (s, *ArC^Q*), 128.9-129.7 (*5-8-Q/Q'*), 124.2 (s, en-*Ar^Q*),

123.5 (s, en-Ar^P), 120.4 (s, ex-Ar^Q), 119.8 (s, ex-Ar^P), 119.1 (d, $^3J_{PC}$ = 4, 5-Py), 109.2 (s, 3-Py), 39.5 (d, $^1J_{PC}$ = 20, CH_2^P), 37.2 (s, CH^P), 35.5 (s, CH^Q), 35.3 (s, $CH^{Q'}$), 33.9 (s, 1-$CH_2^{Q'}$), 33.1 (s, 1-$CH_2^{P/Q}$), 32.90 (s, 4-$CH_2^{P/Q}$), 32.82 (s, 4-$CH_2^{P/Q}$), 32.81 (s, 4-$CH_2^{Q'}$), 30.44 (s, 3-$CH_2^{Q'}$), 30.35 (s, 3-$CH_2^{P/Q}$), 30.31 (s, 3-$CH_2^{P/Q}$), 28.9-29.1 (m, 2-$CH_2^{Q'+P/Q}$), 28.87 (s, 2-$CH_2^{P/Q}$), 23.67 (s, 5-$CH_2^{Q'}$), 23.62 (s, 5-$CH_2^{P/Q}$), 23.56 (s, 5-$CH_2^{P/Q}$), 14.8-15.0 (br m, CH_3^{hex}), 13.6 (d, $^1J_{PC}$ = 16, CH_3^P).

^{31}P{^{1}H} NMR (C$_6$D$_6$, 162 MHz, *selected data*): δ 135.6 (s, *PO*), −46.0 (s, *PC*).

HR ESI-MS (positive ion, 4 kV): 1454.5816, [*M-O+Na*]$^+$ (calcd 1454.5831) *m/z*.

6.3.11. Reaction of Crude **14/27** with MeI
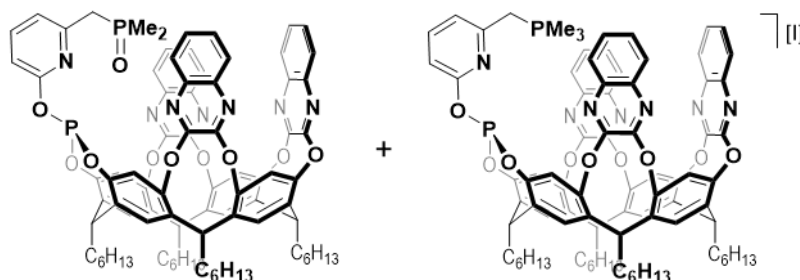
An NMR tube fitted with a J Young's valve was loaded with crude **14/27** (27.7 mg) and 1,2-C$_6$H$_4$F$_2$ (500 μL). To this was added an excess of MeI (3 μL, 50 μmol) and the mixture was agitated at ambient temperature for 16 hours. A cream solid was precipitated, which was filtered, dried *in vacuo* and assigned as **28**. Crude yield: 6 mg. The filtrate was retained and volatiles were removed under reduced pressure to yield a white solid. This was assigned as **27**. Crude yield: 17.5 mg.

*Data for Rc-PONP(=O)-Me$_2$, **27**:*
^{1}H NMR (C$_6$D$_6$, 500 MHz, *selected data*): δ 8.82 (s, 2H, ex-Ar^Q), 7.85-8.10 (5-8-Q/Q'), 7.81 (s, ex-Ar^P), 7.72-7.81 (5-8-Q/Q'), 7.72 (s, 2H, en-Ar^P), 7.70 (s, 3H, en-Ar^Q), 6.86-6.69 (5-8-Q,Q'), 6.81 (app. t, J_{HH} = 7.7, 4-Py), 6.35-6.40 (m, $3,5$-Py), 6.12-6.16 (m, CH^Q), 6.09 (t, $^3J_{HH}$ = 8.5, 2H, $CH^{Q'}$), 5.15 (t, $^3J_{HH}$ = 8.2, 1H, CH^P), 3.15 (d, $^2J_{PH}$ = 17, 2H, CH_2^P), 2.20-2.49 (br m, 1-CH_2), 1.35-1.56 (br m, $2,3$-CH_2), 1.13-1.35 (br m, $4,5$-CH_2), 1.04 (d, $^2J_{PH}$ = 13, 5H, CH_3^P), 0.72-0.98 (br m, CH_3^{hex}).

^{13}C{^{1}H} NMR (C$_6$D$_6$, 126 MHz, *selected data*): δ 160.0 (d, $^2J_{PC}$ = 7, 2-Py), 159.9 (HMBC, 6-Py), 153.4-154.4 ($ArO^{Q,QQ,PQ'}$ + 2-3-Q/Q'), 148.2 (d, $^2J_{PC}$ = 6, ArO^P), 141.1 (s, $1/4$-Q/Q'), 141.0 (s, 4-Py), 140.9 (s, $1/4$-Q/Q'), 140.8 (s, $1/4$-Q/Q'), 139.0 (d, $^3J_{PC}$ = 2, ArC^P), 137.4 (s, $ArC^{Q/Q'}$), 137.3 (s, $ArC^{Q/PQ'}$), 137.0 (s, ArC^{QQ}), 128.0-130.2 (5-8-Q/Q'), 124.1 (s, en-$Ar^{P/Q}$), 123.8 (s, en-$Ar^{P/Q}$), 120.4 (s, ex-Ar^Q), 119.9-120.0 (m, 5-Py), 119.3 (s, ex-Ar^P), 110.3 (s, 3-Py), 43.2 (d, $^1J_{PC}$ = 60, CH_2^P), 37.2 (s, CH^P), 35.5 (s, CH^Q), 35.3 (s, $CH^{Q'}$), 33.7 (s, 1-$CH_2^{Q'}$), 33.3 (s, 1-$CH_2^{P/Q}$), 32.88 (s, 4-$CH_2^{P/Q}$), 32.82 (s, 4-$CH_2^{P/Q}$), 32.81 (s, 4-$CH_2^{Q'}$), 32.3 (s, 1-$CH_2^{P/Q}$),

30.41 (s, $2/3\text{-}CH_2^{Q'}$), 30.34 (s, $2/3\text{-}CH_2^{P/Q}$), 30.27 (s, $2/3\text{-}CH_2^{P/Q}$), 29.01 (s, $2/3\text{-}CH_2^{Q'}$), 28.90 (s, $2/3\text{-}CH_2^{P/Q}$), 28.85 (s, $2/3\text{-}CH_2^{P/Q}$), 23.65 (s, $5\text{-}CH_2^{Q'}$), 23.61 (s, $5\text{-}CH_2^{P/Q}$), 23.55 (s, $5\text{-}CH_2^{P/Q}$), 17.0 (d, $^1J_{PC} = 69$, CH_3^P), 14.7-14.9 (m, CH_3^{hex}).

$^{31}P\{^1H\}$ NMR (C_6D_6, 162 MHz, *selected data*): δ 134.9 (s, *PO*), 36.7 (s, *PC*).

Data for [Rc-PONP-Me₃][I], 28:

^1H NMR (THF-d_8, 500 MHz, *selected data*): δ 8.38 (s, $ex\text{-}Ar^Q$), 8.01-8.08 (m, $5\text{-}8\text{-}Q/Q'$), 7.96 (vt, $J_{HH} = 7.8$, *4-Py*), 7.79-7.87 (m, $5\text{-}8\text{-}Q/Q'$), 7.66-7.73 (m, *3/5-Py* + $5\text{-}8\text{-}Q/Q'$), 7.62 (s, $en\text{-}Ar^P$), 7.55 (s, $en\text{-}Ar^Q$), 7.36 (s, $ex\text{-}Ar^P$), 7.06 (d, $^3J_{HH} = 8.1$, *3/5-Py*), 5.87 (t, $^3J_{HH} = 8.2$, CH^Q), 5.82 (t, $^3J_{HH} = 8.2$, $CH^{Q'}$), 4.65-4.77 (m, $CH_2^P + CH^P$), 2.37-2.59 (br m, $1\text{-}CH_2$), 2.03 (d, $^2J_{PH} = 15$, CH_3^P), 1.45-1.65 (br m, $2\text{-}3\text{-}CH_2$), 1.34-1.45 (br m, $4\text{-}5\text{-}CH_2$), 0.88-1.04 (br m, CH_3^{hex}).

$^{13}C\{^1H\}$ NMR (THF-d_8, 126 MHz, *selected data*): δ 160.9 (d, $^2J_{PC} = 7$, *2-Py*), 154.0-154.4 ($ArO^{Q,QQ,PQ'} + 2\text{-}3\text{-}Q/Q'$), 151.1 (d, $^2J_{PC} = 9$, *6-Py*), 148.1 (d, $^2J_{PC} = 7$, ArO^P), 143.4 (s, *4-Py*), 141.45 (s, $1/4\text{-}Q/Q'$), 141.41 (s, $1/4\text{-}Q/Q'$), 141.2 (s, $1/4\text{-}Q/Q'$), 139.4 (s, ArC^P), 138.0 (s, $ArC^{Q/PQ'}$), 137.9 (s, $ArC^{Q/PQ'}$), 137.6 (s, $ArC^{QQ'}$), 129.4-132.0 ($5\text{-}8\text{-}Q/Q'$), 125.6 (s, $en\text{-}Ar^P$), 125.2 (s, $en\text{-}Ar^Q$), 122.9 (d, $^3J_{PC} = 8$, *3/5-Py*), 120.2 (s, $ex\text{-}Ar^Q$), 119.0 (s, $ex\text{-}Ar^P$), 113.0 (s, *3/5-Py*), 37.8 (s, CH^P), 35.9 (s, CH^Q), 35.8 (s, $CH^{Q'}$), 33.79 (s, $1\text{-}CH_2^{Q'}$), 33.68 (s, $1\text{-}CH_2^{P/Q}$), 33.63 (s, $4\text{-}CH_2^{P/Q}$), 33.59 (s, $4\text{-}CH_2^{P/Q}$), 33.56 (s, $4\text{-}CH_2^{Q'}$), 33.47 (s, $1\text{-}CH_2^{P/Q}$), 32.9 (d, $^1J_{PC} = 35$, CH_2^P), 31.3 (s, $2/3\text{-}CH_2^{P/Q}$), 30.7-31.0 (br s, $2/3\text{-}CH_2^{Q'+P/Q}$), 29.68 (s, $2/3\text{-}CH_2^{Q'+P/Q}$), 29.74 (s, $2/3\text{-}CH_2^{P/Q}$), 24.25 (s, $5\text{-}CH_2^{P/Q}$), 24.22 (s, $5\text{-}CH_2^{Q'}$), 24.18 (s, $5\text{-}CH_2^{P/Q}$), 15.0-15.2 (m, CH_3^{hex}), 10.1 (d, $^1J_{PC} = 55$, CH_3^P).

$^{31}P\{^1H\}$ NMR (THF-d_8, 162 MHz, *selected data*): δ 134.0 (s, *PO*), 27.3 (s, *PC*).

HR ESI-MS (positive ion, 4 kV): 1414.6210, $[M]^+$ (calcd 1414.6270) *m/z*.

## 6.3.12. Attempted Synthesis of $^tBu_2$-PONP-Me₂, 29
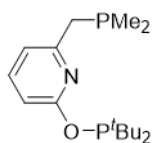
An NMR tube fitted with a J Young's valve was loaded with **25** (6.9 mg, 41 μmol) and KHMDS (8.1 mg, 41 μmol). THF (500 μL) was added and the solution was agitated at ambient temperature for 1 hour. To this was added $^tBu_2PCl$ (8.0 μL, 42 μmol) and the yellow solution was agitated for a further hour. Characterised *in situ*.

^1H NMR (THF-H_8, 400 MHz, *selected data*): δ 7.81 (app. t, $J_{HH} = 7.7$, *4-Py*), 7.04 (d, $^3J_{HH} = 7.2$, *3/5-Py*), 6.97 (d, $^3J_{HH} = 8.0$, *3/5-Py*), 1.49 (d, $^2J_{PH} = 11$, CH_3^P), 0.36 (s, CH_3^{tBu}).

31P{1H} NMR (THF-H_8, 162 MHz, *selected data*): δ 152.1 (s, *PO*), −45.0 (s, *PC*).

### 6.3.13. Synthesis of Np2-PONP(BH3)-Me2, **30**
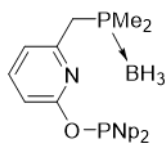
A suspension of **26** (38.3 mg, 0.209 mmol) and KHMDS (42.6 mg, 0.214 mmol) in THF (1 mL) was stirred at ambient temperature for 30 minutes. A solution of Np2PCl (43.4 mg, 0.208 mmol) in THF (1 mL) was added and the mixture was stirred for a further 2 hours. Volatiles were removed under educed pressure to give a colourless oil. Crude yield: 47.3 mg.

1H NMR (1,2-$C_6H_4F_2$, 400 MHz, *selected data*): 7.26 (app. t, J_{HH} = 7.8, 1H, *4-Py*), 6.55-6.59 (m, *3/5-Py*), 6.48 (d, $^3J_{HH}$ = 8.3, 1H, *5/3-Py*), 2.95 (d, $^2J_{PH}$ = 10, 3H, CH_2^{Py}), 1.94 (dd, $^2J_{HH}$ = 14, $^2J_{PH}$ = 2, 2H, CH_2^{Np}), 1.36 (dd, $^2J_{HH}$ = 14, $^2J_{PH}$ = 5, 2H, CH_2^{Np}), 1.04 (s, 8H, CH_3^{P}), 0.96 (s, 21H, CH_3^{Np}).

11B{1H} NMR (1,2-$C_6H_4F_2$, 96 MHz, *selected data*): −38.0 (d, $^1J_{PB}$ = 60).

31P{1H} NMR (1,2-$C_6H_4F_2$, 162 MHz, *selected data*): δ 125.6 (s, *PO*), 5.04-8.00 (br m, *PC*).

6.3.14. Deprotection of **30**
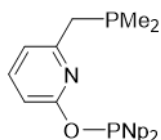
An NMR tube fitted with a J Young's valve was loaded with **30** (14.1 mg). This was suspended in Et2NH (500 µL) and heated to 80 °C for 208 hours/8 days. Volatiles were removed under reduced pressure. Pentane (300 µL) was added and the tube was agitated. Volatiles were again removed under reduced pressure and the resulting colourless oil was dried *in vacuo*.

1H NMR (1,2-$C_6H_4F_2$, 300 MHz, *selected data*): δ 2.69 (s, 2H, CH_2^{P}), 2.03 (d, $^2J_{PH}$ = 14, 2H, CH_2^{Np}), 1.39 (d, $^2J_{PH}$ = 14, 2H, CH_2^{Np}), 1.00 (s, 16H, CH_3^{Np}), 0.89 (d, $^2J_{PH}$ = 3, 5H, CH_3^{P}).

31P{1H} NMR (1,2-$C_6H_4F_2$, 121 MHz, *selected data*): δ 124.7 (s, *PO*), −45.2 (s, *PC*).

6.3.15. Synthesis of [Rh(Np$_2$-PONP-Me$_2$)(PPh$_3$)][Cl], 31
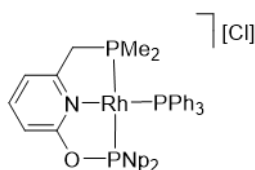
Compound **30** (14.1 mg, 39.7 μmol) was dissolved in 1,2-C$_6$H$_4$F$_2$ (500 μL) and added to a suspension of Wilkinson's catalyst (37.0 mg, 40.0 μmol) in 1,2-C$_6$H$_4$F$_2$ (3 mL). The suspension was heated at 80 °C for 41 hours. Volatiles were removed under reduced pressure to give an orange solid. This was recrystallised *via* slow diffusion of Et$_2$O into a CH$_2$Cl$_2$ solution, giving a deep red solid. Crude yield: 29.0 mg.

^{1}H NMR (CD$_2$Cl$_2$, 400 MHz, *selected data*): δ 7.88 (app. t, $^3J_{HH}$ = 7.9, 1H, *4-Py*), 7.57-7.63 (m, 6H, *Ph*), 7.44-7.54 (m, 8H, *Ph*), 7.41 (d, $^3J_{HH}$ = 7.6, 1H, *3/5-Py*), 6.94 (d, $^3J_{HH}$ = 8.3, 1H, *5/3-Py*), 3.80 (d, $^2J_{PH}$ = 11, 2H, *CH$_2$^{P}*), 1.88 (dd, $^2J_{HH}$ = 16, $^2J_{PH}$ = 5, 1H, *CH$_2$^{Np}*), 1.84 (dd, *J* = 16, $^2J_{PH}$ = 5, 1H, *CH$_2$^{Np}*), 1.07 (d, $^2J_{HH}$ = 15, 1H, *CH$_2$^{Np}*), ~1.05 (under CH$_3$, *CH$_2$^{Np}*), 1.00-1.04 (m, 23H, *CH$_3$^{P} + CH$_3$^{Np}*).

^{31}P{^{1}H} NMR (CD$_2$Cl$_2$, 162 MHz): δ 178.3 (ddd, $^2J_{PP}$ = 317, $^1J_{RhP}$ = 146, $^2J_{PP}$ = 31, *PNp$_2$*), 41.6 (ddd, $^1J_{RhP}$ = 166, $^2J_{PP}$ = 44, 31, *PPh$_3$*), 11.4 (ddd, $^2J_{PP}$ = 317, $^1J_{RhP}$ = 129, $^2J_{PP}$ = 44, *PMe$_2$*).

6.3.16. Synthesis of [Rh(Np$_2$-PONP-Me$_2$)(PPh$_3$)][BAr$^F_4$], 32
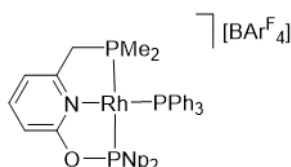
A solution of crude **31** (29.0 mg) in CD$_2$Cl$_2$ (500 μL) was transferred onto Na[BAr$^F_4$] (39.1 mg, 44.1 μmol) in an NMR tube fitted with a J Young's valve and agitated for 30 minutes. The solution was filtered and compound was recrystallised *via* slow diffusion of hexane into the CD$_2$Cl$_2$ solution. Crude yield: 49.1 mg.

^{1}H NMR (CD$_2$Cl$_2$, 300 MHz): δ 7.76 (app. t, $^3J_{HH}$ = 7.8, 1H, *4-Py*), 6.68-7.75 (m, 9H, o-*Ar^F*), 7.52-7.62 (m, 10H, p-*Ar^F* + *Ph*), 7.40-7.51 (m, 7H, *Ph*), 7.16-7.19 (m, 3H, *Ph*), 7.14 (d, $^3J_{HH}$ = 7.8, 1H, *3/5-Py*), 6.92 (d, $^3J_{HH}$ = 8.3, 1H, *5/3-Py*), 3.55 (d, $^2J_{PH}$ = 10, 2H, *CH$_2$^{P}*), 1.88 (dd, $^2J_{HH}$ = 17, $^2J_{PH}$ = 5, 1H, *CH$_2$^{Np}*), 1.82 (dd, $^2J_{HH}$ = 17, $^2J_{PH}$ = 6, 1H, *CH$_2$^{Np}*), 1.08 (d, $^2J_{HH}$ = 15, 1H, *CH$_2$^{Np}*), 1.06 (d, $^2J_{HH}$ = 16, 1H, *CH$_2$^{Np}*), 1.00 (s, 16H, *CH$_3$^{Np}*), 0.94 (d, $^2J_{PH}$ = 8.9, *CH$_3$^{P}*).

^{31}P{^{1}H} NMR (CD$_2$Cl$_2$, 121 MHz): δ 179.0 (ddd, $^2J_{PP}$ = 318, $^1J_{RhP}$ = 146, $^2J_{PP}$ = 31, *PNp$_2$*), 41.1 (ddd, $^1J_{RhP}$ = 165, $^2J_{PP}$ = 43, 31, *PPh$_3$*), 10.9 (ddd, $^2J_{PP}$ = 318, $^1J_{RhP}$ = 130, $^2J_{PP}$ = 43, *PMe$_2$*).

6.3.17. Synthesis of Rc-PONP(BH₃)-Me₂, 33
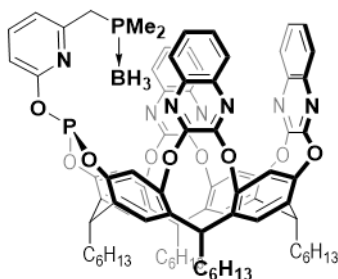

A suspension of **26** (11.5 mg, 62.8 μmol) and KHMDS (12.6 mg, 63.2 μmol) in THF (5 mL) was stirred at ambient temperature for 30 minutes. This was transferred onto RcO₂PCl (79.6 mg, 62.8 μmol) at 0 °C and stirred at 22 °C for 30 minutes. Volatiles were removed under reduced pressure and the resulting white solid was recrystallised from hexane. Crude yield: 59.7 mg.

¹¹B{¹H} NMR (CD₂Cl₂, 96 MHz): δ −35.3.−40.4 (br m).

³¹P{¹H} NMR (CD₂Cl₂, 121 MHz, *selected data*): δ 135.0 (s, *PO*), 3.2-8.0 (br, *PC*).

6.3.18. Synthesis of [Rh(PONOP-^{t}Bu)(CO)][BAr$^F_4$], A32
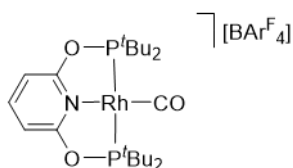
An NMR tube fitted with a J Young's valve was loaded with PONOP-^{t}Bu (8.0 mg, 20 μmol), [Rh(CO)₂Cl]₂ (3.9 mg, 10 μmol) and Na[BAr$^F_4$] (21.0 mg, 23.7 μmol). C₆H₅F was added (500 μL) and the yellow suspension was agitated at ambient temperature for 2 hours. This was filtered and volatiles were removed under reduced pressure. The resulting yellow solid was washed with hexane (500 μL), filtered and dried *in vacuo*. Yield 23 mg (17 μmol, 84 %). Data are consistent with the literature.[57]

¹H NMR (CD₂Cl₂, 500 MHz): δ 7.93 (t, $^3J_{HH}$ = 8.1, 1H, *4-Py*), 7.73 (s, 8H, o-*Ar^F*), 7.57 (s, 3H, p-*Ar^F*), 6.93 (d, $^3J_{HH}$ = 8.2, 2H, *3,5-Py*), 1.42 (vt, J_{PH} = 8.3, 36H, t-*Bu*).

¹³C{¹H} NMR (CD₂Cl₂, 126 MHz): δ 193.2 (dt, $^1J_{RhC}$ = 71, $^2J_{PC}$ = 12, *CO*), 164.7 (vt, J_{PC} = 3, *2,6-Py*), 162.6 (q, $^1J_{CB}$ = 50, i-*Ar^F*), 147.9 (s, *4-Py*), 135.6 (s, o-*Ar^F*), 129.7 (qq, $^2J_{FC}$ = 32, $^3J_{CB}$ = 3, m-*Ar^F*), 125.4 (q, $^1J_{FC}$ = 272, *CF₃*), 118.3 (sept, $^3J_{FC}$ = 4, p-*Ar^F*), 104.7 (vt, J_{PH} = 3, *3,5-Py*), 41.6 (vtd, J_{PC} = 7, $^2J_{RhC}$ = 2, *C^{Bu}*), 28.0 (vt, J_{PC} = 4, *CH₃^{tBu}*).

³¹P{¹H} NMR (CD₂Cl₂, 162 MHz): δ 219.8 (d, $^1J_{RhP}$ = 127).

ATR IR: ν_CO 2017 cm⁻¹.

HR ESI-MS (positive ion, 4 kV): 530.1453, $[M]^+$ (calcd 530.1455) *m/z*.

6.3.19. Synthesis of [Rh(Rc-PONP-Me₂)(CO)][BAr$^F_4$], **34**
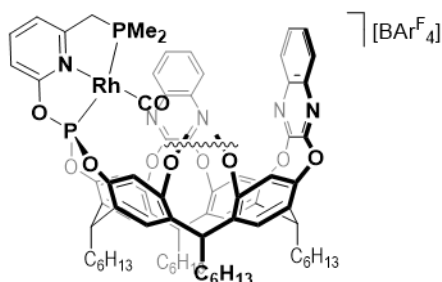
An NMR tube fitted with a J Young's valve was loaded with crude **14** (17.9 mg), [Rh(CO)₂Cl]₂ (2.4 mg, 6.2 μmol) and Na[BAr$^F_4$] (15.5 mg, 17.5 μmol). C₆H₅F was added (500 μL) and the orange suspension was agitated at ambient temperature for 3 hours. This was then filtered and volatiles were removed under reduced pressure, yielding an orange solid. Crude yield: 16 mg.

¹H NMR (CD₂Cl₂, 500 MHz, *selected data for 34 only*): δ 8.01 (s, ex-Ar^Q), 8.01-8.04 (m, *4-Py*), 7.69-7.76 (m, o-Ar^F), 7.55 (s, p-Ar^F), 7.41 (s, en-Ar^P), 7.37 (s, ex-Ar^P), 7.25-7.33 (m, *3,5-Py*), 7.27 (s, en-Ar^Q), 5.47 (t, $^3J_{HH}$ = 8.1, CH$^{Q'}$), 5.15 (t, $^3J_{HH}$ = 8.1, CH^Q), 4.57 (t, $^3J_{HH}$ = 8.1, CH^P), 3.24 (d, $^2J_{PH}$ = 12, CH₂^P), 1.96-2.56 (br m, *1-CH₂*), 1.05-1.70 (br m, CH₂), 0.65-1.01 (br m, CH₃^{hex}), 0.06 (d, $^2J_{PH}$ = 10, CH₃^P).

¹³C{¹H} NMR (CD₂Cl₂, 126 MHz, *selected data for 34 only*): δ 162.6 (q, $^1J_{CB}$ = 50, i-Ar^F), 161.4 (d, $^2J_{PC}$ = 10, *2-Py*), 160.5 (d, $^2J_{PC}$ = 6, *6-Py*), 151.7-154.1 (ArO$^{Q/PQ'/QQ'}$ + *2-3-Q/Q'*), 146.6 (s, ArO^P), 146.2 (s, *4-Py*), 140.3 (s, *1/4-Q/Q'*), 140.4 (s, *1/4-Q/Q'*), 140.6 (s, *1/4-Q/Q'*), 138.4 (s, ArC$^{PQ'/QQ'}$), 137.5 (s, ArC$^{PQ'/QQ'}$), 136.8 (HMBC, ArC^Q), 136.0 (s, ArC^P), 135.6 (s, o-Ar^F), 129.7 (q, $^2J_{FC}$ = 32, m-Ar^F), 125.4 (q, $^1J_{FC}$ = 273, CF₃), 125.1 (s, en-Ar^P), 124.6 (s, en-Ar^Q), 120.4 (d, $^3J_{PC}$ = 12, *5-Py*), 118.5 (s, ex-Ar^Q), 118.2-118.4 (m, p-Ar^F), 117.6 (s, ex-Ar^P), 111.3 (d, $^3J_{PC}$ = 9, *3-Py*), 43.7 (d, $^1J_{PC}$ = 28, CH₂^P), 37.1 (s, CH^P), 36.1 (s, CH^Q), 35.7 (s, CH$^{Q'}$), 32.0-33.1 (m, *1-CH₂*), 29.6-30.6 (m, *2-4-CH₂*), 28.3-28.9 (m, *2-4-CH₂*), 23.0-23.7 (br s, *5-CH₂*), 14.2-14.8 (br s, CH₃^{hex}), 13.0 (s, CH₃^P).

³¹P{¹H} NMR (CD₂Cl₂, 162 MHz, *selected data*): δ 155.3 (dd, $^2J_{PP}$ = 431, $^1J_{RhP}$ = 207, *PO{34}*), 151.8 (d, $^1J_{RhP}$ = 270, *PO{37}*), 61.3 (s, *PC{37}*), 17.3 (dd, $^2J_{PP}$ = 431, $^1J_{RhP}$ = 123, *PC{34}*).

ATR IR: ν$_{CO}$ 2087 (**35**), 2032 (broad, **34**) cm⁻¹.

HR ESI-MS (positive ion, 4 kV): 1530.5100, $[M]^+$ (calcd 1530.5039) *m/z*.

6.3.20. Synthesis of [Rh(Rc-PONP-Me₂)(CO)][Al(OC(CF₃)₃)₄], 35
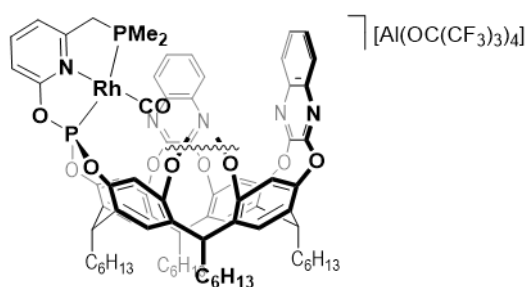
A suspension of crude **14** (42.0 mg), [Rh(CO)₂Cl]₂ (5.8 mg, 15 µmol) and Li[AlOR^F] (29.9 mg, 30.7 µmol) in C₆H₅F was stirred at ambient temperature for 3 hours. The resulting orange suspension was filtered and volatiles were removed under reduced pressure, yielding an orange solid. This was washed with hexane and dried. Crude yield: 65 mg.

¹H NMR (CD₂Cl₂, 500 MHz, *selected data*): δ 8.16 (app. t, J_{HH} = 7.7, *4-Py{38}*), 8.11 (app. t, J_{HH} = 7.7, 1H, *4-Py{35}*), 8.08 (d, $^3J_{HH}$ = 8.4, 2H, *5,8-Q{35}*), 8.05 (s, 2H, *ex-Ar^Q{35}*), 7.93-8.03 (*Q/Q'{38}*), 7.89 (dd, $^3J_{HH}$ = 6.4, $^4J_{HH}$ = 3.5, 2H, *5/8-Q'{35}*), 7.70-7.82 (m, *5/8-Q'{35} + 6,7-Q{35}* + ex-Ar$^{P/Q}${38} + Q/Q'{38}*), 7.64-7.70 (*Q/Q'{38}*), 7.59-7.64 (m, 4H, *6,7-Q'{35}*), 7.50 (s, ex-Ar$^{P/Q}${38}*), 7.47 (d, $^3J_{HH}$ = 8.8, *3-Py{38}*), 7.42 (s, 2H, *en-Ar^P{35}*), 7.38 (s, 2H, *ex-Ar^P{35}*), 7.31-7.36 (m, 3H, *3,5-Py{35}*), 7.31 (s, *en-Ar$^{P/Q}${38}*), 7.29 (s, 2H, *en-Ar^Q{35}*), 7.21 (d, $^3J_{HH}$ = 7.4, *5-Py{38}*), 7.14-7.19 (m, *en-Ar$^{P/Q}${38} + Q/Q'{38}*), 7.07 (t, $^3J_{HH}$ = 8.7, *Q/Q'{38}*), 5.62-5.93 (m, *CH$^{Q'}${38}*), 5.51 (t, $^3J_{HH}$ = 8.1, 2H, *CH$^{Q'}${35}*), 5.21 (t, $^3J_{HH}$ = 8.5, 1H, *CH^Q{35}*), 5.12-5.19 (m, *CH^Q{38}*), 4.61-4.75 (m, *CH^P{38}*), 4.57 (t, $^3J_{HH}$ = 8.1, 1H, *CH^P{35}*), 3.32 (d, $^2J_{PH}$ = 13, *CH₂^P{38}*), 3.23 (d, $^2J_{PH}$ = 12, 2H, *CH₂^P{35}*), 2.01-2.53 (br m, *1-CH₂*), 1.08-1.59 (br m, *CH₂*), 0.70-1.03 (br m, *CH₃^{hex}*), 0.08 (s, *CH₃^P{38}*), −0.02 (d, $^2J_{PH}$ = 10, 6H, *CH₃^P{35}*).

¹³C{¹H} NMR (CD₂Cl₂, 126 MHz, *selected data*): δ 161.5 (dm, $^2J_{PC}$ = 14, *2-Py*), 160.4-160.6 (m, *6-Py*), 153.6 (s, *ArO^Q{35}*), 153.5 (s, *ArO$^{PQ'}${35}*), 153.1 (s, *ArO$^{QQ'}${35}*), 152.86 (s, *2/3-Q/Q'{35}*), 152.83 (s, *2/3-Q/Q'{35}*), 152.4 (s *2/3-Q/Q'{35}*), 146.6 (s, *ArO^P{35}*), 146.3 (s, *4-Py*), 146.0 (s, *ArO^P{38}*), 140.6 (s, *1/4-Q/Q'*), 140.4 (s, *1/4-Q/Q'*), 140.3 (s, *1/4-Q/Q'*), 138.5 (s, *ArC$^{PQ'/QQ'}${35}*), 137.6 (s, *ArC$^{PQ'/QQ'}${35}*), 135.9-136.3 (br, *ArC^{P+Q}{35}*), 130.7 (s, *5-8-Q/Q'*), 130.6 (s, *5-8-Q/Q'*), 130.3 (s, *5-8-Q/Q'*), 129.1 (s, *5-8-Q/Q'*), 128.6 (s, *5-8-Q/Q'*), 128.5 (s, *5-8-Q/Q'*), 125.1 (s, *en-Ar^P{35}*), 124.9 (s, *en-Ar$^{P/Q}${38}*), 124.7 (s, *en-Ar^Q{35}*), 124.5 (s, *en-Ar$^{P/Q}${38}*), 123.7 (HMBC, *5-Py{38}*), 122.1 (q, $^1J_{FC}$ = 292, *CF₃*), 120.5 (d, $^3J_{PC}$ = 12, *5-Py{35}*), 118.6 (s, *ex-Ar^Q{35}*), 118.0 (s, *ex-Ar$^{P/Q}${38}*), 117.9 (s, *ex-Ar$^{P/Q}${38}*), 117.6-117.8 (s, *ex-Ar^P{35}*), 112.6 (HSQC, *3-Py{38}*), 111.3 (d, $^3J_{PC}$ = 10, *3-Py{35}*), 43.6 (d, $^1J_{PC}$ = 28, *CH₂^P{35}*), 39.8 (HSQC, *CH₂^P{38}*), 37.2 (s, *CH^P{35}*), 37.0 (s, *CH^P{38}*), 36.1 (s, *CH^Q{38}*), 36.0 (s, *CH^Q{35}*), 35.7 (s, *CH$^{Q'}${35}*), 35.0-35.3 (m, *CH$^{Q'}${38}*), 31.8-33.2 (m,

$1\text{-}CH_2 + 4\text{-}CH_2$), 29.9-30.6 (m, $2/3\text{-}CH_2$), 28.3-28.9 (m, $2/3\text{-}CH_2$), 22.9-23.7 (m, $5\text{-}CH_2$), 14.3-14.8 (m, CH_3^{hex}), 13.0 (s, $CH_3^P\{38\}$), 12.8 (s, $CH_3^P\{35\}$).

^{31}**P{^{1}H} NMR** (CD$_2$Cl$_2$, 202 MHz): δ 155.5 (dd, $^2J_{PP}$ = 430, $^1J_{RhP}$ = 207, $PO\{35\}$), 151.8 (d, $^1J_{RhP}$ = 276, $PO\{38\}$), 61.3 (s, $PC\{38\}$), 17.2 (dd, $^2J_{PP}$ = 431, $^1J_{RhP}$ = 123, $PC\{35\}$).

ATR IR: ν_{CO} 2113 (**38**), 2036 (**35**) cm^{-1}.

HR ESI-MS (positive ion, 4 kV): 1530.5049, $[M]^+$ (calcd 1530.5039); 1546.4962, $[M+O]^+$ (calcd 1546.4988) *m/z*.

6.3.21. Synthesis of [Rh(Rc-PONP-Me$_2$)(CO)][HCB$_{11}$Me$_5$I$_6$], 36
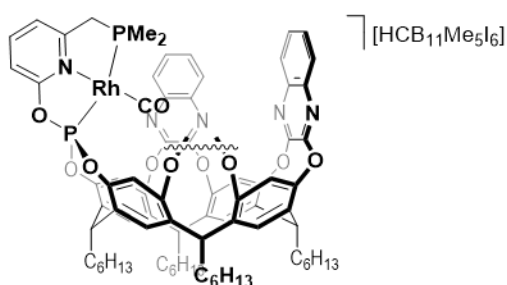
An NMR tube fitted with a J Young's valve was loaded with [Rh(nbd)][HCB$_{11}$Me$_5$I$_6$] (15.4 mg, 13.2 μmol) and CD$_2$Cl$_2$ (500 μL). This was transferred onto crude **14** (18.4 mg) in a second NMR tube, forming an orange solution. After 5 minutes at ambient temperature, the solution was freeze-pump-thaw degassed and backfilled with CO (1 bar). The solution immediately lightened to yellow. Volatiles were removed under reduced pressure and the yellow solid was recrystallised *via* slow diffusion of hexane into a CH$_2$Cl$_2$ solution. Crude yield: 12.5 mg.

^{1}**H NMR** (CD$_2$Cl$_2$, 500 MHz, *selected data for 36 only*): δ 8.21 (s, ex-Ar^Q), 8.14 (app. t, J_{HH} = 8.2, $4\text{-}Py$), 7.56 (d, $^3J_{HH}$ = 7.5, $5\text{-}Py$), 7.41 (s, en-Ar^P), 7.40 (s, ex-Ar^P), 7.32 (d, $^3J_{HH}$ = 8.7, $3\text{-}Py$), 7.29 (s, en-Ar^Q), 5.57 (t, $^3J_{HH}$ = 8.1, $CH^{Q'}$), 5.24 (t, $^3J_{HH}$ = 8.1, CH^Q), 4.55 (t, $^3J_{HH}$ = 7.9, CH^P), 3.41-3.47 (under Et$_2$O*, CH_2^P), 2.75 (s, 1H, HCB), 2.13-2.49 (br m, $1\text{-}CH_2$), 1.20-1.60 (br m, CH_2), 0.74-1.01 (br m, CH_3^{hex}), 0.28 (s, 14H, CH_3^B), −0.21 (d, $^2J_{PH}$ = 10, CH_3^P).

^{13}**C{^{1}H} NMR** (CD$_2$Cl$_2$, 126 MHz, *selected data for 36 only*): δ 161.0 (HMBC, $6\text{-}Py$), 151.1-154.7 ($2/3\text{-}Q/Q' + ArO^{Q/PQ'/QQ'}$), 146.8 (s, ArO^P), 146.3 (s, $4\text{-}Py$), 140.2-140.7 ($1,4\text{-}Q/Q'$), 135.1-138.7 ($ArC^{P/Q/PQ'/QQ'}$), 128.3-131.4 ($5\text{-}8\text{-}Q/Q'$), 125.0 (s, en-Ar^P), 124.6 (s, en-Ar^Q), 121.2-121.5 (m, $5\text{-}Py$), 117.8-119.7 (ex-$Ar^{P/Q}$), 111.1-111.2 (m, $3\text{-}Py$), 62.5 (s, CB), 43.9 (s, CH_2^P), 37.2 (s, CH^P), 35.6 (s, $CH^{Q'}$), 35.7 (s, CH^Q), 31.9-33.4 (br m, CH_2), 29.6-30.8 (br m, CH_2), 28.2-29.0 (br m, CH_2), 23.3-23.8 (br s, CH_2), 14.4-14.9 (m, CH_3^{hex}), 12.9 (d, $^1J_{PC}$ = 30, CH_3^P), 4.0 (HSQC, CH_3^B).

* NMR spectrum contains residual Et$_2$O from an unsuccessful recrystallisation attempt.

6.3.22. Attempted Synthesis of [Rh(Rc-PONP-Me$_2$)(CO)(Cl)$_2$][BAr$^F_4$], **40**
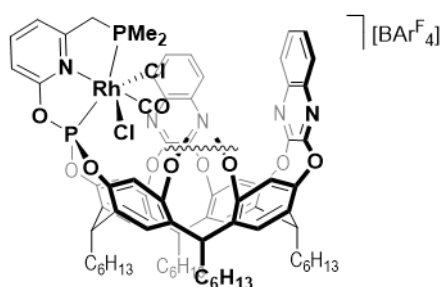
An NMR tube fitted with a J Young's valve was loaded with PhICl$_2$ (1.9 mg, 6.9 μmol). Onto this was transferred a solution of crude **34** (15.9 mg) in C$_6$H$_5$F (500 μL). The orange solution was agitated at ambient temperature for 2 hours and filtered. Volatiles were removed under reduced pressure. The resulting orange solid was washed with hexane (500 μL) and dried *in vacuo*. Crude yield: 10 mg.

33.0 (s, *1-CH₂$^{P/Q}$*), 32.72 (s, *4-CH₂ $^{P/Q}$*), 32.64 (s, *4-CH₂$^{Q'}$*), 32.62 (s, *4-CH₂ $^{P/Q}$*), 32.4 (s, *1-CH₂$^{Q'}$*), 31.6 (s, *1-CH₂$^{P/Q}$*), 30.18 (s, *3-CH₂ $^{P/Q}$*), 30.12 (s, *3-CH₂ $^{Q'}$*), 30.06 (s, *3-CH₂ $^{P/Q}$*), 28.75 (s, *2-CH₂ $^{P/Q}$*), 28.68 (s, *2-CH₂ $^{Q'}$*), 28.56 (s, *2-CH₂ $^{P/Q}$*), 23.51 (s, *5-CH₂$^{P/Q}$*), 23.47 (s, *5-CH₂$^{Q'}$*), 23.44 (s, *5-CH₂$^{P/Q}$*), 14.7 (s, *CH₃$^{Q'}$*), 14.6-14.7 (m, *CH₃^{P,Q}*), 12.1 (d, $^1J_{PC}$ = 4, *CH₃^P*), 11.8 (d, $^1J_{PC}$ = 4, *CH₃^P*).

³¹P{¹H} NMR (CD₂Cl₂, 162 MHz, *selected data*): δ 113.9 (dd, $^2J_{PP}$ = 665, $^1J_{RhP}$ = 121, *PO*), 41.6 (dd, $^2J_{PP}$ = 666, $^1J_{RhP}$ = 75, *PC*).

ATR IR: ν$_{CO}$ 2089 (*42*), 2019 (*40*) cm⁻¹.

6.3.23. <u>Attempted Synthesis of [Rh(Rc-PONP-Me₂)(CO)(Cl)₂][Al(OC(CF₃)₃)₄], **41**</u>
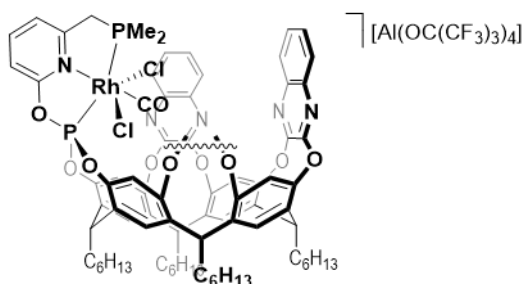
A solution of crude **35** (65.3 mg) and PhICl₂ (7.5 mg, 27 μmol) in C₆H₅F (1 mL) was stirred at ambient temperature for 2 hours and filtered. Volatiles were removed under reduced pressure. The resulting orange solid was washed with hexane (500 μL) and dried *in vacuo*. Crude yield: 54 mg.

¹H NMR (CD₂Cl₂, 500 MHz, *selected data*): δ 8.33 (app. t, J_{HH} = 7.7, *4-Py{43}*), 8.26 (app. t, J_{HH} = 8.1, *4-Py{41}*), 8.23 (s, *ex-Ar^Q{41}*), 8.02-8.07 (m, *5-8-Q/Q'*), 7.90-8.01 (m, *5-8-Q/Q'*), 7.88 (s, *ex-Ar^P{41}*), 7.86 (s, *5-8-Q/Q'*), 7.68-7.82 (m, *5-8-Q/Q'*), 7.58-7.68 (*3-Py{41}* + *5-8-Q/Q'*), 7.58-7.62 (m, *5-Py{41}*), 7.51-7.56 (m, *3/5-Py{43}* + *5-8-Q/Q'*), 7.55 (d, $^3J_{HH}$ = 8.2, *3-Py{41}*), 7.46-7.51 (m, *3/5-Py{43}*), 7.43 (s, *en-Ar^P{41}*), 7.41 (s, *5-8-Q/Q'*), 7.37 (s, *en-Ar^Q{41}*), 7.27-7.35 (m, *5-8-Q/Q'*), 5.68 (t, $^3J_{HH}$ = 7.8, *CH$^{Q,Q'}${41}*), 5.50-5.65 (m, *CH$^{Q,Q'}${43}*), 4.70 (t, $^3J_{HH}$ = 7.9, *CH^P{41}*), 4.59 (t, $^3J_{HH}$ = 7.6, *CH^P{43}*), 4.24 (dm, $^2J_{PH}$ = 14, *CH₂^P{41}*), 4.01 (d, $^2J_{PH}$ = 14, *CH₂^P{43}*), 1.89 (d, $^2J_{PH}$ = 13, *CH₃^P{41}*), 1.88 (d, $^2J_{PH}$ = 13, *CH₃^P{41}*), 2.05-2.61 (br m, *1-CH₂*), 1.09-1.67 (br m, *CH₂*), 0.47-1.02 (br m, *CH₃^{hex}*).

¹³C{¹H} NMR (CD₂Cl₂, 126 MHz, *selected data*): δ 158.9 (d, $^3J_{PC}$ = 10, *2-Py*), 158.2 (d, $^3J_{PC}$ = 7, *6-Py*), 153.7 (s, *ArO$^{Q/PQ'/QQ'}${41}*), 153.4 (s, *ArO$^{Q/PQ'/QQ'}${41}*), 153.3 (s, *ArO$^{Q/PQ'/QQ'}${41}*), 152.8 (s, *2-3-Q/Q'*), 152.7-152.8 (m, *2-3-Q/Q'*), 152.7 (s, *2-3-Q/Q'*), 147.5 (HSQC, *4-Py{43}*, 147.3 (s, *4-Py{41}*), 145.5 (HMBC, *ArO^P{43}*), 145.0 (s, *ArO^P{41}*), 140.6 (s, *1/4-Q/Q'*), 140.4 (s, *1/4-Q/Q'*), 140.3 (s, *1/4-Q/Q'*), 139.0 (s, *ArC$^{QQ'}${41}*), 136.7 (s, *ArC^Q{41}*), 136.6 (s, *ArC^{PQ}{41}*), 135.7 (s, *ArC^P{41}*), 128.3-131.3 (*5-8-Q/Q'*), 124.9 (s, *en-Ar^Q{41}*), 124.7 (s,

en-Ar^P{**41**}), 122.13 (d, $^3J_{PC}$ = 13, *5-Py{**41**}*), 122.07 (q, $^1J_{FC}$ = 292, *CF$_3$*), 119.3-119.4 (m, ex-Ar^Q{**41**}), 118.8-118.9 (m, ex-Ar^P{**41**}), 113.4 (d, $^3J_{PC}$ = 9, *3-Py{**41**}*), 43.6 (d, $^1J_{PC}$ = 34, *CH$_2^P${**41**}*), 38.8 (HSQC, *CH$_2^P${**43**}*), 37.2 (s, *CH^P{**41**} + CH^P{**43**}*), 35.7 (s, *CH$^{Q'}$*), 35.4 (s, *CH^Q*), 33.0 (s, *1-CH$_2^{P/Q}$*), 32.72 (s, *4-CH$_2^{P/Q}$*), 32.65 (s, *4-CH$_2^{Q'}$*), 32.63 (s, *4-CH$_2^{P/Q}$*), 32.4 (s, *1-CH$_2^{Q'}$*), 31.7 (s, *1-CH$_2^{P/Q}$*), 30.18 (s, *3-CH$_2^{P/Q}$*), 30.13 (s, *3-CH$_2^{Q'}$*), 30.10 (s, *3-CH$_2^{P/Q}$*), 28.8 (s, *2-CH$_2^{P/Q}$*), 28.7 (s, *2-CH$_2^{Q'}$*), 28.6 (s, *2-CH$_2^{P/Q}$*), 23.51 (s, *5-CH$_2^{P/Q}$*), 23.47 (s, *5-CH$_2^{Q'}$*), 23.45 (s, *5-CH$_2^{P/Q}$*), 14.64 (s, *CH$_3^{Q'}$*), 14.66 (s, *CH$_3^{P/Q}$*), 14.69 (s, *CH$_3^{P/Q}$*), 12.0 (d, $^1J_{PC}$ = 3, *CH$_3^P${**41**}*), 11.7 (d, $^1J_{PC}$ = 3, *CH$_3^P${**41**}*).

^{31}P{^{1}H} NMR (CD$_2$Cl$_2$, 162 MHz, *selected data*): δ 114.2 (dd, $^2J_{PP}$ = 664, $^1J_{RhP}$ = 121, *PO{**41**}*), 94.4 (d, $^1J_{RhP}$ = 162, *PO{**43**}*), 63.1 (s, *PC{**43**}*), 41.8 (dd, $^2J_{PP}$ = 665, $^1J_{RhP}$ = 75, *PC{**41**}*).

ATR IR: ν$_{CO}$ 2095 (**43**), 2030 (**41**) cm^{-1}.

6.4. Experimental Data for Chapter 4

6.4.1. Synthesis of [Rh(dppe)(acac)], 44
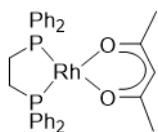
A solution of dppe (0.2046 g, 0.514 mmol) in toluene (10 mL) was transferred onto [Rh(CO)$_2$(acac)] (0.1325 g, 0.514 mmol) and the resulting yellow suspension was stirred at room temperature for 2 hours. Solvent was removed under reduced pressure to give a yellow residue. This was washed with hexane, filtered, and dried and the resulting yellow solid was extracted into THF. Solvent was removed from filtrate to give a brown foam. A small amount of toluene was added to help break up the foam, giving the product as a brown solid. Yield: 0.2164 g (0.359 mmol, 70 %). Single crystals suitable for X-ray diffraction were obtained by slow diffusion of hexane into a C$_6$H$_5$F solution at ambient temperature. ^{31}P NMR data is consistent with the literature.[371]

^{1}H NMR (C$_6$D$_6$, 500 MHz): δ 8.00-8.07 (m, 8H, o-*PPh$_3$*), 7.01-7.10 (m, 12H, m,p-*PPh$_3$*), 5.40 (s, 1H, *CH^{acac}*), 1.85 (s, 6H, *CH$_3$^{acac}*), 1.82 (d, $^2J_{PH}$ = 17, 4H, *CH$_2$*).

^{13}C{^{1}H} NMR (C$_6$D$_6$, 126 MHz): δ 185.6 (s, *C(O)*), 137.6-138.6 (m, i-*PPh$_3$*), 133.9 (t, $^2J_{PC}$ = 5, o-*PPh$_3$*), 129.9 (s, *PPh$_3$*), 128.9 (s, m/p-*PPh$_3$*), 128.7 (s, m/p-*PPh$_3$*), 100.3-100.4 (m, *CH^{acac}*), 28.6-28.7 (m, *CH$_3$^{acac}*), 28.3 (td, $^1J_{PC}$ = 25, $^2J_{RhC}$ = 4, *CH$_2$*).

^{31}P{^{1}H} NMR (C$_6$D$_6$, 162 MHz): δ 70.2 (d, $^1J_{RhP}$ = 193).

6.4.2. Synthesis of [Rh(S_{ax},S,S-BOBPHOS)(acac)], 45
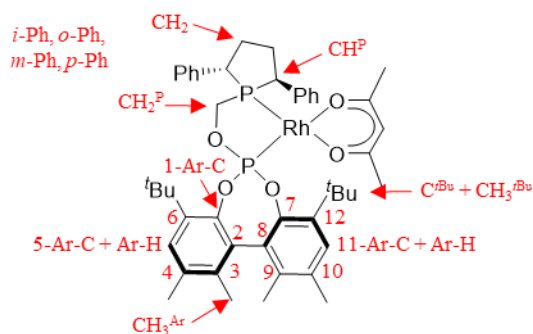
NMR assignments of (S$_{ax}$,S,S)-BOBPHOS are based on this system

A solution of (S_{ax},S,S)-BOBPHOS (0.203 g, 0.311 mmol) in toluene (15 mL) was transferred onto [Rh(CO)$_2$(acac)] (0.0804 g, 0.312 mmol) and the resulting yellow suspension was stirred at room temperature for 2 hours. Volatiles were removed under reduced pressure to give an

orange residue. This was washed with hexane at −78 °C, filtered and dried *in vacuo*. Yield: 0.193 g (0.226 mmol, 73 %). Single crystals suitable for X-ray diffraction were obtained from a hexane solution at −30 °C.

^{1}H NMR (C$_6$D$_6$, 500 MHz): δ 7.74 (d, $^3J_{HH}$ = 8.0, 2H, o-*Ph*), 7.48 (d, $^3J_{HH}$ = 8.0, 2H, o-*Ph*), 7.20-7.29 (m, 5H, m-*Ph* + *Ar-H*), 7.17 (s, 1H, *Ar-H*), 7.05-7.12 (m, 2H, p-*Ph*), 5.27 (s, 1H, *CH^{acac}*), 4.42-4.45 (m, 1H, *CH^P*), 3.26-3.37 (m, 2H, *CH$_2$^{P}*), 2.97-3.05 (m, 1H, *CH^P*), 2.20-2.35 (m, 1H, *CH$_2$*), 2.14 (s, 3H, *CH$_3$^{Ar}*), 2.07-2.19 (m, under *CH$_3$^{Ar}*, 2H, *CH$_2$*), 2.03 (s, 3H, *CH$_3$^{Ar}*), 1.93 (s, 3H, *CH$_3$^{acac}*), 1.85 (s, 3H, *CH$_3$^{Ar}*), 1.73 (s, 9H, ^{t}*Bu*), 1.66-1.71 (m, 1H, *CH$_2$*), 1.65 (s, 3H, *CH$_3$^{Ar}*), 1.41 (s, 3H, *CH$_3$^{acac}*), 1.33 (s, 9H, *CH$_3$^{tBu}*).

^{1}H{^{31}P} NMR (C$_6$D$_6$, 500 MHz, *selected data*): δ 4.46 (dd, $^3J_{HH}$ = 12, 7, 1H, *CH^P*), 3.33 (d, $^2J_{HH}$ = 12, 1H, *CH$_2$^{P}*), 3.30 (d, $^2J_{HH}$ = 12, 1H, *CH$_2$^{P}*), 3.01 (dd, $^3J_{HH}$ = 12, 7, 1H, *CH^P*), 2.28 (app. ddd, J = 25, 12, 5, 1H, *CH$_2$*), 1.69 (app. dd, J_{HH} = 13, 6, 1H, *CH$_2$*).

^{13}C{^{1}H} NMR (C$_6$D$_6$, 126 MHz): δ 186.6 (s, *C(O)*), 184.5 (s, *C(O)*), 147.1 (d, $^2J_{PC}$ = 16, *1/7-Ar-C*), 146.7 (d, $^2J_{PC}$ = 4, *1/7-Ar-C*), 141.8 (d, $^2J_{PC}$ = 3, i-*Ph*), 138.9 (d, $^3J_{PC}$ = 4, *6/12-Ar-C*), 138.5 (d, $^2J_{PC}$ = 4, i-*Ph*), 137.8 (s, *6/12-Ar-C*), 135.4 (s, *3/4/9/10-Ar-C*), 135.2 (s, *3/4/9/10-Ar-C*), 132.4 (s, *3/4/9/10-Ar-C*), 132.3 (s, *3/4/9/10-Ar-C*), 131.7 (d, $^3J_{PC}$ = 2, *2/8-Ar-C*), 131.5 (s, *2/8-Ar-C*), 130.6 (d, $^3J_{PC}$ = 6, o-*Ph*), 129.4-129.6 (m, m-*Ph*), 128.9-129.0 (m, o-*Ph*), 128.62 (under C$_6$D$_6$, *Ar-H*), 127.4 (d, $^5J_{PC}$ = 2, p-*Ph*), 127.3 (d, $^5J_{PC}$ = 2, p-*Ph*), 100.3 (d, $^3J_{RhC}$ = 2, *CH^{acac}*), 64.9 (t, $^1J_{PC}$ = 20, *CH$_2$^{P}*), 51.2 (d, $^1J_{PC}$ = 21, *CH^P*), 46.3 (d, $^1J_{PC}$ = 19, *CH^P*), 36.2 (d, $^2J_{PC}$ = 5, *CH$_2$*), 36.1 (s, *C^{tBu}*), 35.4 (s, *C^{tBu}*), 33.9 (s, *CH$_3$^{tBu}*), 32.6 (s, *CH$_3$^{tBu}*), 31.7 (s, *CH$_2$*), 28.8 (d, $^3J_{RhC}$ = 8, *CH$_3$^{acac}*), 28.1 (d, $^3J_{RhC}$ = 5, *CH$_3$^{acac}*), 21.0 (s, *CH$_3$^{Ar}*), 20.9 (s, *CH$_3$^{Ar}*), 17.4 (s, *CH$_3$^{Ar}*), 17.2 (s, *CH$_3$^{Ar}*).

^{31}P{^{1}H} NMR (C$_6$D$_6$, 202 MHz): δ 164.80 (dd, $^1J_{RhP}$ = 318, $^2J_{PP}$ = 72, *PO*), 113.3 (dd, $^1J_{RhP}$ = 192, $^2J_{PP}$ = 72, *PC*).

HR ESI-MS (positive ion, 4 kV): 877.2629, [*M+Na*]$^+$ (calcd 877.2628) *m/z*.

Anal. Calcd for C$_{46}$H$_{57}$O$_5$P$_2$Rh (854.81 g mol^{-1}): C, 64.63; H, 6.72; Found: C, 64.84; H, 6.71.

6.4.3. Synthesis of [Rh(**A124**)(acac)], **46**
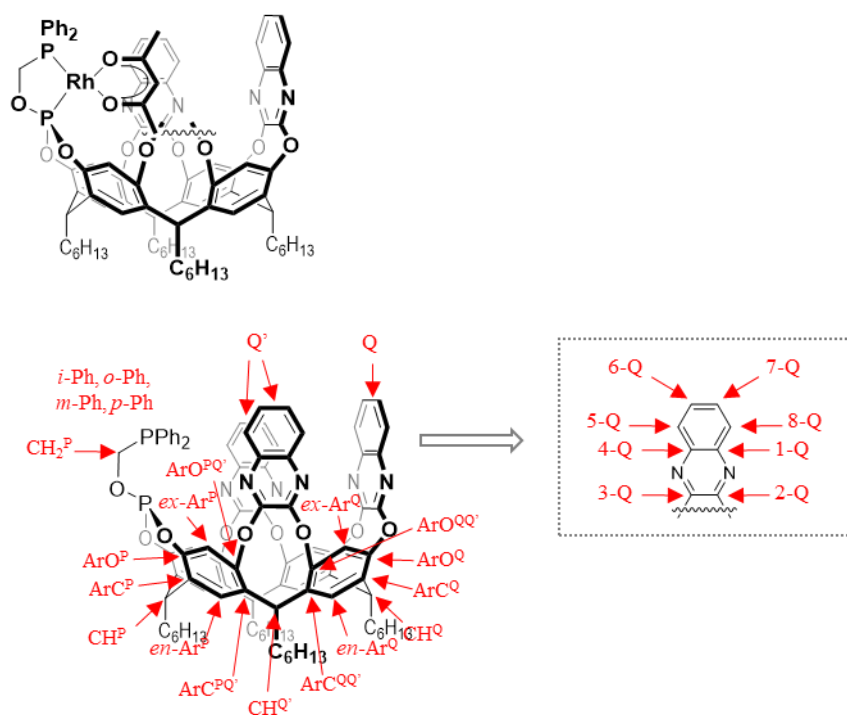
Hex: CH$_3^{hex}$, 5-CH$_2$, 4-CH$_2$, 3-CH$_2$, 2-CH$_2$, 1-CH$_2$

*NMR assignments of **A124** are based on this system*

A solution of **A124** (0.1001 g, 69.1 μmol) in toluene (10 mL) was transferred onto [Rh(CO)$_2$(acac)] (0.0178 g, 69.0 μmol) and the resulting green solution was stirred at room temperature for 2.5 hours. Solvent was removed under reduced pressure to give a green residue. This was washed with –78 °C hexane (2 x 5 mL), filtered and dried to give a pale yellow solid. Yield: 0.0918 g (55.6 μmol, 80 %).

^{1}H NMR (C$_6$D$_6$, 500 MHz): δ 8.94 (s, 2H, ex-Ar^Q), 8.14 (s, 2H, ex-Ar^P), 7.95-7.99 (m, 2H, *5,8-Q*), 7.84-7.90 (m, 6H, m-*PPh$_3$* + *5/8-Q'*), 7.55 (s, 2H, en-Ar^P), 7.53 (s, 2H, en-Ar^Q), 7.45 (dd, $^3J_{HH}$ = 8.3, $^4J_{HH}$ = 1.5, 2H, *5/8-Q'*), 7.21-7.27 (m, 4H, o-*PPh$_3$*), 7.17 (under C$_6$H$_6$, p-*PPh$_3$*), 7.09-7.13 (m, 2H, *6,7-Q*), 7.06 (ddd, $^3J_{HH}$ = 8.4, 6.9, $^4J_{HH}$ = 1.5, 2H, *6/7-Q'*), 7.00 (ddd, $^3J_{HH}$ = 8.4, 7.0, $^4J_{HH}$ = 1.6, 2H, *6/7-Q'*), 6.01-6.07 (m, 3H, *CH$^{Q,Q'}$*), 5.26 (t, $^3J_{HH}$ = 8.0, 1H, *CH^P*), 4.18 (d, $^2J_{PH}$ = 20, 2H, *CH$_2^P$*), 2.21-2.37 (m, 8H, *1-CH$_2$*), 1.14-1.46 (m, 29H, *CH$_2$*), 0.94 (s, 1H, *CH^{acac}*), 0.85-0.93 (m, 13H, *CH$_3^{hex}$*), −0.01 (s, 3H, ex-*CH$_3^{acac}$*), −2.75 (s, 3H, en-*CH$_3^{acac}$*).

^{13}C{^{1}H} NMR (C$_6$D$_6$, 126 MHz): δ 182.9 (s, en-*C(O)*), 182.2 (s, ex-*C(O)*), 154.4 (s, *2/3-Q/Q'* or *ArO^Q* or *ArO$^{QQ'}$*) 154.14 (s, *2/3-Q/Q'* or *ArO^Q* or *ArO$^{QQ'}$*), 154.10 (s, *2/3-Q/Q'* or *ArO^Q* or *ArO$^{QQ'}$*), 153.7 (s, *2/3-Q/Q'* or *ArO^Q* or *ArO$^{QQ'}$*), 153.3 (s, *2/3-Q/Q'* or *ArO^Q* or *ArO$^{QQ'}$*), 153.1 (s, *ArO$^{PQ'}$*), 148.7 (s, *ArO^P*), 141.0 (s, *1/4-Q/Q'*), 140.8 (s, *1/4-Q/Q'*), 140.6 (s, *1/4-Q/Q'*), 137.7 (s, *ArC$^{Q/PQ'/QQ'}$*), 136.9 (s, *ArC^P*), 135.4 (s, *ArC$^{Q/PQ'/QQ'}$*), 135.1 (s, i-*Ph*), 134.2 (d, $^3J_{PC}$

= 12, m-*Ph*), 131.0 (s, p-*PPh$_3$*), 129.4 (s, *6,7-Q*), 129.2-129.3 (m, *5,8-Q + 5/8-Q' +* o-*Ph*), 129.13 (s, *6/7-Q'*), 129.06 (s, *6/7-Q'*), 128.9 (s, *5/8-Q'*), 124.9 (s, en-*Ar^Q*), 122.6 (s, en-*Ar^P*), 121.1 (s, ex-*Ar^P*), 121.0 (s, ex-*Ar^Q*), 94.6 (s, *CH^{acac}*), 69.9 (dd, $^1J_{PC}$ = 34, $^2J_{PC}$ = 18, *CH$_2^P$*), 37.1 (s, *CH^P*), 35.2-35.4 (m, *CH$^{Q,Q'}$*), 33.7 (s, *1-CH$_2^{Q'}$*), 33.2 (s, *1-CH$_2^{P/Q}$*), 32.86 (s, *4-CH$_2^{P/Q}$*), 32.83 (s, *4-CH$_2^{P/Q}$*), 32.79 (s, *4-CH$_2^{Q'}$*), 32.0 (s, *1-CH$_2^{P/Q}$*), 30.43 (s, *3-CH$_2^{Q'}$*), 30.40 (s, *3-CH$_2^{P/Q}$*), 30.3 (s, *3-CH$_2^{P/Q}$*), 28.99 (s, *2-CH$_2^{Q'}$*), 28.96 (s, *2-CH$_2^{P/Q}$*), 28.88 (s, *2-CH$_2^{P/Q}$*), 27.4 (d, $^3J_{RhC}$ = 8, ex-*CH$_3^{acac}$*), 23.64 (s, *5-CH$_2^{Q'}$*), 23.63 (s, *5-CH$_2^{P/Q}$*), 23.58 (s, *5-CH$_2^{P/Q}$*), 22.0 (d, $^3J_{RhC}$ = 5, en-*CH$_3^{acac}$*), 14.88 (s, *CH$_3^{hex}$*), 14.87 (s, *CH$_3^{hex}$*).

^{31}P{^{1}H} NMR (C$_6$D$_6$, 162 MHz): δ 160.8 (dd, $^1J_{RhP}$ = 305, $^2J_{PP}$ = 79, *PO*), 76.6 (dd, $^1J_{RhP}$ = 181.6, $^2J_{PP}$ = 79, *PC*).

Anal. Calcd for C$_{94}$H$_{95}$N$_6$O$_{11}$P$_2$Rh (1649.68 g mol^{-1}): C, 68.44; H, 5.80; N, 5.09. Found: C, 68.06; H, 5.80; N, 5.00.

6.4.4. General Procedure for Hydroformylation

All reactions were performed using a custom-built high-pressure autoclave equipped with pressure gauge, injection port and addition funnel. Solutions of **44**, **45** or **46** (12.0 µmol) in toluene (1.5 mL) were placed inside autoclave. The atmosphere was evacuated and pressurised with 10 bar of a 1:1 mixture of CO and H$_2$. Solution was heated at the chosen reaction temperature under 10 bar CO/H$_2$ for 30 mins to activate catalyst. The addition funnel was loaded with either 1-hexene (0.60 mL), 1-heptene (0.68 mL) or 1-octene (0.75 mL) in toluene (1 mL) and the atmosphere was evacuated and pressurised with 20 bar CO/H$_2$. After activation of catalyst, olefin solution was added to the autoclave and the reaction was heated at the chosen temperature for a specified time, under 20 bar CO/H$_2$. After this time, the autoclave was cooled to room temperature and the reaction was quenched by the addition of (^{n}BuO)$_3$P (1 mL). An aliquot (0.6 mL) was taken for analysis by NMR spectroscopy.

6.4.5. General Procedure for NMR Analysis of Reaction Mixtures

Conversions and branched to linear ratios were determined using ^{1}H NMR spectroscopy (toluene-*H$_8$*, no C$_6$D$_6$ capillary). Selected data, δ$_H$ 9.35 (t, $^3J_{HH}$ = 1.7, *heptanal CH*), 9.28 (d, $^3J_{HH}$ = 1.8, *2-methylhexanal CH*), 5.61-5.73 (m, *1-hexene CH*), 5.24-5.40 (m, *2-hexene 2x CH*); 9.36 (t, $^3J_{HH}$ = 1.7, *octanal CH*), 9.28 (d, $^3J_{HH}$ = 1.8, *2-methylheptanal CH*), 5.61-5.74 (m, *1-heptene CH*), 5.23-5.39 (m, *2-heptene 2x CH*); 9.36 (t, $^3J_{HH}$ = 1.7, *nonanal CH*), 9.29 (d, $^3J_{HH}$ = 1.8, *2-methyloctanal CH*), 5.61-5.74 (m, *1-octene CH*), 5.24-5.38 (m, *2-octene 2x CH*).

6.4.6. Activation of **46** for Analysis by NMR Spectroscopy

A solution of (15 mg, 9.1 μmol) in toluene (1.5 mL) was stirred under 20 bar 1:1 H_2/CO in a 10 mL reactor for two days at ambient temperature. A 500 μL aliquot of this reaction mixture was then transferred to an NMR tube and analysed under ambient conditions.

^{1}H NMR (toluene-H_8, no C_6D_6 capillary, 500 MHz, *selected data*): δ −9.99 (ddd, $^2J_{PH}$ = 108, 22, $^1J_{RhH}$ = 7, *Rh-H*).

^{1}H{^{31}P$_{δ181.1}$} NMR (toluene-H_8, no C_6D_6 capillary, 500 MHz, *selected data*): δ −9.99 (dd, $^2J_{PH}$ = 108, $^1J_{RhH}$ = 7, *Rh-H*).

^{1}H{^{31}P$_{δ68.6}$} NMR (toluene-H_8, no C_6D_6 capillary, 500 MHz, *selected data*): δ −9.99 (dd, $^2J_{PH}$ = 22, $^1J_{RhH}$ = 7, *Rh-H*).

^{31}P{^{1}H} NMR (toluene-H_8, no C_6D_6 capillary, 202 MHz, *selected data*): δ 181.1 (dd, $^1J_{RhP}$ = 225, $^2J_{PP}$ = 43, *PO*), 68.6 (dd, $^1J_{RhP}$ = 99, $^2J_{PP}$ = 43, *PC*).

6.4.7. High Pressure NMR

Static NMR experiments that needed an atmosphere of CO and/or H_2, were carried out in pressure valved NMR tubes S-5-500-IPV-7, S-5-500-MWIPV-7 and S-5-500—HW-IPV-7 from Norell rated to 6, 9 and 12 bar, respectively. NMR spectra were recorded on a Bruker 500 MHz Advance II+ Ultrashield equipped with a N_2-cooled BBO Prodigy CryoProbe.^{1}H NMR chemical shifts are referenced against $SiMe_4$ (99.5% purity in $CDCl_3$) and ^{31}P NMR shifts are referenced to 85% H_3PO_4. The reaction monitoring software used was InsightMR, and data processing was performed with TopSpin4.0.6 and DynamicCenter 2.5.6.

6.5. <u>Crystallographic Data</u>

Crystallographic data were collected on either a Rigaku Oxford Diffraction SuperNova AtlasS2 CCD diffractometer using graphite monochromated Cu Kα ($\lambda = 1.54178$ Å) radiation and a low-temperature device, or a Rigaku XtaLAB Synergy-S diffractometer using mirror monochromated Mo Kα radiation ($\lambda = 0.71073$ Å), generated using a microfocus sealed X-ray tube source and detected at a HyPix Hybrid Pixel Array Detector.

Data were collected and reduced using CrysAlisPro. All non-hydrogen atoms were refined anisotropically (unless stated otherwise) using SHELXL,[389] through the Olex2 interface.[390] Hydrogen atoms (excluding hydrides) were placed in calculated positions using the riding model. Crystallographic data for compounds **2**, **4**-**10**, **12**, **23**, **24**, **26**, **32**, **44**, **45** and **A131** are given in **Table 6.2**-**Table 6.7**.

Table 6.2. *Crystallographic data for compounds 2, 4-6 (Chapter 2)*

Compound	2	4	5	6
ID	0674abc22s	0578abc19s	0617abc20s	0616abc20s
Empirical formula	$C_{60}H_{63}BF_{24}NOP_2Rh$	$C_{59}H_{63}BF_{24}IrNP_2$	$C_{39}H_{59}NP_2ClRh$	$C_{39}H_{59}ClIrNP_2$
Formula weight	1445.77	1507.05	742.17	831.46
Temperature/K	150(2)	150(2)	150.00(10)	150.00(10)
Crystal system	triclinic	monoclinic	monoclinic	monoclinic
Space group	P-1	Cc	$P2_1/n$	$P2_1/n$
a/Å	13.09645(12)	22.9577(3)	11.89861(13)	11.92395(12)
b/Å	19.11606(13)	18.07420(10)	20.6042(2)	20.60478(19)
c/Å	26.4231(2)	19.5255(3)	15.57616(18)	15.54793(14)
α/°	92.3098(6)	90	90	90
β/°	97.3278(7)	128.175(2)	92.0166(11)	91.9259(9)
γ/°	90.9351(6)	90	90	90
Volume/Å^3	6554.20(9)	6369.15(19)	3816.30(7)	3817.82(6)
Z	4	4	4	4
ρ_{calc}mg/mm^3	1.465	1.572	1.292	1.447
μ/mm^{-1}	1.465	5.506	5.243	8.394
F(000)	2936.0	3008.0	1568.0	1696.0
Crystal size/mm^3	$0.178 \times 0.164 \times 0.128$	$0.412 \times 0.195 \times 0.092$	$0.245 \times 0.142 \times 0.026$	$0.151 \times 0.113 \times 0.018$
Radiation	Cu K$_\alpha$ (λ=1.54184)	Cu K$_\alpha$ (λ=1.54184)	Cu Kα (λ = 1.54184)	Cu Kα (λ = 1.54184)
2Θ range for data collection	12.794 to 140.152°	12.796 to 147.27°	12.828 to 147.32	12.818 to 147.152
Index ranges	$-15 \leq h \leq 15$, $-23 \leq k \leq 23$, $-32 \leq l \leq 32$	$-28 \leq h \leq 28$, $-22 \leq k \leq 21$, $-24 \leq l \leq 23$	$-14 \leq h \leq 14$, $-25 \leq k \leq 19$, $-18 \leq l \leq 19$	$-14 \leq h \leq 14$, $-24 \leq k \leq 25$, $-18 \leq l \leq 19$
Reflections collected	47333	51356	38394	38295
Independent reflections	47333	12476	7641	7622
	[R(int) = 0.0764]	[R(int) = 0.0399]	[R_{int} = 0.0568, R_{sigma} = 0.0371]	[R_{int} = 0.0372, R_{sigma} = 0.0255]
Data/restraints/parameters	47333/993/1784	12476/858/922	7641/0/409	7622/0/409
Goodness-of-fit on F^2	1.044	1.051	1.044	1.045
Final R indexes [I>=2σ (I)]	R_1 = 0.0492, wR_2 = 0.1275	R_1 = 0.0427, wR_2 = 0.1141	R_1 = 0.0350, wR_2 = 0.0900	R_1 = 0.0222, wR_2 = 0.0525
Final R indexes [all data]	R_1 = 0.0555, wR_2 = 0.1316	R_1 = 0.0437, wR_2 = 0.1150	R_1 = 0.0398, wR_2 = 0.0938	R_1 = 0.0265, wR_2 = 0.0549
Largest diff. peak/hole / e Å^{-3}	1.66/-0.67	3.02/-1.09	0.90/-1.23	1.26/-0.68
Flack parameter	-	0.538(10)	-	-

Table 6.3. *Crystallographic data for compound* **7** *(***Chapter 2***).*

Compound	7	7	7
ID	0660abc21s_50K	0660abc21s_100K	0660abc21s_150Ki
Empirical formula	$C_{76}H_{85}BCl_2F_{24}NP_2RhSi$	$C_{76}H_{85}BCl_2F_{24}NP_2RhSi$	$C_{76}H_{85}BCl_2F_{24}NP_2RhSi$
Formula weight	1743.09	1743.09	1743.09
Temperature/K	50(2)	100(2)	150(2)
Crystal system	monoclinic	monoclinic	monoclinic
Space group	$P2_1/n$	$P2_1/n$	$P2_1/n$
a/Å	17.98676(15)	17.99211(8)	18.06899(8)
b/Å	20.29587(15)	20.35918(8)	20.37115(9)
c/Å	22.4987(2)	22.57112(10)	22.74137(9)
α/°	90	90	90
β/°	103.6897(8)	103.5153(4)	103.4587(4)
γ/°	90	90	90
Volume/Å^3	7979.97(12)	8038.95(6)	8140.90(6)
Z	4	4	4
ρ_{calc}mg/mm^3	1.451	1.440	1.422
μ/mm^{-1}	3.738	3.710	3.664
F(000)	3568.0	3568.0	3568.0
Crystal size/mm^3	$0.36 \times 0.16 \times 0.11$	$0.371 \times 0.138 \times 0.12$	$0.359 \times 0.133 \times 0.117$
Radiation	Cu Kα (λ = 1.54184)	Cu Kα (λ = 1.54184)	Cu Kα (λ = 1.54184)
2Θ range for data collection	12.774 to 147.27	12.74 to 147.376°	12.66 to 147.188°
Index ranges	$-21 \leq h \leq 21, -25 \leq k \leq 24,$ $-27 \leq l \leq 23$	$-22 \leq h \leq 22, -25 \leq k \leq 25,$ $-27 \leq l \leq 28$	$-22 \leq h \leq 21, -25 \leq k \leq 24,$ $-28 \leq l \leq 28$
Reflections collected	79403	98760	83442
Independent reflections	15591 $[R_{int} = 0.0489, R_{sigma} = 0.0324]$	16116 $[R(int) = 0.0316]$	16292 $[R(int) = 0.0311]$
Data/restraints/parameters	15591/871/1144	16116/970/1175	16292/970/1177
Goodness-of-fit on F^2	1.021	1.042	1.018
Final R indexes [I>=2σ (I)]	$R_1 = 0.0729, wR_2 = 0.1987$	$R_1 = 0.0419, wR_2 = 0.1099$	$R_1 = 0.0451, wR_2 = 0.1166$
Final R indexes [all data]	$R_1 = 0.0792, wR_2 = 0.2064$	$R_1 = 0.0442, wR_2 = 0.1122$	$R_1 = 0.0477, wR_2 = 0.1194$
Largest diff. peak/hole / e Å^{-3}	2.51/-1.68	1.24/-1.19	1.47/-1.04
Flack parameter	-	-	-

Table 6.4. *Crystallographic data for compound 8 (**Chapter 2**).*

Compound	8	8	8
ID	0687abc22s_50K	0687abc22s_100K	0687abc22s_150K
Empirical formula	$C_{76}H_{85}BCl_2F_{24}IrNP_2Si$	$C_{76}H_{85}BCl_2F_{24}IrNP_2Si$	$C_{76}H_{85}BCl_2F_{24}IrNP_2Si$
Formula weight	1832.38	1832.38	1832.38
Temperature/K	50(2)	100(2)	150(2)
Crystal system	monoclinic	monoclinic	monoclinic
Space group	$P2_1/n$	$P2_1/n$	$P2_1/n$
a/Å	17.97881(10)	18.01404(10)	18.07503(10)
b/Å	20.35324(11)	20.37733(11)	20.39717(12)
c/Å	22.41641(13)	22.53842(13)	22.69009(13)
α/°	90	90	90
β/°	103.6412(6)	103.5871(6)	103.5249(6)
γ/°	90	90	90
Volume/Å^3	7971.38(8)	8041.82(8)	8133.38(8)
Z	4	4	4
ρ_{calc}mg/mm^3	1.527	1.513	1.496
μ/mm^{-1}	5.252	5.206	5.147
F(000)	3696.0	3696.0	3696.0
Crystal size/mm^3	$0.348 \times 0.086 \times 0.063$	$0.342 \times 0.088 \times 0.052$	$0.356 \times 0.078 \times 0.059$
Radiation	Cu Kα (λ = 1.54184)	Cu Kα (λ = 1.54184)	Cu Kα (λ = 1.54184)
2Θ range for data collection	12.81 to 147.242°	12.75 to 147.162°	12.678 to 147.236°
Index ranges	$-22 \leq h \leq 22$, $-22 \leq k \leq 24$, $-27 \leq l \leq 27$	$-22 \leq h \leq 20$, $-23 \leq k \leq 24$, $-27 \leq l \leq 27$	$-22 \leq h \leq 22$, $-23 \leq k \leq 24$, $-28 \leq l \leq 28$
Reflections collected	80451	81629	82799
Independent reflections	15913 [R(int) = 0.0459]	16064 [R(int) = 0.0311]	16264 [R(int) = 0.0290]
Data/restraints/parameters	15913/871/1145	16064/964/1172	16264/970/1174
Goodness-of-fit on F^2	1.044	1.035	1.038
Final R indexes [I>=2σ (I)]	R_1 = 0.0551, wR_2 = 0.1476	R_1 = 0.0461, wR_2 = 0.1156	R_1 = 0.0437, wR_2 = 0.1087
Final R indexes [all data]	R_1 = 0.0574, wR_2 = 0.1500	R_1 = 0.0487, wR_2 = 0.1179	R_1 = 0.0463, wR_2 = 0.1110
Largest diff. peak/hole / e Å^{-3}	6.76/-2.07	5.93/-2.40	5.30/-2.21
Flack parameter	-	-	-

*Table 6.5. Crystallographic data for compounds **9**, **10** and **12** (**Chapter 2**).*

Compound	9	10	12
ID	0696abc22s	0678abc22s	0679abc22s
Empirical formula	$C_{72}H_{71}BF_{24}NOP_2Rh$	$C_{72}H_{71}BF_{24}IrNOP_2$	$C_{68}H_{77}BF_{25}IrNP_2$
Formula weight	1597.95	1687.24	1648.25
Temperature/K	150.00(10)	150(2)	150(2)
Crystal system	orthorhombic	orthorhombic	monoclinic
Space group	$P2_12_12_1$	$Pca2_1$	$P2_1/c$
a/Å	19.87157(17)	18.88454(16)	13.10964(4)
b/Å	19.58214(16)	19.65114(16)	28.08187(9)
c/Å	37.6979(3)	19.85752(18)	19.74276(6)
α/°	90	90	90
β/°	90	90	94.0809(3)
γ/°	90	90	90
Volume/Å^3	14669.3(2)	7369.18(11)	7249.73(4)
Z	8	4	4
ρ_{calc}mg/mm^3	1.447	1.521	1.510
μ/mm^{-1}	3.220	4.839	4.910
F(000)	6512.0	3384.0	3316.0
Crystal size/mm^3	$0.389 \times 0.102 \times 0.073$	$0.25 \times 0.168 \times 0.048$	$0.238 \times 0.126 \times 0.064$
Radiation	Cu Kα (λ = 1.54184)	Cu Kα (λ = 1.54184)	Cu Kα (λ = 1.54184)
2Θ range for data collection	12.694 to 140.152°	12.676 to 147.43°	13.05 to 147.294°
Index ranges	$-24 \le h \le 24$, $-23 \le k \le 23$, $-38 \le l \le 45$	$-23 \le h \le 19$, $-24 \le k \le 24$, $-23 \le l \le 24$	$-16 \le h \le 16$, $-34 \le k \le 30$, $-24 \le l \le 24$
Reflections collected	119751	61966	119163
Independent reflections	27544[R(int) = 0.0381]	14215[R(int) = 0.0503]	14575[R(int) = 0.0259]
Data/restraints/parameters	27544/2520/1862	14215/1711/1041	14575/744/1051
Goodness-of-fit on F^2	1.073	1.072	1.044
Final R indexes [I>=2σ (I)]	$R_1 = 0.1186$, $wR_2 = 0.3090$	$R_1 = 0.0516$, $wR_2 = 0.1285$	$R_1 = 0.0250$, $wR_2 = 0.0639$
Final R indexes [all data]	$R_1 = 0.1275$, $wR_2 = 0.3204$	$R_1 = 0.0553$, $wR_2 = 0.1324$	$R_1 = 0.0261$, $wR_2 = 0.0650$
Largest diff. peak/hole / e Å^{-3}	7.22/-2.28	3.21/-1.76	0.80/-0.64
Flack parameter	0.49(2)	-0.004(12)	-

Table 6.6. *Crystallographic data for compounds **23**, **24**, **26** and **32** (**Chapter 3**).*

Compound	23	24	26	32
ID	0697abc22s	0525abc19s	0691abc22s	0595abc20s
Empirical formula	$C_{46}H_{57}O_5P_2Rh$	$C_{66}H_{76}BF_{24}N_2O_2P_2RhSi_2$	$C_8H_{15}BNOP$	$C_{68}H_{60}BF_{24}NOP_3Rh$
Formula weight	854.76	1617.12	182.99	1569.80
Temperature/K	150(2)	150.00(10)	150(2)	150.00(10)
Crystal system	orthorhombic	monoclinic	monoclinic	triclinic
Space group	$P2_12_12_1$	$P2_1/n$	$P2_1/n$	P-1
a/Å	13.1889(5)	15.59345(6)	12.4353(2)	13.66917(14)
b/Å	20.4841(7)	25.78780(10)	7.23590(10)	13.80697(14)
c/Å	32.0040(10)	18.26966(7)	12.8159(2)	18.91039(18)
α/°	90	90	90	97.7465(8)
β/°	90	92.6989(3)	115.394(2)	96.4094(8)
γ/°	90	90	90	90.2437(8)
Volume/Å^3	8646.3(5)	7338.46(5)	1041.76(3)	3513.61(6)
Z	8	4	4	2
ρ_{calc}mg/mm^3	1.313	1.464	1.167	1.484
μ/mm^{-1}	4.233	3.539	1.969	3.561
F(000)	3584.0	3304.0	392.0	1588.0
Crystal size/mm^3	$0.23 \times 0.14 \times 0.02$	$0.358 \times 0.215 \times 0.076$	$0.298 \times 0.207 \times 0.093$	$0.198 \times 0.135 \times 0.068$
Radiation	Cu Kα (λ = 1.54184)	Cu Kα (λ = 1.54184)	Cu Kα (λ = 1.54184)	Cu Kα (λ = 1.54184)
2Θ range for data collection	12.942 to 140.126	12.826 to 140.152	13.126 to 140.034	12.944 to 140.152
Index ranges	$-16 \le h \le 16, -24 \le k \le 24,$ $-39 \le l \le 29$	$-19 \le h \le 19, -31 \le k \le 31,$ $-22 \le l \le 22$	$-15 \le h \le 15, -8 \le k \le 8,$ $-15 \le l \le 15$	$-16 \le h \le 16, -16 \le k \le 16,$ $-23 \le l \le 23$
Reflections collected	55220	117529	10618	85456
Independent reflections	16020	13919	1980	13319
	[R_{int} = 0.1465, R_{sigma} = 0.1201]	[R_{int} = 0.0322, R_{sigma} = 0.0159]	[R_{int} = 0.0183, R_{sigma} = 0.0122]	[R_{int} = 0.0305, R_{sigma} = 0.0194]
Data/restraints/parameters	16020/0/488	13919/441/1001	1980/0/113	13319/342/956
Goodness-of-fit on F^2	1.045	1.039	1.065	1.043
Final R indexes [I>=2σ (I)]	R_1 = 0.1473, wR_2 = 0.3356	R_1 = 0.0323, wR_2 = 0.0830	R_1 = 0.0297, wR_2 = 0.0800	R_1 = 0.0299, wR_2 = 0.0754
Final R indexes [all data]	R_1 = 0.1651, wR_2 = 0.3470	R_1 = 0.0338, wR_2 = 0.0844	R_1 = 0.0306, wR_2 = 0.0810	R_1 = 0.0306, wR_2 = 0.0760
Largest diff. peak/hole / e Å^{-3}	4.74/-1.47	0.67/-0.43	0.26/-0.24	0.66/-0.76
Flack parameter	0.04(3)	-	-	-

Table 6.7. *Crystallographic data for compounds **44**, **45** and **A131** (**Chapter 4**).*

Compound	44	45	A131
ID	0655abc21s	0697abc22s	0549abc19s
Empirical formula	$C_{31}H_{31}O_2P_2Rh$	$C_{46}H_{57}O_5P_2Rh$	$C_{114}H_{122}B_{11}F_2I_6N_6O_9P_2Rh$
Formula weight	600.41	854.76	2803.33
Temperature/K	150(2)	150(2)	150(2)
Crystal system	tetragonal	orthorhombic	triclinic
Space group	$P\text{-}42_1c$	$P2_12_12_1$	P-1
a/Å	25.3571(5)	13.1889(5)	12.00058(12)
b/Å	25.3571(5)	20.4841(7)	22.3381(2)
c/Å	8.5173(3)	32.0040(10)	24.6293(3)
α/°	90	90	114.7777(10)
β/°	90	90	97.2236(8)
γ/°	90	90	99.4706(9)
Volume/Å^3	5476.5(3)	8646.3(5)	5771.42(11)
Z	8	8	2
ρ_{calc}mg/mm^3	1.456	1.313	1.613
μ/mm^{-1}	0.767	4.233	14.548
F(000)	2464.0	3584.0	2772.0
Crystal size/mm^3	$0.3 \times 0.12 \times 0.12$	$0.23 \times 0.14 \times 0.02$	$0.264 \times 0.161 \times 0.059$
Radiation	Mo Kα (λ = 0.71073)	Cu Kα (λ = 1.54184)	Cu Kα (λ = 1.54184)
2Θ range for data collection	5.982 to 69.938	12.942 to 140.126	12.892 to 140.152
Index ranges	$-40 \le h \le 40, -40 \le k \le 40,$ $-13 \le l \le 12$	$-16 \le h \le 16, -24 \le k \le 24,$ $-39 \le l \le 29$	$-14 \le h \le 14, -27 \le k \le 27,$ $-29 \le l \le 30$
Reflections collected	64300	55220	111730
Independent reflections	11974	16020	21879
	[R_{int} = 0.0567, R_{sigma} = 0.0498]	[R_{int} = 0.1465, R_{sigma} = 0.1201]	[R_{int} = 0.0437, R_{sigma} = 0.0279]
Data/restraints/parameters	11974/12/328	16020/0/488	21879/405/1401
Goodness-of-fit on F^2	0.935	1.045	1.043
Final R indexes [I>=2σ (I)]	R_1 = 0.0437, wR_2 = 0.1212	R_1 = 0.1473, wR_2 = 0.3356	R_1 = 0.0410, wR_2 = 0.1068
Final R indexes [all data]	R_1 = 0.0679, wR_2 = 0.1412	R_1 = 0.1651, wR_2 = 0.3470	R_1 = 0.0454, wR_2 = 0.1110
Largest diff. peak/hole / e Å^{-3}	0.66/-0.80	4.74/-1.47	2.76/-1.47
Flack parameter	0.50(4)	0.04(3)	-

Appendix – The 18-Electron Rule

The 18-electron rule can be used to predict or explain the structures of transition metal complexes, in a similar manner to the way in which the octet rule can be used in main group systems. The principle is that the sum of the number of electrons in valence orbitals of the metal and those donated by the ligands should be equal to 18. This originates from the presence of nine valence orbitals for a d block metal: five d orbitals, three p orbitals and one s orbital. Combined, these give a total of nine bonding orbitals and nine antibonding orbitals. When the bonding orbitals are completely filled, leaving the antibonding orbitals unoccupied, there are 18 bonding electrons. Generally speaking, compounds that obey this rule are relatively stable and unreactive, with complexes that don't obey the rule typically being more reactive and chemically interesting.[391, 392]

However, transition metal coordination compounds do not necessarily follow this rule and it should really only be considered as a guideline when electron-counting complexes. Firstly, the example of octahedral, first row transition metal complexes with weak field ligands (*e.g.* chloride, water, ammonia) should be considered. The small splitting, Δ_o, between the t_{2g} and e_g orbitals (**Figure A1**) results in non-bonding character for the t_{2g} orbitals and only weakly antibonding character for the e_g orbitals. Consequently, there are no significant preferences for the number of electrons that can occupy these orbitals, and the valence electron count can vary from 12 to 22.
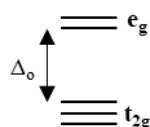
Figure A1. Simplified molecular orbital diagram showing the d-orbital splitting for an octahderal transition metal complex.

Secondly, second row transition metal complexes, or first row complexes with strong field ligands (*e.g.* cyanide) possess a larger Δ_o. As a result of this, the t_{2g} orbitals retain non-bonding character but the e_g orbitals now have stronger antibonding character. The non-bonding orbitals are preferably filled, leaving the antibonding orbitals unoccupied. This results in a valence electron count of 18 electrons or fewer.

The final case to consider is transition metal complexes bearing strong field organometallic ligands, such as carbonyl, olefins and arenes, which are also good π-acceptors. These stabilise the t_{2g} orbitals, lowering their energy and giving them fully bonding character, whilst the e_g orbitals remain antibonding. Therefore, 6 electrons should occupy the t_{2g} orbitals. When the other six bonding orbitals are taken into account, this gives a total of 18 electrons. The majority of transition metal complexes bearing organometallic ligands (including those discussed in this thesis) fall into this category.

Within this class of complexes that should obey the 18-electon rule, there are further exceptions. These can primarily be rationalised by steric and electronic considerations.

For early transition metals, their lower d-electron count requires coordination of a larger number of ligands in order to satisfy the 18-electron rule. The steric hindrance between these coordinated ligands can results in lower electron count complexes.

Of the greatest importance to the work described in this thesis is the situation of late transition metal d^8 and d^{10} complexes. As atomic number increases, the effective nuclear charge increases (a consequence of the poor shielding ability of diffuse d-orbitals), resulting in a stabilisation of the d-orbitals. Towards the end of the row, the d-electrons display increasingly greater core electron character. As a result, their ability to engage in metal-ligand bonding is diminished: the potential for π-backdonation onto coordinated ligands as a means of attaining electroneutrality is reduced (the π-accepting capabilities of the coordinated ligands is, therefore, also an important factor).

In the case of M(I) d^8 complexes, where M is rhodium or iridium, these complexes have a strong tendency to form square planar 16-electron complexes. The occupied d_{z2} orbital, perpendicular to the metal-ligand bonding plane, is not involved in ligand bonding. These complexes can be seen throughout this thesis (**Figure A2**), for example the pincer-supported metal carbonyl complexes **2** and **3** (**Chapter 2**) and **A32**, **34**-**36** (**Chapter 3**). Other examples include dihydrogen complex **13** (**Chapter 2**), complexes **23**, **24**, **31** and **32** (**Chapter 3**) and acac complexes **44**-**46** (**Chapter 4**).

The fact that complexes such as this do not obey the 18-electron rule makes them chemically interesting. A consequence of this is that they can undergo classical, two-electron reactivity such as oxidative addition (requiring an increase of 2 in the valence electron count). The reverse also applies: an 18-electron complex can undergo reductive elimination (requiring a decrease of 2 in the valence electron count), to give a 16-electron complex. These processes generally form the key steps in group 9 complex-mediated catalysis.

A final example of complexes that do not appear to obey the 18-electron rule, and which are particularly relevant in the context of this thesis, is those which are stabilised by agostic interactions (**Figure A3**). Complexes **4** and **12** appear to be square-based pyramidal, 16-electron M(III) complexes, but if the agostic interaction at the vacant coordination site is taken into account, these actually become octahedral, 18-electron complexes that do not violate the rule.
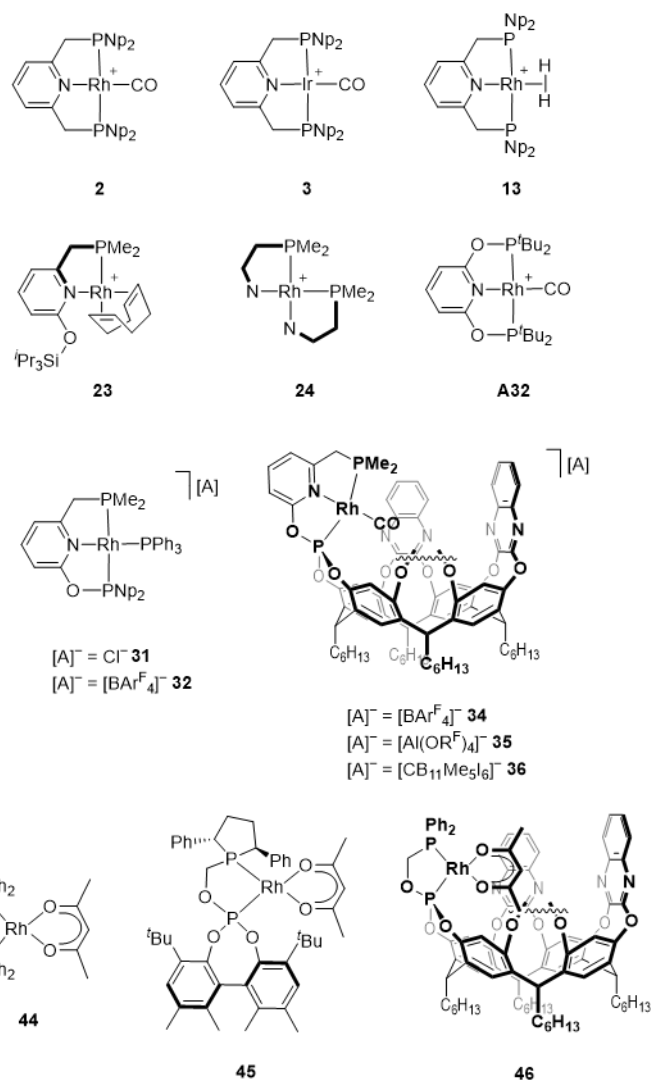
Figure A2. *Examples of 16-electron, square planar d^8 complexes described in this thesis.*
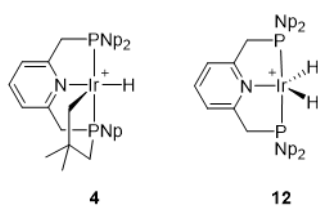
Figure A3. *Examples of formally 16-electron, d^6 complexes described in this thesis, which can be considered as 18-electron complexes when agostic interactions are taken into account.*

References

1. C.A. Tolman, *Chem. Rev.*, 1977, **77**, 313.

2. A. Roodt, S. Otto, G. Steyl, *Coord. Chem. Rev.*, 2003, **245**, 121.

3. S. Otto, A. Roodt, *Inorg. Chim. Acta*, 2004, **357**, 1.

4. R.A. Kelly III, H. Clavier, S. Giudice, N.M. Scott, E.D. Stevens, J. Bordner, I. Samardjiev, C.D. Hoff, L. Cavallo, S.P. Nolan, *Organometallics*, 2008, **27**, 202.

5. T. Dröge, F. Glorius, *Angew. Chem., Int. Ed.*, 2010, **49**, 6940.

6. D.J. Nelson, S.P. Nolan, *Chem. Soc. Rev.*, 2013, **42**, 6723.

7. D. Setiawan, R. Kalescky, E. Kraka, D. Cremer, *Inorg. Chem.*, 2016, **55**, 2332.

8. D. Cremer, E. Kraka, *Dalton Trans.*, 2017, **46**, 8323.

9. D.W. Allen, B.F. Taylor, *J. Chem. Soc., Dalton Trans.*, 1982, 51.

10. U. Beckmann, D. Süslüyan, P.C. Kunz, *Phosphorus Sulfur*, 2011, **186**, 2061.

11. A.C. Hillier, W.J. Sommer, B.S. Yong, J.L. Petersen, L. Cavallo, S.P. Nolan, *Organometallics*, 2003, **22**, 4322.

12. H. Clavier, S.P. Nolan, *Chem. Commun.*, 2010, **46**, 841.

13. C.P. Casey, G.T. Whiteker, *Isr. J. Chem.*, 1990, **30**, 299.

14. M. Kranenburg, Y.E.M. van der Burgt, P.C.J. Kamer, P.W.N.M. van Leeuwen, K. Goubitz, J. Fraanje, *Organometallics*, 1995, **14**, 3081.

15. P. Dierkes, P.W.N.M. van Leeuwen, *J. Chem. Soc., Dalton Trans.*, 1999, 1519.

16. P.W.N.M. van Leeuwen, P.C.J. Kamer, J.N.H. Reek, P. Dierkes, *Chem. Rev.*, 2000, **100**, 2741.

17. L.A. van der Veen, P.H. Keeven, G.C. Schoemaker, J.N.H. Reek, P.C.J. Kamer, P.W.N.M. van Leeuwen, M. Lutz, A.L. Spek, *Organometallics*, 2000, **19**, 872.

18. P.W.N.M. van Leeuwen, J.N.H. Reek, *Acc. Chem. Res.*, 2001, **34**, 895.

19. M.-N. Birkholz, Z. Freixa, P.W.N.M. van Leeuwen, *Chem. Soc. Rev.*, 2009, **38**, 1099.

20. S.H.A.M. Leenders, R. Gramage-Doria, B. de Bruin, J.N.H. Reek, *Chem. Soc. Rev.*, 2015, **44**, 433.

21. V. Mouarrawis, R. Plessius, J.I. van der Vlugt, J.N.H. Reek, *Front. Chem.*, 2018, **6**, 623.

22. J.N.H. Reek, B. de Bruin, S. Pullen, T.J. Mooibroek, A.M. Kluwer, X. Caumes, *Chem. Rev.*, 2022, **122**, 12308.

23. C. Jeunesse, D. Armspach, D. Matt, *Chem. Commun.*, 2005, 5603.

24. R.J. Puddephatt, *Can. J. Chem.*, 2006, **84**, 1505.

25. A.W. Kleij, J.N.H. Reek, *Chem.- Eur. J.*, 2006, **12**, 4218.

26. R.J. Hooley, J. Rebek, Jr., *Chem. Biol.*, 2009, **16**, 255.

27. R. Gramage-Doria, D. Armspach, D. Matt, *Coord. Chem. Rev.*, 2013, **257**, 776.

28. D. Sémeril, D. Matt, *Coord. Chem. Rev.*, 2014, **279**, 58.

29. J.-N. Rebilly, B. Colasson, O. Bistri, D. Over, O. Reinaud, *Chem. Soc. Rev.*, 2015, **44**, 467.

30. T. Iwasawa, *Tetrahedron Lett.*, 2017, **58**, 4217.

31. N. Natarajan, E. Brenner, D. Sémeril, D. Matt, J. Harrowfield, *Eur. J. Org. Chem.*, 2017, 6100.

32. S. Roland, J.M. Suarez, M. Sollogoub, *Chem.- Eur. J.*, 2018, **24**, 12464.

33. G.R.F. Orton, B.S. Pilgrim, N.R. Champness, *Chem. Soc. Rev.*, 2021, **50**, 4411.

34. D. Matt, J. Harrowfield, *ChemCatChem*, 2021, **13**, 153.

35. J. Trouvé, R. Gramage-Doria, *Chem. Soc. Rev.*, 2021, **50**, 3565.

36. D. Morales-Morales, C.M. Jensen, *The Chemistry of Pincer Compounds*, Elsevier, Amsterdam, 2007.

37. G. van Koten, D. Milstein, *Organometallic Pincer Chemistry*, Springer-Verlag, Berlin-Heideberg, 2013.

38. K.J. Szabó, O.F. Wendt, *Pincer and Pincer-Type Complexes*, Wiley-VCH, Weinheim, 2014.

39. A. Kasera, J.P. Biswas, A.A. Alshehri, S.A. Al-Thabaiti, M. Mokhtar, D. Maiti, *Coord. Chem. Rev.*, 2023, **475**, 214915.

40. C. Zhou, M.-H. Huang, K.-W. Huang, in *Rhodium Pincer Complexes: Coordination, Reactivity and Catalysis*, Eds. E.C. Constable, G. Parkin, L. Que, Jr., Elsevier, Amsterdam, 2021, vol. 6, ch. 6.03, pp. 43–107.

41. M. Albrecht, G. van Koten, *Angew. Chem., Int. Ed.*, 2001, **40**, 3750.

42. C. Gunanthan, D. Milstein, *Chem. Rev.*, 2014, **114**, 12024.

43. A. Kumar, T.M. Bhatti, A.S. Goldman, *Chem. Rev.*, 2017, **117**, 12357.

44. E. Peris, R.H. Crabtree, *Chem. Soc. Rev.*, 2018, **47**, 1959.

45. R.E. Andrew, L. González-Sebastián, A.B. Chaplin, *Dalton Trans.*, 2016, **45**, 1299.

46. M. Asay, D. Morales-Morales, *Dalton Trans.*, 2015, **44**, 17432.

47. M.A. Esteruelas, M. Oliván, A. Vélez, *Inorg. Chem.*, 2013, **52**, 5339.

48. W.V. Dahlhoff. S.M. Nelson, *J. Chem. Soc. A*, 1971, 2184.

49. C.J. Moulton, B.L. Shaw, *J. Chem. Soc., Dalton Trans.*, 1976, 1020.

50. D. Hermann, M. Gandelman, H. Rozenberg, L.J.W. Shimon, D. Milstein, *Organometallics*, 2002, **21**, 812.

51. E. Ben-Ari, M. Gandelman, H. Rozenberg, L.J.W. Shimon, D. Milstein, *J. Am. Chem. Soc.*, 2003, **125**, 4714.

52. E. Ben-Ari, R. Cohen, M. Gandelman, L.J.W. Shimon, J.M.L. Martin, D. Milstein, *Organometallics*, 2006, **25**, 3190.

53. M. Kanzelberger, B. Singh, M. Czerw, K. Krogh-Jespersen, A.S. Goldman, *J. Am. Chem. Soc.*, 2000, **122**, 11017.

54. M. Feller, E. Ben-Ari, T. Gupta, L.J.W. Shimon, G. Leitus, Y. Diskin-Posner, L. Weiner, D. Milstein, *Inorg. Chem.*, 2007, **46**, 10479.

55. A.B. Chaplin, A.S. Weller, *Organometallics*, 2011, **30**, 4466.

56. M. Feller, Y. Diskin-Posner, G. Leitus, L.J.W. Shimon, D. Milstein, *J. Am. Chem. Soc.*, 2013, **135**, 11040.

57. G.M. Adams, F.M. Chadwick, S.D. Pike, A.S. Weller, *Dalton Trans.*, 2015, **44**, 6340.

58. A. Anaby, M. Feller, Y. Ben-David, G. Leitus, Y. Diskin-Posner, L.J.W. Shimon, D. Milstein, *J. Am. Chem. Soc.*, 2016, **128**, 9941.

59. S.M. Kloek, D.M. Heinekey, K.I. Goldeberg, *Angew. Chem., Int. Ed.*, 2007, **46**, 4736.

60. S. Kloek Hanson, D.M. Heinekey, K.I. Goldberg, *Organometallics*, 2008, **27**, 1454.

61. M.R. Gyton, T.M. Hood, A.B. Chaplin, *Dalton Trans.*, 2019, **48**, 2877.

62. M.R. Gyton, B. Leforestier, A.B. Chaplin, *Angew. Chem., Int. Ed.*, 2019, **58**, 15295.

63. W.B. Tolman, *Angew. Chem., Int. Ed.*, 2010, **49**, 1018.

64. T. Yano, Y. Moroe, M. Yamashita, K. Nozaki, *Chem. Lett.*, 2008, **37**, 1300.

65. M. Yamashita, Y. Moroe, T. Yano, K. Nozaki, *Inorg. Chim. Acta*, 2011, **369**, 15.

66. Z. Tang, E. Otten, J.N.H. Reek, J.I. van der Vlugt, B. de Bruin, *Chem.- Eur. J.*, 2015, **21**, 12683.

67. S. Takegasa, M.M. Lee, K. Tokuhiro, R. Nakano, M. Yamashita, *Chem.- Eur. J.*, 2022, **28**, e2022018.

68. M. Hollering, B. Dutta, F.E. Kühn, *Coord. Chem. Rev.*, 2016, **309**, 51.

69. T. Ito, K. Takahashi, N. Iwasawa, *Organometallics*, 2019, **38**, 205.

70. K. Takahashi, Y. Hirataka, T. Ito, N. Iwasawa, *Organometallics*, 2020, **39**, 1561.

71. S. Manzini, A. Cadu, A.-C. Schmidt, N. Huguet, O. Trapp, R. Paciello, T. Schaub, *ChemCatChem*, 2017, **9**, 2269.

72. S. Lapointe, E. Khaskin, R.R. Fayzullin, J.R. Khusnutdinova, *Organometallics*, 2019, **38**, 1581.

73. E. Khaskin, Y. Diskin-Posner, L. Weiner, G. Leitus, D. Milstein, *Chem. Commun.*, 2013, **49**, 2771.

74. S. Acosta-Calle, A.J.M. Miller, *Acc. Chem. Res.*, 2023, **56**, 971.

75. M.R. Kita, A.J.M. Miller, *J. Am. Chem. Soc.*, 2014, **136**, 14519.

76. J. Grajeda, M.R. Kita, L.C. Gregor, P.S. White, A.J.M. Miller, *Organometallics*, 2016, **35**, 306.

77. L.C. Gregor, J. Grajeda, M.R. Kita, P.S. White, A.J. Vetter, A.J.M. Miller, *Organometallics*, 2016, **35**, 3074.

78. M.R. Kita, A.J.M. Miller, *Angew. Chem., Int. Ed.*, 2017, **56**, 5498.

79. A.M. Camp, M.R. Kita, P.T. Blackburn, H.M. Dodge, C.-H. Chen, A.J.M. Miller, *J. Am. Chem. Soc.*, 2021, **143**, 2792.

80. H.M. Dodge, M.R. Kita, C.-H. Chen, A.J.M. Miller, *ACS Catal.*, 2020, **10**, 13019.

81. J.B. Smith, A.M. Camp, A.H. Farquhar, S.H. Kerr, C.-H. Chen, A.J.M. Miller, *Organometallics*, 2019, **38**, 4392.

82. D. Fieldler, D.H. Leung, R.G. Bergman, K.N. Raymond, *Acc. Chem. Res.*, 2005, **38**, 351.

83. M.D. Pluth, R.G. Bergman, K.N. Raymond, *Acc. Chem. Res.*, 2009, **42**, 1650.

84. D.H. Leung, D. Fieldler, R.G. Bergman, K.N. Raymond, *Angew. Chem., Int. Ed.*, 2004, **43**, 963.

85. D.H. Leung, R.G. Bergman, K.N. Raymond, *J. Am. Chem. Soc.*, 2007, **129**, 2746.

86. Z.J. Wang, C.J. Brown, R.G. Bergman, K.N. Raymond, F.D. Toste, *J. Am. Chem. Soc.*, 2011, **133**, 7358.

87. C.C. James, D. Wu, E.O. Bobylev, A. Kros, B. de Bruin, J.N.H. Reek, *ChemCatChem*, 2022, **14**, e2022009.

88. L.J. Jongkind, M. Rahimi, D. Poole, III, S.J. Ton, D.E. Fogg, J.N.H. Reek, *ChemCatChem*, 2020, **12**, 4019.

89. S. Hkiri, M. Steinmetz, R. Schurhammer, D. Sémeril, *Chem.- Eur. J.*, 2022, **28**, e202201887.

90. M.A. Sarmentero, H. Fernández-Pérez, E. Zuidema, C. Bo, A. Vidal-Ferran, P. Ballester, *Angew. Chem., Int. Ed.*, 2010, **49**, 7489.

91. V.F. Slagt, J.N.H. Reek, P.C.J. Kamer, P.W.N.M. van Leeuwen, *Angew. Chem., Int. Ed.*, 2001, **40**, 4271.

92. V.F. Slagt, P.C.J. Kamer, P.W.N.M. van Leeuwen, J.N.H. Reek, *J. Am. Chem. Soc.*, 2004, **126**, 1526.

93. M. Kuil, T. Soltner, P.W.N.M. van Leeuwen, J.N.H. Reek, *J. Am. Chem. Soc.*, 2006, **128**, 11344.

94. V. Bocokić, A. Kalkan, M. Lutz, A.L. Spek, D.T. Gryko, J.N.H. Reek, *Nat. Commun.*, 2013, **4**, 2670.

95. T. Besset, D.W. Norman, J.N.H. Reek, *Adv. Synth. Catal.*, 2013, **355**, 348.

96. X. Wang, S.S. Nurttila, W.I. Dzik, R. Becker, J. Rodgers, J.N.H. Reek, *Chem.- Eur. J.*, 2017, **23**, 14769.

97. L.J. Jongkind, J.N.H. Reek, *Chem.- Asian J.*, 2020, **15**, 867.

98. T. Keijer, J.N.H. Reek, in *Porphyrin-based Supramolecular Architectures: From Hierarchy to Functions*, Eds. S. Ma, G. Verma, Royal Society of Chemistry, London, 2022, ch. 2, pp. 59–105.

99. V. Mouarrawis, E.O. Bobylev, B. de Bruin, J.N.H. Reek, *Eur. J. Inorg. Chem.*, 2021, 2890.

100. D.J. Cram, *Science*, 1983, **219**, 1177.

101. V.V. Shinde, D. Jeong, S. Jung, *Catalysts*, 2019, **9**, 111.

102. N. Şahin, D. Sémeril, E. Brenner, D. Matt, İ. Özdemir, C. Kaya, L. Toupet, *ChemCatChem*, 2013, **5**, 1116.

103. N. Şahin, D. Sémeril, E. Brenner, D. Matt, C. Kaya, L. Toupet, *Turk. J. Chem.*, 2015, **39**, 1171.

104. M. Kaloğlu, D. Sémeril, E. Brenner, D. Matt, İ. Özdemir, L. Toupet, *Eur. J. Inorg. Chem.*, 2016, 1115.

105. N. Şahin, D. Sémeril, E. Brenner, D. Matt, İ. Özdemir, C. Kaya, L. Toupet, *Eur. J. Org. Chem.*, 2013, 4443.

106. N. Natarajan, T. Chavagnan, D. Sémeril, E. Brenner, D. Matt, R. Ramesh, L. Toupet, *Eur. J. Inorg. Chem.*, 2018, 890.

107. M. Guitet, P. Zhang, F. Marcelo, C. Tugny, J. Jiménez-Barbero, O. Buriez, C. Amatore, V. Mouriès-Mansuy, J.-P. Goddard, L. Fensterbank, Y. Zhang, S. Roland, M. Ménand, M. Sollogoub, *Angew. Chem., Int. Ed.*, 2013, **52**, 7213.

108. P. Zhang, C. Tugny, J. Meijide Suárez, M. Guitet, E. Derat, N. Vanthuyne, Y. Zhang, O. Bistri, V. Mouriès-Mansuy, M. Ménand, S. Roland, L. Fensterbank, M. Sollogoub, *Chem*, 2017, **3**, 174.

109. P. Zhang, J. Meijide Suárez, T. Driant, E. Derat, Y. Zhang, M. Ménand, S. Roland, M. Sollogoub, *Angew. Chem., Int. Ed.*, 2017, 129, 10961.

110. J. Meijide Suárez, O. Bistri-Aslanoff, S. Roland, M. Sollogoub, *ChemCatChem*, 2022, **14**, e202101411.

111. X. Fang, B.L. Scott, J.G. Watkin, C.A.G. Carter, G.J. Kubas, *Inorg. Chim. Acta*, 2001, **317**, 276.

112. J. Emerson-King, S. Pan, M.R. Gyton, R. Tonner-Zech, A.B. Chaplin, *Chem. Commun.*, 2023, **59**, 2150.

113. M. Petroselli, Y.-Q. Chen, J. Rebek Jr., Y. Yu, *Green Synth. Catal.*, 2021, **2**, 123.

114. A.G.S. Hörberg, *J. Org. Chem.*, 1980, **45**, 4498.

115. J.R. Moran, S. Karbach, D.J. Cram, *J. Am. Chem. Soc.*, 1982, **104**, 5826.

116. C. Gibson, J. Rebek, Jr., *Org. Lett.*, 2002, **4**, 1887.

117. T. Iwasawa, Y. Nishimoto, K. Hama, T. Kamei, M. Nishiuchi, Y. Kawamura, *Tetrahedron Lett.*, 2008, **49**, 4758.

118. M.P. Schramm, M. Kanaura, K. Ito, M. Ide, T. Iwasawa, *Eur. J. Org. Chem.*, 2016, 813.

119. N. Endo, M. Kanaura, M.P. Schramm, T. Iwasawa, *Eur. J. Org. Chem.*, 2016, 2514.

120. M. Kanaura, N. Endo, M.P. Schramm, T. Iwasawa, *Eur. J. Org. Chem.*, 2016, 4970.

121. N. Endo, M. Kanaura, M.P. Schramm, T. Iwasawa, *Tetrahedron Lett.*, 2016, **57**, 4754.

122. N. Endo, M. Inoue, T. Iwasawa, *Eur. J. Org. Chem.*, 2018, 1136.

123. M. Inoue, K. Ugawa, T. Maruyama, T. Iwasawa, *Eur. J. Org. Chem.*, 2018, 5304.

124. T.D. Ho, M.P. Schramm, *Eur. J. Org. Chem.*, 2019, 5678.

125. M. Inoue, S. Kamiguchi, K. Ugawa, S. Hkiri, J. Bouffard, D. Sémeril, T. Iwasawa, *Eur. J. Org. Chem.*, 2019, 6261.

126. L.E. Rusali, M.P. Schramm, *Tetrahedron Lett.*, 2020, **61**, 152333.

127. P.P. Castro, G. Zhao, G.A. Masangkay, C. Hernandez, L.M. Gutierrez-Tunstad, *Org. Lett.*, 2004, **6**, 333.

128. S.L. Craig, S. Lin, J. Chen, J. Rebek, Jr., *J. Am. Chem. Soc.*, 2002, **124**, 8780.

129. A. Shivanyuk, J. Rebek, Jr., *J. Am. Chem. Soc.*, 2002, **124**, 12074.

130. I. Martín-Torres, G. Ogalla, J.-M. Yang, A. Rinaldi, A.M. Echavarren, *Angew. Chem., Int. Ed.*, 2021, **60**, 9339.

131. J. Emerson-King, PhD Thesis, University of Warwick, 2019.

132. V.A. Azov, B. Jaun, F. Diederich, *Helv. Chim. Acta*, 2004, **87**, 449.

133. T. Gottschalk, B. Jaun, F. Diederich, *Angew. Chem., Int. Ed.*, 2007, **46**, 260.

134. J.J. Schneider, *Angew. Chem., Int. Ed. Engl.*, 1996, **35**, 1068.

135. S.E. Bromberg, H. Yang, M.C. Asplund, T. Lian, B.K. McNamara, K.T. Kotz, J.S. Yeston, M. Wilkens, H. Frei, R.G. Bergman, C.B. Harris, *Science*, 1997, **278**, 260.

136. J.A. Labinger, J.E. Bercaw, *Nature*, 2002, **417**, 507.

137. R.H. Crabtree, *Chem. Rev.*, 1985, **85**, 245.

138. A.E. Shilov, G.B. Shul'pin, *Chem. Rev.*, 1997, **97**, 2879.

139. J.A. Labinger, J.E. Bercaw, *Nature*, 2002, **417**, 507.

140. R.H. Crabtree, *J. Organomet. Chem.*, 2004, **689**, 4083.

141. K. Godula, D. Sames, *Science*, 2006, **312**, 67.

142. T. Gensch, M.N. Hopkinson, F. Glorius, J. Wencel-Delord, *Chem. Soc. Rev.*, 2016, **45**, 2900.

143. K.M. Altus, J.A. Love, *Commun. Chem.*, 2021, **4**, 173.

144. C. Hall, R.N. Perutz, *Chem. Rev.*, 1996, **96**, 1068.

145. A.S. Weller, F.M. Chadwick, A.I. McKay, *Adv. Organomet. Chem.*, 2016, **66**, 223.

146. M. Brookhart, M.L.H. Green, *J. Organomet. Chem.*, 1983, **250**, 395.

147. M. Brookhart, M.L.H. Green, L.-L. Wong, *Prog. Inorg. Chem.*, 1988, **36**, 1.

148. W. Scherer, G.S. McGrady, *Angew. Chem., Int. Ed.*, 2004, **43**, 1782.

149. M. Brookhart, M.L.H. Green, G. Parkin, *P. Natl. Acad. Sci. U.S.A.*, 2007, **104**, 6908.

150. E. Clot, O. Eisenstein, *Struct. Bond.*, 2004, **113**, 1.

151. R.H. Crabtree, E.M. Holt, M. Lavin, S.M. Morehouse, *Inorg. Chem.*, 1985, **24**, 1986.

152. A.J. Martínez-Martínez, B.E. Tegner, A.I. McKay, A.J. Bukvic, N.H. Rees, G.J. Tizzard, S.J. Coles, M.R. Warren, S.A. Macgregor, A.S. Weller, *J. Am. Chem. Soc.*, 2018, **140**, 14958.

153. A.G. Algarra, A.L. Burnage, M. Iannuzzi, T. Krämer, S. A. Macgregor, R.E.M. Pirie, B. Tegner, A.S. Weller, *Struct. Bond.*, 2020, **186**, 183.

154. W.D. Jones, *Inorg. Chem.*, 2005, **44**, 4475.

155. A.C. Cooper, W.E. Streib, O. Eisenstein, K.G. Caulton, *J. Am. Chem. Soc.*, 1997, **119**, 9069.

156. G. Ujaque, A.C. Cooper, F. Maseras, O. Eisenstein, K.G. Caulton, *J. Am. Chem. Soc.*, 1998, **120**, 361.

157. A.C. Cooper, E. Clot, J.C. Huffman, W.E. Streib, F. Maseras, O. Eisenstein, K.G. Caulton, *J. Am. Chem. Soc.*, 1999, **121**, 97.

158. T.M. Douglas, A.B. Chaplin, A.S. Weller, *Organometallics*, 2008, **27**, 2918.

159. L.J. Sewell, A.B. Chaplin, J.A.B. Abdalla, A.S. Weller, *Dalton Trans.*, 2010, **39**, 7437.

160. R. Dorta, E.D. Stevens, S.P. Nolan, *J. Am. Chem. Soc.*, 2004, **126**, 5054.

161. N.M. Scott, R. Dorta, E.D. Stevens, A. Correa, L. Cavallo, S.P. Nolan, *J. Am. Chem. Soc.*, 2005, **127**, 3516.

162. N.M. Scott, V. Pons, E.D. Stevens, D.M. Heinekey, S.P. Nolan, *Angew. Chem., Int. Ed.*, 2005, **44**, 2512.

163. C.Y. Tang, A.L. Thompson, S. Aldridge, *J. Am. Chem. Soc.*, 2010, **132**, 10578.

164. C.Y. Tang, N. Phillips, M.J. Kelly, S. Aldridge, *Chem. Commun.*, 2012, **48**, 11999.

165. N. Phillips, J. Rowles, M.J. Kelly, I. Riddlestone, N.H. Rees, A. Dervisi, I.A. Fallis, S. Aldridge, *Organometallics*, 2012, **31**, 8075.

166. S.K. Brayshaw, J.C. Green, G. Kociok-Köhn, E.L. Sceats, A.S. Weller, *Angew. Chem., Int. Ed.*, 2006, **45**, 452.

167. S.K. Brayshaw, E.L. Sceats, J.C. Green, A.S. Weller, *P. Natl. Acad. Sci. U.S.A.*, 2007, **104**, 6921.

168. H.A. Sparkes, T. Krämer, S.K. Brayshaw, J.C. Green, A.S. Weller, J.A.K. Howard, *Dalton Trans.*, 2011, **40**, 10708.

169. A.B. Chaplin, J.C. Green, A.S. Weller, *J. Am. Chem. Soc.*, 2011, **133**, 13162.

170. A.B. Chaplin, A.S. Weller, *J. Organomet. Chem.*, 2013, **730**, 90.

171. G.M. Adams, D.E. Ryan, N.A. Beattie, A.I. McKay, G.C. Lloyd-Jones, A.S. Weller, *ACS Catal.*, 2019, **9**, 3657.

172. J.J. Race, M.J. Webb, T.M. Boyd, A.S. Weller, *Eur. J. Inorg. Chem.*, 2022, e202200174.

173. A.B. Chaplin, R. Tonner, A.S. Weller, *Organometallics*, 2010, **29**, 2710.

174. R.C. Knighton, J. Emerson-King, J.P. Rourke, C.A. Ohlin, A.B. Chaplin, *Chem.- Eur. J.*, 2018, **24**, 4927.

175. C.N. Iverson, W.D. Jones, *Organometallics*, 2001, **20**, 5745.

176. Z. Lu, C.-H. Jun, S.R. de Gala, M.P. Sigalas, O. Eisenstein, R.H. Crabtree, *J. Chem. Soc., Chem. Commun.*, 1993, 1877.

177. Z. Lu, C.-H. Jun, S.R. de Gala, M.P. Sigalas, O. Eisenstein, R.H. Crabtree, *Organometallics*, 1995, **14**, 1168.

178. M.R. Gyton, B. Leforestier, A.B. Chaplin, *Organometallics*, 2018, **37**, 3963.

179. T.M. Hood, M.R. Gyton, A.B. Chaplin, *Dalton Trans.*, 2020, **49**, 2077.

180. T.M. Hood, A.B. Chaplin, *Dalton Trans.*, 2021, **50**, 2472.

181. T.M. Hood, B. Leforestier, M.R. Gyton, A.B. Chaplin, *Inorg. Chem.,* 2019, **58**, 7593.

182. R.B. King, J.C. Cloyd Jr., R.H. Reimann, *J. Org. Chem.*, 1976, **41**, 972.

183. B. Leforestier, M.R. Gyton, A.B. Chaplin, *Dalton Trans.*, 2020, **49**, 2087.

184. T.M. Hood, PhD Thesis, University of Warwick, 2020.

185. T. Imamoto, T. Kusumoto, N. Suzuki, K. Sato, *J. Am. Chem. Soc.*, 1985, **107**, 5301.

186. G.C. Lloyd-Jones, N.P. Taylor, *Chem.- Eur. J.*, 2015, **21**, 5423.

187. G.L. Parker, S. Lau, B. Leforestier, A.B. Chaplin, *Eur. J. Inorg. Chem.*, 2019, 3791.

188. C. Maddox, MChem Thesis, University of Warwick, 2022.

189. O. Kühl, *Phosphorus-31 NMR Spectroscopy*, Springer, Berlin, 2008.

190. P.S. Pregosin, *NMR in Organometallic Chemistry*, Wiley-VCH, Weinheim, 2012.

191. M.R. Gyton, A.E. Kynman, B. Leforestier, A. Gallo, J.R. Lewandowski, A.B. Chaplin, *Dalton Trans.*, 2020, **49**, 5791.

192. E.W. Poole, I. Bustos, T.M. Hood, J.E. Smart, A.B. Chaplin, *Dalton Trans.*, 2023, **52**, 1096.

193. J.M. Rummey, M. C. Boyce, *J. Chem. Educ.*, 2004, **81**, 762.

194. M. Findlater, K.M. Schultz, W.H. Bernskoetter, A. Cartwright-Sykes, D.M. Heinekey, M. Brookhart, *Inorg. Chem.*, 2012, **51**, 4672.

195. R.H. Crabtree, *Chem. Rev.*, 2016, **116**, 8750.

196. J.J. Turner, M.W. George, M. Poliakoff, R.N. Perutz, *Chem. Soc. Rev.*, 2022, **51**, 5300.

197. M.A. Graham, R.N. Perutz, M. Poliakoff, J.J. Turner, *J. Organomet. Chem.*, 1972, **34**, C34.

198. M. Poliakoff, J.J. Turner, *J. Chem. Soc., Dalton Trans.*, 1974, 2276.

199. R.N. Perutz, J.J. Turner, *J. Am. Chem. Soc.*, 1975, **97**, 4791.

200. A.J. Rest, J.R. Sodeau, D.J. Taylor, *J. Chem. Soc., Dalton Trans.*, 1978, 651.

201. A. Horton-Mastin, M. Poliakoff, J.J. Turner, *Organometallics*, 1986, **5**, 405.

202. A.J. Rest, I. Whitwell, *J. Chem. Soc., Dalton Trans.*, 1987, 1181.

203. M. Brookhart, W. Chandler, R.J. Kessler, Y. Liu, N.J. Pienta, C.C. Santini, C. Hall, R.N. Perutz, J.A. Timney, *J. Am. Chem. Soc.*, 1992, **114**, 3802.

204. R.J. Mawby, R.N. Perutz, M.K. Whittlesey, *Organometallics*, 1995, **14**, 3268.

205. G. Wang, S. Lai, M. Chen, M. Zhou, *J. Phys. Chem. A*, 2005, **109**, 9514.

206. H. Hermann, F.-W. Grevels, A. Henne, K. Schaffner, *J. Phys. Chem.*, 1982, **86**, 5151.

207. S.P Church, F.-W. Grevels, H. Hermann, K. Schaffner, *Inorg. Chem.*, 1985, **24**, 418.

208. L. Wang, X. Zhu, K.G. Spears, *J. Am. Chem. Soc.*, 1988, **110**, 8695.

209. P.M. Hodges, S.A. Jackson, J. Jacke, M. Poliakoff, J.J. Turner, F.-W. Grevels, *J. Am. Chem. Soc.*, 1990, **112**, 1234.

210. J.R. Sprague, S.M. Arrivo, K.G. Spears, *J. Phys. Chem.*, 1991, **95**, 10528.

211. M.W. George, M.T. Haward, P.A. Hamley, C. Hughes, F.P.A. Johnson, V.K. Popov, M. Poliakoff, *J. Am. Chem. Soc.*, 1993, **115**, 2286.

212. S.K. Nayak, T.J. Burkey, *J. Am. Chem. Soc.*, 1993, **115**, 6391.

213. B.S. Creaven, M.W. George, A.L. Ginzburg, C. Hughes, J.M. Kelly, C. Long, I.M. McGrath, M.T. Pryce, *Organometallics*, 1993, **12**, 3127.

214. D.W. Lee, C.M. Jensen, *J. Am. Chem. Soc.,* 1996, **118**, 8749.

215. X.-Z. Sun, D.C. Grills, S.M. Nikiforov, M. Poliakoff, M.W. George, *J. Am. Chem. Soc.*, 1997, **119**, 7521.

216. S. Geftakis, G.E. Ball, *J. Am. Chem. Soc.*, 1998, **120**, 9953

217. C.J. Breheny, J.M. Kelly, C. Long, S. O'Keeffe, M.T. Pryce, G. Russell, M.M. Walsh, *Organometallics*, 1998, **17**, 3690.

218. G.I. Childs, C.S. Colley, J. Dyer, D.C. Grills, X.-Z. Sun, J. Yang, M.W. George, *J. Chem. Soc., Dalton Trans.*, 2000, 1901.

219. M.K. Kuimova, W.Z. Alsindi, J. Dyer, D.C. Grills, O.S. Jina, P. Matousek, A.W. Parker, P. Portius, X.-Z. Sun, M. Towrie, C. Wilson, J. Yang, M.W. George, *Dalton Trans.*, 2003, 3996.

220. D.J. Lawes, S. Geftakis, G.E. Ball, *J. Am. Chem. Soc.*, 2005, **127**, 4134.

221. D.J. Lawes, T.A. Darwish, T. Clark, J.B. Harper, G.E. Ball, *Angew. Chem., Int. Ed.*, 2006, **45**, 4486.

222. G.E. Ball, C.M. Brookes, A.J. Cowan, T.A. Darwish, M.W. George, H.K. Kawanami, P. Portius, J.P. Rourke, *P. Natl. Acad. Sci. U.S.A.*, 2007, **104**, 6927.

223. S.B. Duckett, M.W. George, O.S. Jina, S.L. Matthews, R.N. Perutz, X.-Z. Sun, K.Q. Vuong, *Chem. Commun.*, 2009, 1401.

224. J.A. Calladine, S.B. Duckett, M.W. George, S.L. Matthews, R.N. Perutz, O. Torres, K.Q. Vuong, *J. Am. Chem. Soc.*, 2011, **133**, 2303.

225. R.D. Young, A.F. Hill, W. Hillier, G.E. Ball, *J. Am. Chem. Soc.*, 2011, **133**, 13806.

226. R.D. Young, D.J. Lawes, A.F. Hill, G.E. Ball, *J. Am. Chem. Soc.*, 2012, **134**, 8294.

227. W.H. Breckenridge, N. Sinai, *J. Phys. Chem.*, 1981, **85**, 3557.

228. Y. Ishikawa, C.E. Brown, P.A. Hackett, D.M. Rayner, *Chem. Phys. Lett.*, 1988, **150**, 506.

229. C.E. Brown, Y. Ishikawa, P.A. Hackett, D.M. Rayner, *J. Am. Chem. Soc.*, 1990, **112**, 2530.

230. A.J. Cowan, M.W. George, *Coord. Chem. Rev.*, 2008, **252**, 2504.

231. R.D. Young, *Chem.- Eur. J.*, 2014, **20**, 12704.

232. W.H. Bernskoetter, C.Y. Schauer, K.I. Goldberg, M. Brookhart, *Science*, 2009, **326**, 553.

233. W.H. Bernskoetter, S.K. Hanson, S.K. Buzak, Z. Davis, P.S. White, R. Swartz, K.I. Goldberg, M. Brookhart, *J. Am. Chem. Soc.*, 2009, **131**, 8603.

234. M.D. Walter, P.S. White, C.K. Schauer, M. Brookhart, *J. Am. Chem. Soc.*, 2013, **135**, 15933.

235. J.D. Watson, L.D. Field, G.E. Ball, *Nat. Chem.*, 2022, **14**, 801.

236. J.D. Watson, L.D. Field, G.E. Ball, *J. Am. Chem. Soc.*, 2022, **144**, 17622.

237. D.R. Evans, T. Drovetskaya, R. Bau, C.A. Reed, P.D.W. Boyd, *J. Am. Chem. Soc.*, 1997, **119**, 3633.

238. I. Castro-Rodriguez, H. Nakai, P. Gantzel, L.N. Zakharov, A.L. Rheingold, K. Meyer, *J. Am. Chem. Soc.*, 2003, **125**, 15734.

239. E.D. Bloch, W.L. Queen, R. Krishna, J.M. Zadrozny, C.M. Brown, J.R. Long, *Science*, 2012, **335**, 1606.

240. S.D. Pike, A.L. Thompson, A.G. Algarra, D.C. Apperley, S.A. Macgregor, A.S. Weller, *Science*, 2012, **337**, 1648.

241. S.D. Pike, F.M. Chadwick, N.H. Rees, M.P. Scott, A.S. Weller, T. Krämer, S.A. Macgregor, *J. Am. Chem. Soc.*, 2015, **137**, 820.

242. S.D. Pike, T. Krämer, N.H. Rees, S.A. Macgregor, A.S. Weller, *Organometallics*, 2015, **34**, 1487.

243. S.D. Pike, A.S. Weller, *Phil. Trans. R. Soc. A*, 2015, **373**, 20140187.

244. F.M. Chadwick, N.H. Rees, A.S. Weller, T. Krämer, M. Iannuzzi, S.A. Macgregor, *Angew. Chem., Int. Ed.*, 2016, **55**, 3677.

245. F.M. Chadwick, T. Krämer, T. Gutmann, N.H. Rees, A.L. Thompson, A.J. Edwards, G. Buntkowsky, S.A. Macgregor, A.S. Weller, *J. Am. Chem. Soc.*, 2016, **138**, 13369.

246. F.M. Chadwick, A.I. McKay, A.J. Martínez-Martínez, N.H. Rees, T. Krämer, S.A. Macgregor, A.S. Weller, *Chem. Sci.*, 2017, **8**, 6014.

247. A.I. McKay, T. Krämer, N.H. Rees, A.L. Thompson, K.E. Christensen, S.A. Macgregor, A.S. Weller, *Organometallics*, 2017, **36**, 22.

248. A.I. McKay, A.J. Martínez-Martínez, H.J. Griffiths, N.H. Rees, J.B. Waters, A.S. Weller, T. Krämer, S.A. Macgregor, *Organometallics*, 2018, **37**, 1.

249. A.I. McKay, A.J. Martínez-Martínez, H.J. Griffiths, N.H. Rees, J.B. Waters, A.S. Weller, T. Krämer, S.A. Macgregor, *Organometallics*, 2018, **37**, 3524.

250. A.I. McKay, A.J. Bukvic, B.E. Tegner, A.L. Burnage, A.J. Martínez-Martínez, N.H. Rees, S.A. Macgregor, A.S. Weller, *J. Am. Chem. Soc.*, 2019, **141**, 11700.

251. A.J. Martínez-Martínez, C.G Royle, S.K. Furfari, K. Suriye, A.S. Weller, *ACS Catal.*, 2020, **10**, 1984.

252. T.M. Boyd, B.E. Tegner, G.J. Tizzard, A.J. Martinez-Martinez, S.E. Neale, M.A. Hayward, S.J. Coles, S.A. Macgregor, A.S. Weller, *Angew. Chem., Int. Ed.*, 2020, **59**, 6177.

253. A.J. Bukvic, D.G. Crivoi, H.G. Garwood, A.I. McKay, T.T.D. Chen, A.J. Martínez-Martínez, A.S. Weller, *Chem. Commun.*, 2020, **56**, 4328.

254. S.K. Furfari, B.E. Tegner, A.L. Burnage, L.R. Doyle, A.J. Bukvic, S.A. Macgregor, A.S. Weller, *Chem.- Eur. J.*, 2021, **27**, 3177.

255. A.J. Bukvic, A.L. Burnage, G.J. Tizzard, A.J. Martínez-Martínez, A.I. McKay, N.H. Rees, B.E. Tegner, T. Krämer, H. Fish, M.R. Warren, S.J. Coles, S.A. Macgregor, A.S. Weller, *J. Am. Chem. Soc.*, 2021, **143**, 5106.

256. L.R. Doyle, M.R. Galpin, S.K. Furfari, B.E. Tegner, A.J. Martínez-Martínez, A.C. Whitwood, S.A. Hicks, G.C. Lloyd-Jones, S.A. Macgregor, A.S. Weller, *Organometallics*, 2022, **41**, 284.

257. L.R. Doyle, E.A. Thompson, A.L. Burnage, A.C. Whitwood, H.T. Jenkins, S.A. Macgregor, A.S. Weller, *Dalton Trans.*, 2022, **51**, 3661.

258. E. Dalcanale, P. Soncini, G. Bacchilega. F. Ugozzoli, *J. Chem. Soc., Chem. Commun.*, 1989, 500.

259. R.J. Hooley, H.J. van Anda, J. Rebek, *J. Am. Chem. Soc.*, 2006, **128**, 3894.

260. R.J. Hooley, H.J. van Anda, J. Rebek, *J. Am. Chem. Soc.*, 2007, **129**, 13464.

261. T. Gottschalk, P.D. Jarowski, F. Diederich, *Tetrahedron*, 2008, **64**, 8307.

262. J. Hornung, D. Fankhauser, L.D. Shirtcliff, A. Praetorius. W.B. Schweizer, F. Diederich, *Chem.- Eur. J.*, 2011, **17**, 12362.

263. D. Fankhauser, D. Kolarski, W.R. Grüning, F. Diederich, *Eur. J. Org. Chem.*, 2014, 3575.

264. R.C. Knighton, A.B. Chaplin, *Tetrahedron*, 2017, **73**, 4591.

265. A. Carroy, J.-M. Lehn, *J. Chem. Soc., Chem. Commun.*, 1986, 1232.

266. K. Yamamoto, K. Higuchi, M. Ogawa, H. Sogawa, S. Kuwata, Y. Hayashi, S. Kawauchi, T. Takata, *Chem.- Asian J.*, 2020, **15**, 356.

267. D. Sooksawat, S.J. Pike, A.M.Z. Slawin, P.J. Lusby, *Chem. Commun.*, 2013, **49**, 11077.

268. D. Peng, Y. Zhang, X. Du, L. Zhang, X. Leng, M.D. Walter, Z. Huang, *J. Am. Chem. Soc.*, 2013, **135**, 19154.

269. X. Jia, Z. Huang, *Sci. China Chem.*, 2015, **58**, 1340.

270. L.S. Jongbloed, D. García-López, R. van Heck, M.A. Siegler, J.J. Carbó, J.I. van der Vlugt, *Inorg. Chem.*, 2016, **55**, 8041.

271. M.R. Eberhard, S. Matsukawa, Y. Yamamoto, C.M Jensen, *J. Organomet. Chem.*, 2003, **687**, 185.

272. A.J. Nawara-Hultzsch, J.D. Hackenberg, B. Punji, C. Supplee, T.J. Emge, B.C. Bailey, R.R. Schrock, M. Brookhart, A.S. Goldman, *ACS Catal.*, 2013, **3**, 2505.

273. R. Barrios-Francisco, E. Balaraman, Y. Diskin-Posner, G. Leitus, L.J.W. Shimon, D. Milstein, *Organometallics*, 2013, **32**, 2973.

274. J.I. van der Vlugt, J.N.H. Reek, *Angew. Chem., Int. Ed.*, 2009, **48**, 8832.

275. A.K. Bhattacharya, G. Thyagarajan, *Chem. Rev.*, 1981, **81**, 415.

276. A.P.T. Athanasopoulos, Master of Science Thesis, University of Waterloo, 2009.

277. S. Kloß, D. Selent, A. Spannenberg, R. Franke, A. Börner, M. Sharif, *Catalysts*, 2019, **9**, 1036.

278. M.J.G. Sinclair, A.B. Chaplin, *Inorg. Chim. Acta*, 2020, **513**, 119948.

279. A.J. Lupinetti, G. Frenking, S.H. Strauss, *Angew. Chem., Int. Ed.*, 1998, **37**, 2113.

280. A.J. Lupinetti, S.H. Strauss, G. Frenking, *Prog. Inorg. Chem.*, 2001, **49**, 1.

281. G.L. Parker, R. Van Lommel, N. Roig, M. Alonso, A.B. Chaplin, *Chem.- Eur. J.*, 2022, **28**, e202202283.

282. H. Valdés, E. Rufino-Felipe, G. van Koten, D. Morales-Morales, *Eur. J. Inorg. Chem.*, 2020, 4418.

283. W.A. Herrmann, B. Cornils, *Angew. Chem., Int. Ed. Engl.*, 1997, **36**, 1048.

284. P.W.N.M. van Leeuwen, C. Claver, *Rhodium Catalyzed Hydroformylation*, Kluwer, Dordrecht, 2000.

285. P.W.N.M. van Leeuwen, *Homogeneous Catalysis: Understanding the Art*, Kluwer, Dordrecht, 2004.

286. M. Beller, J. Seayad, A. Tillack, H. Jiao, *Angew. Chem., Int. Ed.*, 2004, **43**, 3368.

287. R. Franke, D. Selent, A. Börner, *Chem. Rev.*, 2012, **112**, 5675.

288. M.L. Clarke, *Curr. Org. Chem.*, 2005, **9**, 701.

289. Y.Ning, T. Ohwada, F.-E. Chen, *Green Synth. Catal.*, 2021, **2**, 247.

290. R.F. Heck, D.S. Breslow, *J. Am. Chem. Soc.*, 1961, **83**, 4023.

291. J.A. Osborn, G. Wilkinson, J.F. Young, *Chem. Commun. (London)*, 1965, 17.

292. J.A. Osborn, F.H. Jardine, J.F. Young, G. Wilkinson, *J. Chem. Soc. A*, 1966, 1711.

293. M.C. Baird, J.T. Mague, J.A. Osborn, G. Wilkinson, *J. Chem. Soc. A*, 1967, 1347.

294. M.C. Baird, C.J. Nyman, G. Wilkinson, *J. Chem. Soc. A*, 1968, 348.

295. D. Evans, G. Yagupsky, G. Wilkinson, *J. Chem. Soc. A*, 1968, 2660.

296. D. Evans, J.A. Osborn, G. Wilkinson, *J. Chem. Soc. A*, 1968, 3133.

297. C.K. Brown, G. Wilkinson, *Tetrahedron Lett.*, 1969, 1725.

298. M. Yagupsky, C.K. Brown, G. Yagupsky, G. Wilkinson, *J. Chem. Soc. A*, 1970, 937.

299. G. Yagupsky, C.K. Brown, G. Wilkinson, *J. Chem. Soc. A*, 1970, 1392.

300. C.K. Brown, G. Wilkinson, *J. Chem. Soc. A*, 1970, 2753.

301. M. Sparta, K.J. Børve, V.R. Jensen, *J. Am. Chem. Soc.*, 2007, **129**, 8487.

302. I. Jacobs, B. de Bruin, J.N.H. Reek, *ChemCatChem.*, 2015, **7**, 1708.

303. M. Diéguez, C. Claver, A.M. Masdeu-Bultó, A. Ruiz, P.W.N.M. van Leeuwen, G.C. Schoemaker, *Organometallics*, 1999, **18**, 2107.

304. M. Caporali, P. Frediani, A. Salvini, G. Laurenczy, *Inorg. Chim. Acta*, 2004, **357**, 4537.

305. R. Bellini, J.N.H. Reek, *Chem.- Eur. J.*, 2012, **18**, 13510.

306. C. Kubis, R. Ludwig, M. Sawall, K. Neymeyr, A. Börner, K.-D. Wiese, D. Hess, R. Franke, D. Selent, *ChemCatChem*, 2010, **2**, 287.

307. C. Kubis, M. Sawall, A. Block, K. Neymeyr, R. Ludwig, A. Börner, D. Selent, *Chem.- Eur. J.*, 2014, **20**, 11921.

308. R.C. How, P. Dingwall, R.T. Hembre, J.A. Ponasik, G.S. Tolleson, M.L. Clarke, *Mol. Catal.*, 2017, **434**, 116.

309. P. Dingwall, J.A. Fuentes, E. Crawford, A.M.Z. Slawin, M. Bühl, M.L. Clarke, *J. Am. Chem. Soc.*, 2017, **139**, 15921.

310. I.T. Horváth, R.V. Kastrup, A.A. Oswald, E.J. Mozeleski, *Catal. Lett.*, 1989, **2**, 85.

311. C. Bianchini, H.M. Lee, A. Meli, F. Vizza, *Organometallics*, 2000, **19**, 849.

312. D.A. Foley, A.L. Dunn, M.T. Zell, *Magn. Reson. Chem.*, 2016, **54**, 451.

313. A. Martínez-Carrión, M.G. Howlet, C. Alamillo-Ferrer, A.D. Clayton, R.A. Bourne, A. Codina, A. Vidal-Ferran, R.W. Adams, J. Burés, *Angew. Chem., Int. Ed.*, 2019, **58**, 10189.

314. A.C. Brezny, C.R. Landis, *J. Am. Chem. Soc.*, 2017, **139**, 2778.

315. A.C. Brezny, C.R. Landis, *ACS Catal.*, 2019, **9**, 2501.

316. A. Bara-Estaún, C.L. Lyall, J.P. Lowe, P.G. Pringle, P.C.J. Kamer, R. Franke, U. Hintermair, *Faraday Discuss.*, 2021, **229**, 422.

317. A. Bara-Estaún, C.L. Lyall, J.P. Lowe, P.G. Pringle, P.C.J. Kamer, R. Franke, U. Hintermair, *Catal. Sci. Technol.*, 2022, **12**, 5501.

318. A. Bara-Estaún, C.L. Lyall, J.P. Lowe, P.G. Pringle, P.C.J. Kamer, R. Franke, U. Hintermair, *ChemCatChem*, 2023, e202201204.

319. M. Tanaka, T. Hayashi, I. Ogata, *Bull. Chem. Soc. Jpn.*, 1977, **50**, 2351.

320. A.R. Sanger, *J. Mol. Catal.*, 1978, **3**, 221.

321. O.R. Hughes, J.D. Unruh, *J. Mol. Catal.*, 1981, **12**, 71.

322. C.P. Casey, G.T. Whiteker, M.G. Melville, L.M. Petrovich, J.A. Gavney, Jr., D.R. Powell, *J. Am. Chem. Soc.*, 1992, **114**, 5535 and 10680.

323. M. Miyazawa, S. Momose, K. Yamamoto, *Synlett*, 1990, **1990**, 711.

324. K. Yamamoto, S. Momose, M. Funahashi, S. Ebata, H. Ohmura, H. Komatsu, M. Miyazawa, *Chem. Lett.*, 1994, **23**, 189.

325. A. van Rooy, P.C.J. Kamer, P.W.N.M. van Leeuwen, K. Goubitz, J. Fraanje, N. Veldman, A.L. Spek, *Organometallics*, 1996, **15**, 835.

326. P.D. Achord, P. Kiprof, B. Barker, *J. Mol. Struc.- THEOCHEM*, 2008, **849**, 103.

327. H. Fernández-Pérez, P. Etayo, A. Panossian, A. Vidal-Ferran, *Chem. Rev.*, 2011, **111**, 2119.

328. S.H. Chikkali, J.I. van der Vlugt, J.N.H. Reek, *Coord. Chem. Rev.*, 2014, **262**, 1.

329. A. Pizzano, *Chem. Rec.*, 2016, **16**, 2599.

330. A. Cunillera, C. Godard, A. Ruiz, *Top. Organomet. Chem.*, 2018, **61**, 99.

331. N. Sakai, S. Mano, K. Nozaki, H. Takaya, *J. Am. Chem. Soc.*, 1993, **115**, 7033.

332. N. Sakai, K. Nozaki, H. Takaya, *J. Chem. Soc., Chem. Commun.*, 1994, 395.

333. K. Nozaki, N. Sakai, T. Nanno, T. Higashijima, S. Mano, T. Horiuchi, H. Takaya, *J. Am. Chem. Soc.*, 1997, **119**, 4413.

334. K. Nozaki, H. Takaya, T. Hiyama, *Top. Catal.*, 1997, **4**, 175.

335. T. Horiuchi, T. Ohta, E. Shirakawa, K. Nozaki, H. Takaya, *J. Org. Chem.*, 1997, **62**, 4285.

336. S. Deerenberg, P.C.J. Kamer, P.W.N.M. van Leeuwen, *Organometallics*, 2000, **19**, 2065.

337. M. Rubio, A. Suárez, E. Álvarez, C. Bianchini, W. Oberhauser, M. Peruzzini, A. Pizzano, *Organometallics*, 2007, **26**, 6428.

338. C.G. Arena, F. Faraone, C. Graiff, A. Tiripicchio, *Eur. J. Inorg. Chem.*, 2002, 711.

339. H. Fernández-Pérez, J. Benet-Buchholtz, A. Vidal-Ferran, *Org. Lett.*, 2013, **15**, 3634.

340. H. Fernández-Pérez, J. Benet-Buchholtz, A. Vidal-Ferran, *Chem.- Eur. J.*, 2014, **20**, 15375.

341. J.R. Lao, J. Benet-Buchholtz, A. Vidal-Ferran, *Organometallics*, 2014, **33**, 2960.

342. G.M. Noonan, J.A. Fuentes, C.J. Cobley, M.L. Clarke, *Angew. Chem., Int. Ed.*, 2012, **51**, 2477.

343. G.M. Noonan, C.J. Cobley, T. Mahoney, M.L. Clarke, *Chem. Commun.*, 2014, **50**, 1475.

344. R. Pittaway, J.A. Fuentes, M.L. Clarke, *Org. Lett.*, 2017, **19**, 2845.

345. L. Iu, J.A. Fuentes, M.E. Janka, K.J. Fontenot, M.L. Clarke, *Angew. Chem., Int. Ed.*, 2019, **58**, 2120.

346. J.A. Fuentes, M.E. Janka, J. Rodgers, K.J. Fontenot, M. Bühl, A.M.Z. Slawin, M.L. Clarke, *Organometallics*, 2021, **40**, 3966.

347. S.S. Nurttila, P.R. Linnebank, T. Krachko, J.N.H. Reek, *ACS Catal.*, 2018, **8**, 3469.

348. C. Bauder, D. Sémeril, *Eur. J. Inorg. Chem.*, 2019, 4951.

349. F. Hapiot, H. Bricout, S. Tilloy, E. Monflier, *Eur. J. Inorg. Chem.*, 2012, 1571.

350. F. Hapiot, S. Menuel, H. Bricout, S. Tilloy, E. Monflier, *Appl. Organometal. Chem.*, 2015, **29**, 580.

351. F.-X. Legrand, N. Six, C. Slomianny, H. Bricout, S. Tilloy, E. Monflier, *Adv. Synth. Catal.*, 2011, **353**, 1325.

352. D.N. Tran, F.-X. Legrand, S. Menuel, H. Bricout, S. Tilloy, E. Monflier, *Chem. Commun.*, 2012, **48**, 753.

353. M. Jouffroy, R. Gramage-Doria, D. Armspach, D. Sémeril, W. Oberhauser, D. Matt, L. Toupet, *Angew. Chem., Int. Ed.*, 2014, **53**, 3937.

354. J. Leblond, J. Potier, S. Menuel, H. Bricout, C. Machut-Binkowski, D. Landy, S. Tilloy, E. Monflier, F. Hapiot, *Catal. Sci. Technol.*, 2017, **7**, 3823.

355. M. Dauchy, M. Ferreira, J. Leblond, H. Bricout, S. Tilloy, G.S. Smith, E. Monflier, *Pure Appl. Chem.*, 2018, **90**, 845. M. Dauchy, M. Ferreira, J. Leblond, H. Bricout, S. Tilloy, G.S. Smith, E. Monflier, *Pure Appl. Chem.*, 2018, **90**, 845.

356. Z. Csók, G. Szalontai, G. Czira, L. Kollár, *J. Organomet. Chem.*, 1998, **570**, 23.

357. R. Paciello, L. Siggel, M. Röper, *Angew. Chem., Int. Ed.*, 1999, **38**, 1920.

358. C.J. Cobley, D.D. Ellis, A.G. Orpen, P.G. Pringle, *J. Chem. Soc., Dalton Trans.*, 2000, 1109.

359. F.J. Parlevliet, C. Kiener, J. Fraanje, K. Goubitz, M. Lutz, A.L. Spek, P.C.J. Kamer, P.W.N.M. van Leeuwen, *J. Chem. Soc., Dalton Trans.*, 2000, 1113.

360. C. Kunze, D. Selent, I. Neda, M. Freytag, P.G. Jones, R. Schmutzler, W. Baumann, A. Börner, *Z. Anorg. Allg. Chem.*, 2002, **628**, 779.

361. D. Sémeril, C. Jeunesse, D. Matt, L. Toupet, *Angew. Chem., Int. Ed.*, 2006, **45**, 5810.

362. D. Sémeril, D. Matt, L. Toupet, *Chem.- Eur. J.*, 2008, **14**, 7144.

363. L. Monnereau, D. Sémeril, D. Matt, L. Toupet, *Adv. Synth. Catal.*, 2009, **351**, 1629.

364. L. Monnereau, D. Sémeril, D. Matt, *Eur. J. Org. Chem.*, 2010, 3068.

365. D. Sémeril, D. Matt, L. Toupet, W. Oberhauser, C. Bianchini, *Chem.- Eur. J.*, 2010, **16**, 13843.

366. F. Plourde, K. Gilbert, J. Gagnon, P.D. Harvey, *Organometallics*, 2003, **22**, 2862.

367. F. Elaieb, D. Sémeril, D. Matt, M. Pfeffer, P.-A. Bouit, M. Hissler, C. Goulaouen, J. Harrowfield, *Dalton Trans.*, 2017, **46**, 9833.

368. N. Natarajan, M.-C. Pierrevelcin, D. Sémeril, C. Bauder, D. Matt, R. Ramesh, *Catal. Commun.*, 2019, **118**, 70.

369. W.L. Steffen, G.J. Palenik, *Inorg. Chem.*, 1976, **15**, 2432.

370. L.A. van der Veen, P.H. Keeven, G.C. Schoemaker, J.N.H. Reek, P.C.J. Kamer, P.W.N.M. van Leeuwen, M. Lutz, A.L.Spek, *Organometallics*, 2000, **19**, 872.

371. P.J. Fennis, P.H.M. Budzelaar, J.H.G. Frijns, A.G. Orpen, *J. Organomet. Chem.*, 1990, **393**, 287.

372. S. Güven, M.M.L. Nieuwenhuizen, B. Hamers, R. Franke, M. Priske, M. Becker, D. Vogt, *ChemCatChem*, 2014, **6**, 603.

373. M.Y.S. Ibrahim, J.A. Bennett, D. Mason, J. Rodgers, M. Abolhasani, *J. Catal.*, 2022, **409**, 105.

374. Hans Reich's Collection. NMR Spectroscopy., https://organicchemistrydata.org/hansreich/resources/nmr/?page=05-hmr-01-integration%2F, (accessed September 2023).

375. A.R. Rossi, R. Hoffman, *Inorg. Chem.*, 1975, **14**, 365.

376. T. Robert, Z. Abiri, J. Wassenaar, A.J. Sandee, S. Romanski, J.-M. Neudörfl, H.-G. Schmalz, J.N.H. reek, *Organometallics*, 2010, **29**, 478.

377. E. Zuidema, E. Daura-Oller, J.J. Carbó, C. Bo, P.W.N.M. van Leeuwen, *Organometallics*, 2007, **26**, 2234.

378. M. Nishio, Y. Umezawa, M Hirota, Y. Takeuchi, *Tetrahedron*, 1995, **51**, 8665.

379. F.R. Pinacho Crisóstomo, A. LLedó, S.R. Shenoy, T. Iwasawa, J. Rebek, Jr., *J. Am. Chem. Soc.*, 2009, **131**, 7402.

380. S. Mosca, Y. Yu, J.V. Gavette, K.-D. Zhang, J. Rebek, Jr., *J. Am. Chem. Soc.*, 2015, **137**, 14582.

381. Y. Zhu, M. Tang, H. Zhang, F.-U. Rahman, P. Ballester, J. Rebek, Jr., C.A. Hunter, Y. Yu, *J. Am. Chem. Soc.*, 2021, **143**, 12397.

382. J.A. McCleverty, G. Wilkinson, *Inorg. Synth.*, 1990, **28**, 84.

383. G.E.M. Crisenza, N. G. McCreanor and J. F. Bower, *J. Am. Chem. Soc.*, 2014, **136**, 10258.

384. W.E. Buschmann, J.S. Miller, *Inorg. Synth.*, 2002, **33**, 83.

385. E. Neumann, A. Pfaltz, *Organometallics*, 2005, **24**, 2008.

386. J.A. Osborn, G. Wilkinson, *Inorg. Synth.*, 1990, **28**, 77.

387. I. Krossing, *Chem. Eur. J.*, 2001, **7**, 490.

388. J. Yu and C. Zhang, *Synthesis*, 2009, **2009**, 2324.

389. G.M. Sheldrick, *Acta Cryst. A*, 2008, **64**, 112.

390. O.V. Dolomanov, L.J. Bourhis, R.J. Gildea, J.A.K. Howard and H. Puschmann, *J. Appl. Crystallogr.*, 2009, **42**, 339.

391. P.R. Mitchell, R.V. Parish, J. Chem. Ed., 1969, 46, 811.

392. C. Elschenbroich, Organometallics, Wiley-VCH, Weinheim, 3rd edn., 2016.